AN ABSTRACT OF THE THESIS OF

Lisa B. Eisner for the degree of Doctor of Philosophy in Oceanography presented on May 2, 2003. Title: Relationships of In Situ Spectral Absorption, Pigment Ratios and Environmental Parameters for Phytoplankton Assemblages in Coastal Waters.

Abstract approved: Redacted for privacy

Timothy J. Cowles

In situ optical measurements of spectral absorption and beam attenuation provide information on the fine scale horizontal and vertical variations in phytoplankton pigments and other measures of phytoplankton photophysiology and ecology in coastal waters. Phytoplankton pigment ratios from discrete sample analyses with High Performance Liquid Chromatography were compared to in situ spectral absorption, hydrography, light and nutrients in protected waters in East Sound, Washington and in coastal waters off Oregon. Clear linear relationships were seen between ratios of photoprotective: photosynthetic carotenoids (PPC: PSC) and the shape of the in situ phytoplankton absorption (a_{ph}) spectra in East Sound. Linear relationships between PPC: PSC ratios and a_{ph} spectra were also found for Oregon coastal waters within groups of samples (grouped by collection date, location and temperature salinity characteristics). Inshore samples showed a similar relationship as East Sound samples. Diatoms were dominant in East Sound and Oregon shelf waters, with prokaryotes and prymnesiophytes important in Oregon waters further offshore.

Environmental parameters were associated with variations in PPC: PSC ratios. Light was clearly an important factor in East Sound with a strong positive association seen between PPC: PSC ratios and recent light history. In Oregon waters, PPC: PSC ratios varied with prior light exposure, nutrients and temperature. Light exposure and temperature predicted 61% of the variability in PPC: PSC ratios for samples with low nutrients (dissolved inorganic nitrogen < 2 μM). In situ optical measurements indicated considerable spatial variation in phytoplankton photophysiology and taxonomic composition in the Oregon costal region. Phytoplankton assemblages often had lower PPC: PSC ratios, flatter particle size distributions slopes suggesting greater contributions by large particles, higher chlorophyll *a* per particle, and more packaging in the nutrient-rich upwelled waters near shore compared to further offshore.

These results indicate that in situ measurements of spectral absorption and beam attenuation can predict PPC: PSC ratios and other photophysiological and taxonomic indices in coastal waters. Such data provide high-resolution information on phytoplankton characteristics on the same temporal and spatial scales as physical properties such as temperature and salinity, and offer important insights into light history and the transfer of absorbed light within phytoplankton cells.

Relationships of In Situ Spectral Absorption, Pigment Ratios and Environmental Parameters for Phytoplankton Assemblages in Coastal Waters

by
Lisa B. Eisner

A THESIS

submitted to

Oregon State University

in partial fulfillment of
the requirements for the
degree of

Doctor of Philosophy

Presented May 2, 2003
Commencement June 2003

Doctor of Philosophy thesis of Lisa B. Eisner presented on May 2, 2003.

APPROVED:

Redacted for privacy

Major Professor, representing Oceanography

Redacted for privacy

Dean of College of Oceanic and Atmospheric Sciences

Redacted for privacy

Dean of Graduate School

I understand that my thesis will become part of the permanent collection of Oregon State University libraries. My signature below authorizes release of my thesis to any reader upon request.

Redacted for privacy

Lisa B. Eisner, Author

ACKNOWLEDGMENTS

I wish to thank my major advisor, Tim Cowles, for his continued support, guidance, patience and friendship throughout my time at COAS. He has suggested a great many thoughtful ideas and approaches, and always helped me to keep the bigger picture in mind. I also greatly appreciate all the edits and suggestions during my manuscript and thesis preparations and his confidence in my abilities. Finally, Tim's kindness and dedication to his family, laboratory group and the overall COAS community are exemplary examples to follow.

I thank Pat Wheeler, Ricardo Letelier, Ron Zaneveld, Scott Pegau and Steve Giovannoni for serving on my thesis committee. I am indebted to Ricardo Letelier for always being there to answer my questions and offer insights and new ways of evaluating a problem. He has greatly helped me to improve my approach to science and to think creatively. I also thank Ricardo for his great enthusiasm and love of science, which have helped me to maintain my own excitement. Pat Wheeler has helped me gain a much better understanding of phytoplankton physiology and has offered helpful feedback on my manuscripts. I also appreciate the opportunities Pat gave me to peer review articles for the Journal of Phycology, a valuable experience. Scott Pegau and Ron Zaneveld offered many helpful suggestions on understanding and applying optical techniques in my research. I especially thank Ron for agreeing to serve on my committee on late notice and offering several useful ideas on my thesis work. Steve Giovannoni has had many interesting questions about my research, in addition to serving as my graduate representative.

I thank everyone in Tim Cowles Lab group for all the help and friendship and sense of humor over the years. Chris Wingard and Russ Desiderio helped with data collection, processing, and data interpretation. I am grateful to Russ for his insightful discussions and extremely helpful advice (and the free cups of coffee for poor starving graduate students such as myself). I thank Chris Wingard for all his help with MATLAB programming and the infamous Figure 2 in my first manuscript. Nathan Potter helped with the East Sound fieldwork and I appreciate the interesting discussions over years.

Margaret Sparrow offered endless advice on High Performance Liquid Chromatography (HPLC) and was always willing to help out. I also appreciate Claudia Mengelt's effort getting the HPLC up and running as well as her valuable suggestions and ideas. I am grateful to Fred Prahl and Bob Collier for many interesting conversations and the opportunity to conduct research in Crater Lake. I thank Jack Barth for his endless patience in teaching me how to teach, and thank both Jack Barth and Kelly Falkner and for their advice and support in proposal writing. Countless other professors, research assistants and students gave me support and aid and participated in many great science talks during my time at COAS. Thank you!

There are numerous students and friends who have offered encouragement, camaraderie, entertainment and friendship over the years. I especially want to thank John Lyman, Caroline Broadbent, Dylan and Narra Riggi, Sam Laney, Malinda Sutor, Krista Longnecker, Cidney Howard, Jonathan Nash, Brigid Gearen, Daniel and Kelly Palacios, Mark Baumgartner, Kipp and Courtney Shermann, Amanda Ashe, Jacob and Maria Huyer, Sue Gries, Matt and Cara Robinson. I cannot express how appreciative I

am for all the get-togethers and BBQ's, climbing, fishing, kayaking, and skiing trips, poker games, adventures and laughs. You are all wonderful! I also thank all the craft night ladies (especially Sheila O'Keefe, Leah Bandstra and Melissa Feldberg) for teaching me the valuable life skill of knitting. I am also quite grateful to the women scientists who inspired me along my career in biological oceanography. Mary Jane Perry, Monica Orellano, Mary Kay Talbot and Carol Janzen offered much enthusiasm and support for all my scientific endeavors. Thanks also to my family for all their love and caring and belief that I would succeed.

Finally, and most of all, I thank my husband, Jody White. I am enormously appreciative for his support during my long effort in returning to school and his endless love and patience during this time. Jody's wonderful sense of humor and role as social coordinator also kept my spirits high. I could not have done this without him. I have no words to say how truly grateful I am. Last of all I am grateful for the companionship of Zoe, my joyful bouncing dog who constantly shows me that nothing is more important in life than taking time to enjoy the world around you.

CONTRIBUTION OF AUTHORS

Dr. Timothy J. Cowles was highly involved in the execution of research, data analysis and writing of all chapters. Dr. Michael Twardowski significantly contributed to sample collection, data analysis and writing of chapter two, and offered many insightful and valuable suggestions. Dr. Mary Jane Perry provided particulate absorption measurements, aided in sample collection and provided helpful editorial suggestions for chapter two. Dr. Ricardo Letelier collected the High Performance Liquid Chromatography samples, collected and analyzed the particulate absorption samples and assisted in data interpretation for chapters three and four (as well as offering many insights for chapter two).

TABLE OF CONTENTS

TABLE OF CONTENTS (CONTINUED)

TABLE OF CONTENTS (CONTINUED)

TABLE OF CONTENTS (CONTINUED)

LIST OF FIGURES

LIST OF FIGURES (CONTINUED)

LIST OF FIGURES (CONTINUED)

LIST OF FIGURES (CONTINUED)

LIST OF TABLES

DEDICATION

I wish to dedicate this doctoral dissertation to my late father, Steve Eisner. My father was a chemist for his primary career and a writer and world traveler during his retirement. His curiosity, fascination with science and love of life were beneficial for all of his ambitions. I was very fortunate to have a father who immensely enjoyed his field of work and was able to pass that excitement along to me. And so, my father was instrumental in my draw to science and choice of career. Most importantly he taught me to try to approach a problem from many different angles and open my mind to all the possibilities. I thank him deeply.

Relationships of in situ spectral absorption, pigment ratios and environmental parameters for phytoplankton assemblages in coastal waters

CHAPTER 1

GENERAL INTRODUCTION

Phytoplankton ecologists have long strived to monitor and understand the interaction of algal physiology, taxonomic composition and environmental conditions in the oceans (Mann and Lazier 1991 and references therein, Riley 1942, Sverdrup 1953, Eppley 1972). Of particular interest have been the effects of light and nutrients on the rates of photosynthesis of various assemblages of phytoplankton species, given that each species possesses a mixture of light-absorbing pigments, most of which aid in the translation of light energy into chemical energy in the cell. Extensive laboratory research on the pigment complexes in algae over the past decades (Rowan 1989, Jeffrey 1997, Macintyre 2002) has provided a broad base of knowledge on the types of pigments found in different taxa, the general shifts in pigment composition that can occur under light and nutrient stress, and an initial understanding of the kinetics of those shifts in pigment composition. It is not clear, however, how to translate our laboratory-derived insights into sound interpretation of in-situ processes. It is this "translation problem " that has motivated the work presented in this thesis. The recent use of in situ instrumentation for measurement of spectral light absorption and

attenuation allows scientists to begin to monitor photophysiological and taxonomic changes over small temporal and spatial scales that are similar to those obtained for physical oceanography, such as temperature and salinity. Spectral absorption reflects variations in pigment composition and packaging (SooHoo et al. 1986; Johnsen et al.1994) that can be tied to the photosynthetic machinery of the cell. Spectral beam attenuation, on the other hand, may be used to understand variations in particle size distributions of the phytoplankton assemblage (Kitchen et al.1982, Boss et al.2001). Taxonomic variations are reflected by spectral absorption (Johnsen and Sakshaug 1996) and beam attenuation, since different phytoplankton species have different pigmentation, packaging, and cell sizes. Accordingly, a major goal in recent years has been to discover proxies for phytoplankton physiology and taxonomic composition, such as phytoplankton pigment ratios, that can be monitored by in situ optics.

Phytoplankton pigments provide a means to characterize photophysiological state, composition and biomass of the phytoplankton assemblage (Raven and Falkowski, 1997). Pigments absorb light and transfer the light energy to chlorophyll *a* in the reaction center for use in photochemistry or dissipate excess energy as fluorescence or heat. The pigments (carotenoids and chlorophylls) involved in photochemistry are termed photosynthetic, while the carotenoid pigments thought to be involved in heat dissipation (or the transfer of energy with reduced efficiency) are termed photoprotective since they help prevent the cell from damage by excess light energy. Photoprotective carotenoid (PPC) concentrations can be compared to photosynthetic carotenoids (PSC), chlorophyll *a* (chl *a*) or total pigment

concentrations to provide photophysiological indices that may be indicative of energy transfer within the photosynthetic apparatus of the chloroplast (MacIntyre et al, 2002).

Saturating irradiances have been associated with relative increases in PPC and decreases in chl *a* in phytoplankton laboratory cultures and field assemblages (Claustre et al.1994, Moline 1998, Schluter 2000). Limiting nutrients (nitrogen or phosphate) can produce similar responses in pigmentation (Geider et al.1993, 1998, Latasa 1995), since cells that are nutrient stressed may have fewer functional reaction centers and thus are able to use less of the absorbed light in photosynthesis. So, for a given saturating irradiance, nutrient-stressed cells may produce more PPC than nutrient replete cells, suggesting there is an interaction between light and nutrients in PPC formation. Ratios of PPC relative to photosynthetic pigments also provide an indication of recent light or nutrient history since pigments are synthesized and degraded on scales of hours to days (Falkowski and Raven 1997). Xanthophyll cycling between some photoprotective carotenoids (such as diadinoxanthin and diatoxanthin in chromophytes) occurs over shorter time periods (on the order of 1-10 minutes, reviewed in Porra et al, 1997) and thus best reflect the immediate light environment.

In order to apply these components of the photosynthetic process to populations of autotrophs, it is necessary to evaluate these components within the changing light and nutrient conditions of the ocean. In this study, I have examined phytoplankton pigments, spectral absorption and spectral beam attenuation, in conjunction with environmental parameters, to develop an in situ assessment of photoacclimation and taxonomic composition.

Phytoplankton pigments are quantified using High Performance Liquid Chromatography (HPLC) on discrete water samples (reviewed in Wright and Jeffery 1997). In contrast, in situ spectral absorption measurements, obtained with an ac-9, a nine-wavelength absorption and beam attenuation meter, provide high-resolution information on the in-water assemblages. So, one primary goal of my research has been to find an index of the relative amount of PPC in field phytoplankton assemblages, using in situ optical measurements. Pigment classes have specific wavelengths of absorption (Bidigare, 1990) that influence the shape of the in situ absorption spectra. The PPC have peak absorptions at shorter wavelengths (further toward the blue end of the spectrum) than PSC (Figure 1.1, adapted from Bidigare 1990). The PPC: PSC ratios (from HPLC analyses) are used to indicate the photoadaptive state of the phytoplankton. These ratios are compared to the shape of the in situ phytoplankton absorption (a_{ph}) spectra, defined by an a_{ph} slope index. The a_{ph} slope = $(a_{ph}488\text{-}a_{ph}532)/((a_{ph}676) \cdot (488\text{-}532\ \text{nm}))$. The a_{ph} spectra are derived from the ac-9 a_p spectra by removing the detrital absorption (a_d) component, based on estimates from discrete samples using the Quantitative Filter Technique (Yentsch 1962; Mitchell and Kiefer 1988) with the Kishino method (Kishino et al.1985; Roesler 1992). The removal of a_d is critical to these calculations (Roesler et al.1989), and therefore is covered in detail. I also describe package effects (intracellular self-shading, Duysens 1956) since they affect the shape of the absorption spectra and reflect variations in pigment compliment, size and shape (Kirk 1994). The relationships of phytoplankton taxonomic composition to PPC: PSC ratios and pigment packaging are also considered. Finally I investigate the relationship of PPC:

PSC ratios and absorption measurements to physical forcing mechanisms and water mass characteristics described by variations in light, nutrients, temperature and stratification. The mixing history of the phytoplankton assemblages is quite important (Cullen and Lewis, 1988). For example, natural phytoplankton from stratified depths in Puget Sound exhibited photoacclimation effects (photosynthetic pigment absorption coefficient: total phytoplankton absorption coefficient was inversely related to irradiance), while cells in mixed layers did not show a discernable photoacclimation trend (Culver and Perry, 1999).

In chapter 2, I evaluate the relationship between PPC: PSC ratios and a_{ph} slopes for protected marine waters in East Sound, an inlet of Orcas Island, Washington. These samples were collected over a 10-day period during Mid-June 1998 from a barge moored at a single location near the head of the inlet. Vertical optical profiles and water samples were collected from the near surface (2-3 m) to near bottom (18 m).

In chapters 3 and 4, sampling was conducted over a 9000-km^2 area of the Oregon coastal region during the upwelling season for a 3-week period in mid-August, 2001. The relationships between PPC: PSC ratios and ac-9 a_{ph} slopes are described for samples grouped by water mass characteristics (temperature, salinity), location, and collection date. Vertical profiles of optics and water samples were collected close to shore in active upwelling regions, at mid-shelf locations and further offshore in areas influenced by the Columbia River plume. Water depths varied from 30 m to 300 m with considerable mesoscale variability observed cross shelf and alongshore. This

work was part of the NSF sponsored Coastal Ocean Advances in Shelf Transport (COAST) project.

The progression of my research was from a single station-sampling scheme in East Sound to a large area multi-station sampling strategy off the Oregon Coast. This progression allowed me to develop my relationships using East Sound data and then test the applicability of these relationships using data from the highly variable (temporally and spatially) environment of the Oregon coastal region (Small and Menzies 1981). The calibration of in situ absorption measurements with PPC: PSC ratios allow environmental parameters, pigment ratios and optical parameters to be compared over a wide variety of conditions at high spatial and temporal resolution. These comparisons are an important step toward understanding the factors driving variations in phytoplankton physiology and taxonomic composition in coastal phytoplankton assemblages.

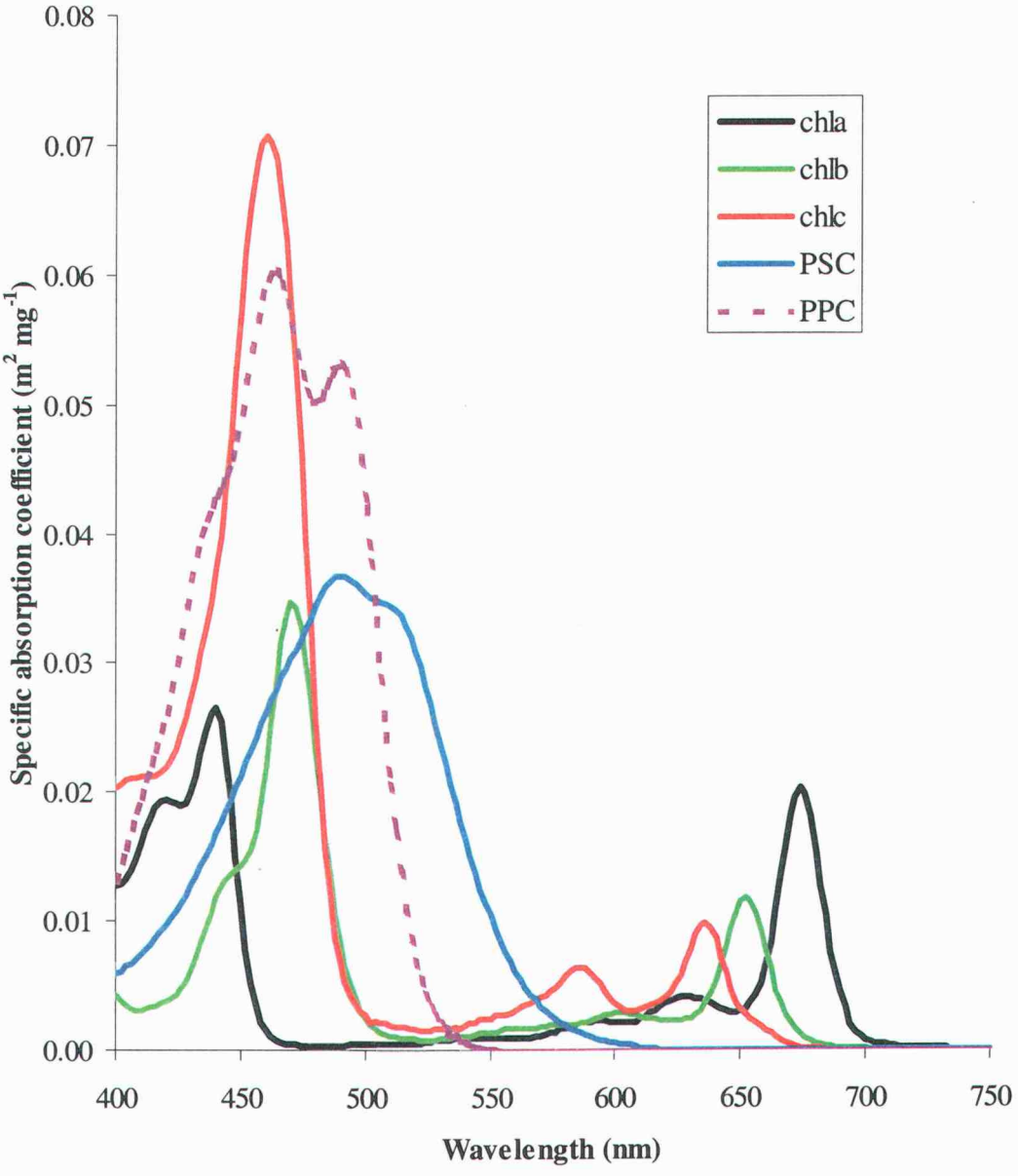

Figure 1.1. Specific absorption coefficient spectra for chlorophylls *a*, *b* and *c* (chl *a*, chl *b* chl *c*), photosynthetic carotenoids (PSC: 19-hexanoyloxyfucoxanthin,19-butanoyloxyfucoxanthin, fucoxanthin, peridinin), and photoprotective carotenoids (PPC: alloxanthin, β-carotene, diadinoxanthin, diatoxanthin, lutein/zeaxanthin, violaxanthin). Phycobilipigments are not shown. Adapted from Bidigare et al. (1990).

CHAPTER 2

RESOLVING PHYTOPLANKTON PHOTOPROTECTIVE: PHOTOSYNTHETIC CAROTENOID RATIOS ON FINE SCALES USING IN SITU SPECTRAL ABSORPTION MEASUREMENTS

Lisa B. Eisner, Michael S. Twardowski, Timothy J. Cowles and Mary Jane Perry

Published in *Limnology & Oceanography*
ASLO Business Office, 5400 Bosque Boulevard, Suite 680, Waco, Texas 76710-4446
Volume 48, Number 2 (March 2003), Pages 632-646.

Abstract

Temporal changes in phytoplankton pigments and spectral absorption were evaluated during June 1998 in East Sound, Orcas Island, Washington. High-resolution vertical profiles of in situ spectral absorption were obtained with a WET Labs ac-9 (nine-wavelength absorption and beam attenuation meter), and pigment concentrations were determined for discrete water samples using High Performance Liquid Chromatography (HPLC). Fucoxanthin was the most abundant carotenoid, indicating the dominance of diatoms. We computed a "slope" index to evaluate changes in shapes of the in-situ particulate absorption coefficient (a_p) spectra, a_p slope = (a_p488-a_p532)/((a_p676) · (488-532 nm)). A clear linear relationship was seen between ratios of photoprotective: photosynthetic carotenoids (PPC: PSC) and these a_p slopes. While pigment package effects may alter the absorption spectra, in our data set we still found a significant relationship between pigment ratios and in situ a_p slopes. Retrieval of this relationship was facilitated by the low and relatively constant detrital absorption coefficient (a_d) values in our study area. Similar relationships were found between PPC: PSC ratios and the estimated phytoplankton absorption coefficient (a_{ph}) spectra. High PPC: PSC ratios and steeper a_p slopes were associated with high light levels. Our results suggest that in situ absorption measurements can be used to estimate PPC: PSC ratios in areas where a_d contribution is low or can be estimated. These variations in pigment ratios and spectral absorption reflect photoacclimation responses and/or changes in phytoplankton species composition, and suggest in situ absorption

measurements may be used to estimate pigmentation changes over fine temporal and spatial scales.

Introduction

Rapid, in situ assessment of phytoplankton physiological condition has been a goal of plankton ecologists for many decades. The recent development and field use of multi-wavelength bio-optical instrumentation has brought us closer to that goal, and provides the opportunity to quantify the relationship between in situ observations and traditional, discrete sample analyses of physiological condition. The work described in this paper was motivated by that opportunity, and in particular, tested the effectiveness of measurements of in situ absorption spectra as indicators of the photoadaptive state of the phytoplankton assemblage.

Pigments are widely used to characterize phytoplankton physiological state, species identity and biomass in marine and freshwater environments (Falkowski and Raven 1997). Light harvesting pigments in the photosystem absorb light that impinges on chloroplasts within the cell. This absorbed light energy has three main fates, 1) carbon assimilation via photosynthesis, 2) dissipation as fluorescence or 3) dissipation as heat. Photoprotective carotenoid (PPC) pigments help prevent damage to the chloroplast from excess light energy, while photosynthetic carotenoid (PSC) pigments are involved in transfer of energy to reaction centers during photosynthesis. Therefore, PPC: PSC ratios may serve as indicators of energy transfer pathways within phytoplankton cells.

Variations in the relative proportions of carotenoid accessory pigments also alter the shape of the phytoplankton absorption coefficient (a_{ph}) spectrum. Changes in the a_{ph} spectra have been used to differentiate low light and high light adapted cultures for a variety of different phytoplankton taxa (SooHoo et al. 1986; Johnsen et al.1994). The slope of the a_{ph} spectra from 490 to 530 nm (normalized to 676 nm) has been found to be steeper in high light compared to low light adapted cultures (Johnsen et al.1994). Such a_{ph} spectral variations are due to physiological changes in cellular pigment ratios and pigment packaging (intracellular self-shading; Duysens 1956). Under high light, increases in PPC, decreases in PSC and a reduction in pigment packaging may cause the a_{ph} spectral slopes to become steeper, while the reverse is true for low light conditions. The in situ a_{ph} spectra also can reflect variations in taxonomic composition (Johnsen and Sakshaug 1996) and absorption by pigmented heterotrophic organisms.

Research over the past few decades has shown that changes in pigments and absorption coefficients, reflecting changes in phytoplankton physiology and species composition, are tied to fluctuations in the physical and chemical environment (irradiance, stratification, mixing, nutrients). Field studies have shown that variations in PPC and PSC potentially can be used to evaluate changes in light and mixing (Claustre et al.1994; Moline 1998). In laboratory experiments, increases in the photoprotective pigments, diatoxanthin and diadinoxanthin, were associated with both increases in irradiance and decreases in nutrients (Latasa 1995).

These previous studies used discrete sample analyses to evaluate the photoadaptive state of specific samples. Common methodology for particulate

absorption measurements, (the quantitative filter technique (QFT) (Yentsch 1962; Mitchell and Kiefer 1988)), requires filtration of discrete water samples and analysis with a bench-top spectrophotometer to obtain a_p. The QFT allows estimation of the detrital absorption coefficient (a_d) following extraction of pigments from the filter (Kishino method, Kishino et al.1985; Roesler 1992), thus providing an estimate of the phytoplankton absorption coefficient (a_{ph}). In contrast to this discrete sample analysis, the use of in situ multi-wavelength optical instrumentation such as the WET Labs ac-9 now allows the absorption coefficients for particulate (a_p) spectra to be estimated directly within the water column, enabling vertical profiles of $a_p(\lambda)$ to be easily obtained. Coupled with the measurement of phytoplankton pigment concentration using High Performance Liquid Chromatography (HPLC) on discrete samples, in situ absorption measurements now may provide a tool for assessing fine scale variations in the photoadaptive state of phytoplankton. In addition, the non-intrusive nature of in situ optics provides an advantage over discrete water sample collection since one can eliminate the sampling artifacts during preservation, handling and laboratory analysis. Finally, coincident measurements of physical parameters such as temperature (T) and salinity (S) allow a better correlation of biological and physical properties within the water column.

Our goals in this work were to determine the extent to which in situ a_p measurements can estimate phytoplankton accessory pigment composition over fine scales, and to evaluate the resulting impacts on phytoplankton ecology at these scales. Specifically, we wished to 1) compare PPC and PSC concentrations from HPLC analyses of discrete water samples with in situ absorption spectra for estuarine

phytoplankton assemblages, 2) demonstrate how in situ a_p and a_{ph} measurements can be used to evaluate of PPC: PSC ratios over fine scales, 3) provide examples of the relationship of PPC: PSC ratios and absorption measurements to physical forcing mechanisms (light, nutrients and mixing), and 4) quantify the potential effects of a_d and package effect variations on the relationship between PPC: PSC ratios and a_p and a_{ph} spectra.

Materials and Methods

Sampling site

Data collection occurred from 14 to 24 June 1998 from the R/V Henderson, moored near the head of East Sound (148° 40.62' N and 122° 53.45' W), a fjord type inlet of Orcas Island, Washington (Figure 2.1). The depth of the water column varied from 20 to 22 m depending on tidal stage.

In situ measurements of hydrography and bio-optics

A vertical time series of temperature data (Figure 2.2) was obtained with a thermistor chain located ~100 m east of the R/V Henderson. Vertical profiles of temperature, salinity, fluorescence and spectral absorption were obtained with a free-falling optical instrument package. This package included a high-resolution Conductivity-Temperature-Depth (CTD) sensor (SBE911, Seabird, Inc.), a fluorometer (Wetstar, WET Labs, Inc.), and two nine-wavelength in situ spectral absorption and beam attenuation meters (ac-9, WET Labs, Inc.). A 0.2 μm filter

(maxi-capsule, Gelman) was attached to the intake port of one of the ac-9s to measure the absorption by dissolved materials. Wavelengths for in situ absorption measurements were 412, 440, 488, 510, 532, 555, 650, 676, 715 nm. The ac-9s were calibrated every 2-4 d during the study using the pure water calibration technique (Twardowski et al.1999).

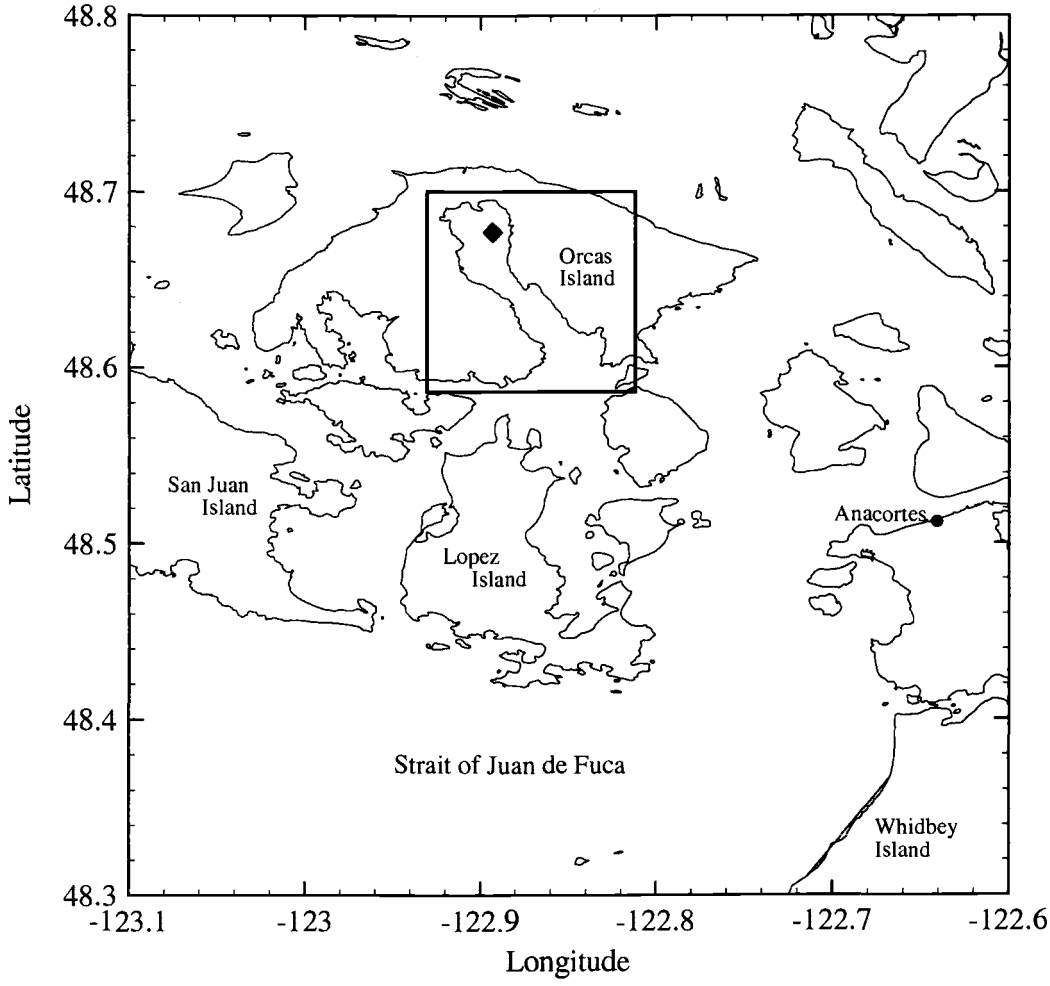

Figure 2.1. Location of sampling site (RV/ Henderson, black diamond) during June 1998 in East Sound, Orcas Island, Washington. East Sound marked by the square outline.

Collection of discrete water samples

Water samples were collected once or twice per day (Figure 2.2) within and outside vertical intervals of high particle concentration. Samples for pigment composition, QFT absorption, nutrients and phytoplankton taxonomy were either siphoned from depth, collected with a separate 5-liter Niskin bottle, or sampled with a rosette system of bottles (20 cm in height; 500 ml capacity) deployed with the optical instrumentation package. T and S signatures from CTD measurements were obtained for both water samples and in situ optical measurements, and then used to match

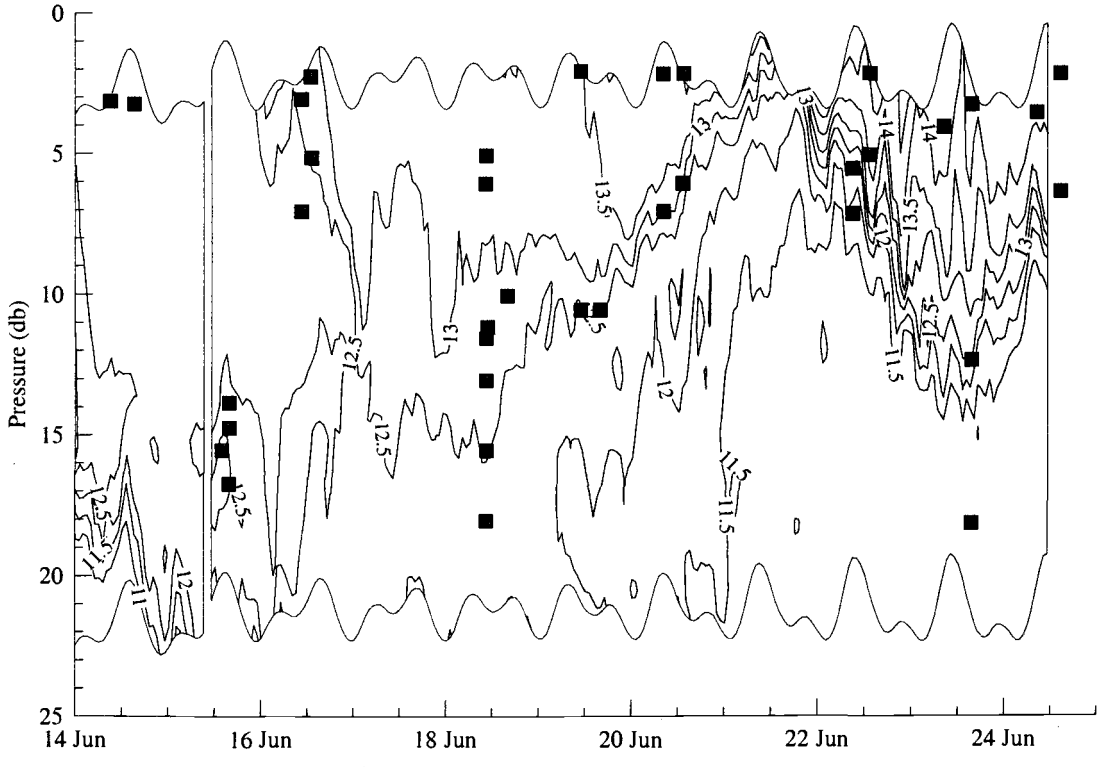

Figure 2.2. Contour plot of thermistor chain data from mooring array for 14-24 June 1998, Pacific Daylight Time (PDT). The cyclic oscillations in thermistor sampling depths are due to tidal variations in water height. Black squares indicate depths of HPLC sample collection.

depths of water sample collection with optical measurements. Water samples and optical measurements were collected within 2.5 h of each other with the majority (80%) collected within 1 h.

Phytoplankton pigment analyses

For phytoplankton pigment determinations, water samples (0.5 to 1 L) were filtered onto 25 mm glass fiber filters (GF/F filters, Whatman) and frozen in liquid N_2. Pigments were extracted overnight in cold 90% acetone, sonicated and quantified using reverse-phase HPLC (Ultrasphere C18 column, dual wavelength Spectra System UV2000 absorption detector) following a modified mobile solvent protocol (Wright and Jeffrey 1997). Calibrations were done with external standards. Quantifiable pigments included chlorophylls (*a*, b, c1/c2), chlorophyllide *a*, PSC (19-hexanoyloxyfucoxanthin, 19-butanoyloxyfucoxanthin, fucoxanthin, peridinin), and PPC (alloxanthin, β-carotene, diadinoxanthin, diatoxanthin, lutein/zeaxanthin, violaxanthin). To use chlorophyll *a* as a biomass reference level in pigment ratios, we computed the sum of chlorophyll *a* (chl *a*) and chlorophyllide *a*, noted as Tchl *a*.

The output voltage of the Wetstar fluorometer on the profiling package was converted to chl *a* equivalents using fluorometric analyses of extracted chl *a* and pheopigments from discrete water samples collected with the rosette sampler. Samples were filtered and extracted in cold 90% acetone and analyzed with a Turner Model AU –10 fluorometer (Parsons et al, 1984). Chl *a* concentration from extracted samples was linearly correlated with the in situ fluorometer voltage ($r^2 = 0.89$, $p < 0.0001$).

Discrete sample absorption spectra analyses

Discrete water sample a_p, a_{ph} and a_d spectra were obtained following methods described in Culver and Perry (1999). A dual beam spectrophotometer (SLM-Amico DW2) was used to measure a_p spectra using the QFT (Yentsch 1962; Mitchell and Kiefer 1988). Phytoplankton pigments were removed using methanol (Kishino et al. 1985) and filters were re-scanned to measure the a_d spectra. The a_{ph} spectra were determined by subtracting a_d from a_p spectra.

Nutrient analyses

Nutrient samples were immediately frozen after collection and analyzed within six months for total nitrate, nitrite, ammonium, phosphate and silicate. Nutrient concentrations were determined with a Technicon auto analyzer following standard colorimetry protocols (UNESCO 1994).

In situ particulate absorption spectra

The total in situ absorption coefficient (a_t) spectrum consists of absorption coefficients for water (a_w), particulates (a_p) and dissolved constituents (a_g). Pure water absorption is removed in the calibration methodology, so that the ac-9 measures $a_p + a_g$, denoted a_{pg}. Corrections for the temperature dependence of pure water absorption and variations in salinity were applied (Pegau et al. 1997), while the scattering error in our a_p measurements was removed by subtracting a_p715 nm from all wavelengths (Zaneveld et al, 1994). Data from the two ac-9s were used to estimate a_p

by subtraction of a_g from a_{pg}. A time-lag correction for a slower flow rate was applied to the filtered ac-9 data in order to align the particulate and dissolved measurements.

Calculation of slopes from absorption spectra

To evaluate changes in the shape of the a_{ph}, and a_p spectra from 488 to 532 nm, we normalized the absorption data to 676 nm. The "slopes" of the normalized absorption curves from 488 to 532 nm were computed:

$$a_x \text{ slope} = (a_x488 - a_x532) / (a_x676 \cdot (488 - 532 \text{ nm})),$$

where a_x is denoted as a_{ph} or a_p.

The ac-9 slope measurements were averaged over 1-m intervals (~50 data points at a profiler descent rate of 0.12 m s^{-1}). The a_{ph} and a_p slopes from the ac-9 and discrete samples were then compared to the PPC: PSC ratios from HPLC. A steeper slope was assumed to indicate an increase in relative amounts of PPC and/or a decrease in PSC based on the wavelength of maximum absorption and spectral shape of these pigment groups. The peak in vivo absorption for PPC is ~ 460 nm with specific absorption dropping near zero (0.001 m^2 mg^{-1}) at ~ 540 nm (Bidigare et al. 1990). In comparison, the peak in vivo absorption for PSC is ~ 490 nm, dropping near zero at ~ 590 nm. Chlorophyll c (chl *c*) absorbs within the wavelengths of interest (488 to 532 nm), so absorption slopes also were compared to chl *c*: PSC, chl *c*: PPC and chl *c*: Tchl *a* ratios. We used model 2 linear regression analysis for all comparisons.

Detrital absorption (a_d) estimation

We investigated three methods to estimate and remove a_d from the ac-9 a_p measurements to obtain a_{ph}. Method 1 used the a_d results from specific discrete water samples collected close in time and depth to the ac-9 samples and analyzed with the QFT (and Kishino method). Method 2 used a mean a_d spectrum derived from all QFT data combined. Method 3 involved modeling the a_d shape and magnitude following methods in Roesler et al. (1989), using the equation:

$$a_d(\lambda) = a_d 440 \, e^{(-s\,(\lambda-440))},$$

where $a_d 440 = a_p 440 - a_{ph} 440$. We measured $a_p 440$ with the ac-9, but needed to estimate $a_{ph} 440$ and the exponent, s, to apply this method. We assumed that $a_{ph} 676 \sim a_p 676$ (since a_d decays exponentially from blue to red wavelengths, little detrital absorption is expected in the red region of the spectrum). We then assumed $a_{ph} 440 = 1.61 \cdot a_p 676$, where1.61 was the mean blue: red value from QFT results. We used s = 0.0065 nm^{-1}, since it gave a_{ph} slopes insignificantly different from slopes found using QFT a_d from specific samples (95% CI for regression line slope, s = 0.0060 to 0.0072 nm^{-1}).

We then calculated ac-9 a_{ph} slopes based on the a_{ph} (λ) that resulted from each of the three a_d correction methods outlined above. The linear regressions between a_{ph} slopes and PPC: PSC ratios were not significantly different using any of the methods ($p < 0.05$), after removal of one outlier (which had no comparable QFT data). For our data set consisting of ac-9 data and discrete pigment samples, we used the QFT a_d

from specific discrete water samples (method 1) to calculate a_{ph} slopes for all samples, except for one outlier. Since QFT data were limited in number, some QFT a_d data were used for more than one ac-9/HPLC sample pair (QFT, n = 21; HPLC, n = 35 (excluding outlier)). For the single outlier and for fine-scale vertical profiles of ac-9 derived a_{ph} slopes, we used method 3 (or a variation of this method with a different s) to estimate a_d and subsequently a_{ph} slopes, since comparable QFT a_d data were unavailable, particularly for deep samples.

The relative importance of a_d to the a_p spectra was evaluated by comparing ratios of a_p412: a_p440 from ac-9 measurements. Detritus has higher absorption at 412 nm than at 440 nm while phytoplankton show the opposite trend. A ratio of a_p412: a_p440 greater than 0.96 was assumed to indicate the presence of detritus, since QFT samples were never found to have $a_{ph}412$: $a_{ph}440$ ratios exceeding 0.96. We used this indicator to identify depths within specific vertical profiles that may have had high a_d relative to a_p, when discrete sample a_d data were unavailable.

Package effects

We examined the effects of packaging on our data set by reconstructing unpackaged a_{ph} spectra from phytoplankton pigment concentrations (determined by HPLC) using methods in Bidigare et al. (1990). We calculated the unpackaged phytoplankton absorption coefficient ($a_{ph}'(\lambda)$) from:

$$a_{ph}'(\lambda) = \sum_{i=1}^{n} c_i \, a^*_i(\lambda),$$

where c_i is the concentration of pigment i (mg m^{-3}) and a^*_i (λ) is the specific absorption coefficient of pigment i (m^2 mg^{-1}) at wavelength (λ). The percent loss of pigment absorption due to the package effect (Qa*, Morel and Bricaud 1981) can be calculated as in Nelson et al. (1993):

$Qa^*(\lambda)$ = measured a_{ph} (includes packaging) /reconstructed a_{ph}' (unpackaged).

We used Qa* (676) to compare package effects. Absorption at 676 nm is due almost entirely to Tchl *a*, and thus is not confounded by possible errors resulting from misidentified or missing pigments (phycobiliproteins) in the blue green region of the spectrum (Nelson et al.1993).

Photosynthetically available radiation (PAR)

Irradiance measurements were obtained from a Tethered Spectral Radiometer Buoy (TSRB, Satlantic, Inc.; *see* Cullen et al, 1997), deployed 30 m from the R/V Henderson from mid-morning to late afternoon during 18-20 June and 22-24 June 1998. Downward irradiance (E_d) just above the surface was measured at 6 Hz at seven wavelengths (412, 443, 490, 555, 670, 684, 700 nm).

The E_d (λ) from TSRB data was integrated from 400 to 715 nm to estimate PAR above the water surface. Subsurface irradiance was obtained using:

$$E_d(z) = E_d(0)\, e^{-(Kd)\, z},$$

where E_d (z) is the downward irradiance at depth z in meters, E_d (0) is the downward irradiance just below the water surface, and K_d is the average vertical attenuation coefficient from 0 to z m. We assumed 5% loss of light at the air-water interface during calm conditions. $K_d(\lambda)$ was approximated by $K_E(\lambda)$, the vertical attenuation coefficient for net downward irradiance, where $K_E(\lambda) = a_t(\lambda)$ / μ-bar(λ), and μ-bar(λ) is the average cosine for the light field. We used $a_t(\lambda)$ values estimated from ac-9 data and average mixed layer μ-bar(λ) values from sub-surface measurements made with a Satlantic SeaWiFS profiling multi-channel spectral radiometer and an ac-9 from a nearby vessel in East Sound (A. Barnard, pers. comm.). Subsurface PAR values were derived from the integral (400-715 nm) of estimated E_d (z). To estimate prior light exposure, subsurface PAR values were averaged over the depth of mixing. Mixing was assumed to occur over a depth range that had a sigma-theta (density anomaly) differential < 0.01 kg m^{-3}.

Results

Slopes of absorption spectra in relation to pigments

Clear linear relationships were found between PPC: PSC ratios and normalized a_{ph} and a_p slopes from ac-9 measurements ($r^2 = 0.93$, $p < 0.001$; Figure 2.3a, c) and from QFT analysis of discrete samples ($r^2 = 0.81$ to 0.82, $p < 0.001$; Figure 2.3b, d). The relationship between PPC: PSC ratios and ac-9 a_p slopes was robust throughout the entire range of values. There were only four data points in the higher (>0.5 g: g) PPC: PSC range; however, removal of these points did not significantly alter the linear

Figure 2.3. Relationship of PPC: PSC ratios from HPLC analysis to normalized absorption slopes, slope = (a488-a532)/(a676 · (488-532nm)), from measurements of a) in situ ac-9 phytoplankton absorption coefficients (a_{ph}), b) discrete sample QFT a_{ph}, c) in situ ac-9 particulate absorption coefficients (a_p), and d) discrete sample QFT a_p. Open symbols are near surface samples (< 5 m) and closed squares are deep samples (> 5 m). Circles indicate surface mixed layer extends deeper than 5 m; diamonds indicate surface mixed layer < 5 m; triangles indicate a continuously stratified surface layer. The plus sign (+) indicates a single outlier that appeared to contain high levels of detritus (see text). Model 2 linear regressions shown for n = 36 samples in panel a, n = 35 samples (excludes the outlier) in panel c and n = 21 samples in panels b, d.

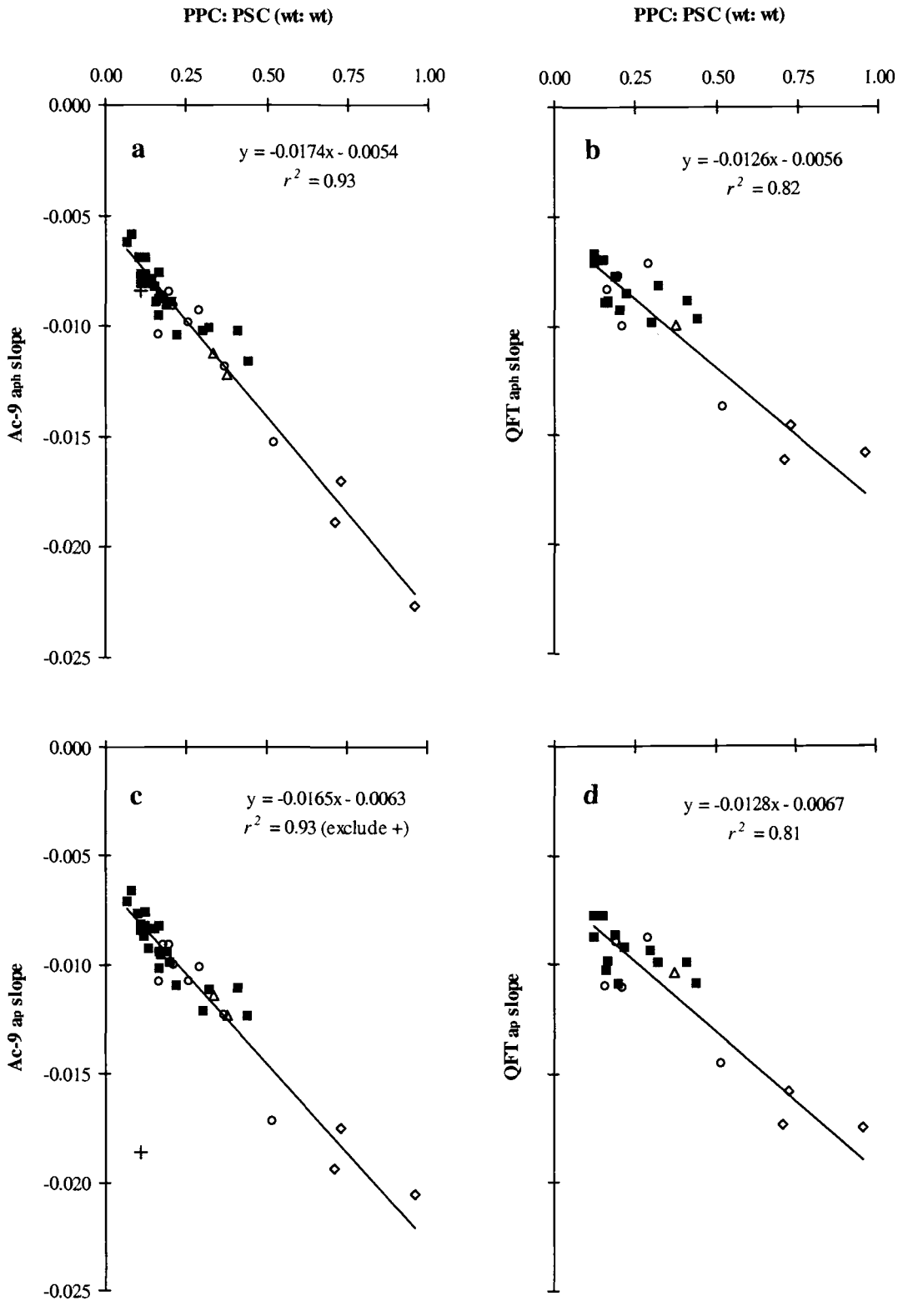
PPC: PSC (wt: wt)
0.00
0.25
0.50
0.75
1.00
0.000
-0.005
-0.010
-0.015
-0.020
-0.025
a
y = -0.0174x - 0.0054
r² = 0.93
Ac-9 aph slope
b
y = -0.0126x - 0.0056
r² = 0.82
QFT aph slope
c
y = -0.0165x - 0.0063
r² = 0.93 (exclude +)
Ac-9 ap slope
d
y = -0.0128x - 0.0067
r² = 0.81
QFT ap slope

Figure 2.3.

regression ($p < 0.05$), but reduced the r^2 to 0.80. The PPC: PSC ratios for the entire HPLC data set (two replicates per sample) had coefficients of variation (CV) of 0.1 to 15.1% with a mean CV of 4.5% for all samples. For the co-located water parcels, ac-9 a_p slopes had CVs ranging from 20 to 76% with a mean CV of 40%. The derived ac-9 a_{ph} slopes had CVs ranging from 28 to 128% with a mean of 47%.

The regression line slopes and intercepts for a_{ph} and a_p slopes and PPC: PSC ratios were not significantly different from each other ($p < 0.05$) for either ac-9 derived data (Figure 2.3a, c) or QFT data (Figure 2.3b, d). These results suggest that detrital absorption had an insignificant effect on a_p slopes for our data set, with the

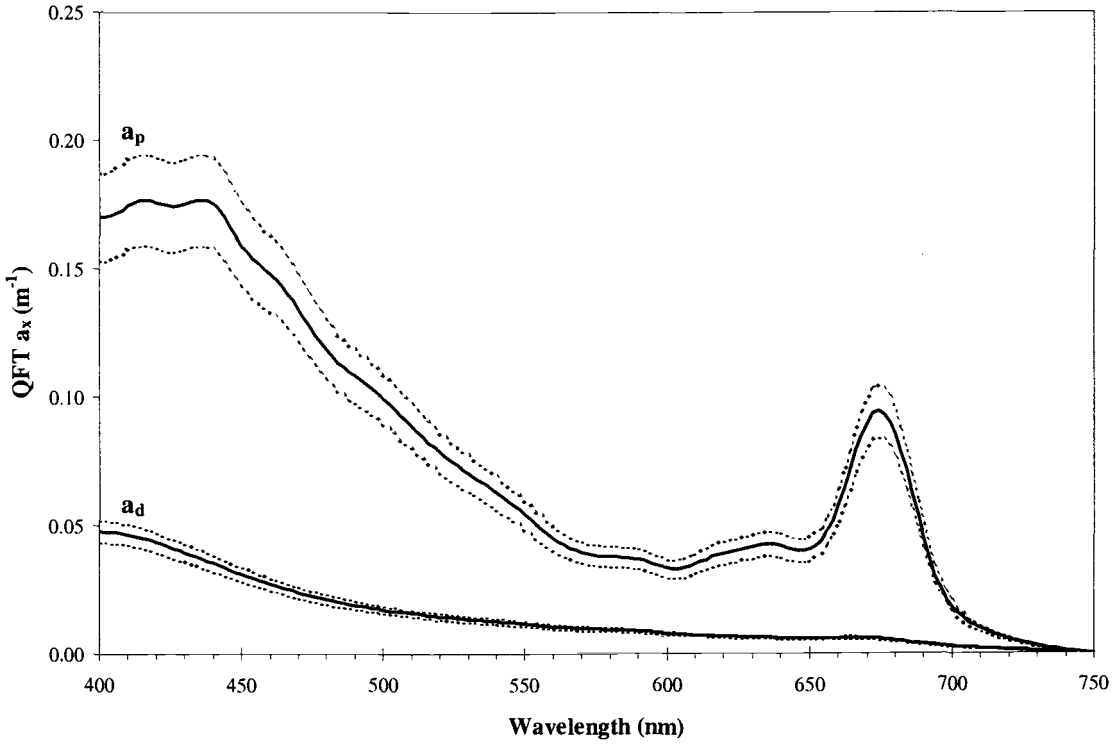

Figure 2.4. Mean a_p and a_d spectra (solid lines) for QFT samples collected concurrently with HPLC samples, $n = 21$. Standard errors indicated by dashed lines.

exclusion of a single outlier (+ symbol in Figure 2.3 c). This conclusion was supported by the low a_d relative to a_p seen in QFT samples (Figure 2.4).

For the outlier, we calculated a_d and subsequently the a_{ph} slope using a variation of the method 3 a_d correction (see Methods), assuming s = 0.011 nm^{-1}, since s = 0.0065 nm^{-1} (as applied to the other samples) did not yield a sufficient a_d correction. This higher s (steeper exponential slope) allowed the outlier sample point to fall close to the regression line for the PPC: PSC ratio and a_{ph} slope relationship (Figure 2.3 a). This single deep sample (18.1 m) from 23 June 1998 appeared to contain high a_d based on high ratios of a_p412: a_p440 (1.12 for this outlier compared to a range of 0.87 to 1.03 for the other data points shown in regressions). This correction implies that the a_d shape and magnitude were different (steeper exponential slope and higher magnitude) for this outlier compared to the remaining samples (all but one collected at shallower depths).

Slopes compared to a_{ph} ratios, Tchl a, and other pigment ratios

We compared the ac-9 a_{ph} slope calculations and the more straightforward ratios of $a_{ph}488$: $a_{ph}676$ and $a_{ph}488$: $a_{ph}532$ and found that the PPC: PSC ratios had a stronger correlation with a_{ph} slopes (r^2 = 0.93) than with these a_{ph} ratios (r^2 = 0.84 and 0.70, respectively).

A comparison of Tchl *a* to a_p slopes showed that Tchl *a* had a much weaker relationship to a_p slopes than was found for PPC: PSC ratios (r^2 = 0.45 compared to 0.93). Removing the four lowest Tchl *a* values (and also steepest a_p slopes) from the analysis yielded an even weaker relationship (r^2 = 0.20). In contrast, strong linear

relationships were found between ac-9 a_p slopes and ratios (g: g) of PPC: total pigments (chlorophylls, PSC and PPC) and PPC: total carotenoids (r^2 = 0.90 and 0.93 respectively, $p < 0.001$). Weak linear relationships were seen between absorption slopes and ratios (g: g) of chl *c*: PSC, chl *c*: PPC or chl *c*: Tchl *a* (r^2 = 0.12, 0.36 and 0.36, respectively).

Effects of a_d magnitude and shape on slopes

The ac-9 a_p data and subsequent a_p slope calculations are influenced by phytoplankton and detrital absorption. In other coastal and oceanic environments containing high and/or variable detritus concentrations, it is critical to understand how the a_p spectra are affected by variations in a_d magnitude and shape. These variations will in turn influence the relationship between a_p slopes and PPC: PSC ratios. To this end, we examined how variations in magnitude and shape (exponential slope, s) of a_d spectra might affect the relationship of ac-9 derived a_p slopes to PPC: PSC ratios. Specific sample a_d values (QFT data) were used for all analyses. We varied the a_d magnitude by multiplying a_d by 1, 2, 4, 6, 10, 20 times (yielding a_d412: a_p412 ratios of 0.21, 0.32, 0.50, 0.58, 0.70, 0.82, respectively) and added these a_d values to prior estimates of ac-9 a_{ph} values. We observed strong linear relationships between these new a_p slopes and PPC: PSC ratios up to 10 a_d (r^2 = 0.88 and 0.71 for 4 and 10 a_d, respectively) (Figure 2.5a). The linear relationship between a_p slopes and PPC: PSC ratios weakened at 20 a_d (r^2 = 0.44, data not shown). The intercepts were significantly different ($p < 0.05$) than seen for the original ac-9 a_p regression for detrital additions

Figure 2.5. Relationship of PPC: PSC ratios from HPLC analysis to a_p slopes derived by adding estimates of a_d to ac-9 a_{ph} values using a) a_d magnitudes of 4 and 10 times measured a_d, b) a_d spectral slopes, s, of 0.004, 0.008, 0.012, and c) varying magnitudes and spectral shapes (s = 0.004 and 0.012 with 1 and 4 times measured a_d). Linear regression lines (solid lines) for varying a_d estimates are shown. Dashed lines show the linear regression of ac-9 a_p slopes as in Figure 2.3a. The a_p slope was calculated as in Figure 2.3.

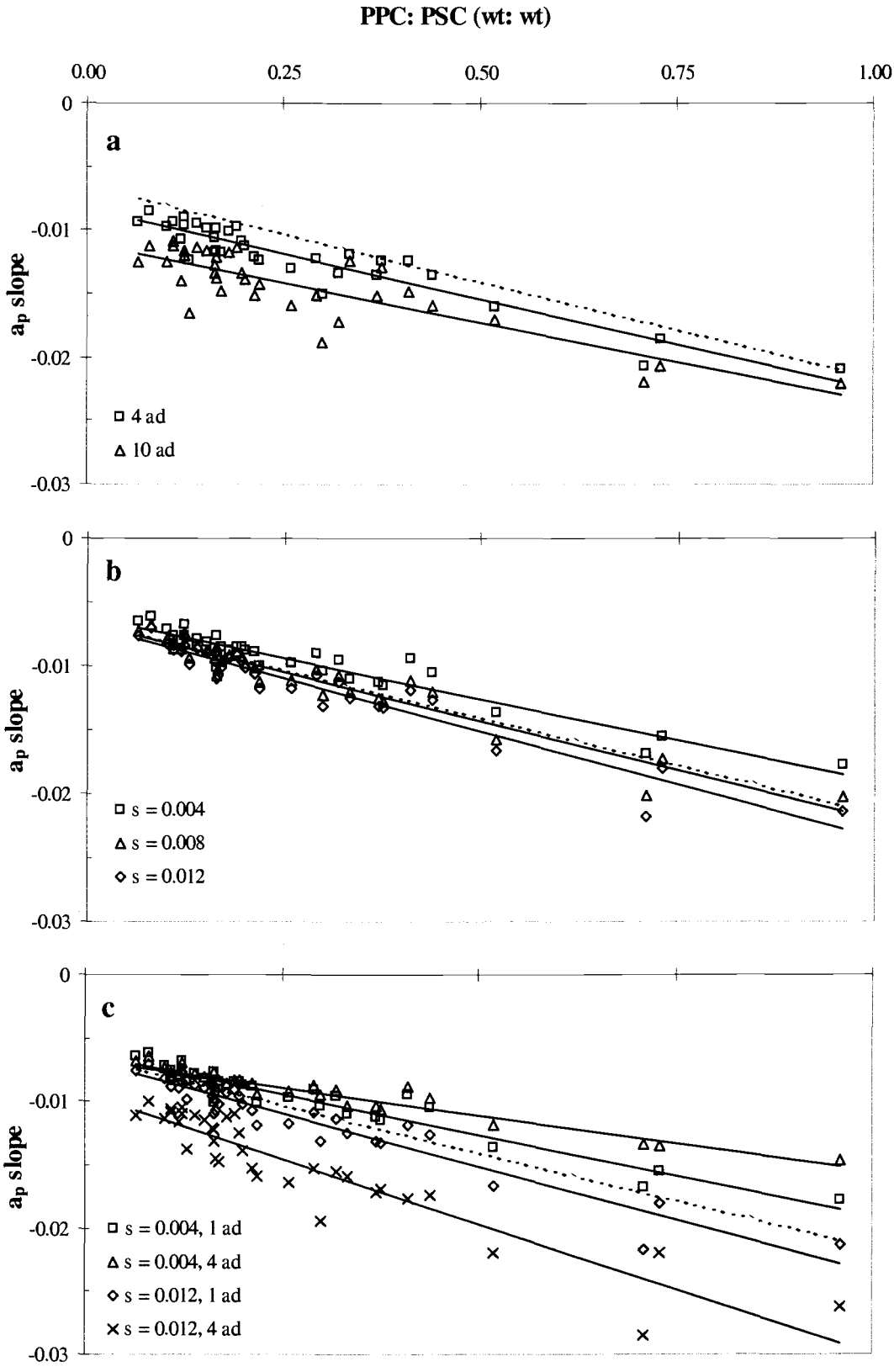
PPC: PSC (wt: wt)
0.00
0.25
0.50
0.75
1.00
a
b
c
a_p slope
0
-0.01
-0.02
-0.03
4 ad
10 ad
s = 0.004
s = 0.008
s = 0.012
s = 0.004, 1 ad
s = 0.004, 4 ad
s = 0.012, 1 ad
s = 0.012, 4 ad

Figure 2.5.

greater than 4 a_d, while the slopes of the regression lines were not significantly different for any multiple of a_d.

We next varied the shape of the a_d spectra using a_d440 from each sample and s = 0.004, 0.006, 0.008, 0.010, 0.012 nm^{-1}, to obtain new a_p spectra (Roesler et al. 1989). A strong linear relationship was seen between the resulting a_p slopes and PPC: PSC ratios for all values of s (Figure 2.5b). In this test, the slopes of the linear regression were significantly different ($p < 0.05$) from that seen for the original ac-9 a_p regression, for $s \leq 0.005$ nm^{-1} and $s > 0.0125$ nm^{-1}. The intercepts were not significantly different.

Finally, we varied both the magnitude and shape (s values) of the a_d spectra. Magnitudes of 1 and 4 a_d and s values of 0.004, 0.012 nm^{-1} were used to calculate new a_d spectra for a_p slope estimates (Figure 2.5c). Linear relationships between a_p slope and PPC: PSC ratios were found for all combinations of a_d magnitude and spectral shape, s. At the higher values of s, we observed greater differences in regression line intercepts between low and high a_d magnitudes.

The above analyses did not examine the effects of large variations in a_d between samples within one data set. We lacked the data to conduct such an analysis, but consideration of all points in Figure 2.5c (as if the various a_d corrections were from a single data set), yields a linear association ($p < 0.001$, $r^2 = 0.55$) with significant differences in a_p slopes seen for PPC: PSC differences of 0.1 or greater (e.g. PPC: PSC ratios of 0.2 compared to 0.3, $p < 0.04$, two-sided t-test).

Effects of packaging on a_{ph} slopes

Package effects result from a combination of intracellular pigment (composition and concentration) and cell size variations. These variations can reduce the optical cross section of the cell and alter the a_p and a_{ph} spectra and slopes. Therefore, we attempted to quantify the effects of pigment packaging on a_{ph} slope variability.

Cell size (ranging from 0.6 to > 50 μm diameter) can have an important influence on phytoplankton package effects between and within taxonomic groups (Morel and Bricaud 1981, Bricaud et al.1983). The influence of cell size on packaging for diatoms was recently examined by Zinkel (2001), who found that, under low light conditions (25 μmol photons m^{-2} s^{-1}), larger diatom species had increased packaging effects. To evaluate the potential impact of these cell size package effects on our a_{ph} slope method, we estimated a_{ph} slopes from the specific absorption coefficient data (a^*, m^2 mg chl a^{-1}, Zinkel 2001, see her Figure 2a) for small (n = 3) and large (n = 4) diatom species, assuming similar pigment composition for all species (Zinkel 2001). The resulting mean a_{ph} slopes were not significantly different for small compared to large diatoms ($p > 0.75$, mean slopes were –0.0073 and –0.0069 for small and large species, respectively). In this case, large size variations in diatoms (and presumed differences in packaging) did not significantly alter a_{ph} slope estimates.

Packaging effects for our data set were estimated using Qa*(676) derived from our QFT data. These Qa*(676) values ranged from 0.87 to 0.35 with a mean of 0.57. Qa*(676) values were significantly higher for surface depths (≤ 5 m) than for depths ≥ 10 m (mean Qa*(676) values of 0.59 compared to 0.44; *t*-test, $p < 0.05$), suggesting

that cells located near the surface had less packaging than cells located at depth. The trends in Qa*(676) are similar for ac-9 derived Qa*(676) data. For comparison, Qa*(675) ranged from ~0.98 to 0.6 for a variety of diatom cultures reported in literature (Nelson et al, 1993). Bricaud et al. (1995) found Qa*(675) values of ~0.9 to < 0.3 for samples with Tchl *a* ranging from 1.5 to 20 μg/L (overlapping the Tchl *a* range in our study), with Qa*(675) showing a general decrease with increasing Tchl *a*. We observed a weak trend of decreasing Qa*(676), with increasing Tchl *a* (although the scatter was large and the slope of the linear regression was not significantly different from zero). We found no significant relationships ($p > 0.05$) between Qa*(676) and a_{ph} slopes or PPC: PSC ratios.

Lastly, we evaluated the variations in packaging on ac-9 a_{ph} slopes by comparing measured a_{ph} slopes to the a_{ph} slopes derived from a_{ph}' (unpackaged) data using varying percentages of packaging. The a_{ph} slopes with 0%, 50% and 75% of their original packaging were on average 1.88 1.48, and 1.25 times steeper than measured a_{ph} slopes ($p < 0.05$, *t*-tests, Figure 2.6). A comparison of these ac-9 a_{ph} slopes to PPC: PSC ratios indicates that decreasing the package effect increases the magnitude of the regression line intercept, but does not change the regression line slope appreciably. Similar results were obtained for reconstructed a_{ph} slopes derived ratios for all packaging levels ($r^2 = 0.91$ to 0.93). As with the a_d evaluations, these analyses did not address the effects of large variations in packaging between samples within one data set (as may occur in many oceanographic regions). If all packaging variations are considered at once (as if the various package effects shown in Figure 2.6

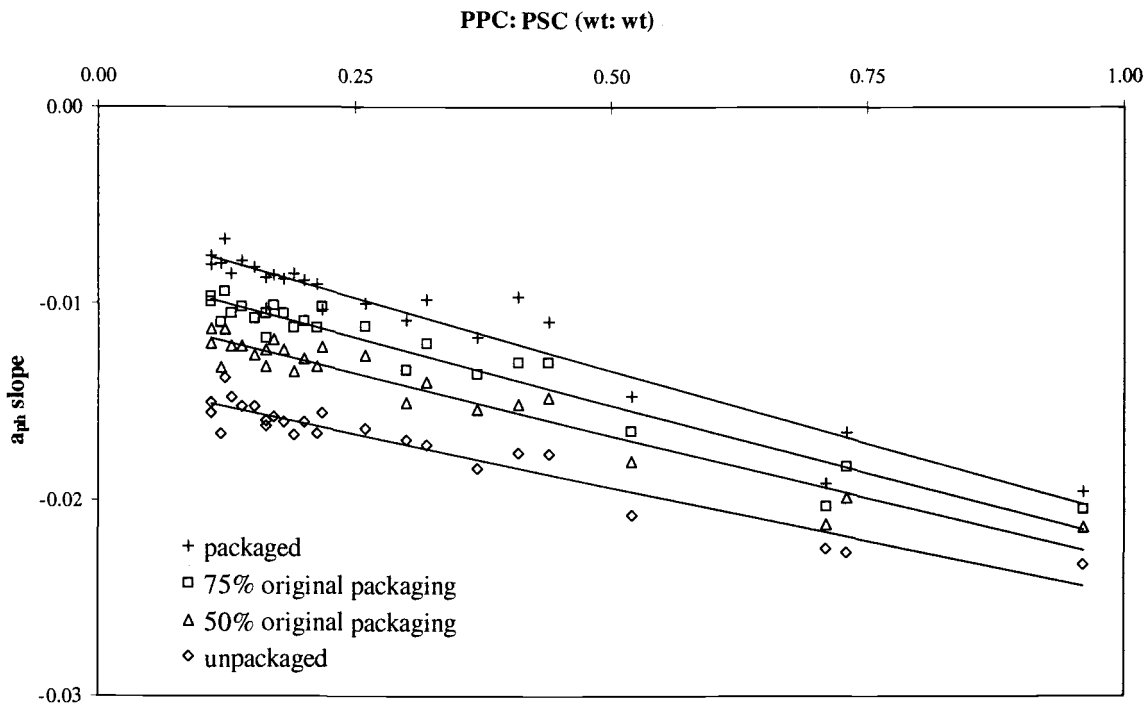

Figure 2.6. Relationship of PPC: PSC ratios from HPLC analysis to a_{ph} slopes derived from HPLC data (as described in text) with varying amounts (0%, 50%, 75% 100%) of packaging. Linear regression lines are shown (r^2 = 0.91 to 0.93). Data collected between 18 to 24 June, 1998. The a_{ph} slope was calculated as in Figure 2.3. from QFT data. We found linear relationships between a_{ph} slopes and PPC: PSC

were from a single data set), a linear association between ac-9 a_{ph} slopes and PPC: PSC ratios is still found ($p < 0.001$; $r^2 = 0.54$).

Stratification, light and nutrients

The thermistor-chain record (Figure 2.2) indicates that surface temperatures and mixed layer depths varied considerably over the 10-day survey period. Surface temperatures increased and surface mixed layers shoaled from 14 to 21 June 1998, with decreases in surface temperatures and deepening of surface mixed layers from 21 to 24 June 1998. Mean above surface PAR between 1000 and 1600 h was moderate

on 18 June 1998 (800 μmol quanta m^{-2} s^{-1}), high on 19, 20 and 22 June 1998 (1250, 1450 and 1550 μmol quanta m^{-2} s^{-1}, respectively) and low on 23 and 24 June 1998 (600 μmol quanta m^{-2} s^{-1}). Total N (nitrate-N + ammonium-N + nitrite-N) in surface waters (< 5m) had minimum concentrations of 0.7, 2.1, 4.8, 1.6 μM and N: P ratios of 1.5, 3.0, 6.5, 4.0 on 20, 22, 23, 24 June 1998, respectively. Nitrogen was likely the limiting nutrient during this period, assuming Redfield ratios of 16: 1 for N: P.

Vertical and temporal variations of a_p slopes and pigment ratios

Steeper a_p and a_{ph} slopes and higher PPC: PSC ratios were observed more often near the surface than at depth (Figure 2.3). Vertical ac-9 profiles of a_p slopes and a_{ph} slopes were used to document finescale variations in PPC: PSC ratios (Figure 2.7). Deeper in the water column (below the main pycnocline), the greater magnitude a_p slopes were likely due to higher a_d in these waters (based on a_p412: a_p440 ratios). To estimate a_{ph} slopes, we derived a_d using method 3 (see Methods), with a slight variation for deep samples. We assumed that s = 0.0065 nm^{-1} in waters above the pycnocline with low a_d, and s = 0.011 nm^{-1} (as used for the single outlier) in deeper waters with high a_d (see Figure 2.7 caption). These estimated a_{ph} slopes appear to be fairly low and constant below the pycnocline (with the possible exception of the 24 June profile), suggesting that PPC: PSC ratios were low and did not change appreciably in these deep waters. Note that these a_{ph} slope estimates are dependent on the assumptions made for a_d estimates (e.g. s = 0.011 nm^{-1} is an appropriate value for deep waters with high a_d).

Figure 2.7. Vertical profiles of density in sigma-theta (bold line), chlorophyll a calculated from in situ fluorescence (thin line), ac-9 a_p slopes (open diamonds) and a_{ph} slopes (closed diamonds) collected within a half hour of solar noon on a) 20 June, b) 22 June, c) 23 June and d) 24 June 1998. The a_{ph} slopes were derived from ac-9 a_p data using the method 3 a_d correction (see Methods text) assuming $a_{ph}440$: $a_{ph}676$ = 1.61 and an exponential slope, s, based on ac-9 a_p412: a_p440 ratios. For samples with a_p412: a_p440 ratios > 0.96 (typically located below 10-15 m), we used s = 0.011 nm^{-1}. For all other samples we assumed s = 0.0065 nm^{-1}. The a_p and a_{ph} slopes were calculated as in Figure 2.3 and multiplied by negative 1000 for scaling purposes. Error bars on a_p and a_{ph} slopes indicate ± 1 standard error. The a_p slopes that were significantly different (95% confidence level) from the1-meter interval directly above, are indicated by an X. Significant differences were calculated only for depths with a_p412: a_p440 ratio < 0.96 (i.e. samples that did not appear to contain high levels of detritus). The mean PAR value for the hour prior to sample collection is displayed on each panel. Note the large changes in a_p and a_{ph} slopes in panels a and b compared to c and d.

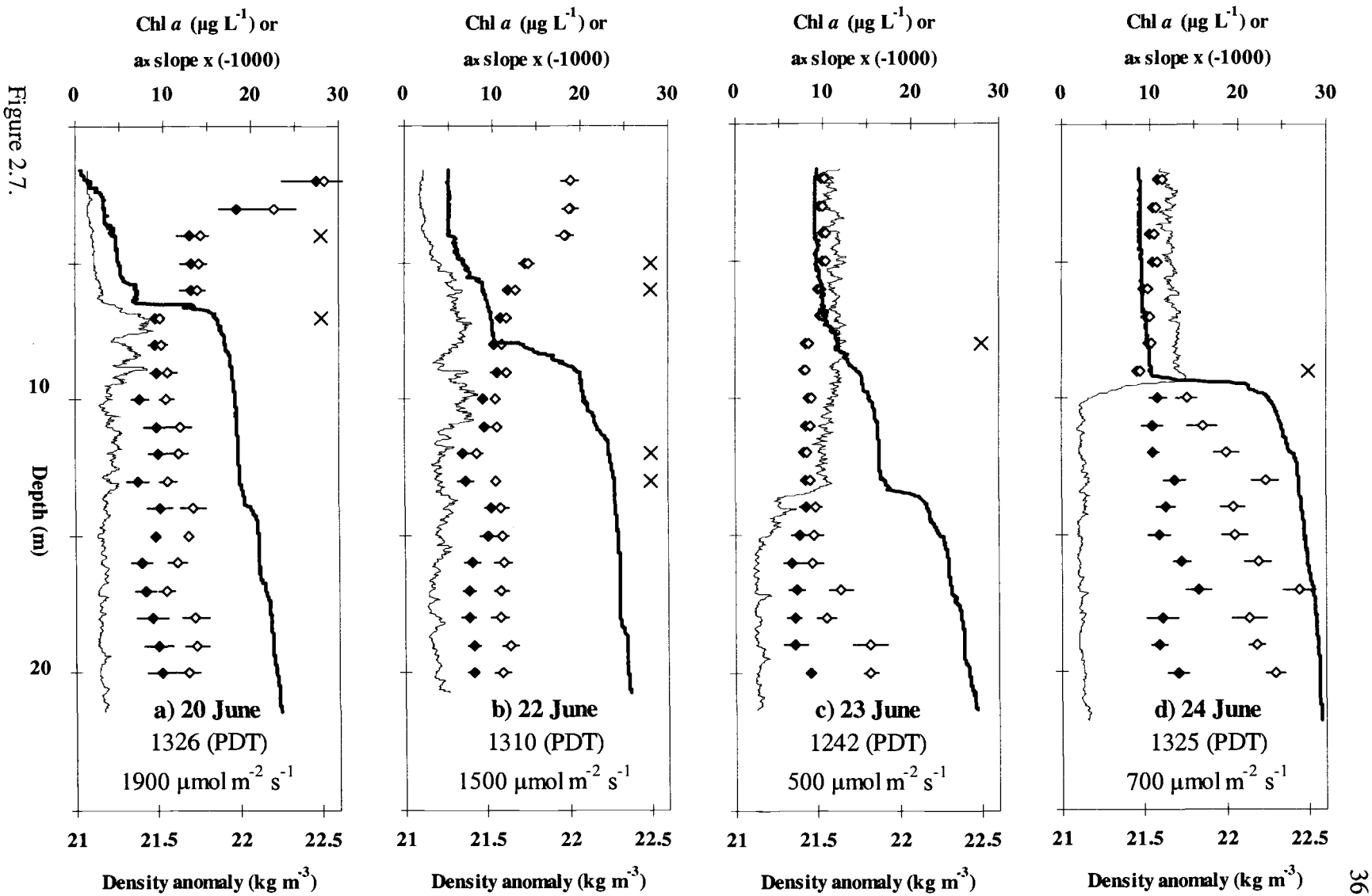
Chl a (µg L-1) or
ax slope x (-1000)
0
10
20
30
Depth (m)
10
20
a) 20 June
1326 (PDT)
1900 µmol m-2 s-1
b) 22 June
1310 (PDT)
1500 µmol m-2 s-1
c) 23 June
1242 (PDT)
500 µmol m-2 s-1
d) 24 June
1325 (PDT)
700 µmol m-2 s-1
21
21.5
22
22.5
Density anomaly (kg m-3)

Figure 2.7.

The data from all four days (20, 22, 23 and 24 June 1998) show that a_p and a_{ph} slopes changed significantly at depths with large density gradients. For example, on 20 June 1998 (Figure 2.7a), the a_p slopes were significantly steeper at 3 m than 4 m and at 6 m than 7 m (*t*-tests, $p < 0.002$). Both of these transitions occurred over large density steps. A prediction of PPC: PSC ratios from these ac-9 a_p slopes (y = -55.43x - 0.292, $r^2 = 0.94$, model 1 linear regression) suggests that the PPC: PSC ratios were twice as high at 3 m than 4 m (difference of 0.46 g: g) and at 6 m than 7 m (difference of 0.24 g: g). Taxonomic data collected on 20 June 1998 revealed greater variation in species composition across the pycnocline than seen within waters above or below the pycnocline (D. Gifford, pers. comm.).

Temporal variations in a_p slopes and pigment ratios can also be seen in the profiles shown in Figure 2.7. Surface a_p and a_{ph} slopes were steeper on 20 and 22 June relative to 23 and 24 June 1998. The higher irradiance levels and shallower surface mixed layer depths on 20 and 22 June (Figure 2.2, 2.7) likely contributed to these slope differences between the dates. The 2-m phytoplankton populations, for example, were exposed to average irradiances four times higher on 20 and 22 June than on 23 and 24 June 1998 (~950 compared to ~250 μmol quanta m^{-2} s^{-1}).

Pigment ratios and a_p slopes in relation to light

We compared prior light exposures for samples collected between 1100 h and 1600 h to pigment ratios and a_p slopes. Positive associations were seen between mean PAR for the hour prior to sample collection and (diatoxanthin + diadinoxanthin): PSC ratios, (diatoxanthin + diadinoxanthin): (Tchl *a*) ratios, PPC: PSC ratios and a_p slopes

(linear regression r^2 = 0.92, 0.98. 0.96, and 0.94, respectively; Figure 2.8). Similar but slightly weaker relationships to pigment ratios and a_p slopes were seen for PAR averaged over 30 minutes or 2 hours prior to sample collection (data not shown). Since the TSRB was not deployed until ~ 4 hours after dawn, we did not have enough data to adequately assess cumulative irradiance effects from the start of the light period.

Dominant phytoplankton species

The chemotaxonomic pigments with the highest concentrations were fucoxanthin, peridinin, and alloxanthin; these pigments were used to assess the relative abundances of diatoms, dinoflagellates, and cryptophytes (Jeffrey and Vesk 1997), respectively. The fucoxanthin: Tchl *a*, peridinin: Tchl *a,* and alloxanthin: Tchl *a* ratios indicate that taxonomic composition varied temporally and as a function of depth (Table 2.1). Fucoxanthin: Tchl *a* ratios were typically an order of magnitude higher than other biomarkers indicating that diatoms were the most abundant species (Table 2.1). *Chaetoceros socialis*, a colonial diatom, frequently was the most numerous diatom sampled, although its relative proportion of the assemblage varied over depth, time and location within East Sound (D. Gifford, J. Rines, pers. comm.).

Discussion

The key findings of this study were the strong relationships found between the ac-9 a_{ph} and a_p slopes and the HPLC-derived PPC: PSC ratios (Figure 2.3). These

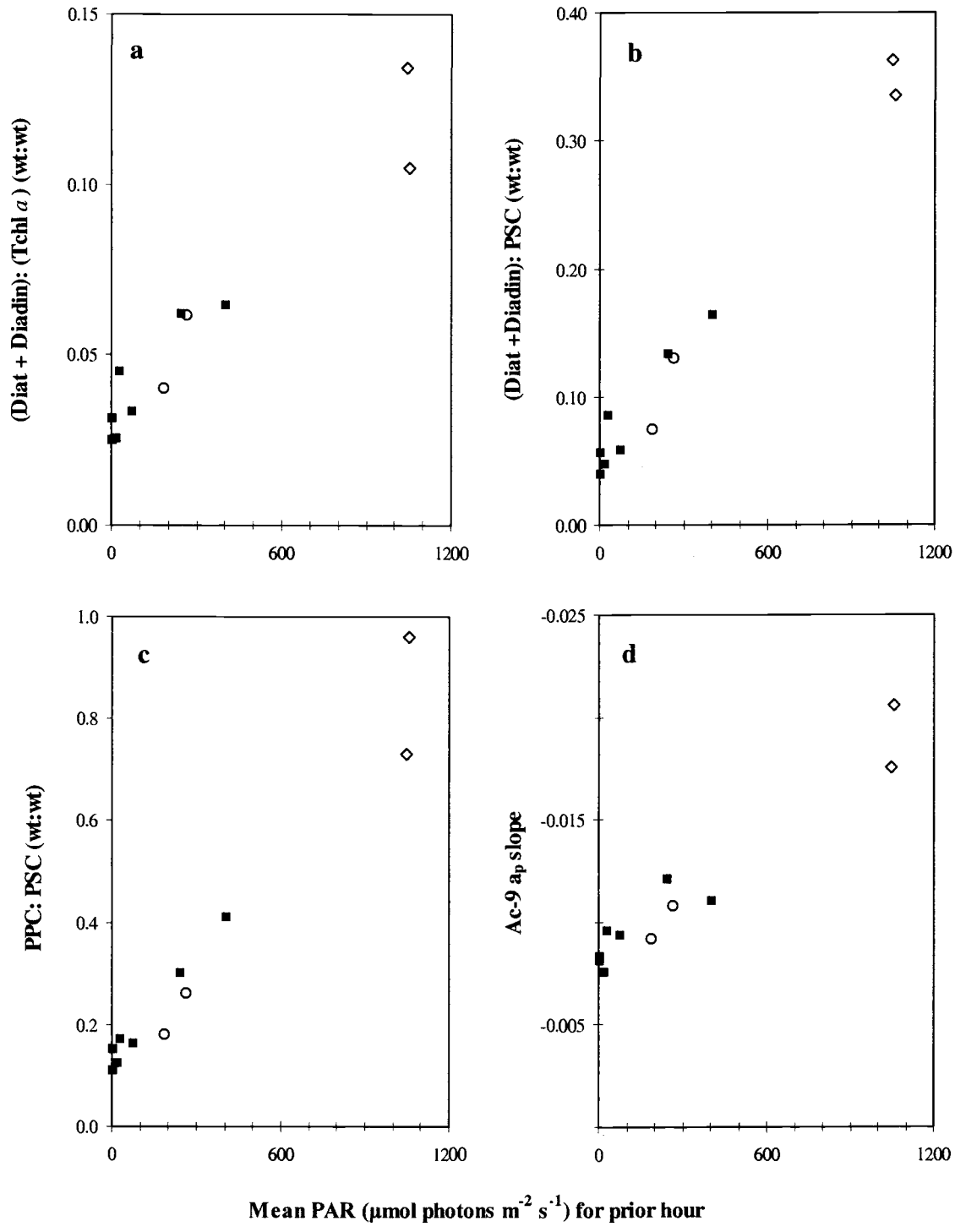

Figure 2.8. Relationship of mean in-water PAR for the hour prior to sample collection to a) (diatoxanthin + diadinoxanthin): (Tchl *a*), b) (diatoxanthin + diadinoxanthin): PSC, c) PPC: PSC, and d) ac-9 a_p slopes. Samples collected between 1100 and 1600 (PDT) on 18-20 June and 22-24 June 1998. PAR calculated as described in text. Symbols and a_p slope calculation as in Figure 2.3.

Table 2.1. HPLC-determined pigment concentrations (μg L^{-1}) and ratios (wt: wt). Pigment types are abbreviated as follows: chlorophyll *a* + chlorophyllide *a* (Tchl *a*), chlorophyll c1/c2 (chl c), fucoxanthin (Fuco), peridinin (Peri), alloxanthin (Allo), diatoxanthin + diadinoxanthin (DtDd), β-carotene (Bcar), photoprotective carotenoids (PPC), photosynthetic carotenoids (PSC). Total pigment concentrations (total) were calculated as Tchl *a* + chl c + PPC + PSC. Dates and times are Pacific Daylight Time. Samples > 5 m shown in bold. NA indicates no data available. Each data point represents the mean of two replicate samples unless indicated as no replicate (nr).

							PSC: Tchl *a*		PPC: Tchl *a*		
Date	Time	Depth (m)	Tchl *a*	Chl c	PP:PS	PP:total	Fuco:Tchl *a*	Peri:Tchl *a*	Allo:Tchl *a*	DtDd:Tchl *a*	Bcar:Tchl *a*
14 Jun	910	3.6	6.36	1.45	0.29	0.083	0.485	0.039	0.039	0.081	0.047
	1520	3.7	6.01	1.81	0.20	0.065	0.655	0.014	0.029	0.060	0.048
15 Jun	**1355**	**16.0**	**5.45**	**1.40**	**0.12**	**0.045**	**0.719**	**0.018**	**0.007**	**0.038**	**0.034**
	nr1551	**13.8**	**10.42**	**1.87**	**0.08**	**0.028**	**0.653**	**0.000**	**0.003**	**0.025**	**0.024**
	nr1551	**14.7**	**6.77**	**1.29**	**0.07**	**0.027**	**0.690**	**0.009**	**0.000**	**0.030**	**0.028**
	nr1551	**16.7**	**8.75**	**1.86**	**0.10**	**0.036**	**0.707**	**0.000**	**0.005**	**0.030**	**0.028**
16 Jun	1030	3.0	7.01	1.17	0.33	0.082	0.402	0.006	0.034	0.059	0.042
	1030	**7.0**	**12.73**	**2.75**	**0.16**	**0.055**	**0.598**	**0.027**	**0.013**	**0.046**	**0.034**
	1255	2.6	8.17	1.44	0.38	0.095	0.404	0.006	0.064	0.053	0.055
	1310	**5.6**	**8.92**	**2.29**	**0.17**	**0.057**	**0.658**	**0.020**	**0.020**	**0.052**	**0.035**
18 Jun	1030	5.0	6.47	1.14	0.37	0.094	0.386	0.038	0.048	0.052	0.055
	nr1030	**11.5**	**10.06**	**2.21**	**0.11**	**0.035**	**0.572**	**0.000**	**0.013**	**0.026**	**0.031**
	1030	**13.0**	**14.84**	**3.06**	**0.14**	**0.043**	**0.559**	**0.001**	**0.009**	**0.028**	**0.032**
	1030	**15.5**	**12.50**	**2.79**	**0.13**	**0.039**	**0.554**	**0.000**	**0.007**	**0.027**	**0.029**
	1030	**18.0**	**7.95**	**1.60**	**0.12**	**0.040**	**0.619**	**0.013**	**0.007**	**0.029**	**0.029**
	1020	**6.5**	**7.26**	**1.47**	**0.22**	**0.060**	**0.459**	**0.011**	**0.028**	**0.032**	**0.034**
	1053	**11.5**	**18.59**	**3.72**	**0.15**	**0.046**	**0.544**	**0.002**	**0.013**	**0.031**	**0.028**
	1600	**10.0**	**19.16**	**3.71**	**0.12**	**0.037**	**0.514**	**0.003**	**0.004**	**0.025**	**0.022**
19 Jun	1100	2.0	3.34	0.55	0.52	0.122	0.315	0.054	0.060	0.064	0.070
	1100	**10.5**	**10.96**	**2.16**	**0.19**	**0.058**	**0.529**	**0.013**	**0.024**	**0.034**	**0.036**
	1600	**10.5**	**9.92**	**2.19**	**0.16**	**0.050**	**0.553**	**0.007**	**0.014**	**0.033**	**0.029**
20 Jun	805	2.6	2.40	0.33	0.71	0.150	0.285	0.034	0.065	0.075	0.077
	820	**7.5**	**6.16**	**1.13**	**0.44**	**0.100**	**0.323**	**0.044**	**0.070**	**0.042**	**0.066**
	nr1333	2.5	1.62	0.23	0.96	0.170	0.262	0.037	0.096	0.105	0.060
	nr1322	**6.5**	**9.32**	**2.32**	**0.41**	**0.091**	**0.349**	**0.040**	**0.045**	**0.064**	**0.040**
22 Jun	**911**	**6.0**	**6.33**	**1.19**	**0.32**	**0.082**	**0.434**	**0.015**	**0.041**	**0.055**	**0.048**
	904	**7.6**	**6.03**	**1.30**	**0.20**	**0.058**	**0.499**	**0.000**	**0.028**	**0.031**	**0.045**
	1328	2.5	3.04	0.48	0.73	0.150	0.322	0.012	0.057	0.134	0.057
	1318	**5.4**	**6.21**	**1.31**	**0.30**	**0.076**	**0.434**	**0.020**	**0.028**	**0.062**	**0.039**
23 Jun	830	4.0	10.58	2.10	0.16	0.050	0.557	0.015	0.015	0.036	0.035
	1541	3.2	11.36	2.66	0.18	0.051	0.525	0.010	0.017	0.040	0.029
	1541	**12.3**	**12.03**	**2.84**	**0.11**	**0.034**	**0.617**	**0.000**	**0.006**	**0.025**	**0.025**
	1541	**18.1**	**2.05**	**0.41**	**0.11**	**0.039**	**0.711**	**0.000**	**0.004**	**0.036**	**0.029**
24 Jun	830	3.5	14.84	3.08	0.21	0.061	0.506	0.019	0.016	0.055	0.033
	nr1445	2.1	8.33	1.92	0.26	0.067	0.427	0.027	0.018	0.062	0.036
	nr1445	**6.3**	**10.31**	**2.82**	**0.17**	**0.048**	**0.527**	**0.000**	**0.009**	**0.045**	**0.031**

relationships suggest that absorption measurements from in situ instrumentation may be used to estimate PPC: PSC ratios in field phytoplankton assemblages. The relationship between ac-9 a_p slopes and pigment ratios was robust in East Sound except in deeper waters where a_d was likely high. The general applicability of this approach in other coastal and oceanic waters is dependent upon consideration of the contributions of detrital absorption (a_d), pigment packaging, species composition, and irradiance to the shape of the absorption spectrum at specific depths. For both the a_d and packaging sensitivity analyses, we were restricted by the narrow range of values in our particular data set. Analysis with a wider ranging data set that possesses larger variations in a_d and packaging would allow us to more fully evaluate the impact of these variations. In addition, a more extensive data set would permit us to address the combined effects of variations in a_d and packaging on the relationship of a_{ph} and a_p slopes to PPC: PSC ratios.

Our analysis of variable contributions of a_d to our estimated a_p slopes suggests that over a large range of a_d magnitudes (a_d412: a_p412 up to 0.5) and spectral shapes (s from 0.004 to 0.012 calculated over 440 to 676 nm range, Figure 2.5c) it is possible to infer PPC: PSC ratios from a_p slopes derived from in situ absorption measurements. Ideally, a_d values should be determined using the QFT for a representative number of samples. Measured, mean or modeled (Roesler et al, 1989; Cleveland and Perry, 1994) values of a_d can then be subtracted from the ac-9 a_p spectra to estimate a_{ph} values and slopes for samples collected within similar water masses. We suggest that in situ absorption measurements always be made with coincident measurements of water mass properties and the local light field to permit assignment of groups of a_p

slopes to particular water mass types, thus reducing the impact of variable a_d magnitudes and spectral shapes on the interpretation of estimated PPC: PSC ratios.

Variation in pigment packaging may further complicate the interpretation of pigment ratios from absorption data (Hoepffner and Sathyendranath 1991). Within the data set we analyzed, we had a range of package effects (indicated by Qa*(676) of 0.35 to 0.9). In spite of this variation, we were able to derive a clear linear relationship between PPC: PSC ratios and a_p and a_{ph} slopes. Our sensitivity analysis using a_{ph} data from the current study indicated that variable package effects can degrade the relationship between a_{ph} slopes and PPC: PSC ratios, if packaging varies while PPC: PSC ratios are held constant. In the natural environment, package effects may co-vary inversely with PPC: PSC ratios. For our data set, we found significantly higher package effects in deep than in surface samples, while PPC: PSC ratios were higher in the surface than at depth (although, there was not a significant linear relationship between these two parameters). Since both decreases in packaging and increases in the PPC: PSC ratios can increase a_{ph} slopes (and vise versa), it will be necessary to evaluate the effects of both these factors on a_{ph} slopes to explain a_{ph} slope variability in other marine systems with a range of phytoplankton taxa. We suggest that estimates of HPLC derived pigment concentrations and cell size (perhaps based on pigment biomarkers (Vidussi et al, 2001) or size fractionation of pigments) accompany in situ measurements of absorption to evaluate the effects of packaging on a_{ph} slopes.

Short-term temporal changes in a_{ph} slope may reflect photoacclimation responses to variations in irradiance, and provide clues to the light history of the

phytoplankton community. If turnover (mixing) of the water column is slower than the time required for pigment synthesis, then indicators of photoacclimation such as (diatoxanthin + diadinoxanthin): chl *a* ratios can show a vertical gradient within the water column (Moline 1998). Culver and Perry (1999) found that natural phytoplankton from stratified depths in Puget Sound exhibited photoacclimation effects (photosynthetic pigment absorption coefficient: total phytoplankton absorption coefficient increased as irradiance decreased), while cells in mixed layers did not show a discernable photoacclimation trend. In our study, higher (diatoxanthin + diadinoxanthin): Tchl *a* ratios, PPC: PSC ratios, steeper a_p and a_{ph} slopes and higher prior (1 h) light exposures were seen in stratified surface waters than in deeper waters (Table 2.1, Figure 2.8), reflecting the reduced vertical mixing associated with shallow stratification. Additional studies at intermediate to high light levels are required to quantify the time scales of response between irradiance, pigment ratios and ac-9 a_p slopes, and the intersection of these time scales with the longer time scales of species compositional changes within a water mass.

Variations in nutrient concentrations also can promote changes in physiology (Geider, et al. 1993) and phytoplankton species succession that influence the relative pigment concentrations of the phytoplankton assemblage. However, the absence of an appreciable change in surface N levels, with the exception of 20 June 1998, suggests that for the most part, light influenced pigmentation more than nutrients during our study period.

Changes in PPC: PSC ratios can reflect physiological changes at the cellular level or indicate a shift in species composition with different light tolerances or

nutrient requirements. During monospecific (or low species diversity) phytoplankton blooms, changes in the shape of the a_{ph} spectrum indicate physiological acclimation rather than taxonomic diversity. The phytoplankton assemblages in this study had differing species compositions (although diatoms were always the most abundant), photoacclimation responses and/or light histories, all of which could influence a_{ph} slopes and pigment ratios. For example, the high PPC: PSC ratios, and steep a_p and a_{ph} slopes seen in surface waters on 20 June 1998 likely resulted from photoacclimation as indicated by high diatoxanthin + diadinoxanthin: Tchl *a* ratios, in addition to taxonomic variation (presence of non-diatom species) as suggested by the relatively lower fucoxanthin: Tchl *a* ratios and relatively higher alloxanthin: Tchl *a*, peridinin: Tchl *a* ratios (Table 2.1).

Finally, our results indicate that in situ a_p slope measurements may reveal significant differences in estimated PPC: PSC ratios on vertical scales of ~1 m. This finescale resolution, obtained with free-fall deployment methods, also allows estimates of a_p slopes and pigment ratios to be directly compared with parameters such as temperature, salinity, density, and fluorescence measured over the same vertical scales. These sharp vertical gradients in bio-optical properties are consistent with other observations of finescale planktonic structure in East Sound (Dekshenieks et al. 2001, Rines et al. 2002, Alldredge et al. 2002), over the continental shelf (Cowles et al. 1993, 1998), and in the Baltic (Bjornsen and Nielsen 1991).

In conclusion, our results suggest that absorption measurements from in situ instrumentation can be used to estimate PPC: PSC ratios in field phytoplankton assemblages in areas with low detrital concentrations or where the a_d contribution can

be adequately estimated. We show that the use of in situ optical instrumentation can provide a continuous vertical profile or temporal record of in-water optical properties, such as the normalized a_p spectral slope (488 to 532 nm), that can detect changes in pigmentation on finer scales than possible with conventional discrete water sampling methods. Pigmentation and in situ absorption changes were observed in response to changes in light and stratification, with increases in PPC: PSC ratios and a_p slopes associated with increases in irradiance and shoaling of the mixed layer. Such in situ-derived estimates of phytoplankton pigmentation changes may also provide insight into the recent light history of a particular phytoplankton population. For example, a time series of in situ absorption measurement could be used to estimate synthesis of PPC relative to PSC, given that advection effects are minimal or a single water mass can be monitored. While pigment package effects or a_d variations may alter the absorption spectra, in our data set we still found a significant relationship between pigment ratios and in situ a_p slopes. Further work is needed, however, to extend our understanding of the effects of packaging and a_d on the relationship developed in this study. With careful consideration of the range of factors influencing in situ absorption, these measurements can provide valuable information for deciphering the spatial, temporal and physical factors driving photoacclimation and species diversity in field phytoplankton populations. We look forward to additional comparisons of in situ a_p, HPLC-derived pigment composition and a_d estimates in other oceanic regions to confirm the general utility of a_{ph} and a_p slopes to estimate PPC: PSC ratios.

Acknowledgements

This research was supported by an AASERT grant (#N00014-96-10933) from the Office of Naval Research. Comments from Heidi M. Sosik and an anonymous reviewer substantially improved this manuscript. We thank Dian Gifford for assistance in water sample collection and for providing phytoplankton species data, Jan Rines for information concerning phytoplankton species, Chris Wingard and Russ Desiderio for help with data collection, data processing and graphics, Andrew Barnard for spectral radiometer measurements, Van Holliday for help with sample collection, and Claudia Mengelt, Ricardo Letelier and Margaret Sparrow for advice and support with HPLC analysis. Kathy Krogslund from the Marine Chemistry Laboratory at the University of Washington conducted nutrient analyses.

References

Alldredge, A.L., T.J. Cowles, S. MacIntyre, J.E.B. Rines, P.L. Donaghay, C.F. Greenlaw, D.V. Holliday, M.M. Dekshenieks, J.M. Sullivan, J.R.V. Zaneveld. 2002. Occurrence and mechanisms of formation of a dramatic thin layer of marine snow in a shallow Pacific fjord. Mar. Ecol. Prog. Ser. **233**: 1-12

Bidigare, R.R, M.E. Ondrusek, J.H. Morrow, and D.E. Kiefer. 1990. In vivo absorption properties of algal pigments. SPIE Ocean Optics X. **1302**: 290-302.

Bjornsen, P.K. and T.G. Nielsen. 1991. Decimeter scale heterogeneity in plankton during a pycnocline bloom of Gyrodinium aureolum. Mar. Ecol. Prog. Ser. **73**: 263-267.

Bricaud, A., M. Babin, A. Morel, and H. Claustre. 1995. Variability in the chlorophyll-specific absorption coefficients of natural phytoplankton: Analysis and parameterization. J. Geophys. Res. **100**: 13321-13332.

Bricaud, A., A. Morel and L. Prieur. 1983. Optical efficiency factors of some phytoplankters. Limnol. Oceanogr. **28**: 816-832.

Claustre, H., P. Kerherve, J.C. Marty, and L. Prieur. 1994. Phytoplankton photoadaption related to some frontal physical processes. J. Mar. Systems. **5**: 251-265.

Cleveland, J.S., and M.J. Perry. 1994. A model for partitioning absorption into phytoplanktonic and detrital components. Deep Sea Res. Part I. **41**: 197-221.

Cowles, T.J., R.A. Desiderio, and S. Neuer. 1993. *In situ* characterization of phytoplankton from vertical profiles of fluorescence emission spectra. Mar. Biol. **115**: 217-222

Cowles, T.J., R.A. Desiderio, and M-E. Carr. 1998. Small-scale planktonic structure: persistence and trophic consequences. Oceanography **11**: 4-9

Cullen, J.J., A.M. Ciotti, R.F. Davis, and M.L. Lewis. 1997. Optical detection and assessment of algal blooms. Limnol. Oceanogr. **42**: 1223-1239.

Culver, M.E., and M.J. Perry. 1999. The response of photosynthetic absorption coefficients to irradiance in culture and in tidally mixed estuarine waters. Limnol. Oceanogr. **44**: 24-36.

Dekshenieks, M.M., P.L. Donaghay, and J.M. Sullivan, J.E. Rines, T.R. Osborn, and M.S. Twardowski. 2001. Temporal and spatial occurrence of thin phytoplankton layers in relation to physical processes. Mar. Ecol. Prog. Ser. **223**: 61-71.

Duysens, L.N.M. 1956. The flattening of the absorption spectrum of suspensions, as compared to that of solutions. Biochim. Biophys. Acta. **19**: 1-12.

Falkowski, P.G., and J.A. Raven. 1997. Aquatic Photosynthesis. Blackwell Science.

Geider, R.J., J. La Roche, R.M. Greene, and M. Olaizola. 1993. Response of the photosynthetic apparatus of *Phaeodactylum tricornutum* (Bacillariophyceae) to nitrate, phosphate, or iron starvation. J. Phycol. **29**: 755-766.

Hoepffner, N., and S. Sathyendranath. 1991. Effect of pigment composition on absorption properties of phytoplankton. Mar. Ecol. Prog. Ser. **73**:11-23.

Jeffrey, S.W., and M. Vesk. 1997. Introduction to marine phytoplankton and their pigment signatures, p.37-84. *In:* S.W. Jeffrey, R.F. Mantoura, and S.W. Wright [eds.],

Phytoplankton pigments in oceanography: guidelines to modern methods. Unesco Publishing.

Johnsen G., and E. Sakshaug. 1996. Light harvesting in bloom-forming marine phytoplankton: species-specificity and photoacclimation. Sci. Mar. **60** (Supl.1): 47-56.

Johnsen, G., O. Samset, L. Granskog, and E. Sakshaug. 1994. In vivo absorption characteristics in 10 classes of bloom-forming phytoplankton: taxonomic characteristics and responses to photoadaptation by means of discriminate and HPLC analysis. Mar. Ecol. Prog. Ser. **105**: 149-157.

Kishino, M., M. Takahashi, N. Okami, and S. Ichimura. 1985. Estimation of the spectral absorption coefficients of phytoplankton in the sea. Bull. Mar. Sci. **37**: 634-642.

Latasa, M. 1995. Pigment composition of *Heterocapsa* sp. and *Thalassiosira weissflogii* growing in batch cultures under different irradiances. Sci. Mar. **59**: 25-37.

Mitchell, B.G., and D.A. Kiefer. 1988. Chlorophyll *a* specific absorption and fluorescence excitation spectra for light-limited phytoplankton. Deep Sea Res. **35**: 639-663.

Moline, M.A. 1998. Photoadaptive response during the development of a coastal Antarctic diatom bloom and relationship to water column stability. Limnol. Oceanogr. **43**: 146-153.

Morel, A. and A. Bricaud. 1981. Theoretical results concerning light absorption in a discrete medium, and application to specific absorption of phytoplankton. Deep Sea Res. **28A**:1375-1393.

Nelson, N.B., B.B. Prezelin and R.R. Bidigare. 1993. Phytoplankton light absorption and the package effect in California coastal waters. Mar. Ecol. Prog. Ser. **94**: 217-227.

Parsons, T. R., Y. Maita, and C.M. Lalli. 1984. A manual of chemical and biological methods for seawater analysis. Pergamon Press.

Pegau, W.S., D. Gray, and J.R.V. Zaneveld. 1997. Absorption and attenuation of visible near-infrared light in water: dependence on temperature and salinity. Applied Optics. **36**: 6035-6046.

Rines, J.E.B., P.L. Donaghay, M.M. Dekshenieks, J.M. Sullivan, and M.S. Twardowski. 2002. Thin layers and camouflage: hidden Pseudo-nitzschia populations in a fjord in the San Juan Islands, Washington, USA. Mar. Ecol. Prog. Ser. **225**: 123-137

Roesler, C.S. 1992. The determination of in situ phytoplankton spectral absorption coefficients: Direct measurements, modeled estimates, and applications to bio-optical modeling. PhD. Dissertation, Univ. of Washington, Seattle.

Roesler, C.S., M.J. Perry, and K.L. Carder. 1989. Modeling in situ phytoplankton absorption form total absorption spectra in productive inland marine waters. Limnol. Oceanogr. **34**: 1510-1523.

SooHoo, J.B., D.A. Kiefer, D.J. Collins, and I.S. McDermid. 1986. In vivo fluorescence excitation and absorption spectra of marine phytoplankton: I. Taxonomic characteristics and responses to photoadaptation. J. Plankton Res. **8**: 197-214.

Twardowski, M.S., J.M. Sullivan, P.L. Donaghay, and J.R.V. Zaneveld. 1999. Microscale quantification of the absorption by dissolved and particulate material in coastal waters with an ac-9. J. Atmos. Ocean. Technol. **16**: 691-707

UNESCO. 1994. Protocols for the Joint Global Ocean Flux Study (JGOFS) core measurements. IOC Manual and Guides **29**.

Vidussi, F., H. Claustre, B.B. Manca, A. Luchetta and J. Marty. 2001. Phytoplankton pigment distribution in relation to upper thermocline circulation in the eastern Mediterranean Sea during winter. J. Geophys. Res. **106**: 19,939-19,956.

Wright, S.W., and S.W. Jeffrey. 1997. High-resolution HPLC system for chlorophylls and carotenoids of marine phytoplankton, p.327-341. *In:* S.W. Jeffrey, R.F. Mantoura, and S.W. Wright [eds.], Phytoplankton pigments in oceanography: guidelines to modern methods. Unesco Publishing.

Yentsch, C.S. 1962. Measurement of visible light absorption by particulate matter in the ocean. Limnol. Oceanogr. **7**: 207-217.

Zaneveld, J.R.V., J.C. Kitchen, and C.C. Moore. 1994. Scattering error correction of reflecting tube absorption meters. Proc. SPIE Int. Soc. Opt. Eng. **12**: 44-55.

Zinkel, Z.V. 2001. Light absorption and size scaling of light-limited metabolism in marine diatoms. Limnol. Oceanogr. **46**: 86-94.

CHAPTER 3

RELATIONSHIP OF PHYTOPLANKTON PHOTOPROTECTIVE: PHOTOSYNTHETIC CAROTENOID RATIOS TO IN SITU SPECTRAL ABSORPTION MEASUREMENTS IN OREGON COASTAL SURFACE WATERS

Lisa B. Eisner, Timothy J. Cowles and Ricardo M. Letelier

Abstract

Phytoplankton pigment ratios were compared to in situ spectral absorption measurements for surface data collected from Oregon coastal waters during August 2001. A towed undulating sled was used to measure hydrographic properties and pump water from depth to in line instruments and water sampling apparatus located on board ship. In situ spectral absorption and beam attenuation were obtained with a WET Labs ac-9 (nine-wavelength absorption and beam attenuation meter), and pigment concentrations were determined for discrete water samples using High Performance Liquid Chromatography (HPLC). Surface samples were divided into three groups based on temperature salinity characteristics, sample date and location. Phytoplankton absorption coefficient (a_{ph}) spectra were derived from in situ ac-9 particulate absorption coefficient (a_p) spectra and discrete sample detrital absorption coefficient (a_d) measurements using the quantitative filter technique (QFT). We computed a "slope" index to evaluate changes in shapes of the a_{ph} spectra, a_{ph} slope = ($a_{ph}488$-$a_{ph}532$)/(($a_{ph}676$) · (488-532 nm)). Significant linear relationships were seen between ratios of photoprotective: photosynthetic carotenoids (PPC: PSC) and the a_{ph} slope indices for each group. The y-intercepts the regression lines were significantly different between groups although slopes of the regression lines were similar. The largest magnitude intercepts (steepest a_{ph} slopes) were found for stations located further offshore influenced by the Columbia River plume (group CR), with mid-range intercepts seen for mid shelf stations (group MID) and lowest intercepts seen for inshore stations (group IN). Package effects were estimated by Qa*676, defined as a_{ph}

676 packaged (from ac-9 data) / a_{ph} unpackaged (from HPLC and ac-9 data). A strong relationship was seen between the mean Qa* 676 and the intercept from the a_{ph} slope/pigment relationship for each group. These results suggest that the samples from group CR had the lowest packaging followed by group MID and lastly by group IN. Relative particles sizes were estimated by fitting a hyperbolic function to the particulate beam attenuation coefficient (c_p) spectra. These results indicated that the particle size was smaller for group CR compared to group MID. The a_d was low in these samples suggesting the c_p spectral variations are due to relative changes in phytoplankton size. Chemotaxonomic analyses indicated that prokaryotes, prymnesiophytes and diatoms were prevalent in group CR samples, whereas diatoms, and to a lesser extent dinoflagellates, were prevalent in group MID samples. This study provides further confirmation that in situ estimates of phytoplankton physiological parameters can be obtained with in situ absorption and beam attenuation meters, in conjunction with occasional discrete sampling for pigment analysis.

Introduction

The in situ assessment of phytoplankton physiological condition is important for evaluating the environmental factors influencing variations in physiology and taxonomy in natural assemblages. Multi-wavelength bio-optical instrumentation such as in situ absorption and beam attenuation meters have been used to assess in the shape of in situ absorption spectra and provide an optical characterization of the particulate and dissolved materials in a number of studies (Bricaud et al.1995, Barnard

et al. 1998, Boss et al.2001, Twardowski and Donaghay 2002). This study is an effort to assess the relationship between in situ observations and traditional, discrete sample analyses of photophysiology including pigment ratios and package effects (Duysens 1956) in phytoplankton populations.

An earlier study (chapter 2, Eisner et al. 2003) was conducted at a single location in East Sound, a fjord estuary in Puget Sound, Washington during a 10-day period in June 1998 to evaluate the relationship between in situ spectra absorption and phytoplankton pigment ratios. High-resolution vertical profiles of in situ spectral absorption were obtained with an ac-9 (nine-wavelength absorption and beam attenuation meter), and discrete sample pigment concentrations were determined with High Performance Liquid Chromatography (HPLC). To evaluate changes in the shapes of the in situ phytoplankton absorption (a_{ph}) spectra, we computed a "slope" index, a_{ph} slope = $(a_{ph}488\text{-}a_{ph}532)/((a_{ph}676) \cdot (488\text{-}532\ \text{nm}))$. A clear linear relationship was seen between ratios of photoprotective: photosynthetic carotenoids (PPC: PSC) and the a_{ph} slopes. The phytoplankton assemblages were largely composed of diatoms.

To further investigate the relationship between in situ absorption and pigment ratios and determine if the results found in East Sound could be applied to other regions with a variety of water types, we conducted sampling in Oregon coastal waters during August 2001 (summer upwelling season) as part of the National Science Foundation (NSF) sponsored Coastal Ocean Advances in Shelf Transport (COAST) program. The study area covered a variety of water masses influenced by dynamic processes such as the southward flowing coastal jet (California Current), wind driven

coastal upwelling and relaxation, and inputs from the Columbia River (Huyer 1976, Small and Menzies 1981, Hickey 1989, Barth et al. 2000). Phytoplankton biomass, taxonomic characteristics and photophysiology are expected to vary across the study region (between water mass types) due to the variations in physical and chemical properties, such as upwelling, stratification, light, and nutrients (e.g. Kokkinakis and Wheeler 1987, Corwith and Wheeler 2002, Hill and Wheeler 2002). If a relationship is found in oceanic waters between in situ absorption spectra and HPLC-determined phytoplankton pigment ratios such as PPC: PSC, we can use ac-9 data to estimate PPC: PSC ratios over fine temporal and spatial scales and more directly compare these changes with physical oceanographic processes, as was found for East Sound (Eisner et al., 2003).

Thus, the overall goals in this work are to determine the extent to which in situ absorption measurements can estimate phytoplankton accessory pigment composition in Oregon Coast waters and to evaluate the effects of photophysiology and taxonomic variations on this relationship. Packaging effects as well as changes in PPC: PSC ratios can influence the shape of the a_{ph} spectra (Ciotti et al, 2002). Increased packaging will lower the blue: red a_{ph} ratios (Duysens 1956) and is expected to reduce the steepness of our a_{ph} slopes. Package effects are influenced by cell size as well as shape and internal pigment concentration (Kirk 1994). In turn, cell size varies with taxonomic composition. Therefore, we wish to evaluate package effects in relation to relative size and chemotaxonomic characteristics of the phytoplankton assemblage. Finally, since detrital absorption (a_d) can interfere with the quantification of phytoplankton absorption from particulate absorption spectra (Roesler et al.1989), we

want to examine the influence of a_d in our Oregon Coast samples. In this chapter, we focus on surface data (top 10 m, generally above the pycnocline) to evaluate the horizontal patterns in phytoplankton chemotaxonomic distributions and photophysiology. These patterns are related to water mass characteristics, which vary by location and collection date.

Specifically, our objectives are to 1) compare surface PPC and PSC concentrations from HPLC analyses of discrete water samples with in situ a_{ph} and particulate absorption (a_p) spectra in a variety of water masses (inshore, mid-shelf, Columbia River/offshore waters), with consideration of the influence of a_d on this relationship, 2) describe the influences of photophysiology and taxonomic variations on the relationship between PPC: PSC ratios and a_p and a_{ph} spectra using estimates of packaging, particle size and biomarker pigments derived from optical (ac-9) and discrete sample (HPLC, Quantitative Filter Technique (QFT)) analyses.

Materials and Methods

Sampling site

Data were collected in Oregon coastal waters during a 3-week cruise onboard the R/V Thompson from 7 to 25 August 2001 (local time) during summer upwelling and relaxation periods. The sampling grid covered an area of ~ 9000 km^2 from 43.86 ° N to 45.01 ° N and 124.04 ° W to 125.00 ° W (3 km to 70 km offshore) (Figure 3.1). The depth of the water column varied from 30 m inshore to 50 m

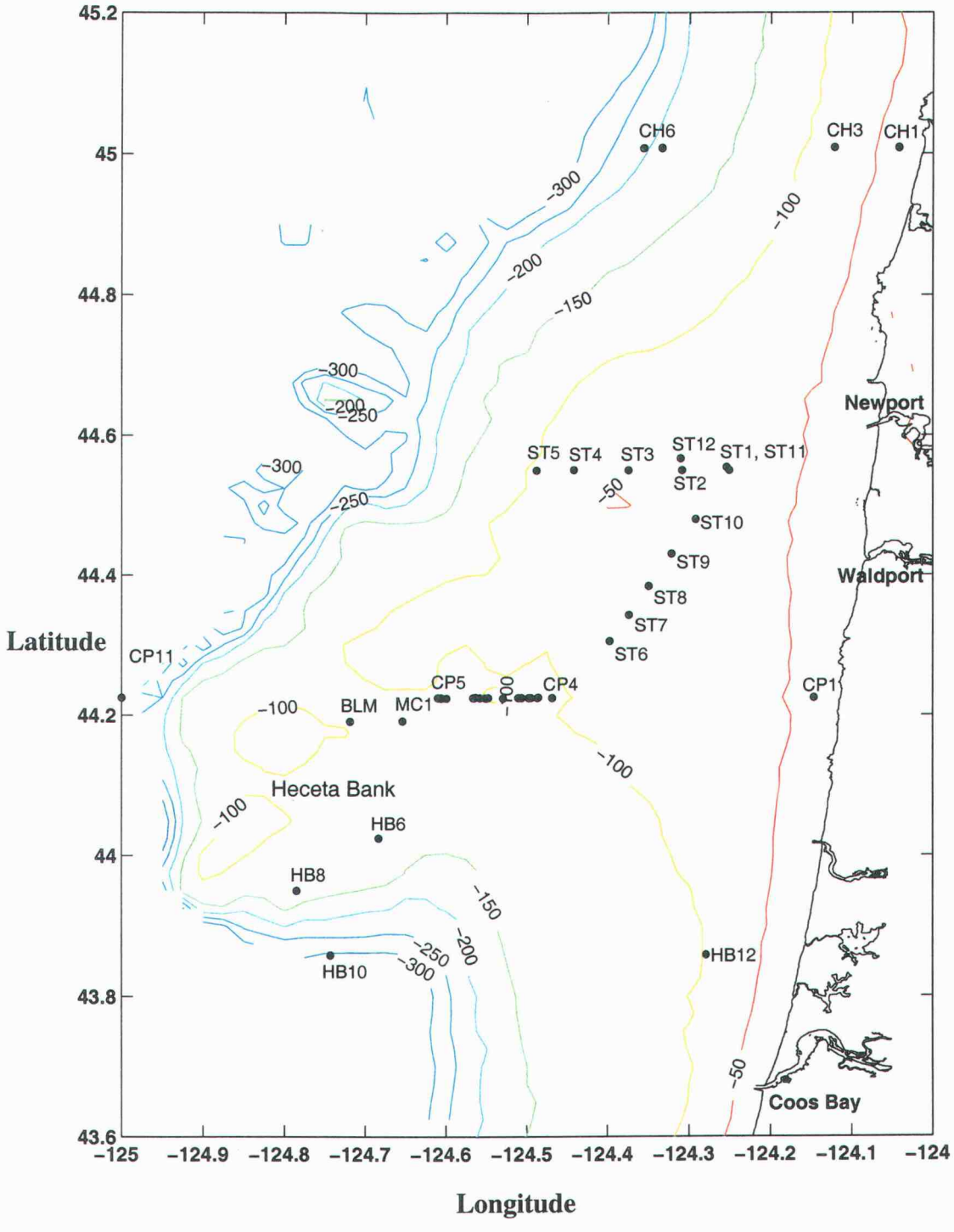

Figure 3.1. Oregon Coast station locations for collection of discrete water samples and in-line optical measurements during August 2001. Bathymetric contours are every 50 m. Latitude and longitude in decimal degrees.

offshore of the shelf break. A tow-yo sled (Dr. B. Hales) was used to map the hydrographic structure of the water column while pumping water to the lab on board the R/V Thompson. The sled maintained a vertical velocity of 0.3 m s^{-1} for both up and down casts.

In situ measurements of hydrography and bio-optics

Vertical profiles of temperature, salinity, fluorescence, transmissometer (beam attenuation at 660 nm) measurements were obtained with in situ instruments attached to the towed undulating sled. Water pumped from the sled to the shipboard laboratory was passed through an in-line bio-optical system. The in line bio-optical system included a Conductivity-Temperature-Depth (CTD) sensor (SBE 911, Seabird, Inc.), a fluorometer (Wetstar, WET Labs, Inc.), and two nine-wavelength in situ spectral absorption and beam attenuation meters (ac-9, WET Labs, Inc.) with one for measurement of total water and one for measurement of dissolved materials (Figure 3.2). The measurement of dissolved constituents was accomplished by diverting part of the inline flow through a 50 μm filter, a 10 μm filter and than a 0.2 μm filter (maxi-capsule, Gelman) prior to passing through the ac-9. Wavelengths for in situ absorption and beam attenuation measurements were 412, 440, 488, 510, 532, 555, 650, 676, 715 nm. The ac-9s were calibrated approximately every 2 days using the pure water calibration technique (Twardowski et al.1999).

Large scale in situ measurements were also collected with a Sea Soar, a towed undulating package, deployed from the R/V Wecoma, a second research vessel participating in the August 2001 COAST sampling. A Flash Pak fluorometer (Wet

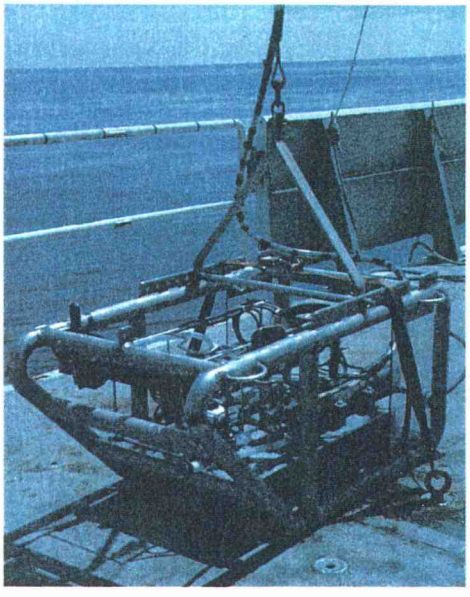

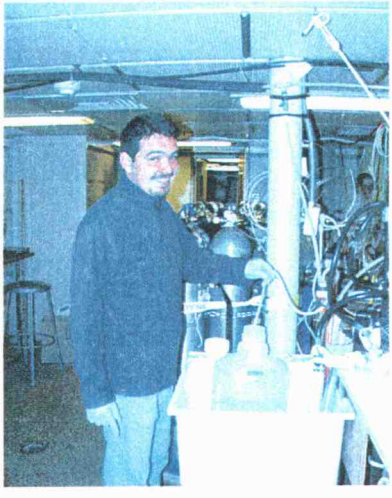

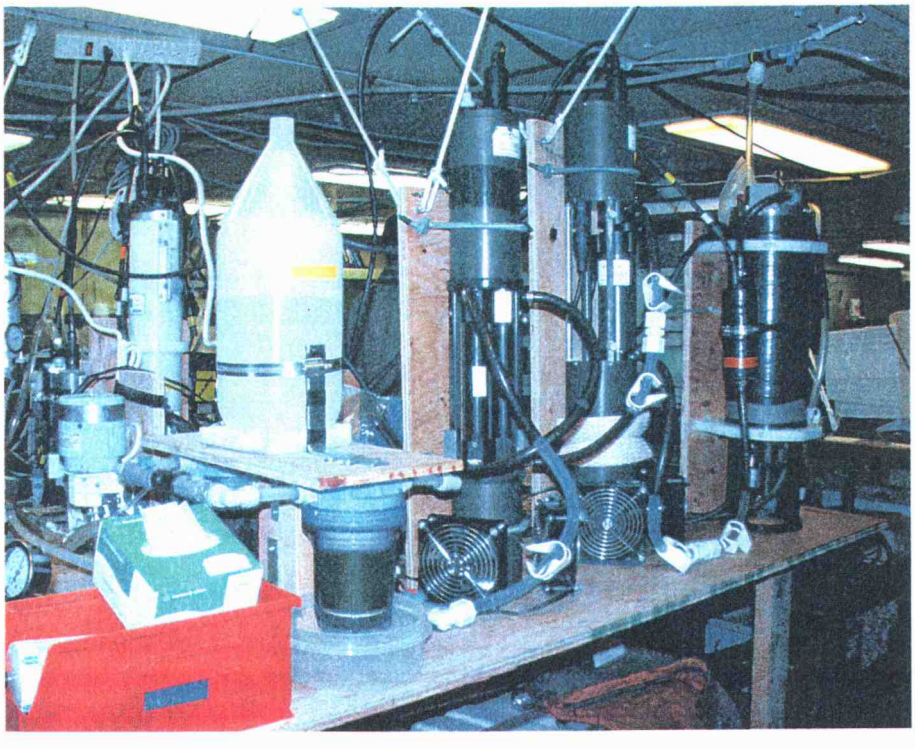

Figure 3.2. Photos of the to-yo sled, discrete water sampling and the in-line optical system on board ship. Instruments for the in-line optics include a Fast Repetition Rate fluorometer, a spectral fluorescence sensor (SAFIRE) two ac-9s (for measurement of total water and dissolved constituents), a Wet Star fluorometer and a Seabird 911 CTD.

Labs) was used to map chlorophyll a concentration and a Seabird 911 CTD was used to map T, S and density. The data were interpolated between the inshore and offshore survey lines using an optimal interpolation to create spatial maps of chlorophyll *a* and temperature. Spatial mapping is courtesy of Dr. J. Barth.

Collection of discrete water samples

Water samples were collected concurrent with the in-line hydrographic and optical measurements on board the R/V Thompson by diverting part of the pumped flow into 20 L plastic carboys. Water samples were collected at select stations (pump stations) from 10-12 depths, surface (5 m) to near-bottom, by holding the sled at each depth for ~ 5 to 20 minutes. Additional surface (3-5 m) water samples were collected every 2 hours for time series sampling (CP45 time series) or at several stations along a transect line (ST stations) (Table 3.1). Water samples were collected for pigment composition (HLPC analyses), and particulate and phytoplankton absorption (QFT analysis with Kishino method) and stored in liquid nitrogen until analysis at our shore-based laboratories. The concurrent CTD data were used to determine the temperature (T) salinity (S) characteristics for each sample.

The depth of the pycnocline (maximum change in density) was deeper than 10 m for all pump stations. In order to evaluate horizontal differences in surface properties across the sampling domain, we restrict our analysis in this paper to samples collected within 10 m of the surface.

Table 3.1. Sampling date, time, depth (dep, m), temperature (temp, °C), salinity, density (kg m^{-3}), bathymetric depth (bathy, m), latitude and longitude (decimal degrees), and group designation (see text) for all stations. Times are local (Pacific Daylight Time). Time series stations between station CP4 and CP5 are indicated by CP45ts.

station	date	time	dep	temp	salin	sig-t	Tchla	bathy	lat (N)	long (W)	group
CH1	7-Aug	17:19	10	12.40	32.85	24.87	9.09	36	45.01	124.04	IN
CH1	7-Aug	17:46	5	12.46	32.79	24.81	9.60	34	45.01	124.04	IN
CH6	8-Aug	4:14	10	14.16	32.30	24.10	1.40	206	45.01	124.36	CR
CH6	8-Aug	4:25	5	14.16	32.30	24.10	1.41	205	45.01	124.36	CR
CH3	9-Aug	14:21	5	9.95	33.06	25.47	2.18	87	45.01	124.12	IN
CH1	10-Aug	20:06	10	10.95	33.14	25.36	4.33	33	45.01	124.04	IN
CH1	10-Aug	20:18	5	11.28	33.00	25.20	4.21	33	45.01	124.04	IN
CH6	11-Aug	10:36	10	13.99	32.34	24.16	1.73	185	45.01	124.33	CR
CH6	11-Aug	10:47	5	15.22	32.26	23.84	1.18	185	45.01	124.33	CR
CP1	12-Aug	2:32	10	10.54	33.50	25.71	5.78	37	44.22	124.15	IN
CP1	12-Aug	3:01	5	11.10	33.45	25.57	8.07	37	44.22	124.15	IN
CP11	13-Aug	15:19	10	15.48	32.31	23.82	0.25	529	44.23	125.00	CR
CP11	13-Aug	15:28	5	15.58	32.30	23.79	0.21	529	44.23	125.00	CR
CP5	14-Aug	3:02	10	12.34	32.79	24.84	3.82	107	44.23	124.61	MID
CP5	14-Aug	3:15	5	12.37	32.57	24.66	2.90	107	44.23	124.61	MID
CP45 ts	14-Aug	12:16	4	13.15	33.07	24.89	3.12	105	44.23	124.56	MID
CP45 ts	14-Aug	14:07	3	13.47	33.12	24.87	2.75	104	44.23	124.51	MID
CP45 ts	14-Aug	16:07	3	13.40	33.10	24.86	3.95	102	44.23	124.49	MID
CP45 ts	14-Aug	16:47	5	13.41	33.12	24.88	4.94	105	44.22	124.51	MID
CP45 ts	14-Aug	18:09	5	13.64	33.11	24.83	2.19	104	44.22	124.55	MID
CP45 ts	14-Aug	20:06	4	12.72	32.57	24.59	6.42	109	44.23	124.61	MID
CP45 ts	14-Aug	21:56	5	12.13	32.68	24.79	7.25	106	44.23	124.56	MID
CP45 ts	15-Aug	0:09	5	13.56	33.12	24.85	1.82	104	44.23	124.51	MID
CP4	15-Aug	3:43	10	13.43	33.12	24.88	3.24	99	44.23	124.47	MID
CP4	15-Aug	3:55	6	13.48	33.12	24.87	3.29	99	44.23	124.47	MID
CP45 ts	15-Aug	6:24	3	13.28	33.10	24.90	2.47	104	44.23	124.50	MID
CP45 ts	15-Aug	8:01	3	12.67	33.00	24.93	6.35	103	44.23	124.55	MID
CP45 ts	15-Aug	9:50	3	11.81	32.61	24.79	5.67	109	44.22	124.60	MID
CP45 ts	15-Aug	12:09	3	13.36	33.06	24.85	4.29	106	44.22	124.57	MID
CP45 ts	15-Aug	14:09	4	13.51	33.09	24.84	5.64	105	44.22	124.51	MID
CP4	15-Aug	20:12	10	11.79	33.13	25.20	2.07	101	44.23	124.47	MID
CP4	15-Aug	20:28	5	13.20	33.10	24.90	3.37	102	44.23	124.47	MID
CP45 ts	16-Aug	0:00	3	12.97	33.17	25.01	6.36	98	44.22	124.53	MID
CP45 ts	16-Aug	2:12	5	12.59	32.83	24.81	13.06	107	44.22	124.61	MID
CP45 ts	16-Aug	4:07	5	12.55	33.15	25.07	4.87	102	44.23	124.55	MID
CP45 ts	16-Aug	6:07	3	12.30	32.94	24.96	6.67	101	44.23	124.49	MID
CP45 ts	16-Aug	7:46	3	12.66	33.03	24.96	6.86	103	44.23	124.49	MID
CP45 ts	16-Aug	10:00	3	12.95	33.16	25.00	3.84	104	44.23	124.56	MID
CP45 ts	16-Aug	12:07	3	12.54	32.70	24.72	18.52	109	44.22	124.61	MID
BLM	16-Aug	18:43	3	12.99	32.68	24.62	17.27	108	44.19	124.72	MID

Table 3.1 continued.

station	date	time	dep	temp	salin	sig-t	Tchla	bathy	lat (N)	long (W)	group
MC1	17-Aug	16:28	10	10.32	32.71	25.14	6.62	116	44.19	124.65	MID
MC1	17-Aug	16:43	5	11.94	32.65	24.79	14.78	116	44.19	124.65	MID
HB6	19-Aug	7:56	10	11.38	32.64	24.90	9.58	131	44.03	124.68	MID
HB6	19-Aug	8:08	5	12.91	32.71	24.66	15.31	131	44.03	124.68	MID
HB8	20-Aug	1:02	10	11.89	32.56	24.74	10.12	129	43.95	124.78	MID
HB8	20-Aug	1:11	5	12.68	32.60	24.62	13.96	129	43.95	124.78	MID
HB10	20-Aug	21:33	10	12.35	32.68	24.75	18.76	309	43.86	124.74	MID
HB10	20-Aug	21:45	5	12.64	32.57	24.60	18.33	309	43.86	124.74	MID
HB12	21-Aug	2:57	5	10.25	33.20	25.53	11.28	102	43.86	124.28	MID
ST 1	24-Aug	6:22	5	11.35	32.80	25.03	21.99	75	44.55	124.25	MID
ST 2	24-Aug	8:31	4	11.54	32.60	24.83	17.02	83	44.55	124.31	MID
ST 3	24-Aug	10:33	4	11.92	32.45	24.65	12.87	62	44.55	124.37	MID
ST 4	24-Aug	12:33	4	11.72	32.49	24.72	11.15	77	44.55	124.44	MID
ST 5	24-Aug	14:06	4	12.49	32.36	24.47	11.05	98	44.55	124.49	MID
ST 6	24-Aug	18:22	4	13.53	32.53	24.40	7.17	92	44.31	124.40	MID
ST 7	24-Aug	20:24	6	12.88	32.43	24.45	11.11	83	44.34	124.37	MID
ST 8	24-Aug	22:29	5	12.80	32.42	24.46	7.91	78	44.38	124.35	MID
ST 9	25-Aug	0:33	5	12.60	32.46	24.53	7.17	71	44.43	124.32	MID
ST 10	25-Aug	2:36	4	12.13	32.61	24.74	13.85	78	44.48	124.29	MID
ST 11	25-Aug	5:54	5	12.18	32.91	24.96	18.57	76	44.55	124.25	MID
ST 12	25-Aug	7:58	4	11.52	32.81	25.00	12.84	84	44.57	124.31	MID

Discrete sample analyses of phytoplankton pigments, particulate absorption

Analysis of phytoplankton pigment composition, and particulate and phytoplankton absorption followed methods described in Eisner et al. (2003). For phytoplankton pigment determinations, water samples (0.5 to 2 L) were filtered onto 25 mm glass fiber filters (GF/F filters, Whatman), frozen in liquid N_2 and analyzed within 8 months using HPLC (Wright and Jeffrey 1997). Quantifiable pigments included chlorophylls (*a*, *b*, *c*1/*c*2, *c*3), chlorophyllide *a*, chlorophyll *a* epimer, PSC (19 hexanoyloxyfucoxanthin (19-hex), 19-butanoyloxyfucoxanthin (19-but), fucoxanthin (fuco), peridinin (perid)), and PPC (alloxanthin (allo), β-carotene (Bcaro),

diadinoxanthin (diad), diatoxanthin (diat), lutein/zeaxanthin (lut/zea), violaxanthin (viol)). Total chlorophyll *a* (Tchl *a*) was computed as the sum of chlorophyll *a* (chl *a*), chlorophyllide *a*, chlorophyll *a* epimer and other unidentified chlorophyll *a* derivatives.

Discrete water sample a_p, a_{ph} and a_d spectra were obtained by filtering water (0.5 to 1 L) onto GF/F filters, freezing samples in liquid N_2 and analyzing samples using the Quantitative Filter technique (QFT; Yentsch 1962; Mitchell and Kiefer 1988) with the Kishino method (Kishino et al. 1985). All samples were processed within 12 months of collection.

In situ particulate absorption spectra

One ac-9 received unfiltered water from the pumped flow stream and measured absorption by particles plus dissolved materials, denoted a_{pg}. The second ac-9 received 0.2 μm filtered water and measured absorption by dissolved material (a_g). We applied corrections for the temperature and salinity dependence of pure water absorption (Pegau et al. 1997), and removed the scattering error in our a_p measurements by subtracting a_p715 nm from all wavelengths (Zaneveld et al, 1994). The a_p was estimated by subtraction of a_g from a_{pg}. Corrections for time lags were applied to all in-line instruments to account for the time it took for a parcel of water to travel from the intake of the sled pump to the in-line flow-through system on board ship. Additional time-lag corrections for the slower flow rates to the filtered ac-9 data were used to align the particulate and dissolved measurements. Sampling frequency for the ac-9s was ~ 6 Hz. Single point data spikes were removed from the ac-9 data

with a 5-point median filter (2 passes). The data were then smoothed with a 7-point running average, averaged into 1-s bins, and merged with 1-s averages of position and hydrographic properties.

Calculation of slopes from absorption spectra

To evaluate changes in the shape of the absorption spectra from 488 to 532 nm, we normalized the absorption data to 676 nm, as described in Eisner et al. (2003). We computed the "slopes" of the absorption curves:

$$a_x \text{ slope} = (a_x488 - a_x532) / (a_x676 \cdot (488 - 532 \text{ nm})),$$

where a_x is denoted as a_{ph} or a_p or a_{pg}.

The ac-9 slope measurements were averaged over the time interval that the sled was held at the sample depth during discrete sample collection (2 to17 minutes). The absorption slopes from both the ac-9 and discrete sample QFT measurements were then compared to the PPC: PSC ratios determined from HPLC analyses of those same discrete samples. We also compared ac-9 a_{ph} slopes and PPC: Tchl *a* ratios. We may expect to see a steeper slope with an increase in relative amounts of PPC and/or a decrease in PSC (or Tchl *a*) based on the wavelength of maximum absorption and spectral shape of these pigment groups (Eisner et al. 2003; Bidigare 1990, *see* Figure 1.1). Model 2 (geometric mean) linear regression analyses were used for all comparisons. For statistical comparisons between model 2 regressions, we determined if the mean values for the regression line slope and intercept for one regression fell

within the 95% confidence intervals (CI) of the other regression. For example, the relationship for PPC: PSC ratios and a_p slopes was assumed to be significantly different than that found for PPC: PSC ratios and a_{ph} slopes if the mean regression line slope and intercept for the a_p slope/pigment relationship fell outside the 95% CI determined for the a_{ph} slope/pigment relationship.

Detrital absorption (a_d) estimation

To estimate ac-9 a_{ph} values we needed to remove a_d from the ac-9 a_p measurements. We estimated a_d using the QFT discrete sample data collected at the same time as the ac-9 samples. We corrected the ac-9 data based on the a_d: a_p ratio from the QFT. The use of the a_d: a_p ratio rather than the a_d value alone permits us to account for differences in the magnitudes of the ac-9 spectra compared to the QFT spectra.

To evaluate the shapes of the a_d spectra, we fit exponential functions to our QFT a_d spectra using mean values for the sample groups IN, MID (for samples without phycobilipigments) and CR (station CH6 only) using a non-linear least squares fit (Press et al.1986) from 440 to 676 nm using the equation (Roesler et al. 1989),

$$a_d(\lambda) = A * e^{(-s\,(\lambda-440))},$$

where A is the magnitude of the fitted a_d spectra at 440 nm and s is the exponential slope.

Package effects

We examined the effects of packaging on our data set by reconstructing unpackaged a_{ph} spectra from phytoplankton pigment concentrations (determined by HPLC) using methods in Bidigare et al. (1990). We calculated the unpackaged phytoplankton absorption coefficient ($a_{ph}'(\lambda)$) from the equation,

$$a_{ph}'(\lambda) = \sum_{i=1}^{n} c_i \, a^*_i(\lambda),$$

where c_i is the concentration of pigment i (mg m^{-3}) and $a^*_i(\lambda)$ is the specific absorption coefficient of pigment i (m^2 mg^{-1}) at wavelength (λ). The ratio of the particulate absorption to the dissolved absorption for a solution of the same absorbing substance is a measure of the package effect (Duysens 1956) defined as the dimensionless factor, Qa* (Morel and Bricaud 1981). Qa* can be calculated from the measured a_{ph} values (from ac-9 or QFT; includes packaging) divided by the reconstructed a_{ph}' values (unpackaged) at the wavelength of interest. We used Qa* at 676 nm (primarily indicating Tchl *a* packaging) to compare package effects between samples and groups. This was the same approach used in Eisner et al. (2003) for East Sound samples.

Size estimations based on c_p spectra

To estimate relative differences in the particle sizes between surface samples, we first estimated the beam attenuation (c) spectra from ac-9 measurements. As was done for determinations of a_p spectra, we subtracted the dissolved attenuation (c_g) spectra, from the total attenuation (c_{pg}) spectra, to get particulate beam attenuation (c_p) spectra. Based on methods in Boss et al.(2001) these c_p spectra were fit using non-linear least squares (Levenberg-Marquardt; Press et al. 1986) using the equation,

$$c_p(\lambda) = C(\lambda/650)^{-\gamma}$$

with 412, 440, 510 532 555 and 650 nm wavelengths from the ac-9. In the above equation, C is the magnitude of the fitted c_p spectra at 650 nm and γ is the hyperbolic exponent. The average root mean square error for fitted compared to measured c_p values was 0.041 (~ 2% of the c_p650 magnitude) assuming standard deviations = 0.005 m^{-1}. The exponent, γ, is expected to be linearly related to the slope of the particle size distribution (PSD) for non-absorbing spheres (Diehl and Haardt 1980, Boss et al. 2001). Thus, γ provides a rough index of relative particle size distribution, with higher γ (steeper hyperbolic slope) associated with a distribution dominated by smaller particle sizes. Therefore we can use γ to estimate the relative particle size distributions between samples and sample groups. Values of γ were compared between groups and for select samples within groups. Ratios of c_p450: c_p650 were also examined since Kitchen et al. (1982) found a correlation between this ratio and the PSD.

Results

Water mass characteristics

The inshore stations (CP1, CH1 on 10 Aug, HB12, CH3) had cold salty surface water suggesting this water was recently upwelled (Figure 3.3, Table 3.1). Stations CP11 and CH6 had warmer fresher (< 32.4) water indicative of Columbia River plume water. The remaining stations (located mid shelf) had mid-range T and S characteristics, although some samples appeared to cluster together (Figure 3.3). For example, station CP4 and nearby stations had relatively warm salty water compared to other mid-shelf stations (Figure 3.3, Table 3.1).

Phytoplankton biomass patterns

We used chl *a* concentration as an estimate of phytoplankton biomass, and observed both temporal and horizontal patterns in chl *a* during our study period. Figure 3.4a displays an example of the spatial variability in chl *a* estimated from in situ fluorometer measurements from Sea Soar transects on 15 to 16 August, and Figure 3.4b shows the concurrent temperature data. The chlorophyll *a* concentrations were typically higher in the colder shelf waters than in the warmer offshore waters. For our discrete samples, the highest surface Tchl *a* values were measured ~ 40-50 km offshore of Cape Perpetua (stations CP5, BLM) during 16 August, over Heceta Bank ~50 km offshore (station HB10) during 20 August, and mid-shelf ~15 km off Newport and Waldport (stations ST1, ST11) during 24 and 25 August (Figure 3.1, Table 3.1, Figure 3.3).

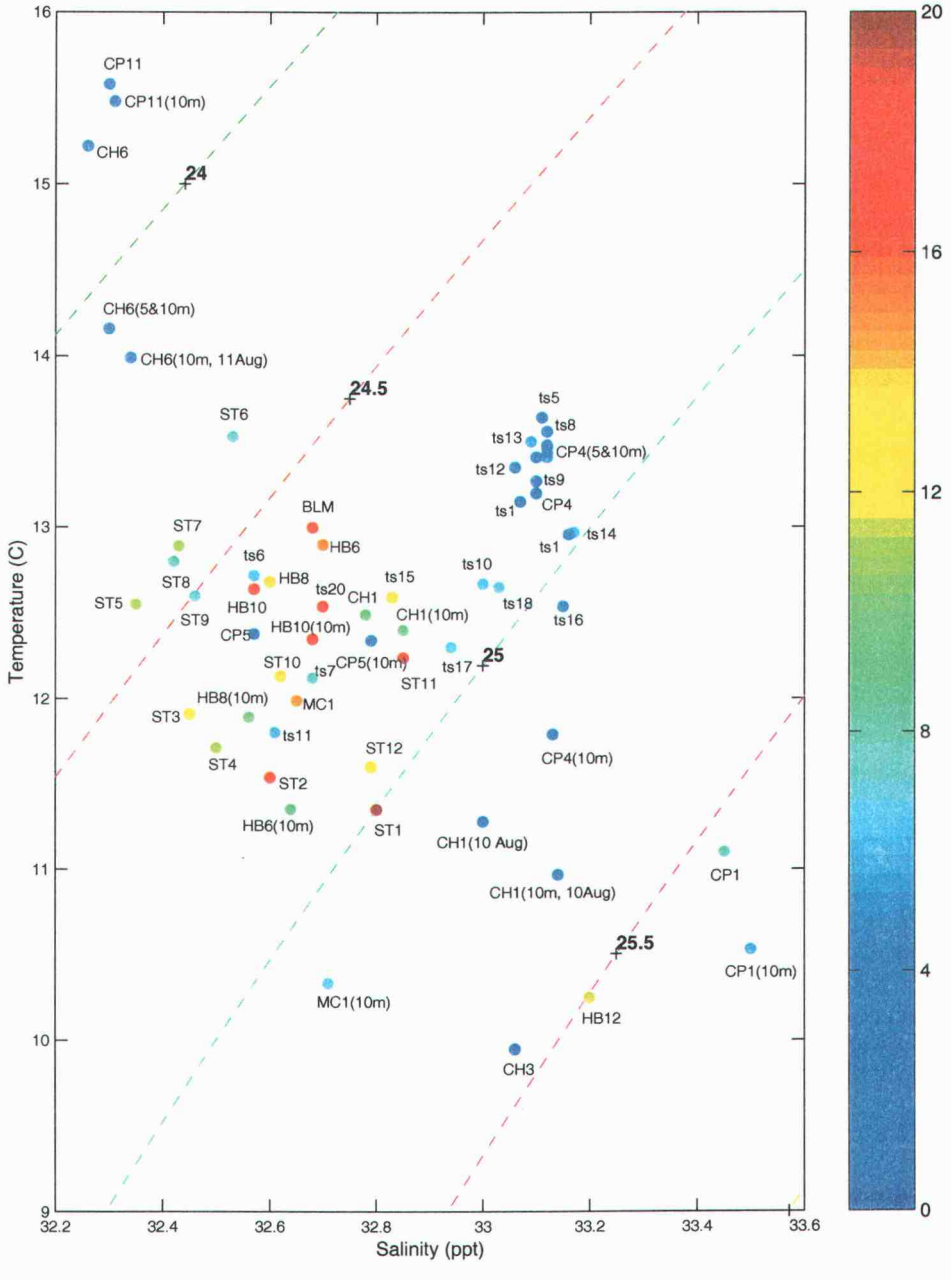

Figure 3.3. Temperature and salinity plot of samples collected in top 10 m (3-10 m) of the water column. Total chlorophyll *a* concentration is indicated with the color bar (maximum value set at 20 μg L^{-1}). Samples are from 3-5 m unless labeled as 10 m. The ts designation indicates the station CP4 to CP5 time series samples with the numbers indicating the order of sampling (1 first, 17 last).

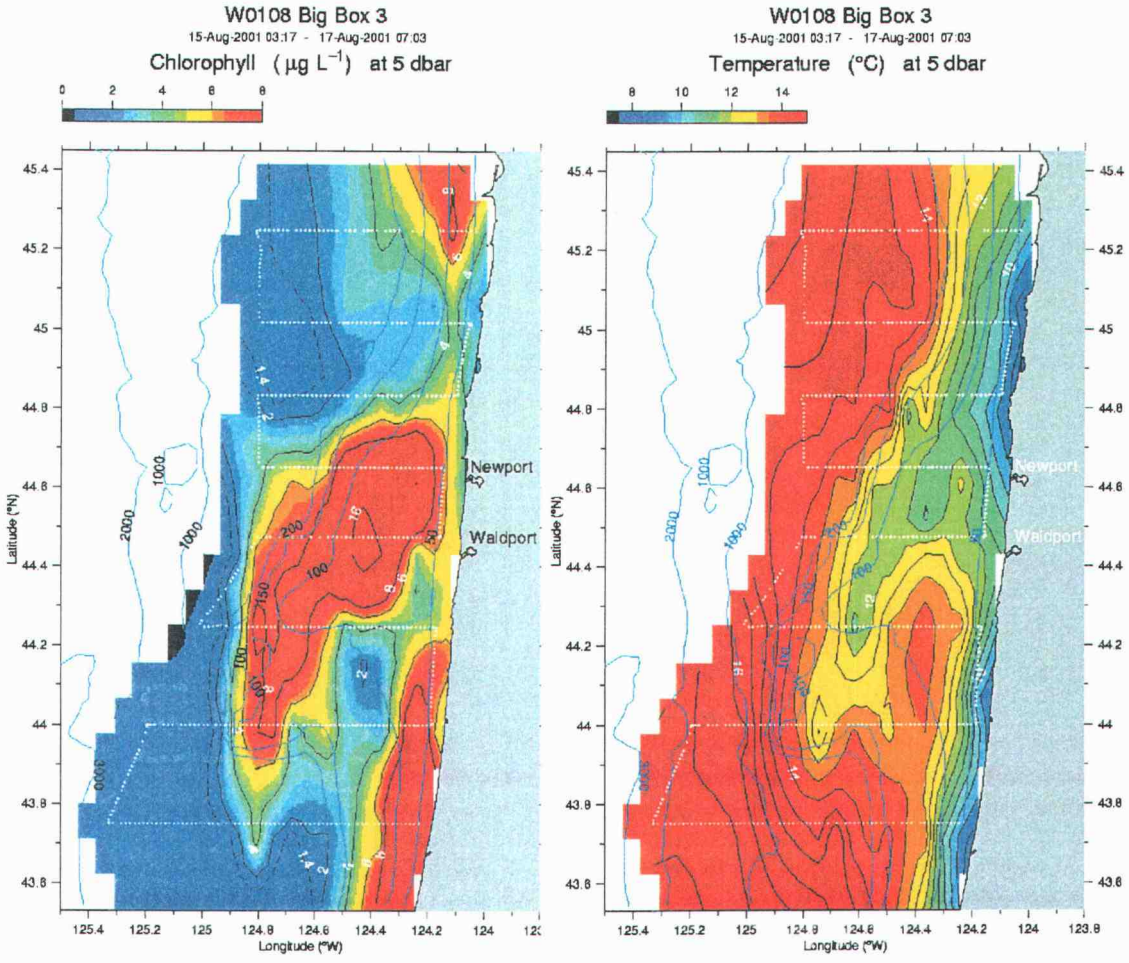

Figure 3.4. 5-m contour maps of a) chlorophyll *a* from an in situ Flash Pak (Wet Labs) fluorometer and b) temperature from 911 CTD (Seabird) during Sea Soar surveys from the R/V Wecoma on 15 to 16 August (local time). GMT time is shown above plots. Transect lines are shown by white dotted lines. Contour maps are courtesy of Dr. Jack Barth.

Grouping of samples

The 61 discrete samples were placed into 3 separate groups based on their location, collection date and TS characteristics (Table 3.1, Figure 3.3).

1) Group IN: This group has the inshore stations CH1, CH3, CP1 (inshore of 124.2° W and north of 44.2° N); collected 7 to12 August 2001; generally high density surface waters with sigma-t from 25.2 to 25.75 kg m^{-3}, S from 33.0 to 33.5 and T from 9.5 to 11.5 °C for all but one station (CH1 on 8 Aug).
2) Group CR: This group consists of Columbia River influenced /offshore stations including CH6 (located the furthest northwest) and CP11, (located the furthest offshore); collected 8 to 13 August 2001; lowest density surface waters with sigma-t from 23.7 to 24.25 kg m^{-3}, S from 32.25 to 32.4, and T from 14 to 16 °C).
3) Group MID: This group consists of all other stations, locations between 124.2° W to 124.8° W and 43.8° N to 44.6° N; data collection on 14 to 25 August 2001; mid-range surface water density with sigma–t from 24.25 to 25.2 kg m^{-3}, S from 32.4 to 33.2 and T from 10.2 to 13.8 °C for all but one sample (HB12, station closest inshore).

We evaluated the differences between groups for factors such as pigment composition, optical parameters (shape of absorption and beam attenuation spectra), and the relationship between pigment ratios and in situ absorption slopes (see methods for details).

These sample groupings did not result in a perfect match for all samples. An overlap of TS characteristics (and densities) between groups occurred for 3 samples,

with station CH1 on 7 Aug (5 and 10 m samples) in group IN showing TS characteristics of group MID, and station HB12 in group MID showing TS characteristics of group IN (Figure 3.3).

Slopes of absorption spectra in relation to pigments

The relationship between PPC: PSC ratios and a_{ph} and a_p slopes were evaluated for ac-9 and QFT spectra for each sample group. In addition, we evaluated the relationship between PPC: PSC ratios and ac-9 a_{pg} slopes, since this can have a broader application when deploying a single ac-9 that measures the total water optical characteristics, solely (e.g. during Sea Soar transects).

To evaluate the relationship between PPC: PSC ratios and normalized absorption slopes, we fit linear regression lines to each group. These results indicate that there are inverse linear relationships between PPC: PSC ratios (g: g) and normalized a_{ph} slopes with $r^2 = 0.61$, 0.66 and 0.94 for groups IN, MID and CR (station CH6 only), respectively ($p< 0.05$ for all; Figure 3.5a, Appendix A). The regression line intercepts became more negative (higher absolute magnitude) from group IN to MID to CR (Figure 3.5a, $p< 0.05$). The regression line slopes between groups were not significantly different ($p>0.05$).

Relationships between PPC: PSC ratios and ac-9 a_p slopes were similar and not significantly different than results found for a_{ph} slopes ($p< 0.05$) for groups MID and CR indicating that a_d had a negligible effect on these relationships (Figure 3.5b, Appendix A). The mean a_d412: a_p412 ratio was < 0.2 for these two groups (range

Figure 3.5. Relationship of photoprotective: photosynthetic carotenoid (PPC: PSC) ratios from HPLC analysis to normalized absorption slopes, slope = (a488-a532)/(a676 · (488-532nm)), from measurements of a) in situ ac-9 phytoplankton absorption coefficients (a_{ph}), b) in situ ac-9 particulate absorption coefficients (a_p), c) in situ ac-9 particulate + dissolved absorption coefficients (a_{pg}), d) discrete sample QFT a_{ph}, and e) discrete sample QFT a_p. Open squares are group IN samples (stations CH1, CP1, CH3). Closed diamonds are group MID samples (stations CP4, CP5, CP4 to CP5 time series, HB stations, MC1, BLM, ST stations). Open triangles are group CR samples with station CH6 only shown in the main plot (for panel a, stations CH6 and CP11 are shown in the inset with CP11 designated by closed triangles). Model 2 linear regression lines are shown. Regression equations are listed in Appendix A.

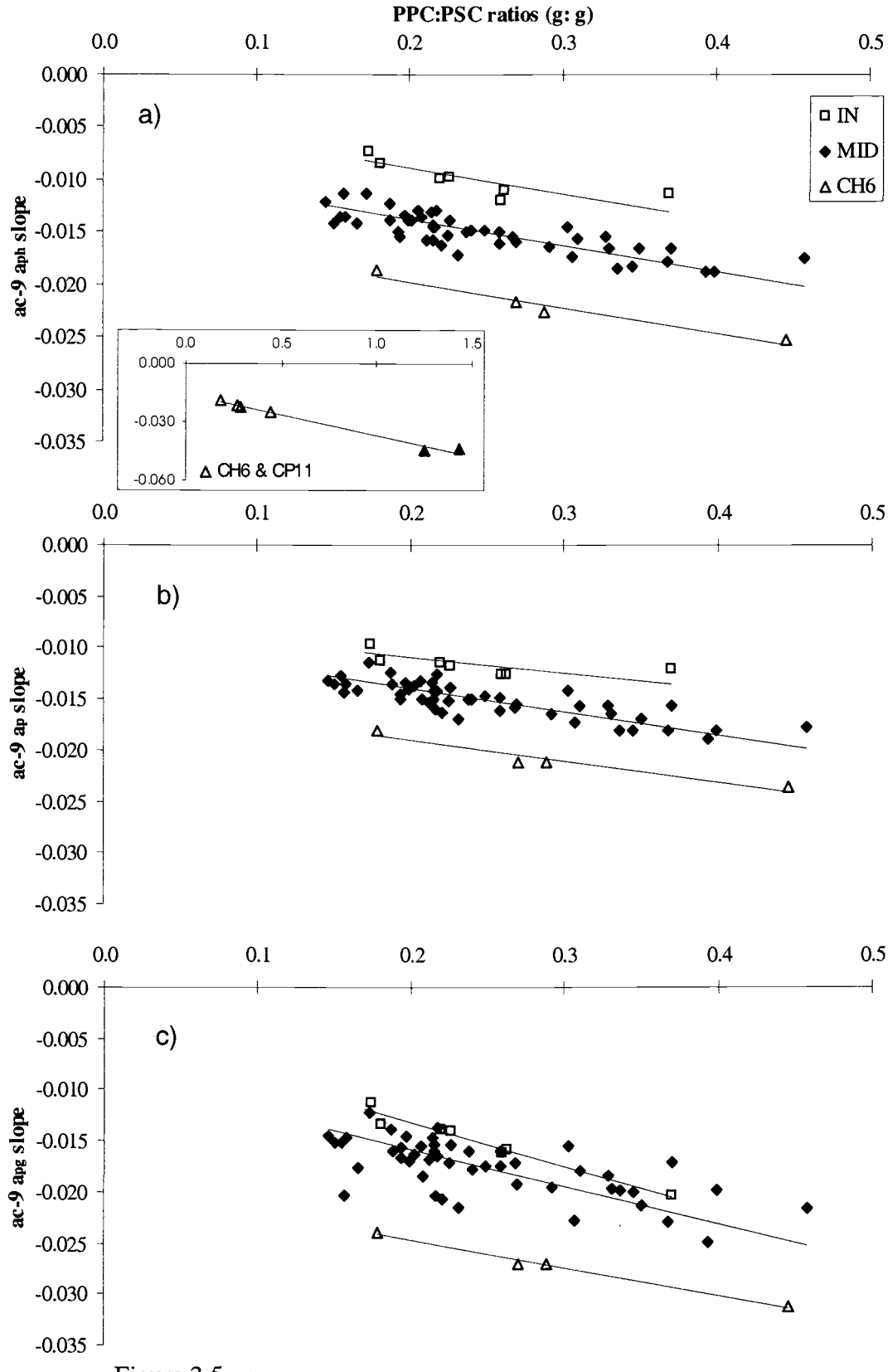
PPC:PSC ratios (g: g)
0.0
0.1
0.2
0.3
0.4
0.5
a)
b)
c)
IN
MID
CH6
ac-9 aph slope
ac-9 ap slope
ac-9 apg slope
0.000
-0.005
-0.010
-0.015
-0.020
-0.025
-0.030
-0.035
0.0
0.5
1.0
1.5
-0.060
CH6 & CP11

Figure 3.5.

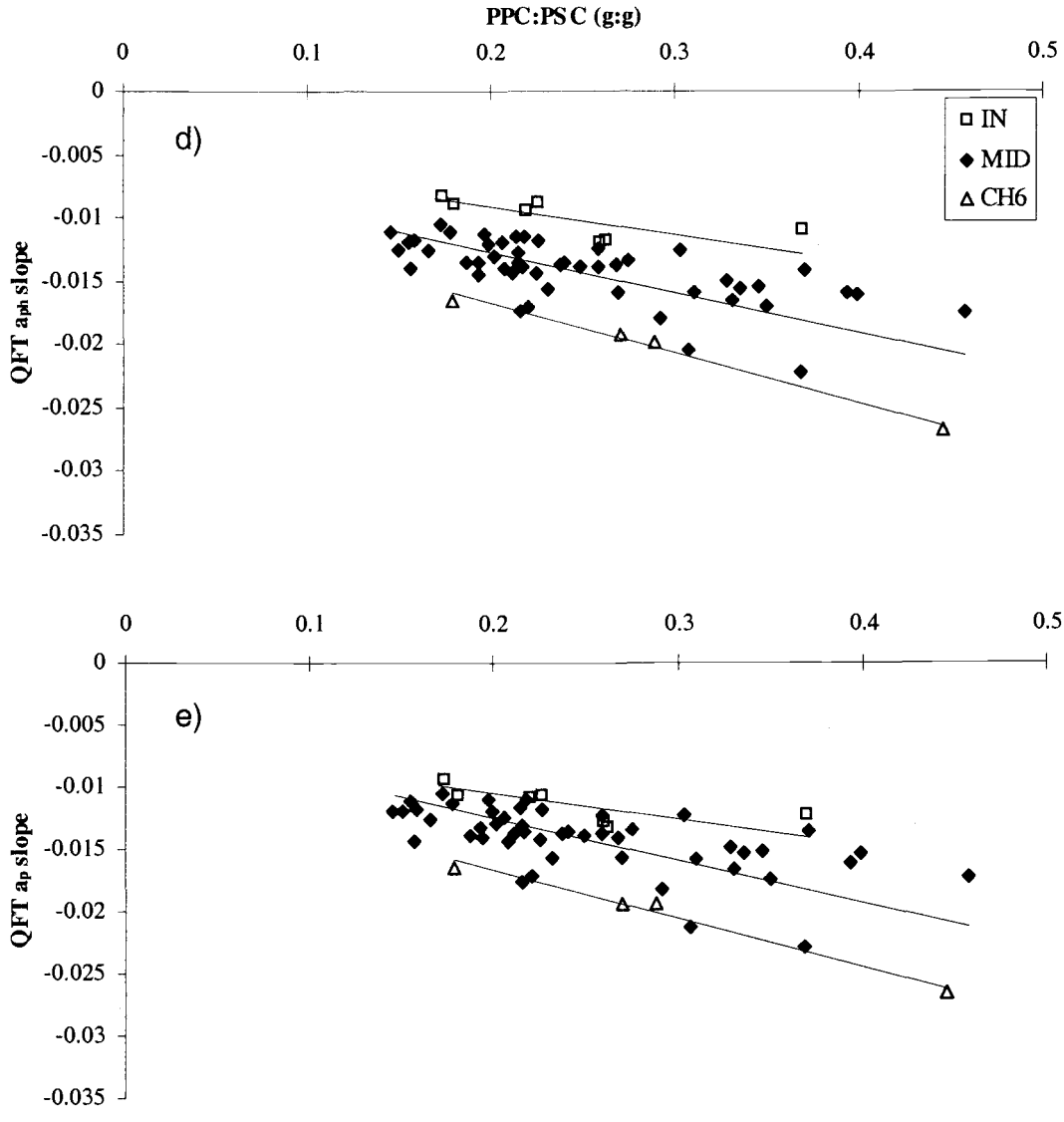

Figure 3.5 continued

0.09 to 0.30). For group IN, the linear regression between PPC: PSC ratios and ac-9 a_p slopes was not significant (p>0.05). However, as seen for groups CR and MID, the regression line slopes and intercepts for the group IN a_p slope/pigment relationship were not significantly different than those seen for the a_{ph} slope/pigment relationship. The high scatter in the a_p slope measurements may have been due to the relatively

high a_d concentrations in group IN (QFT a_d412: a_p412 ranged from 0.3 to 0.5). There were also significant relationships between the PPC: PSC ratios and a_p and a_{ph} slopes for the QFT data although the data in groups IN and MID displayed greater scatter than the ac-9 results (Figure 3.5d and e, Appendix A).

Comparison of the PPC: PSC ratios to ac-9 a_{pg} slopes showed that groups IN and MID could not be distinguished from one another (due to the combined influence of a_d and a_g) although Group CR remained distinct (Figure 3.5c, Appendix A). For group MID, the scatter for the a_{pg} slope relationship was much higher than seen for the a_p and a_{ph} slope relationships, likely due to varying a_g between samples. In contrast, we found a strong relationship between a_{pg} slopes and PPC: PSC ratios ($r^2 = 0.93, p< 0.001$) in East Sound since a_g was essentially constant during the study period and a_d was minimal (Eisner, unpublished results).

Significant inverse relationships were found between PPC: total pigments (mol: mol) and a_{ph} slopes, with r^2 of 0.61, 0.71 and 0.89 for groups IN, MID and CR (station CH6 only), respectively (Appendix A). As was seen for East Sound data (Eisner et al. 2003), the PPC: PSC ratios and PPC: total pigments show similar trends in relation to absorption slopes. We also found linear relationships between PPC: Tchl *a* ratios and ac-9 a_{ph} slopes for all groups combined (excluding station CP11) for Oregon Coast data and for East Sound data ($r^2 = 0.58$ and 0.89, respectively, Figure 3.6). The PPC and Tchl *a* concentrations for Oregon Coast data were strongly linearly related ($r^2 = 0.97$).

Replicates were collected for a third of the surface HPLC samples. For PPC: PSC ratios replicates (two or three replicates per sample) had coefficients of variation

(CV) of 0.8 to 3.3 % with a mean CV of 1.7%. For the co-located water parcels, the derived ac-9 a_{ph} slopes had CVs ranging from 0.29 to 53% with a mean CV of 7.3%. The ac-9 a_p slopes had CVs ranging from 0.33 to 39% with a mean of 6.8%. The ac-9 a_{pg} slopes had CVs ranging from 0.30 to 13% with a mean of 3.3%.

Comparison of a_{ph} slopes and a_{ph} ratios

We evaluated the relationships of PPC: PSC ratios to ac-9 ratios of $a_{ph}440$: $a_{ph}676$ and $a_{ph}488$: $a_{ph}532$ to determine if a simpler calculation than the a_{ph} slope could provide us with a quantitative index of pigment ratios. We found that the PPC: PSC ratios had a stronger correlation with a_{ph} slopes for Group MID ($r^2 = 0.66$) than with $a_{ph}440$: $a_{ph}676$ ratios ($r^2 = 0.47$) (Figure 3.7a, Appendix A). In addition, Group IN could not be adequately distinguished from group MID on the basis of $a_{ph}440$: $a_{ph}676$ ratios ($p>0.05$). Group CR (CH6 only), however, had a strong linear relationship between PPC: PSC ratios and $a_{ph}440$: $a_{ph}676$ ratios and could be distinguished from the other two groups by higher $a_{ph}440$: $a_{ph}676$ values ($p<0.05$). For the $a_{ph}488$: $a_{ph}532$ ratios, group MID showed a weak relationship for PPC: PSC to $a_{ph}488$: $a_{ph}532$ ratios ($r^2 = 0.27$), however, groups IN and CR (CH6 only) did not have significant relationships (Figure 3.7b, Appendix A). In addition, group IN had a negative instead of a positive regression slope, due to the station CH3 sample.

Relationship of a_{ph} slopes to Tchl a, chl c: Tchl a ratios and chl b: Tchl a ratios

The a_{ph} slopes had a weaker linear relationship to Tchl *a* than was found for PPC: PSC ratios for group MID ($r^2 = 0.25$ $p<0.05$) with no significant linear

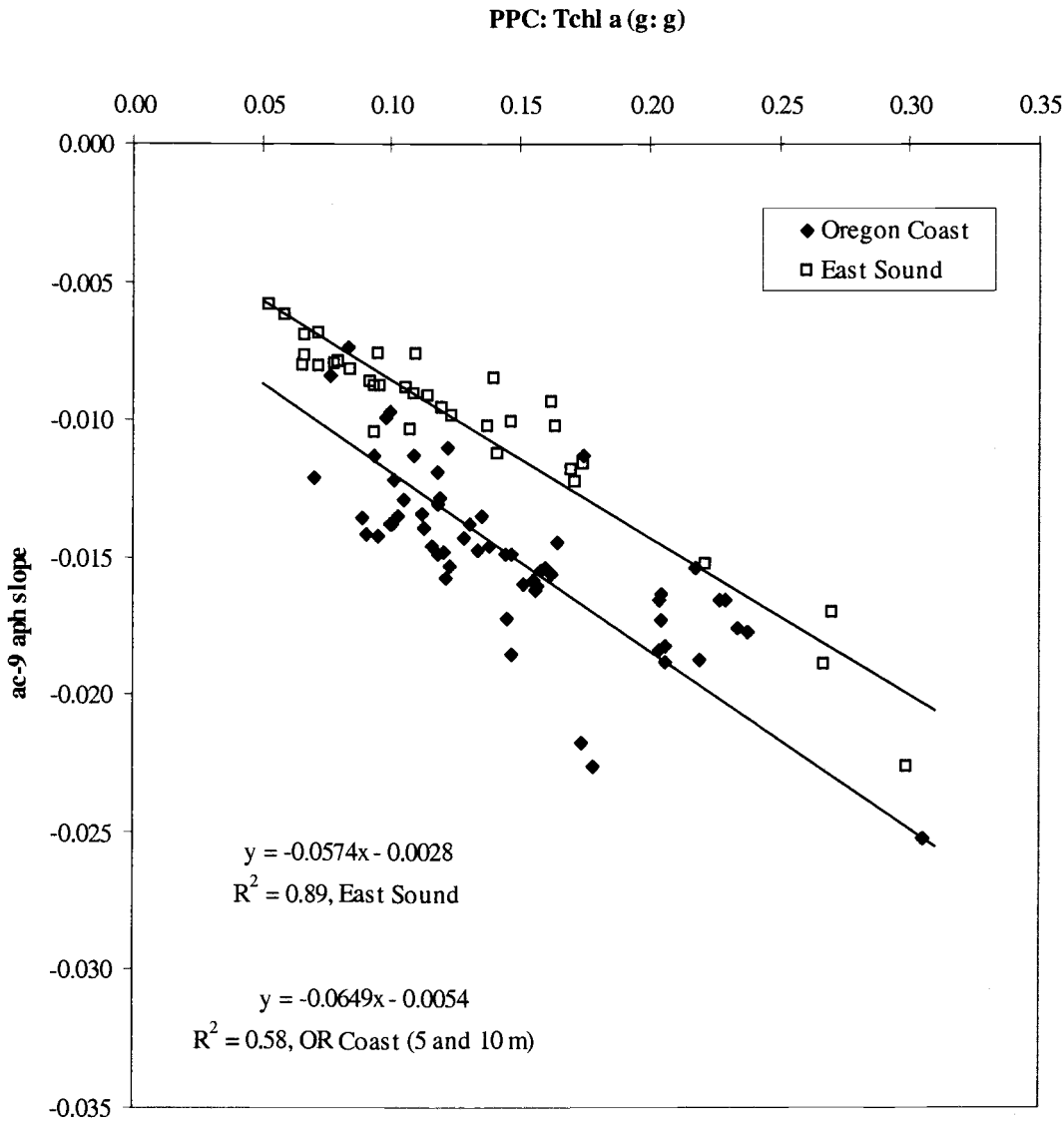

Figure 3.6. Relationship of HPLC derived PPC: Tchl *a* ratios (g: g) to ac-9 a_{ph} slopes for Oregon Coast surface samples (excluding station CP11), closed diamonds, and East sound samples, open squares. Model 2 regressions shown.

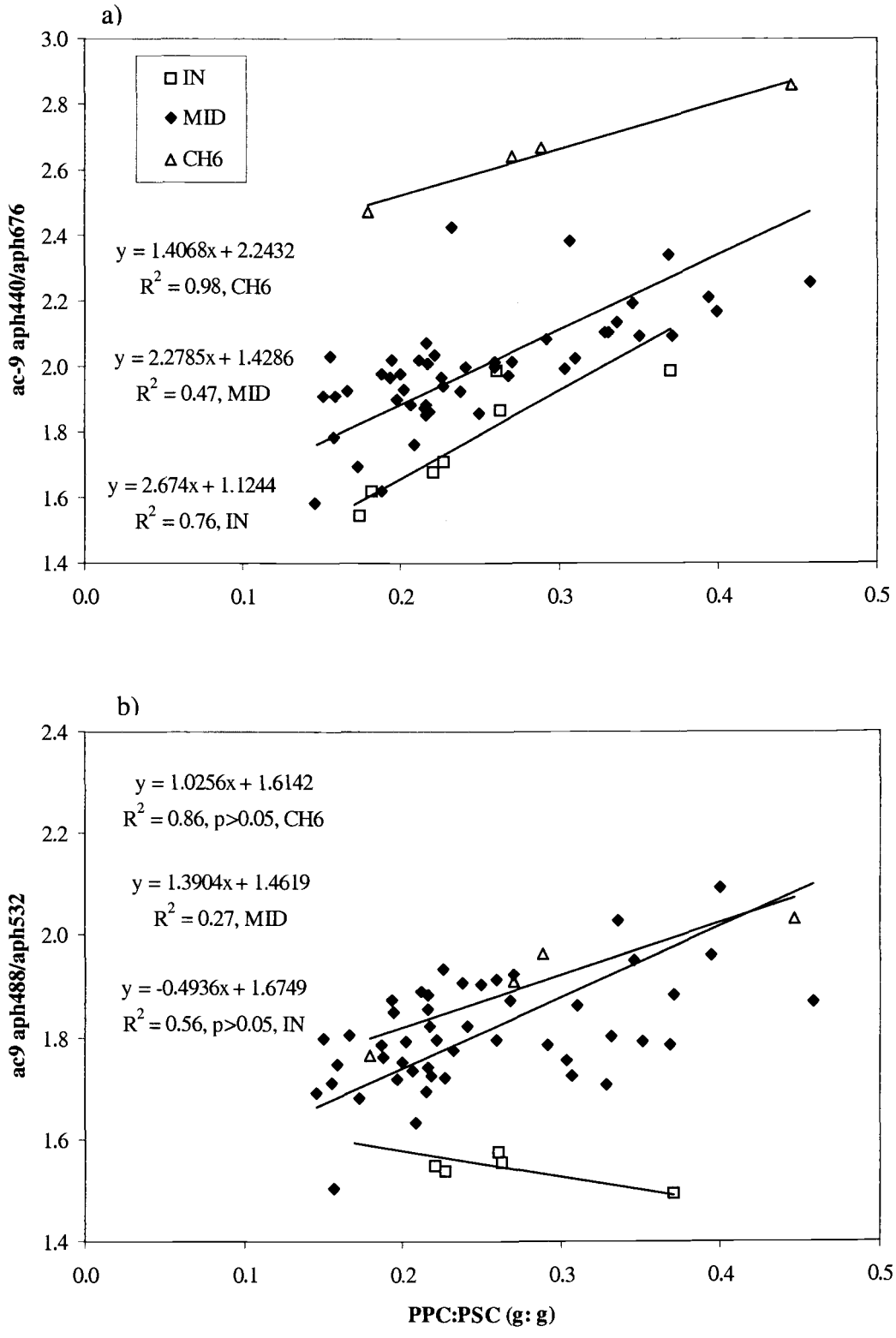

Figure 3.7. Relationship of PPC: PSC ratios from HPLC analysis to a) ac-9 $a_{ph}440$: $a_{ph}676$ ratios and b) ac-9 $a_{ph}488$: $a_{ph}676$ ratios. Symbols as in Figure 5. Model 2 linear regressions are shown.

relationship seen for group IN ($r^2 = 0.18$ $p>0.05$, Appendix A). Conversely, a strong linear relationship with a steep regression line slope was seen for group CR ($r^2 = 0.99$, Appendix A), with steeper slopes seen for samples with very low Tchl *a* concentrations. These results suggest that the a_{ph} slopes are minimally associated with Tchl *a* concentration for the samples in groups IN and MID (across a wide range of Tchl *a* values, 1.8 to 22.0 μg L^{-1}); whereas the a_{ph} slopes appear to be strongly related to Tchl *a* concentration for samples in group CR (with low Tchl *a* values, 0.2 to 1.7 μg L^{-1}).

Comparison of a_{ph} slopes and ratios of chl *c* (*c*1/*c*2 + *c*3): Tchl *a* (g: g) indicated there was no linear relationship for group MID ($r^2 = 0.002$, $p > 0.05$), whereas strong linear associations were seen for groups IN and CR ($r^2 = 0.88$, $p<0.05$ and $r^2 = 0.89$, $p<0.05$, respectively, Appendix A), with steeper slopes seen for samples with lower chl *c*: Tchl *a* ratios. A similar comparison of a_{ph} slopes and ratios of chl *b*: Tchl *a* (g: g) indicated there was a very weak linear relationship for group MID ($r^2 = 0.09$, $p<0.05$) and no significant relationships seen for groups IN and CR once outlier endpoints (CP1, CP11 samples) were removed from the analyses. For all samples combined, except from stations CP1 and CP11, we observed a weak linear relationship between a_{ph} slopes and chl *b*: Tchl *a* ratios ($r^2 = 0.41$, $p<0.05$), with steeper slopes seen for samples with higher chl *b*: Tchl *a* ratios. The very high a_{ph} slopes (-0.04) seen at Station CP11 may have been partially affected by high chl *b*: Tchl *a* ratios (0.2 g: g).

Variations in a_d magnitude and shape

The mean QFT a_d412: a_p412 was 0.21 (similar to that found in East Sound data). The individual samples had a range of a_d412: a_p412 from 0.09 to 0.47 with groups IN, MID, and CR showing means of 0.36, 0.19 and 0.19, respectively. The values of s from exponential fits of mean QFT a_d data were found to be 0.0077, 0.0080 and 0.0089 for groups IN, MID and CR, respectively. Within groups, s ranged from 0.0072 to 0.0086 for group IN, 0.0072 to 0.014 for group MID, and 0079 to 0.011 for group CR.

Effects of packaging on a_{ph} slopes

Package effects result from a combination of intracellular pigment and cell size variations and alter the a_{ph} spectra and slopes. Packaging effects for our data set were estimated using Qa*676 derived from HPLC data and QFT or ac-9 $a_{ph}676$ values. For all samples combined values ranged from 0.39 to > 1 with a median of 0.98 for Qa*676 derived with QFT data and from 0.59 to > 1 with a median of 0.92 for Qa*676 derived from ac-9 data (Appendix A). Qa*676 varied between groups with values for group IN values ranging from 0.65 to 0.99 with a median of 0.74, group CR ranging from 1.6 to 2.5 with a median of 1.6, and group MID ranging from 0.39 to 1.9 with a median of 1.01 for QFT derived data (Table 3.2).

In the Oregon Coast data described in this chapter, comparison of the mean Qa*676 values for each group reveals that there is an increase in the absolute magnitude of the regression line intercepts coincident with a decrease in packaging (increase in Qa*676) (Table 3.2). For groups IN, CR, MID and East Sound data, we

Table 3.2. Phytoplankton pigment ratios, Qa*676 derived from QFT and HPLC data or ac-9 and HPLC data, gamma (hyperbolic coefficient for least squares fit to c_p spectra), ac9 cp440: cp650 ratios and y-intercept of ac9 a_{ph} vs. PPC: PSC relationship. Pigment ratios are g: g. Pigment abbreviations are defined in text.

	Group		PPC	PSC	PPC /PSC	Tchla	fuco /Tchla	fuco /PSC	hex /Tchla	perid /Tchla	zea+ lut /Tchla	allo /Tchla
CH1, CH3, CP1	IN	mean	0.62	2.78	0.24	6.18	0.40	0.88	0.02	0.03	0.00	0.01
		min	0.38	1.03	0.17	2.18	0.34	0.71	0.00	0.01	0.00	0.00
		max	0.94	4.27	0.37	9.60	0.44	0.93	0.03	0.14	0.00	0.01
CH6, CP11	CR	mean	0.22	0.69	0.64	1.03	0.27	0.45	0.26	0.01	0.11	0.04
		min	0.09	0.06	0.18	0.21	0.10	0.31	0.19	0.00	0.02	0.02
		max	0.36	1.42	1.43	1.73	0.52	0.64	0.41	0.02	0.28	0.05
CH6 only		mean	0.28	1.00	0.30	1.43	0.35	0.50	0.28	0.01	0.03	0.03
		min	0.25	0.81	0.18	1.18	0.21	0.31	0.24	0.01	0.02	0.02
		max	0.36	1.42	0.45	1.73	0.52	0.64	0.41	0.02	0.04	0.05
CP11 only		mean	0.10	0.08	1.34	0.23	0.11	0.35	0.20	0.00	0.27	0.04
		min	0.09	0.06	1.25	0.21	0.10	0.34	0.19	0.00	0.27	0.04
		max	0.11	0.09	1.43	0.25	0.12	0.35	0.21	0.01	0.28	0.04
CP45 ts, CP4, CP5		mean	0.81	3.32	0.26	5.67	0.39	0.67	0.11	0.08	0.00	0.01
		min	0.23	1.20	0.16	1.82	0.14	0.22	0.04	0.01	0.00	0.01
		max	2.49	11.17	0.45	18.52	0.54	0.90	0.24	0.37	0.01	0.03
HB, MC1, BLM		mean	1.55	8.03	0.19	13.19	0.55	0.91	0.04	0.01	0.00	0.01
		min	0.59	3.80	0.14	6.62	0.43	0.87	0.02	0.00	0.00	0.00
		max	2.53	12.15	0.26	18.76	0.61	0.94	0.05	0.04	0.00	0.02
ST		mean	1.83	7.15	0.28	12.73	0.51	0.90	0.03	0.01	0.00	0.02
		min	1.45	3.94	0.17	7.17	0.48	0.87	0.02	0.00	0.00	0.01
		max	2.25	11.92	0.40	21.99	0.54	0.94	0.05	0.02	0.01	0.03
CP4, CP5, CP45ts,	MID	mean	1.20	5.16	0.25	8.84	0.45	0.77	0.08	0.05	0.00	0.01
HB, ST, MC1, BLM		min	0.23	1.20	0.14	1.82	0.14	0.22	0.02	0.00	0.00	0.00
		max	2.53	12.15	0.45	21.99	0.61	0.94	0.24	0.37	0.01	0.03

Table 3.2 continued.

	Group		chlb /Tchla	but /Tchla	(diad+ diat) /Tchla	chl c1+c2 /Tchla	Total access pigs /Tchla	Qa* using QFT data	Qa* using ac9 data	gamma =slope of cp spec (412 nm to 650 nm)	cp440/ cp650	y-int. of ac9 aph slope vs PPC: PSC ratos
CH1, CH3, CP1	IN	mean	0.01	0.00	0.08	0.15	0.77	0.76	0.77	0.70	1.32	-0.0039
		min	0.00	0.00	0.06	0.10	0.74	0.65	0.59			
		max	0.02	0.01	0.14	0.18	0.82	0.99	1.55			
CH6, CP11	CR	mean	0.12	0.03	0.09	0.15	1.28	1.90	1.26	1.11	1.62	
		min	0.07	0.00	0.04	0.07	1.01	1.61	1.11			
		max	0.20	0.06	0.18	0.24	1.53	2.52	1.46			
CH6 only		mean	0.09	0.04	0.11	0.18	1.36	1.62	1.26	0.90	1.49	-0.0148
		min	0.07	0.04	0.08	0.16	1.23	1.61	1.11			
		max	0.10	0.06	0.18	0.24	1.53	1.64	1.46			
CP11 only		mean	0.19	0.01	0.05	0.09	1.12	2.46	1.28	1.55	1.88	
		min	0.17	0.00	0.04	0.07	1.01	2.40	1.15			
		max	0.20	0.03	0.06	0.11	1.23	2.52	1.41			
CP45 ts, CP4, CP5		mean	0.04	0.01	0.10	0.17	1.06	1.11	1.00	0.43	1.22	
		min	0.02	0.01	0.05	0.13	0.89	0.39	0.66			
		max	0.09	0.02	0.18	0.22	1.27	1.86	1.70			
HB, MC1, BLM		mean	0.03	0.01	0.08	0.18	1.02	0.97	0.95	0.60	1.33	
		min	0.01	0.00	0.04	0.15	0.89	0.87	0.82			
		max	0.04	0.02	0.13	0.21	1.10	1.18	1.06			
ST		mean	0.03	0.01	0.10	0.17	1.00	0.85	0.87	0.43	1.22	
		min	0.01	0.01	0.05	0.15	0.89	0.56	0.74			
		max	0.03	0.01	0.15	0.18	1.12	1.02	0.96			
CP4, CP5, CP45ts, HB, ST, MC1, BLM	MID	mean	0.04	0.01	0.10	0.17	1.04	1.02	0.96	0.45	1.24	-0.0088
		min	0.01	0.00	0.04	0.13	0.89	0.39	0.66			
		max	0.09	0.02	0.18	0.22	1.27	1.86	1.70			
CP4, nearby stations with high Perid/Tchla		mean								0.31	1.14	
		min										
		max										
East Sound		mean						0.57	0.86			-0.0054
		min						0.35	0.45			
		max						0.87	1.67			

found a strong linear correlation (r^2 = 0.99, p<0.05, Figure 3.8a) between ac-9 derived Qa*676 and the y-intercept for the PPC: PSC ratios vs. ac-9 a_{ph} slope regression. The y-intercepts were also linearly related to gamma, the hyperbolic slope of the cp spectra (an index of particle size distribution) and the total chl *a*: c_p650 (a measure of chl *a* per particle), both of which contribute to packaging variations (Figure 3.8b). The trends in Qa*676 are similar for QFT derived Qa*676 data. Our samples showed a general decrease in QFT Qa*676 with an increase in Tchl *a* in the lower Tchl *a* range (< 5 μg L^{-1}, Figure 3.9) as was seen in Bricaud et al. (1995).

If all packaging levels are considered at once (all groups combined), a weak linear correlation between ac-9 a_{ph} slopes and PPC: PSC ratios is found (p< 0.05; r^2 = 0.36). Likewise, weak linear correlations between ac-9 a_p and a_{pg} slopes and PPC: PSC ratios are also seen (p< 0.05; r^2 = 0.40 and 0.39, respectively). These regressions improve if the absorption slopes within each group are normalized by the mean Qa*676 for that group. For example, the correlation between ac-9 a_{ph} slopes/mean ac-9 Qa*676 and PPC: PSC ratios has an r^2 = 0.58, p< 0.05 (Figure 3.10).

Chemotaxonomic analyses

Bio-marker pigments determined from HPLC analysis provide an indication of the broad taxonomic variations in our sample set. The chemotaxonomic pigments with the highest concentrations relative to Tchl *a* were (in descending order) fuco, 19-hex, zea/lut, and perid (Table 3.2); these pigments were used to assess the relative abundances of diatoms, prymnesiophytes, prokaryotes (*Synechoccocus* or *Prochloroccocus*), and dinoflagellates, respectively (Jeffrey and Vesk 1997). For the

Figure 3.8. Relationships of a) the mean Qa*676 values (derived from ac-9 and HPLC data, see text) and b) the mean Tchl *a*: c_p650 and mean gamma (the slope of the hyperbolic fit to the c_p spectra) for each group to the y-intercept for the linear regression of PPC: PSC ratios and ac-9 a_{ph} slopes for each sample group. Model 2 linear regressions were used to obtain the mean y-intercept values. The solid square indicates East Sound data and solid diamonds are the three Oregon Coast groups (IN, MID, CR (CH6 only)). East Sound model results (Eisner et al., 2003) were determined by removing varying amounts of packaging from the original a_{ph} spectra (assuming original spectra had 100% packaging). The model results between Qa*676 and y-intercepts for the PPC: PSC ratios vs. modeled a_{ph} slopes (with packaging levels of 0%, 50%, 75%) are indicated with open squares. Model 2 linear regressions are shown for panel a, and model 1 linear regressions are shown for panel b.

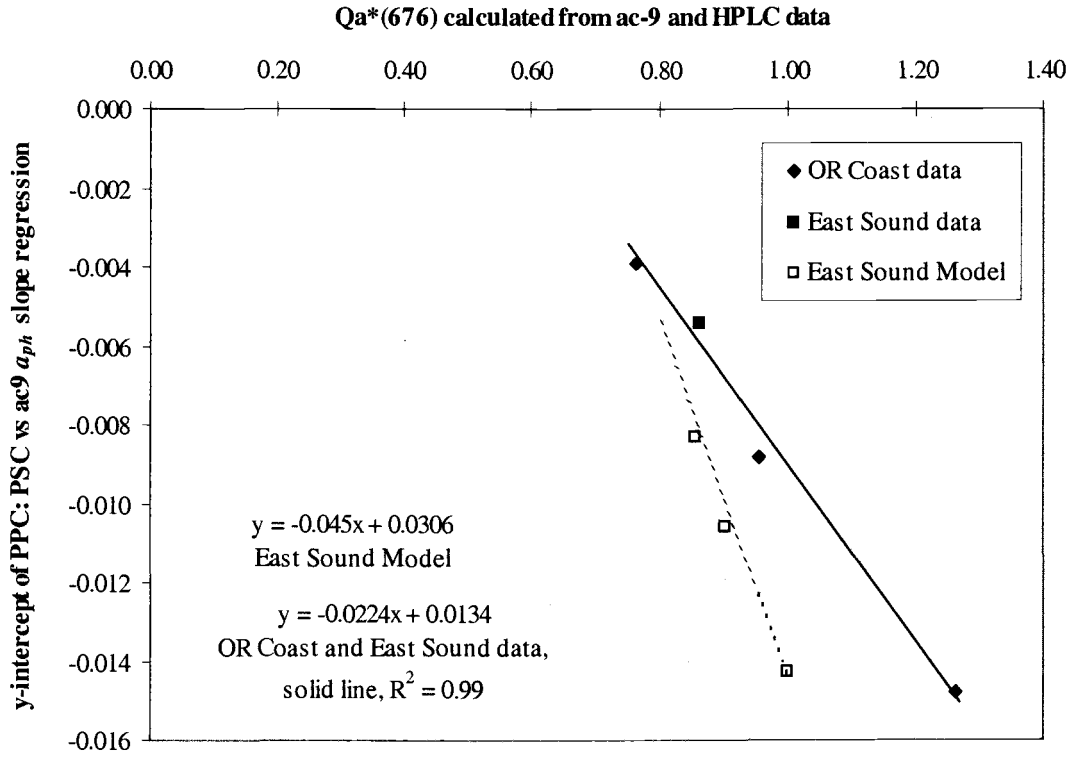
Qa*(676) calculated from ac-9 and HPLC data
y-intercept of PPC: PSC vs ac9 a_{ph} slope regression
0.00
0.20
0.40
0.60
0.80
1.00
1.20
1.40
0.000
-0.002
-0.004
-0.006
-0.008
-0.010
-0.012
-0.014
-0.016
OR Coast data
East Sound data
East Sound Model
y = -0.045x + 0.0306
East Sound Model
y = -0.0224x + 0.0134
OR Coast and East Sound data,
solid line, R^2 = 0.99

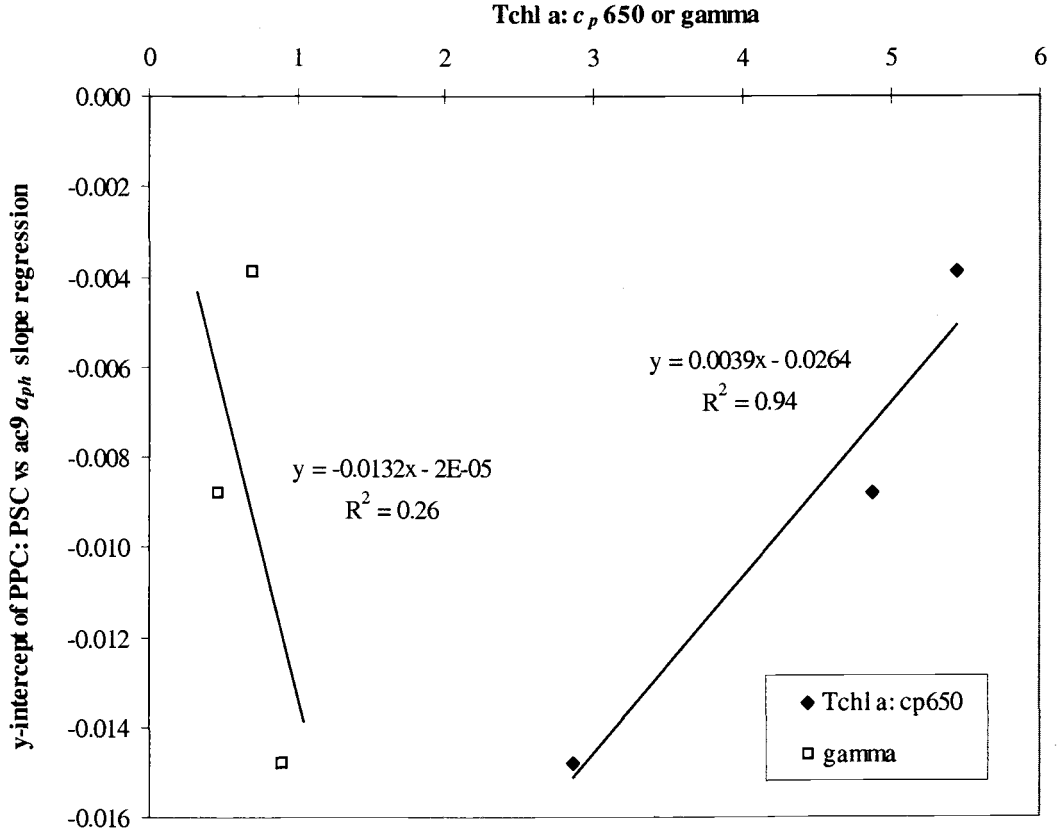
Tchl a: c_p 650 or gamma
y-intercept of PPC: PSC vs ac9 a_{ph} slope regression
0
1
2
3
4
5
6
0.000
-0.002
-0.004
-0.006
-0.008
-0.010
-0.012
-0.014
-0.016
y = 0.0039x - 0.0264
R^2 = 0.94
y = -0.0132x - 2E-05
R^2 = 0.26
Tchl a: cp650
gamma

Figure 3.8.

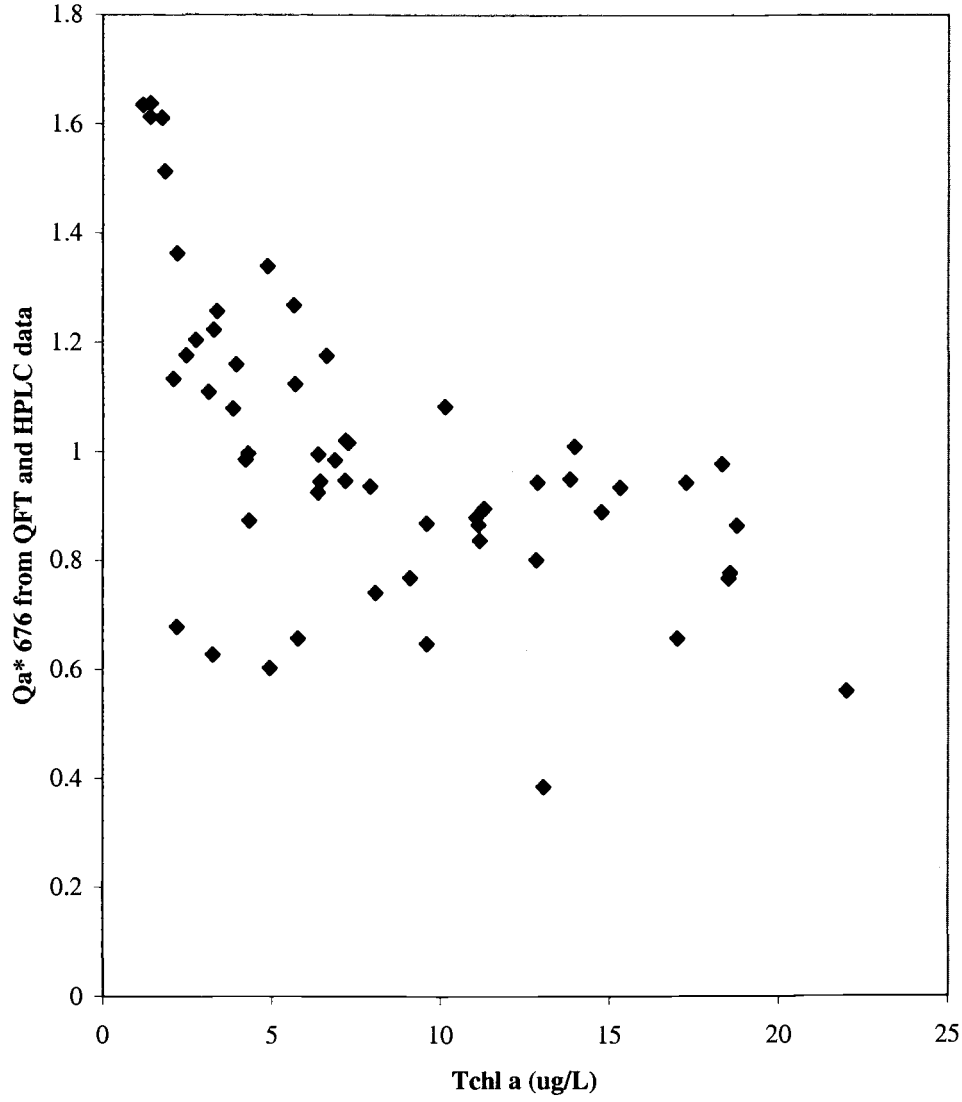

Figure 3.9. Relationship of Tchl *a* (μg L^{-1}) from HPLC analyses to the Qa*676 values (derived from QFT and HPLC data, see text) for all Oregon Coast surface samples.

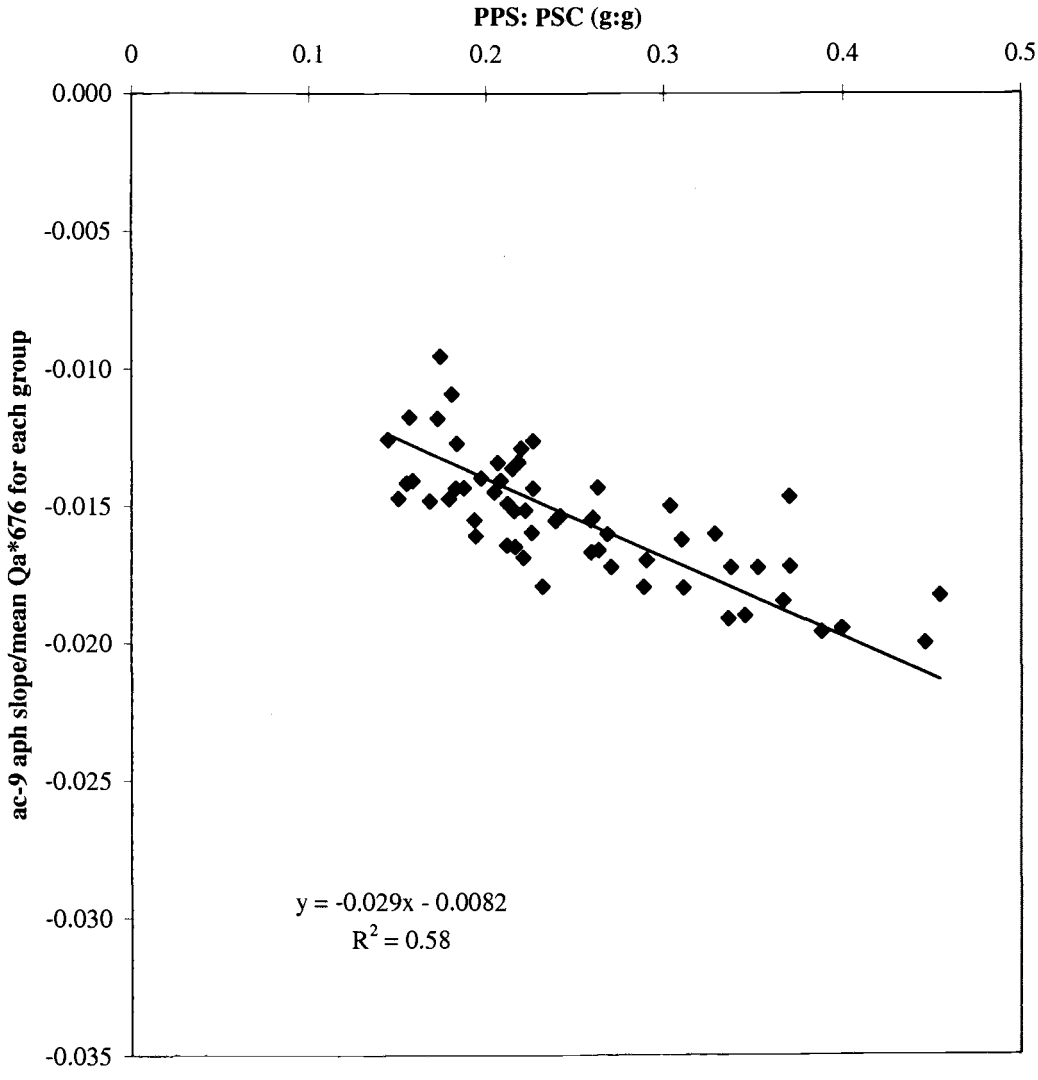

Figure 3.10. Relationship of the PPC: PSC ratios to ac-9 a_{ph} slope values divided by the mean Qa*676 (derived from ac-9 and HPLC data) for each group for all surface samples (except station CP11). A model 2 linear regression is shown.

majority of samples, fuco: Tchl *a* ratios were an order of magnitude higher than other biomarkers indicating that diatoms were the most abundant taxonomic group (Table 3.2).

For group IN, ratios of fuco: PSC were high (> 0.9, Table 3.2), with the exception of station CP1 where perid: Tchl *a* ratios were almost half the magnitude of fuco: Tchl *a* ratios at 10 m depths (fuco: PSC = 0.7). These results indicate that for most samples in group IN, diatoms were by far the dominant species type. Relative to the other groups, group CR had the highest 19-hex: Tchl *a*, zea/lut: Tchl *a*, allo: Tchl *a*, 19-but: Tchl *a*, chl *c*3: Tchl *a* and chl *b*: Tchl *a* ratios and lowest fuco: Tchl *a* ratios (fuco: PSC ratios = 0.3 to 0.6, Table 3.2), although there were some differences between stations. At station CH6 fuco: Tchl *a* and 19-hex: Tchl *a* had the highest ratios, whereas at station CP11 zea/lut: Tchl *a* had the highest ratios followed by 19-hex: Tchl *a*, and then fuco: Tchl *a*. These data suggest that prymnesiophytes (indicated by both 19-hex and 19-but) and diatoms and were dominant at station CH6 and that prokaryotes, followed by prymnesiophytes then diatoms were dominant at station CP11. Cryptophytes (allo: Tchl *a*) made minor contributions at both stations.

Samples in the MID group were collected over a longer time span (12 days) and a broader spatial area than the other groups. This group had the highest fuco: Tchl *a*, perid: Tchl *a*, and (chlc1/c2): Tchl *a* compared to other groups (Table 3.2). Overall, fuco: Tchl *a* ratios were highest followed by perid: Tchl *a* and 19-hex: Tchl *a*. We found taxonomic differences between samples within the MID group as indicated by the wide range of fuco: PSC ratios (0.22 to 0.94). Samples from stations CP4, CP5, and the CP45 time series had higher perid: Tchl *a* ratios (occasionally over twice as

high as fuco: Tchl *a*), higher 19-hex: Tchl *a* ratios and lower fuco: Tchl *a* than observed for the remaining group MID samples (from the HB, MC1, BLM and ST stations). These pigment ratios indicate that stations CP4, CP5, and the CP45 time series was dominated by diatoms, dinoflagellates and prymnesiophytes with relative importance being station specific, whereas, at the remaining stations, diatoms were always prevalent.

We also evaluated the ratios of total accessory pigments (which include chl *b*, chl *c*1/*c*2, chl *c*3, all carotenoids, all derivatives of chl *b*, chl *c* and carotenoids) to Tchl *a* (Appendix C). These data show that ratios of accessory pigments: Tchl *a* are highest in group CR (mean 1.28 g: g) followed by group MID (mean 1.03 g: g) then group IN (mean 0.77 g: g).

Size estimations based on c_p spectra

Comparisons of the exponent, γ, from the hyperbolic fit to the c_p spectra indicate variations in the relative PSD which suggest there was a greater contribution by large particles in groups IN and MID compared to group CR (Table 3.2). The HB-12 sample was excluded from these analyses since its c_p spectra could not be adequately fit with the hyperbolic function (i.e. γ was less than zero). Ratios of c_p440: c_p650 (Kitchen et al. 1982) and γ calculations provided comparable results in the estimation of relative PSD ($r^2 = 0.98$ between these two indices, excluding HB12 sample).

Discussion

Applicability of the a_{ph} and a_p slope and PPC: PSC ratio relationships

We found a significant linear correlation between the ac-9 (and QFT) a_{ph} slopes and the HPLC determined PPC: PSC ratios (or PPC: total pigment ratios) within sample groups representing different water mass types (Figure 3.5). This result extends the correlation between pigment ratios and a_{ph} slopes seen in East Sound (Eisner et al. 2003), to Oregon coastal waters. The phytoplankton assemblages sampled in East Sound and off the Oregon coast were dominated by diatoms and other chromophytes, with the exception of station CP11, the furthest offshore station sampled during our Oregon survey. The linear regression y-intercepts were significantly different for each group, although regression line slopes were similar. The group IN regression was similar to the regression for East Sound samples, suggesting similarities in the variation in the shape of the absorption spectra with changes in PPC: PSC ratios, possibly due to similarities in packaging.

We also found linear relationships between PPC: PSC ratios and a_p slopes that were not significantly different than seen for PPC: PSC ratios and a_{ph} slopes for mid-shelf (MID) and Columbia River plume (CR) groups, since these samples had low a_d: a_p ratios (a_d412: a_p412 = 0.09 to 0.3 with a mean of 0.21). Given the estimated spectral slopes, s (~0.008 to 0.009 for 440 to 676 nm), and low a_d values for our Oregon Coast samples, we do not expect the regression lines for PPC: PSC ratios vs. a_p slopes to vary substantially from the regression for PPC: PSC ratios vs. a_{ph} slopes. In East Sound, at low a_d magnitude (0.21 a_d 412: a_p412), the shape of the a_d spectra

had little effect on the PPC: PSC to a_p slope relationship for s between 0.0065 and 0.012 (see Figure 5b in Eisner et al. (2003), compare the dotted line (s=0.0065) and diamonds). For groups located near shore (IN) we did not find a significant linear relationship between PPC: PSC ratios and a_p slopes, possibly due to the higher a_d: a_p ratios (a_d412: a_p412 = 0.3 to 0.5) in these samples.

Our results indicate that in waters with low a_d, the a_p slope/pigment relationship can serve as a proxy for the a_{ph} slope/pigment relationship. Under these conditions once a relationship between a_p and PPC: PSC is determined for a particular water mass, we could use a_p spectra (derived solely from in situ ac-9 measurements) to estimate the PPC: PSC ratios within that water mass. Obviously, in waters with higher detrital contributions, a_d must be adequately estimated (using discrete water samples and/or modeling (Roesler et al, 1989; Cleveland and Perry, 1994) and then removed from the a_p spectra before a relationship between absorption spectra (using a_{ph} data) and PPC: PSC ratios can be adequately derived and used to map spatial or temporal changes in PPC: PSC ratios.

Taxa containing chl *c* comprised the bulk of the sampled phytoplankton assemblages (Appendix A) and therefore the a_{ph} slope and PPC: PSC relationships were primarily derived using chromophytes. The relative concentration of chl *c* (chl *c*: Tchl *a* ratios) were linearly related to a_{ph} slopes in groups IN and CR suggesting that for these groups, the a_{ph} slope variation may be partially due to variations in the chromophyte taxonomic composition.

In contrast, it is possible that the relationship between PPC: PSC and a_{ph} slopes may be invalidated by high relative abundances of species containing chl *b*. For

example, samples from Crater Lake, Oregon, that had high relative concentrations of chl *b* (*chl b*: T chl *a* ~ 0.35 g: g) had steeper a_{ph} slopes, even though PPC: PSC ratios were lower, relatively (Eisner unpublished data). Thus, the relationship found for ac-9 a_{ph} slopes and HPLC pigment ratios may not be applicable in open ocean areas when chlorophytes comprise a sizeable fraction of the phytoplankton biomass. In addition, in areas with low phytoplankton biomass (< 0.2 μg L^{-1} chl *a*), estimation of ac-9 $a_{ph}676$ approaches the noise level of the instrument (0.005 m^{-1}). Thus, it can be difficult to reliably calculate a_{ph} slopes (with $a_{ph}676$ in the denominator) from ac-9 data in these low biomass or chl *b* rich environments. An estimation of variations in the shape of the absorption spectra using shorter wavelengths of light (blue to green region of the visible spectrum where values are higher) and/or methods that do not normalize to 676 nm may be more successful under low biomass conditions.

Package effects, cell size and chemotaxonomic indicators

Another significant result of this study was the strong correlation between the Qa*676 values, a measure of pigment packaging, and the regression line intercepts for PPC: PSC ratio vs. a_{ph} slope relationships for groups IN, MID, CR (CH6) and East Sound data (Figure 3.8). These results suggest that samples in group IN had the highest amount of packaging, close to that seen for East Sound, followed by group MID and lastly by group CR.

Many of the Qa*676 values were higher than 1, the theoretical limit for this ratio (Morel and Bricaud). Qa*676 values > 1 may be due to the presence of phycobilipigments in the samples that are not detected with our HPLC procedure,

missing or lost pigments due to incomplete extraction, and/or uncertainty in the pathlength amplification factor, β, at low optical density (Bricaud et al, 1995), or scattering errors in the ac-9 data.

Eisner et al. (2003) evaluated the variations in packaging on East Sound ac-9 a_{ph} slopes by comparing measured a_{ph} slopes to modeled a_{ph} slopes derived from a_{ph}' (unpackaged) data using varying percentages of packaging. Linear relationships were seen between a_{ph} slopes and PPC: PSC ratios for all packaging levels. These model results also indicated that a decrease in packaging increased the absolute magnitude of the regression line intercept, but did not change the regression line slope appreciably for the PPC: PSC ratios to a_{ph} slope relationship (Eisner et al., 2003, their Fig 6).

We attempted to find a common packaging relationship between PPC: PSC ratios and a_{ph} slopes for the complete Oregon surface data set. As described in the results, the regression between PPC: PSC ratios and a_{ph} slopes for all three groups combined (IN, MID, CR (CH6 only)) is stronger if the a_{ph} slopes in each group are normalized by the mean Qa*676 for that group (r^2 = 0.58 for normalized compared to r^2 = 0.36 for un-normalized data). For comparison, we evaluated the relationship between a_{ph} slopes normalized to mean Qa*676 and PPC: PSC ratios for East Sound data. This comparison indicates that the regression lines slope is significantly different for Oregon Coast data compared to East Sound data (p<0.05) for ac-9 a_{ph} slopes/mean Qa*676 and PPC: PSC ratios (Figure 3.11 a). However, if the mean Qa*676 values for the East sound samples are reduced by 10%, or the Oregon Coast mean Qa*676 for each group are increased by 10% (by reducing or increasing the

Figure 3.11. a) Relationship of the PPC: PSC ratios to ac-9 a_{ph} slope values divided by the mean Qa*676 (derived from ac-9 and HPLC data) for each group for Oregon Coast data (solid diamonds) compared to East Sound data (open squares), and b) same as panel a except the Qa*676 values (used to determine the mean Qa*676) were reduced by 10% for the East Sound data (see text). Oregon station CP11 excluded from these analyses. Model 2 linear regressions are shown.

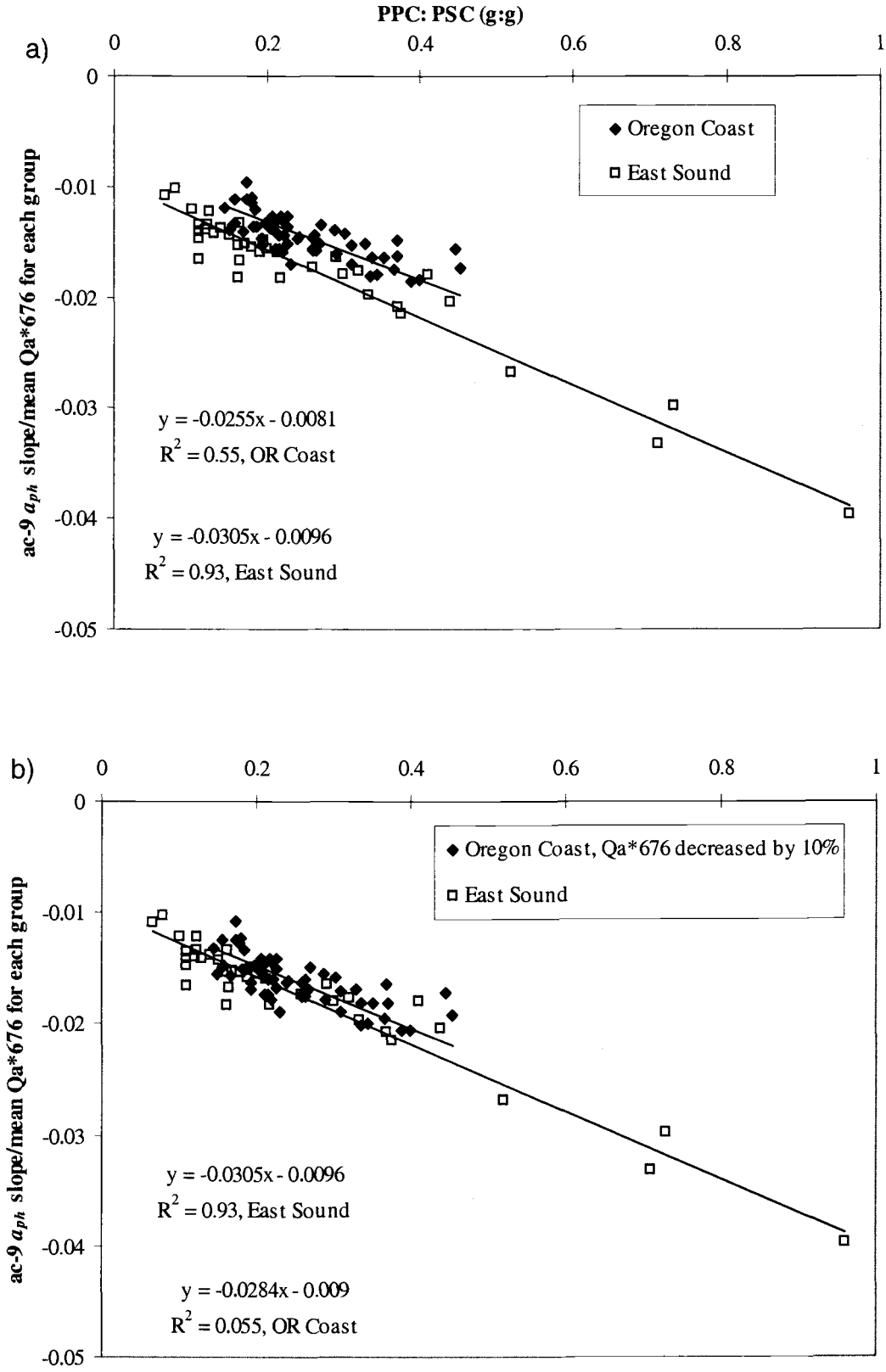
a)
PPC: PSC (g:g)
0
0.2
0.4
0.6
0.8
1
ac-9 a_{ph} slope/mean Qa*676 for each group
-0.01
-0.02
-0.03
-0.04
-0.05
Oregon Coast
East Sound
y = -0.0255x - 0.0081
R^2 = 0.55, OR Coast
y = -0.0305x - 0.0096
R^2 = 0.93, East Sound
b)
Oregon Coast, Qa*676 decreased by 10%
East Sound
y = -0.0305x - 0.0096
R^2 = 0.93, East Sound
y = -0.0284x - 0.009
R^2 = 0.055, OR Coast

Figure 3.11.

QFT a_{ph} values by 10%, accordingly), the relationships found for Oregon Coast and East Sound samples are not significantly different ($p< 0.05$) (Figure 3.11 b). The observed differences can be offset by a 10% adjustment in the a_{ph}, values obtained from the HPLC spectral reconstruction or in the ac-9 a_{ph} values estimated from the ac-9 and QFT data. While we are confident that the shapes of the observed spectra are accurate within the measurement error of the technique, a small magnitude offset in the ac-9 a_{ph} spectra (derived from ac-9 a_p spectra and QFT a_d spectra) or the HPLC pigment determinations is likely.

As shown in the results, there was a stronger correlation seen for PPC: Tchl *a* and a_{ph} slopes than for PPC: PSC ratios and a_{ph} slopes, for all groups combined (Figure 3.6). Thus the a_{ph} slope parameter can provide an estimate of PPC: Tchl *a* ratios, although the relationship is generally not as strong as that seen for a_{ph} slopes and PPC: PSC ratios for individual groups (CR, MID, IN). The advantage of the PPC: Tchl *a* ratio is that PPC concentrations may be predicted from ac-9 data if chl *a* concentrations are known (or estimated from ac-9 $a_{ph}676$ values) and an adequate relationship has been established between ac-9 a_{ph} slopes and PPC: Tchl *a* ratios.

Relative PSD estimates from changes in γ (exponent for hyperbolic fit to the c_p spectra) suggest that the lower package effects observed in group CR were at least partially a result of smaller phytoplankton cell size in group CR compared to group MID (and possibly IN). The higher concentration of detrital particles in Group IN may have contributed to our estimates of γ for this group. In addition, colonial (chain-forming) diatoms, which commonly occur in coastal waters (Kokkinakis and Wheeler

1987), will have large particles sizes, although the cell sizes may be small. Thus, it is possible that phytoplankton cell size may not be adequately described by γ, alone.

Pigments have been used to estimate cell sizes in field assemblages by serving as biomarkers for specific taxonomic groups with characteristic cell diameters (Vidussi et al, 2001). Zeaxanthin is associated with cyanobacteria and prochlorophytes (< 2 μm), total chl *b* with green flagellates and prochlorophytes (< 2 μm), 19-hex and 19-but with chromophyte nanoflagellates (2-20 μm), allo with cryptophytes (2-20 μm), fuco with diatoms (> 20 μm) and perid with dinoflagellates (> 20 μm). Our analysis of HPLC pigments indicated that group CR had high contributions of zea/lut, 19-hex, and fuco whereas groups IN and MID were dominated by fuco, primarily.

The γ values and relative abundances of pigment biomarkers in our sample groupings are consistent with the size class pigment relationships found by Vidussi et al. (2001). For example, station CP11 in group CR had the highest γ and the highest zea/lut: Tchl *a* suggesting that small prokaryotic species were prevalent in these samples. Station CH6, the other station in group CR, had the second highest γ of all stations and had the highest 19-hex: Tchl *a* suggesting that small prymnesiophytes were important. At the other extreme, γ was lowest suggesting a greater contribution from large particles in group MID station CP4, and nearby stations (within 3.3 km due west). These samples had the highest perid: Tchl *a* indicating that large dinoflagellates, as well as diatoms, were important constituents of the phytoplankton assemblage in this location. Further confirmation of these relative size differences between groups would be achieved by inspection of phytoplankton taxonomic samples (whole water, preserved) and/or Coulter Counter analyses.

Future applications

Our results can contribute to the derivation of a bio-optical model using irradiance, packaging and PPC: total pigment ratios, absorption spectra and Tchl *a* to estimate the amount of energy absorbed in situ by phytoplankton. Such a model could explore the dynamics of quantum efficiency shifts between heat, photosynthesis, and fluorescence. Future work should compare the spatial gradients in phytoplankton photophysiology and taxonomy derived from optical and discrete sample analyses with environmental parameters such as nutrient concentration, light exposure and water column stratification. In situ optical instruments such as an ac-9 can collect data over spatial and temporal scales similar to physical oceanography (T, S) sensors. Therefore, the methods described in this paper can be used to compare fine scale variations in factors such as phytoplankton size distribution and pigmentation in relation to hydrographic properties, and provide an integrated physical/biological approach to study phytoplankton ecology.

Acknowledgments

This research was supported by a Coastal Advances in Ocean Transport (COAST) grant (#OCE-9907854) from the National Science Foundation. We thank members of the Ricardo Letelier lab group for water sample collection and particulate absorption analyses, Burke Hales for hydrographic data, Jack Barth for contour maps of chlorophyll *a* and temperature, Chris Wingard and Russ Desiderio for help with data processing, and Margaret Sparrow for advice and support with HPLC analysis.

References

Barnard A., W.S. Pegau and J.R. Zaneveld. 1998. Global relationships of the inherent optical properties of the oceans. J. Geophys. Res. **103**: 24955-24968.

Barth, J.A., Pierce, S.D. and R.L. Smith. 2000. A separating coastal upwelling jet at Cape Blanco, Oregon and its connection to the California Current system. Deep Sea Res. II. 783-810.

Bidigare, R.R, M.E. Ondrusek, J.H. Morrow, and D.E. Kiefer. 1990. In vivo absorption properties of algal pigments. SPIE Ocean Optics X. **1302**: 290-302.

Boss E., W.S. Pegau, W.D. Gardner, J.R. Zaneveld, A.H. Barnard, M.S. Twardowski, G.C. Chang and T.D. Dickey. 2001. Spectral particulate attenuation and particle size distribution in the bottom boundary layer of a continental shelf. J. Geophys. Res. **106**: 9509-9516.

Bricaud, A., M. Babin, A. Morel, and H. Claustre. 1995. Variability in the chlorophyll-specific absorption coefficients of natural phytoplankton: Analysis and parameterization. J. Geophys. Res. **100**: 13321-13332.

Bricaud, A., C. Roesler and R.V. Zaneveld. 1995. In situ methods for measuring the inherent optical properties of ocean waters. Limnol. Oceanogr. **40**: 393-410.

Ciotti, A.M., M.R. Lewis and J.J. Cullen. 2002. Assessment of the relationships between dominant cell size in natural phytoplankton communities and the spectral shape of the absorption coefficient. Limnol. Oceanogr. **47**: 404-417.

Cleveland, J.S., and M.J. Perry. 1994. A model for partitioning absorption into phytoplanktonic and detrital components. Deep Sea Res. Part I. **41**: 197-221.

Corwith, H.L. and P.A.Wheeler. 1987. El nino related variations in nutrient and chlorophyll distributions off Oregon. Progr. Oceanogr. **54**: 361-380.

Diehl, P. and H. Haardt. 1980. Measurement of the spectral attenuation to support biological research in a "plankton tube" experiment. Oceanol. Acta. **3**: 89-96.

Duysens, L.N.M. 1956. The flattening of the absorption spectrum of suspensions, as compared to that of solutions. Biochim. Biophys. Acta. **19**: 1-12.

Eisner, L.B., M.S. Twardowski, T.J. Cowles and M.J. Perry. 2003. Resolving phytoplankton photoprotective: photosynthetic carotenoid ratios on fine scales using in situ spectral absorption measurements. Limnol. Oceanogr. **48**: 632-646.

Hickey, B. M. 1989. Patterns and processes of circulation over the Washington continental shelf and slope. In M.R. Landry & B.M. Hickey (eds.), Coastal Oceanography of Washington and Oregon (p. 607). Elsevier Oceanography Series, 47. Elsevier.

Hill, J.K. and P.A. Wheeler. 2002. Organic carbon and nitrogen in the northern California current system: comparison of offshore, river plume, and coastally upwelled waters. Progr. Oceanogr. **53**: 369-387.

Huyer, A. A comparison of upwelling events in two locations: Oregon and northwest Africa. J. Mar. Res. **34**: 531-546.

Jeffrey, S.W., and M. Vesk. 1997. Introduction to marine phytoplankton and their pigment signatures, p.37-84. *In:* S.W. Jeffrey, R.F. Mantoura, and S.W. Wright [eds.], Phytoplankton pigments in oceanography: guidelines to modern methods. Unesco Publishing.

Kirk, J.T. 1994. Light and photosynthesis in aquatic ecosystems. 2nd ed. Cambridge Univ. Press.

Kishino, M., M. Takahashi, N. Okami, and S. Ichimura. 1985. Estimation of the spectral absorption coefficients of phytoplankton in the sea. Bull. Mar. Sci. **37**: 634-642.

Kitchen, J.C., J.R. Zaneveld and H.Pak. 1982. Effect of particle size distribution and chlorophyll content on beam attenuation spectra. Applied Optics. **21**: 3913-3918.

Kokkinakis, S.A. and P.A. Wheeler. 1987. Nitrogen uptake and phytoplankton growth in coastal upwelling regions. Limnol. Oceanogr. **32**: 1112-1123.

Mitchell, B.G., and D.A. Kiefer. 1988. Chlorophyll *a* specific absorption and fluorescence excitation spectra for light-limited phytoplankton. Deep Sea Res. **35**: 639-663.

Morel, A. and A. Bricaud. 1981. Theoretical results concerning light absorption in a discrete medium, and application to specific absorption of phytoplankton. Deep Sea Res. **28A**:1375-1393.

Pegau, W.S., D. Gray, and J.R.V. Zaneveld. 1997. Absorption and attenuation of visible near-infrared light in water: dependence on temperature and salinity. Applied Optics. **36**: 6035-6046.

Press, W.H., B.P. Flannery, S.A. Teukolsky, and W.T. Vetterling. 1986. Numerical Recipes: The Art of Scientific Computing. Cambridge University Press, Cambridge.

Roesler, C.S., M.J. Perry, and K.L. Carder. 1989. Modeling in situ phytoplankton absorption form total absorption spectra in productive inland marine waters. Limnol. Oceanogr. **34**: 1510-1523.

Small, L.F. and D.W. Menzies. 1981. Patterns of primary productivity and biomass in a coastal upwelling region. Deep Sea Res. **28A**: 123-149.

Twardowski, M.S. and P.L. Donaghay. 2002. Photobleaching of aquatic and dissolved materials: Absorption removal, spectral alteration and their relationship. J. Geophys. Res. **107**, no. 0, 10.1029/1999JC000281.

Twardowski, M.S., J.M. Sullivan, P.L. Donaghay, and J.R.V. Zaneveld. 1999. Microscale quantification of the absorption by dissolved and particulate material in coastal waters with an ac-9. J. Atmos. Ocean. Technol. **16**: 691-707.

Vidussi, F., H. Claustre, B.B. Manca, A. Luchetta and J. Marty. 2001. Phytoplankton pigment distribution in relation to upper thermocline circulation in the eastern Mediterranean Sea during winter. J. Geophys. Res. **106**: 19,939-19,956.

Wright, S.W., and S.W. Jeffrey. 1997. High-resolution HPLC system for chlorophylls and carotenoids of marine phytoplankton, p.327-341. *In:* S.W. Jeffrey, R.F. Mantoura, and S.W. Wright [eds.], Phytoplankton pigments in oceanography: guidelines to modern methods. Unesco Publishing.

Yentsch, C.S. 1962. Measurement of visible light absorption by particulate matter in the ocean. Limnol. Oceanogr. **7**: 207-217.

Zaneveld, J.R.V., J.C. Kitchen, and C.C. Moore. 1994. Scattering error correction of reflecting tube absorption meters. Proc. SPIE Int. Soc. Opt. Eng. **12**: 44-55.

CHAPTER 4

SPATIAL VARIATIONS IN PHYTOPLANKTON PIGMENT RATIOS AND OPTICAL PROPERTIES IN RELATION TO ENVIROMENTAL GRADIENTS IN OREGON COAST WATERS

Lisa B. Eisner and Timothy J. Cowles

Abstract

In situ optics and hydrographic measurements, along with discrete samples for calibration, were used to assess spatial variations in phytoplankton characteristics and taxonomic composition (pigment ratios, relative particle size distribution, chlorophyll *a* (chl *a*) concentration, and chl *a* per particle) in Oregon coastal waters during August 2001. The relationships between environmental parameters (nutrients, light, temperature) and photoprotective: photosynthetic carotenoid (PPC: PSC) ratios and optical parameters were also evaluated. We found significant linear relationships between ratios of photoprotective: photosynthetic carotenoids (PPC: PSC) and absorption spectra slopes (a_{ph} slopes, Eisner et al. 2003) for surface samples grouped by location, date and water mass characteristics (chapter 3). We observed high spatial variability (horizontal and vertical) in the phytoplankton photophysiological and taxonomic indicators derived from our optical measurements. Surface waters had lower PPC: PSC ratios, larger particle size distributions, and higher pigment per particle near the coast in colder upwelled water compared to locations further offshore with warmer, more nutrient deplete water. Smaller scale horizontal variations within these broad trends were also detected. There were large vertical gradients in taxonomic composition, PPC: PSC ratios and a_{ph} slopes, packaging, chl *a*: particle, relative particle size distributions and chl *a* concentration. An additive multiple linear regression model using temperature and PAR explained 42% of the variability in PPC: PSC ratios for all surface samples, and 61% for surface samples with < 2 μM

dissolved inorganic nitrogen. For all depths combined, we could explain 50% of the variability with an additive model using PAR and depth.

Introduction

Considerable spatial and temporal variability in phytoplankton physiology and taxonomic composition has been observed in Oregon coastal waters (Dickson and Wheeler 1995, Kokkinakis and Wheeler 1987, Hood et al.1991, Corwith and Wheeler 2002, Small and Menzies 1981). The environmental factors responsible for changes in phytoplankton ecology, such as light, nutrients and temperature, also vary over small temporal and spatial scales. For example, nutrient concentrations are highly variable due to changes in wind driven upwelling and phytoplankton utilization (Kokkinakis and Wheeler 1987). Assessment of phytoplankton photophysiology and ecology is now possible with recent advances in optical instrumentation and allows sampling of optical and hydrographic properties on the same time and space scales. In situ optical instrumentation provides a means to assess these rapid changes in phytoplankton photophysiology and ecology concurrently with hydrographic measurements of water mass characteristics. In this manuscript we describe how hydrographic measurements, and in situ absorption and beam attenuation, along with discrete samples for calibration, can be used to determine how environmental factors relate to variations in phytoplankton pigment ratios (photoprotective: photosynthetic carotenoids), relative particle size distribution, chlorophyll a (chl *a*) concentration, and chl *a* per particle. These tools also provide high-resolution information on phytoplankton

photophysiology and taxonomic composition in the variable environment of the Oregon upwelling system.

The Oregon coastal region is a dynamic area dominated by coastal upwelling during the spring and summer months (April – September) with a southward flowing (0.5 m s^{-1}) coastal jet, the California current, separating the upwelled waters from the low nutrient offshore waters (Barth and Smith 1998). The location of the upwelling front will move offshore during upwelling and remain closer inshore during relaxation and summer downwelling periods (Hermann et al.1989). Eddies in the southward flowing California current lead to cross shelf variability, as does along-shore variations in coastal topography (Strub and James 2000, Barth et al. 2000). The Columbia River plume contributes to the spatial variability in physical and biological parameters in this coastal region through the addition of low salinity, low nutrient waters over the continental shelf (Hickey et al.1989). In general, however, nutrients supplied by episodic upwelling, in conjunction with light provided by incident solar radiation, along with stratification of the upper water column from warming and the injection of less saline water masses, results in high phytoplankton photosynthetic rates (Hood et al.1991), high growth rates (Kokkinakis and Wheeler, 1987), and high primary production (Small and Menzies 1981) over the Oregon shelf.

These spatial and temporal variations in nutrient and light conditions in upwelling systems also affect the biomass, taxonomic composition and photophysiological characteristics of the phytoplankton assemblages, which in turn, are reflected in the photoprotective and photosynthetic pigment variations of the assemblages. For example, both high light and low nutrient environments are

associated with relative increases in photoprotective carotenoids (PPC) such as diadinoxanthin and diatoxanthin relative to chl *a* (Moline 1998, Johnsen and Sakshaug 1996, Anning et al. 2000, Geider et al.1993, Schluter et al.2000, Babin et al.1996). Earlier work in protected coastal waters (East Sound, Washington, Eisner et al. 2003) showed that high ratios of photoprotective: photosynthetic carotenoids (PPC: PSC) of the largely diatom assemblage were associated with high light levels. In addition, phytoplankton cell size also varies across environmental gradients (Chisholm 1992), with lower nutrient offshore waters containing a greater percentage of small (< 10 μm) phytoplankton cells than observed in the higher nutrient inshore waters during normal summer upwelling periods on the Oregon Coast (Corwith and Wheeler, 2002).

We have shown that the in situ assessment of the photophysiology and taxonomic composition of in-water phytoplankton assemblages, based on indices of photoprotective to photosynthetic pigment ratios and relative particle sizes, can now be estimated on similar scales as physical environmental parameters using in situ spectral absorption and beam attenuation measurements (Eisner et al. 2003). For data collected in East Sound (Eisner et al. 2003) and off the Oregon Coast (Eisner et al. chapter 3), we found linear relationships between the shape of the in situ absorption spectra and PPC: PSC ratios from High Performance Liquid Chromatography (HPLC) of discrete samples. Changes in the shapes of the in situ phytoplankton absorption (a_{ph}) spectra, were computed using a "slope" index, a_{ph} slope = ($a_{ph}488 a_{ph}532$)/ (($a_{ph}676$) · (488-532 nm)). For Oregon Coast surface waters, comparisons of PPC: PSC ratios and a_{ph} slopes showed that the regression line slopes were similar but the regression line y-intercepts were significantly different for different water masses

(defined by TS characteristics, location and sampling date). These differences were related to packaging variations. We also found that the shape of the beam attenuation spectra, a metric of relative particle size distribution, was associated with variations in taxonomic characteristics (determined from HPLC pigment ratios).

We now extend the earlier analysis of the slope of the in situ absorption spectra by examining the influence of environmental parameters on the horizontal and vertical patterns of this proxy for photoacclimation and taxonomic composition. Phytoplankton photophysiological and chemotaxonomic characteristics derived from in situ optical measurements and discrete sample analyses (as described in chapter 3) will be evaluated in relation to water mass characteristics. The specific goals of this study are to 1) examine the relationships of the absorption slope index and PPC: PSC ratios with environmental parameters (light history, nutrients, temperature) for surface waters and vertical profiles and 2) demonstrate how in situ absorption and beam attenuation measurements can be used to estimate phytoplankton PPC: PSC ratios, Tchl *a*, Tchl *a* per particle and particle size distribution with high spatial resolution (horizontal and vertical).

Methods

Sampling site

As described in chapter 3, data were collected in Oregon coastal waters from the R/V Thompson during 7 to 25 August 2001 (Pacific Daylight Time, PDT). The survey area encompassed 43.86 ° N to 45.01 ° N and 124.04 ° W to 125.00° W

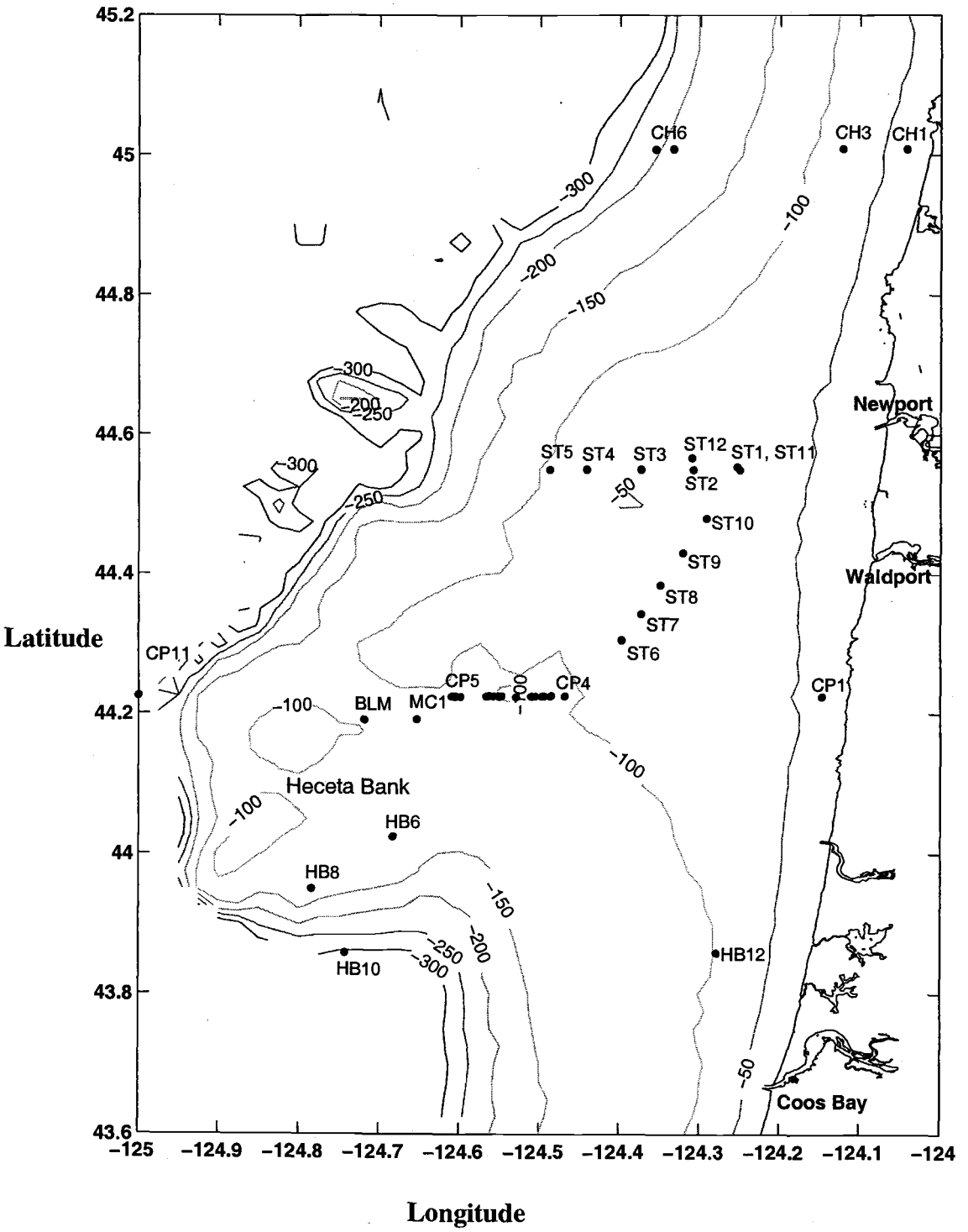

Figure 4.1. Oregon Coast station locations for collection of discrete water samples and in-line optical measurements during August 2001. Bathymetric contours are every 50 m. Latitude and longitude in decimal degrees.

(3 km to 70 km offshore, 130 km north/south) with bottom depths of 30 m to 500 m (Figure 4.1). A tow yo sled (Dr. B. Hales) provided hydrographic (Conductivity-Temperature-Depth, CTD) measurements of the water column while pumping water to the laboratory on board ship. Sampling occurred to 200 m or 5 m from the bottom where bottom depths were less than 200 m.

In situ measurements of hydrography and bio-optics

Water pumped to the shipboard laboratory was passed through an in-line bio-optical system that included a CTD sensor (SBE 911, Seabird, Inc.), and two nine-wavelength (visible light) in situ spectral absorption and beam attenuation meters (ac-9, WET Labs, Inc.) with one for measurement of total water and one for measurement of dissolved materials. Dissolved constituents were measured by diverting part of the inline flow through a set of filters (50 μm, 10 μm, and 0.2 μm (maxi-capsule, Gelman)) before the water passed through the ac-9. Both ac-9s were calibrated every 2 days with the pure water calibration technique (Twardowski et al.1999).

Additional in situ optical and hydrographic measurements were collected with a Sea Soar, a towed undulating package, deployed from the R/V Wecoma, a second research vessel involved in the August 2001 COAST survey. A Seabird 911 CTD was used to map hydrographic parameters and a Flash Pak fluorometer (Wet Labs) was used to map chl *a* concentrations. Optimal interpolation was used to interpolate data and create spatial maps of chlorophyll a and temperature. Maps are courtesy of Dr. J. Barth.

Collection of discrete water samples

Water samples were collected by diverting part of the pumped flow into 20 L carboys while the reminder of the flow went through the in-line optics and CTD system. At select stations (pump stations), water samples were collected every 5 m or 10 m from surface to near-bottom, by holding the sled at each depth for ~ 5 to 20 minutes (Appendix B). Surface (3-6 m) water samples also were collected every 2 hours for time series sampling at stations CP4 to CP5 (CP45 time series) and along a transect (ST stations) (Appendix C). Water samples were collected for nutrients, pigment composition, and particulate and phytoplankton absorption.

Discrete sample analyses of phytoplankton pigments and particulate absorption

Phytoplankton pigment concentrations were quantified with HPLC (Wright and Jeffrey 1997) and particulate absorption measurements were determined by Dr. R. Letelier using the quantitative filter technique (QFT, Yentsch 1962; Mitchell and Kiefer 1988) and the Kishino method (Kishino et al. 1985), as described in chapter 3. Quantifiable pigments included chlorophylls (*a*, *b*, *c*1/*c*2, *c*3), chlorophyllide *a*, chlorophyll *a* epimer, PSC (19-hexanoyloxyfucoxanthin (19-hex), 19-butanoyloxyfucoxanthin (19-but), fucoxanthin (fuco), peridinin (perid)), and PPC (alloxanthin (allo), β-carotene (Bcaro), diadinoxanthin (diad), diatoxanthin (diat), lutein/zeaxanthin (lut/zea), violaxanthin (viol)). Total chlorophyll *a* (Tchl *a*) was computed as the sum of chlorophyll *a* (chl *a*), chlorophyllide *a*, chlorophyll *a* epimer and other unidentified chlorophyll *a* derivatives.

Nutrient analyses

Nutrient samples were immediately frozen after collection and analyzed for total nitrate, nitrite, ammonium, phosphate and silicate using a Technicon AutoAnalyzer following standard colorimetry protocols (Atlas et al. 1971). Nutrient data are courtesy of Dr. P. Wheeler.

In situ particulate absorption spectra

We estimated $a_p(\lambda)$ from the ac-9 data by subtracting the absorption by dissolved material (< 0.2 μm), denoted $a_g(\lambda)$ from the absorption by particles plus dissolved materials, denoted $a_{pg}(\lambda)$. Corrections for temperature and salinity were applied (Pegau et al. 1997), and the scattering error was removed by subtracting a_p715 nm from all $a_p(\lambda)$ (Zaneveld et al, 1994). Single point data spikes were removed from the ac-9 data with a 5-point median filter (2 passes), data were smoothed with a 7-point running average, averaged into 1-s bins, and merged with hydrographic and position data.

Chlorophyll a epimer

The presence of chlorophyll *a* epimer can interfere with baseline scattering corrections of the ac-9 data. For our scattering correction we normally assumed that the $a_{pg}715$ values were primarily due to scattering with a small percentage due chl *a* absorption (tail end of red absorption peak). To account for the contribution by chl *a*, we multiplied the $a_{pg}676$ value by 4% and subtracted this value from $a_{pg}715$ (M. Twardowski pers. comm.). We corrected the other wavelengths by subtraction of

$a_{pg}715$ (after removal of the chl *a* contribution). The chl *a* epimer absorbs at 715 nm (with peak red absorption at ~705 to 710 nm), so when this degradation pigment is present, some of the $a_{pg}715$ may be due to chl *a* epimer. If we do not account for the epimer, we can overestimate the amount of scattering and thus underestimate the magnitudes of the a_{pg} and a_p spectra. We were able to detect the epimer in many of our QFT spectra, particularly in deep samples (Appendix C). We could also detect epimer in our ac-9 data by using the ratio of $(a_p676 - a_p715)/ a_p676$ for uncorrected data. If these ratios were below ~ 0.9 we assumed epimer was present, since we did not expect the chl *a* contribution at 715 nm to be more than 10% of the 676 nm absorption (with 4% of 676 nm absorption considered an average contribution). We estimated the absorption due to epimer by adjusting $a_{pg}715$ until the $(a_p676 - a_p715)/ a_p676$ ratio equaled 0.9. This correction in $a_{pg}715$ was then subtracted from $a_{pg}715$ for all ac-9 data before application of our usual scattering corrections.

Calculation of slopes from absorption spectra

Changes in the shape of the absorption spectra were evaluated by calculating "slopes" of the absorption curves (Eisner et al., 2003):

$$a_x \text{ slope} = (a_x488\text{nm} - a_x532\text{nm}) / (a_x676\text{nm} \cdot (488 - 532\text{ nm})),$$

where a_x is denoted as a_{ph} or a_p.

The ac-9 slope measurements were averaged over time intervals of 2 to 17 minutes for ac-9 data from pump stations and over ~25 seconds during transects when

discrete samples were not collected. The absorption slopes from the ac-9 were compared to the PPC: PSC ratios determined from HPLC analyses, as described in chapter 3. Model 1 linear regression analyses was used to predict PPC: PSC ratios from ac-9 a_p slope measurements.

Detrital absorption (a_d) estimation

We obtained ac-9 a_{ph} values by subtracting the detrital absorption coefficients, a_d, from the ac-9 a_p measurements. The a_d coefficients for ac-9 spectra were obtained by multiplying the ac-9 a_p values by the a_d: a_p ratio from QFT samples collected at the same time. The use of the QFT a_d: a_p ratio rather than the absolute a_d (λ) from QFT, accounts for any differences in the absolute magnitudes of the ac-9 and QFT absorption spectra. Variability in QFT spectra may result from inaccuracies in the path-length amplification factor and variability in the blank filter pad optical density (Roesler, 1998). Whereas, variability in ac-9 spectra may result from the choice of the scattering correction method and pure water calibration errors.

Package effects

Package effects were estimated by reconstructing unpackaged a_{ph} spectra from phytoplankton pigment concentrations obtained by HPLC (Bidigare et al. 1990). The unpackaged phytoplankton absorption coefficient (a_{ph}' (λ)) is calculated as:

$$a_{ph}'(\lambda) = \sum_{i=1}^{n} c_i \, a^*_i(\lambda),$$

where c_i is the concentration of pigment i (mg m^{-3}) and a^*_i (λ) is the specific absorption coefficient of pigment i (m^2 mg^{-1}) at wavelength (λ). The percent loss of pigment absorption due to the package effect at a specific wavelength, Qa*(λ) (Morel and Bricaud 1981), can be calculated from the measured a_{ph} (λ) value divided by the reconstructed a_{ph}' (λ) value. Qa* at 676 nm (indicating Tchl *a* packaging) was used to compare package effects between samples and groups.

Size estimations based on c_p spectra

The relative differences in the particle sizes were estimated from ac-9 beam attenuation (c) spectra (e.g. Boss et al.2001; Kitchen et al, 1982). We subtracted the dissolved attenuation (c_g) spectra, from the total attenuation (c_{pg}) spectra, to get particulate beam attenuation (c_p) spectra. Both, the c_p440: c_p650 ratio and γ, the hyperbolic exponent for a least squares fit to the c_p spectra, have been used to estimate relative particle size distributions (Kitchen et al.1982, Boss et al.2001). In chapter 3, each of these indices showed similar spatial patterns (linear $r^2 = 0.95$). In this study, we use the simpler metric, c_p440: c_p650, to evaluate spatial variations in relative particle size. As shown by Kitchen et al. (1982), lower c_p440: c_p650 ratios indicate the presence of larger particles (within a background of smaller particles), whereas higher ratios indicate a greater contribution by smaller particle sizes in the particle size distribution (PSD).

Horizontal and vertical distributions of nutrients and hydrographic characteristics in relation to optical parameters

We used discrete samples collected between 3 m and 6 m depths to evaluate horizontal patterns in nutrient concentrations, pigments and optical and hydrographic properties. For vertical patterns we evaluated variations in the upper 30 to 50 m of the water column using discrete samples collected every 5 m to10 m. In addition, we made comparisons between the 5 m and 10 m discrete samples since the largest vertical variations in nutrients and PAR often occurred within 10 m of the surface. We used model 1 linear regressions to predict PPC: PSC ratios from the full suite of measured environmental parameters. A stepwise linear regression program was used to conduct all multiple linear regression analyses (SPSS, Statistical Package for the Social Sciences).

We applied the results from the discrete sample analyses to evaluate higher resolution spatial patterns. To evaluate horizontal patterns we used continuous ac-9 and CTD data averaged over 3-7 m depth intervals, collected with the to-yo sled pumped sea water system. We estimated PPC: PSC ratios for a specific water mass based on the linear regression analyses developed from 3-6 m discrete water samples (when ac-9 and discrete sample HPLC and QFT data were concurrently collected).

To evaluate vertical patterns at higher resolution, we used profiles of ac-9 data at selected stations collected within 1 h of completion of pump profiles of discrete samples. Vertical profiles of a_{ph} slopes, $a_{ph}676$, c_p440: c_p650, $a_{ph}676$: c_p650, sigma-t and in situ fluorescence were averaged into 2-m depth bins within the upper 50 m of the water column. We calculated a_{ph} slopes after making detrital corrections of the

measured $a_p(\lambda)$ spectra for each depth bin, using discrete QFT samples collected during the earlier pump profile. We then predicted PPC: PSC ratios from ac-9 a_{ph} slopes using the model I linear regression obtained from ac-9 and discrete sample HPLC data collected during the pump profile.

Photosynthetically available radiation (PAR)

Irradiance measurements were obtained from the R/V Thompson onboard weather station using a quantum sensor. Subsurface irradiance was derived using:

$$E_d(z) = E_d(0)\, e^{-(Kd)\, z},$$

where $E_d(z)$ is the downward irradiance at depth z in meters, $E_d(0)$ is the downward irradiance just below the water surface, and K_d is the average vertical attenuation coefficient from 0 to z m. We assumed 5% loss of light at the air-water interface. $K_d(\lambda)$ was approximated by $K_E(\lambda)$, the vertical attenuation coefficient for net downward irradiance, where $K_E(\lambda) = a_t(\lambda) / \mu\text{-bar}(\lambda)$, and μ-bar(λ) is the average cosine for the light field. We used $a_t(\lambda)$ values from ac-9 data and assumed an average μ-bar(λ) of 0.8. For each sample, the mean $a_t(\lambda)$ at the discrete sample depth was used to derive $K_E(\lambda)$, and we assumed this depth-specific value was representative of the water above. The mean K_d value from 0 to z (the discrete sample depth) may differ slightly from this K_E estimate. We estimated prior light exposure by two methods. For the first method, we used subsurface PAR values averaged over the depth of mixing and assumed this mixing depth remained constant over the time interval of interest

(prior 1 h). Mixing was assumed to occur over a depth range that had a sigma-theta (density anomaly) differential < 0.01 kg m^{-3} at the time of sample collection. For the second method, we assumed the surface waters remained stratified over time (over prior 1 h or prior 24 h). Consequently, for the second method we used the subsurface PAR values at the depth of sample collection to estimate the mean prior PAR exposure (i.e. we assumed the sample depth did not change over the light exposure period, 1 h or 24 h). For 1 h prior light exposure calculations we used samples collected from 0800 h to 1800 h Pacific Daylight Time (PDT), approximately 2 hours after sunrise to 2 hours before sunset.

Wind data

Wind data from the National Oceanographic Data Center (NODC) buoy # 46050 located 20 nautical miles west of Newport, Oregon were used to determine periods of upwelling favorable winds, downwelling favorable winds and summer relaxation (light winds).

Results

Environmental parameters

Stratification, wind, upwelling, temperature

The depth of the surface mixed layer varied from ~ 5 to 20 m for the duration of our study, primarily in response to shifts in wind forcing (Figure 4.2). A 5-day interval of northward winds prevailed prior to the cruise with upwelling favorable

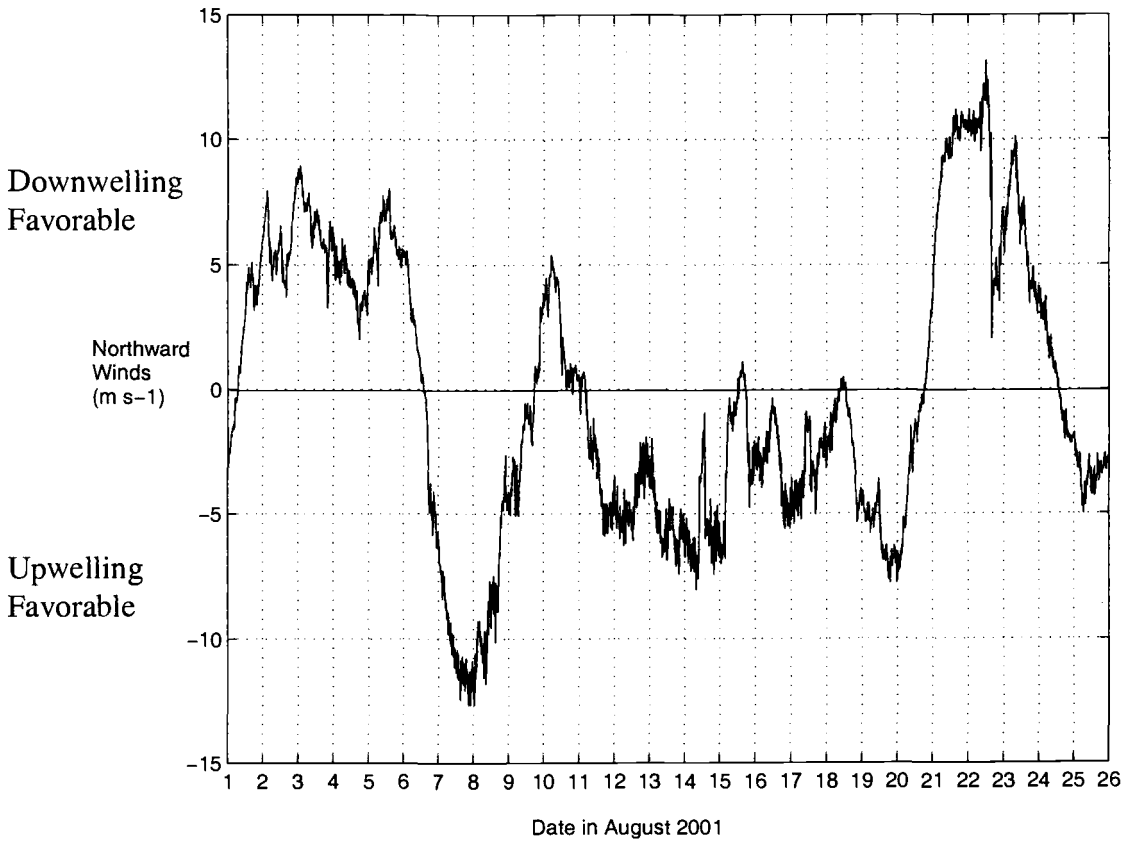

Figure 4.2. Northward wind speeds for August 2001 collected at National Data Buoy Center (NDBC) buoy located 20 nautical miles west of Newport. Northward winds are positive and southward winds are negative.

winds (southward) present during our initial observations (7-9 August, 2001). A brief period of light northward winds occurred on 10 August, followed by a relaxation period with light southward winds from ~ 11-20 August. We then experienced a burst of summer downwelling favorable (northward) winds from 22-24 August that diminished to light winds on 25 August (Figure 4.2). The 5-m temperature contour maps provide examples of areas influenced by the light upwelling favorable winds during mid August (15-17 and 20-22 August), with colder temperatures seen near shore from the upwelling of cold, nutrient rich water and higher temperatures seen offshore beyond the upwelling frontal region (Figure 4.3a and chapter 3 Figure 3.4b). Following the period of strong downwelling winds, during late August (24-25 August), warmer waters were seen over the survey region as upwelling relaxed and high temperature surface waters were advected closer to shore (Figure 4.3b). The temperatures were lower at depth than near the surface with larger vertical gradients often seen for offshore compared to onshore locations (Appendix B).

Nutrients

Dissolved inorganic nitrogen (DIN, ammonium-N+ nitrate-N+ nitrite-N) concentrations in the surface layer were higher inshore than offshore, however, there was considerable variability among mid-shelf stations even when TS characteristics were similar (Figure 4.4, Appendix C). Variability between nearby stations is shown in the CP4 to CP5 time series data where DIN concentrations fluctuated by over two orders of magnitude over a 3 km horizontal distance and within 10 -14 h at a set location (Table 4.1).

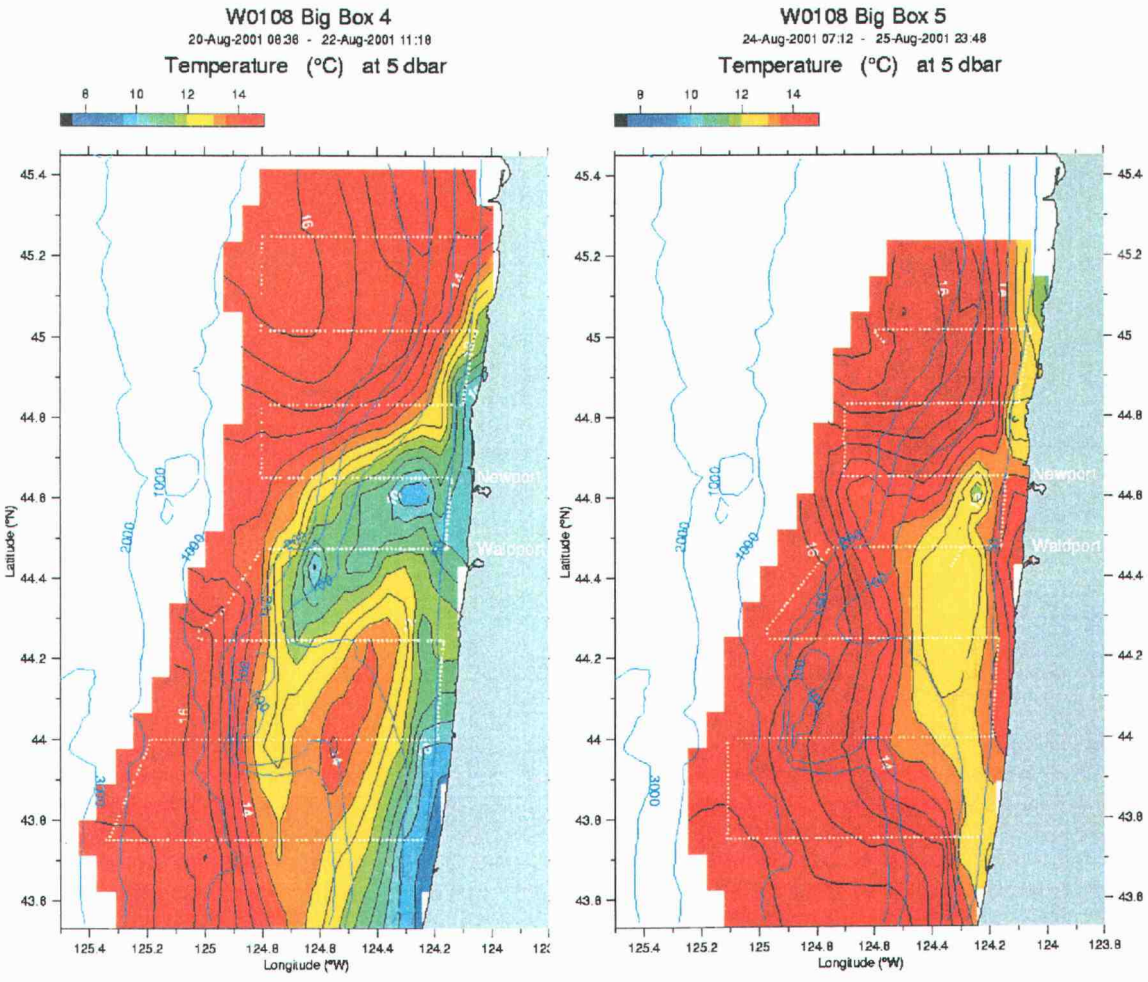

Figure 4.3. 5-m contour maps of temperature from CTD (Seabird 911) measurements during Sea Soar surveys conducted by the R/V Wecoma for a) 20 to 22 August and b) 24 to 25 August (local time). GMT time is shown above plots. Transect lines are shown by white dotted lines. Contour maps are courtesy of Dr. Jack Barth.

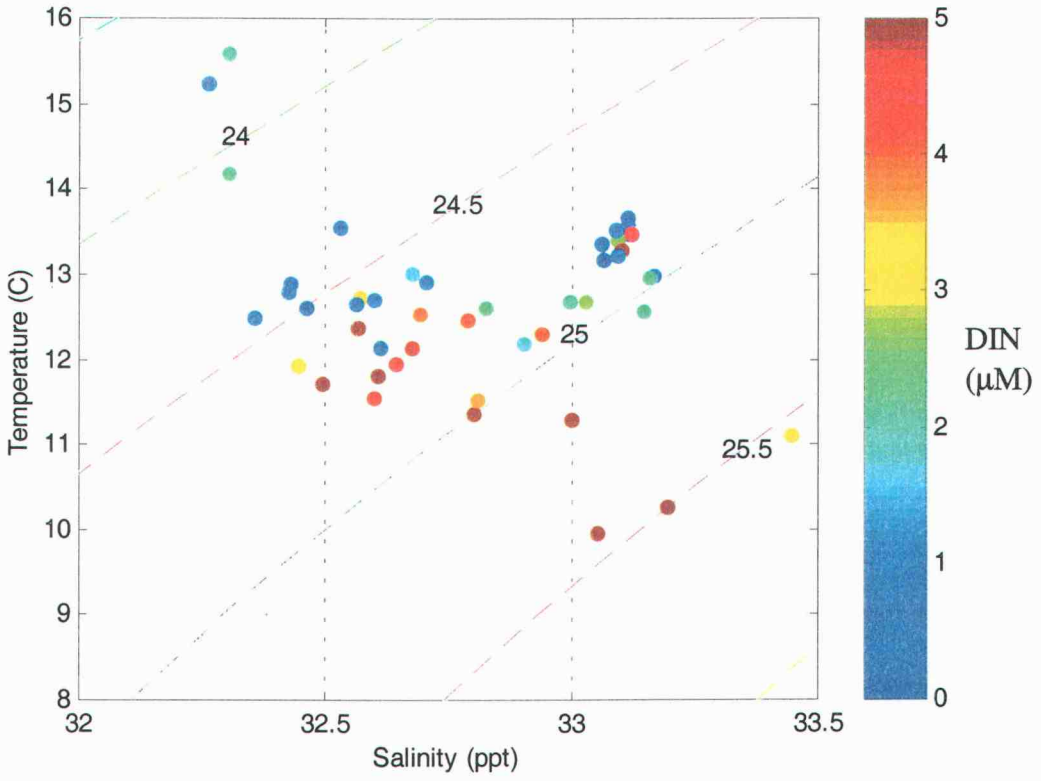

Figure 4.4. Dissolved inorganic nitrogen (DIN) as a function of temperature and salinity for 5 m samples. DIN concentration indicated by the color bar with the maximum range set at 5 μM. Density (sigma-t, kg m^{-3}) contours are also shown.

Table 4.1. Stations CP4 to CP5 time series on 14 to 16 August, 2001 (5 m data). Samples grouped by longitude and ordered by time. Data include silicate (SiO_2) and total dissolved inorganic nitrogen (DIN) in μM, Tchla (μg L^{-1}), perid /Tchla (g: g), hex/Tchla (g: g), PPC: PSC (g: g), temperature (°C), and salinity. Date and time in local time (Pacific Daylight Time).

Station	Date	Time	long	SiO2	DIN	Tchla	per /Tchla	hex /Tchla	PPC /PSC	Temp	Salin
CP45	14-Aug	3:15	124.61	10.16	5.05	2.90	0.01	0.08	0.24	12.37	32.57
CP45	14-Aug	20:06	124.61	7.79	3.52	13.06	0.01	0.09	0.23	12.72	32.57
CP45	15-Aug	9:50	124.60	8.94	6.18	5.67	0.01	0.09	0.31	11.81	32.61
CP45	16-Aug	2:12	124.61	3.03	2.22	6.42	0.01	0.06	0.18	12.59	32.83
CP5	16-Aug	12:07	124.61	9.00	3.93	18.52	0.01	0.04	0.21	12.54	32.70
CP45	14-Aug	12:16	124.56	0.00	0.00	3.12	0.06	0.08	0.39	13.15	33.07
CP45	14-Aug	18:09	124.55	0.00	0.00	2.19	0.10	0.22	0.37	13.64	33.11
CP45	14-Aug	21:56	124.56	3.99	4.84	7.25	0.01	0.07	0.22	12.13	32.68
CP45	15-Aug	8:01	124.55	1.60	2.06	6.35	0.02	0.06	0.19	12.67	33.00
CP45	15-Aug	12:09	124.57	0.00	0.57	4.29	0.05	0.10	0.45	13.36	33.06
CP45	16-Aug	4:07	124.55	0.79	2.11	3.84	0.02	0.09	0.17	12.55	33.15
CP45	16-Aug	10:00	124.56	0.30	2.15	4.87	0.05	0.12	0.26	12.95	33.16
CP45	14-Aug	14:07	124.51	0.00	0.00	4.94	0.17	0.17	0.35	13.47	33.12
CP45	14-Aug	16:47	124.51			2.75	0.19	0.14	0.29	13.41	33.12
CP45	15-Aug	0:09	124.51	0.00	0.05	1.82	0.07	0.24	0.31	13.56	33.12
CP45	15-Aug	14:09	124.51	0.00	0.53	5.64	0.37	0.14	0.33	13.51	33.09
CP45	16-Aug	0:00	124.53	0.42	0.50	6.36	0.01	0.07	0.24	12.97	33.17
CP45	14-Aug	16:07	124.49	0.00	2.58	6.67	0.26	0.20	0.34	13.40	33.10
CP4	15-Aug	3:55	124.47	0.00	4.48	3.29	0.19	0.14	0.22	13.48	33.12
CP45	15-Aug	6:24	124.50	0.00	5.92	2.47	0.14	0.15	0.23	13.28	33.10
CP4	15-Aug	20:28	124.47	0.00	1.06	3.37	0.15	0.15	0.21	13.20	33.10
CP45	16-Aug	6:07	124.49	2.99	4.06	3.95	0.02	0.06	0.18	12.30	32.94
CP45	16-Aug	7:46	124.49	2.18	2.71	6.86	0.02	0.06	0.20	12.66	33.03

Nitrogen concentrations less than 1 to 2 μM may limit phytoplankton growth since coastal diatoms typically have nutrient half saturation (k_s) values in the 1 to 2 μM range (Dr. P. Wheeler pers. comm.). The 5-m DIN concentrations were < 2 μM at a variety of midshelf and offshore stations (n = 20), including a station influenced by the Columbia River plume water (CH6 on 11Aug), Heceta Bank locations (HB6, HB8, HB10, BLM) and select midshelf stations (some ST transect and CP4 to CP5 times series locations) (Appendix C).

The N: P ratios at 5 m ranged from 0.1 to 18.3 with only two samples, from station CP4 and a nearby time series station, showing values above 16 (Redfield ratio) (Appendix C). The mean N: P ratios were 4.6 ± 4.0 (sd) for all sample combined and 1.4 ± 1.2 (sd) for samples with low DIN (< 2 μM). These data suggest that N was more limiting than P. The Si: N ratios at 5 m ranged from 0 to103 with a mean of 10.2 ± 22.8 (sd), with the highest ratios observed at stations on the ST line (ST6, ST7, ST8, ST9, ST10, Appendix C). Without these stations included, the mean 5-m Si: N ratios were 2.9 ± 4.1 (sd).

Nitrate, phosphate and silicate concentrations generally increased from the surface (5 m or 10 m) to the bottom of the water column (Appendix B). In contrast, ammonium often showed mid-depth minima. Overall, the nutrient concentrations for N, P, and Si were higher at 10 m compared to 5 m depths with the exception of stations CH1 on 8Aug, CP5 and CP11, each of which possessed a mixed layer > 10 m thick (Appendix B). DIN concentrations were > 2 μM for samples from 10 m depths

and deeper, with the exception of the offshore station CP11 (10 m DIN = 0.04 μM). N: P ratios for samples from below the surface layer (deeper than 10 m) ranged from 0.8 (at station CP11) to 13, with a mean of 10 ± 2.1 (sd), and were therefore below Redfield ratios (Appendix B). Si: N ratios for samples from below the surface layer ranged from 0.5 to 2.7 with a mean of 1.2 ± 0.4 (sd).

Phytoplankton biomass

We observed moderate to high chl *a* values at inshore and midshelf stations, while offshore stations had low values (Appendices A and B). Most midshelf stations had relatively high chl *a* concentrations in the upper 10 m with much lower values observed below the pycnocline, with considerable mesoscale cross-shelf variability (Figure 3.4a in chapter 3 and Figure 4.5).

Irradiance

Daily maximum above surface PAR varied between 1000-2000 μmol quanta m^{-2} s^{-1} (Figure 4.6). Clearer waters (and deeper light penetration) were indicated at stations CP11 and CH6, and station CH3 since the total absorption was lower, reflected by lower vertical attenuation coefficient (k_d) values, (Appendix B), largely due to reduced phytoplankton biomass at these stations.

Relationships between pigment ratios and environmental parameters

We evaluated the relationships between PPC: PSC ratios and environmental variables (nutrients, PAR, temperature, salinity and depth) using bivariate and

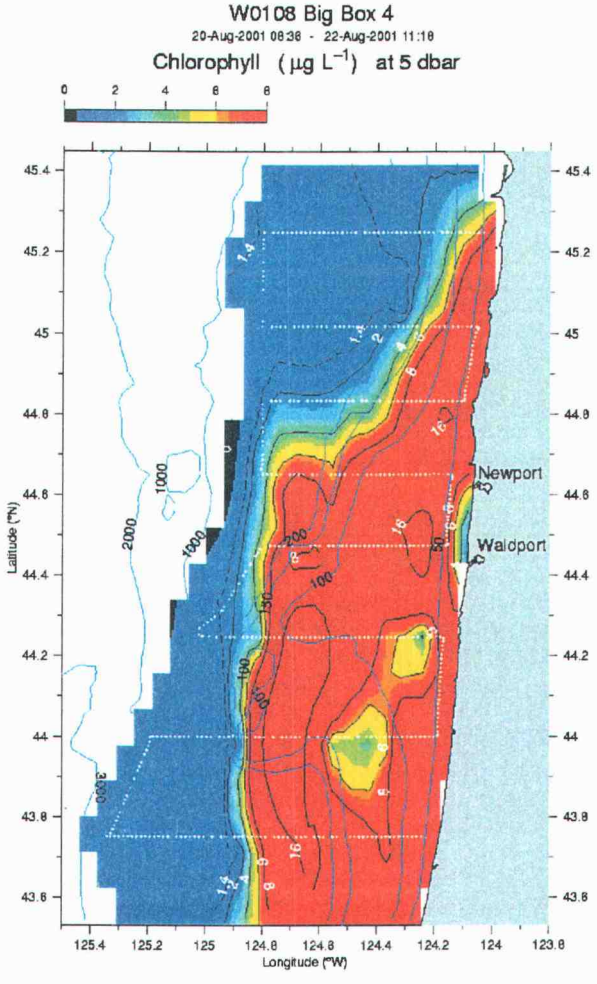

Figure 4.5. 5-m contour maps of chlorophyll a from in situ Flash Pak (Wet Labs) fluorometer measurements during Sea Soar surveys conducted by the R/V Wecoma for 20 to 22 August (local time). GMT time is shown above plots. Transect lines are shown by white dotted lines. Contour maps are courtesy of Dr. Jack Barth.

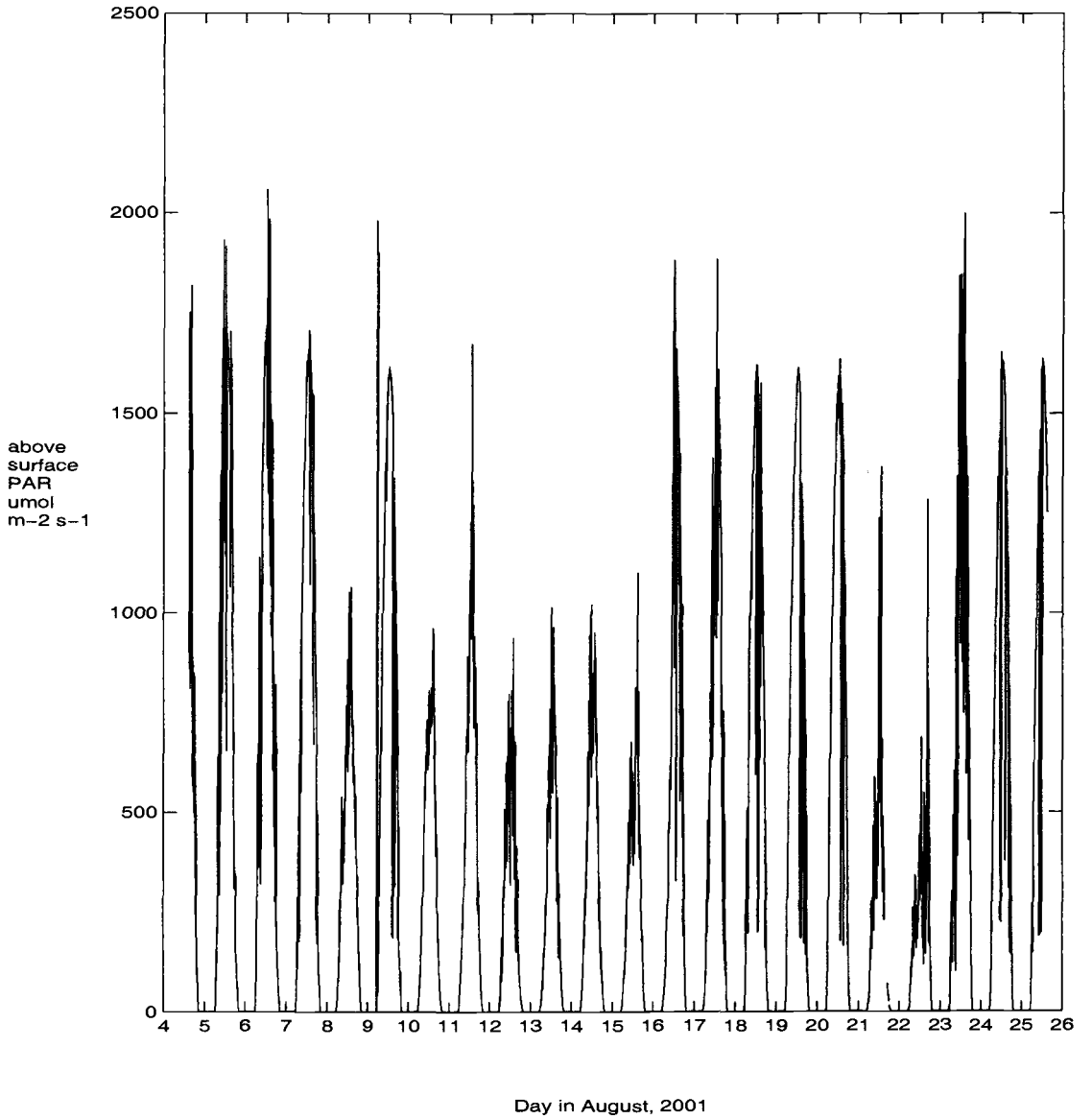

Figure 4.6. Above surface PAR (μmol m^{-2} s^{-1}) for August 2001 collected onboard the R/V Thompson.

multivariate linear regression analyses. Separate analyses were conducted for 5 m samples (for all DIN levels and for data DIN < 2μM) and for all depths combined. Data from station CP11 at 5 and 10 m was excluded from all regression analyses since the PPC: PSC ratios for these samples were > 3 standard deviations from the mean.

We grouped the surface layer samples according to TS characteristics, date of sample collection and location (chapter 3). Samples from stations influenced by Columbia River properties (CH6 and CP11) were assigned to group CR. Samples from stations located closer to shore (CH1, CH3, CP1) were assigned to group IN and the remaining midshelf samples (CP4, CP5, CP4 to CP5 time series, HB6, HB8, HB10, HB12, MC1, BLM and ST stations) were assigned to group MID.

Surface layer (5-m) relationships in pigment ratios and environmental parameters

Nutrients- We did not find a significant linear relationship between DIN (ammonium-N, nitrate-N, nitrite-N) and PPC: PSC ratios (p=0.4). However, we found significantly higher PPS: PSC ratios for samples with low total DIN values (< 2 μM-N) compared to samples with higher total DIN values (> 2 μM-N) (one-sided t tests, p< 0.001, Figure 4.7a). For DIN values < 2 μM, we also found a significant linear relationship between DIN concentration and PPC: PSC ratios, although the correlation coefficient was low (r = -0.4, r^2 = 0.16, p< 0.01). We did not see significant differences in Tchl *a* for low compared to high total DIN values (two sided t-test, p = 0.5, Figure 4.7b). The low DIN values were from groups MID and CR (CH6 only) whereas the high values were from all three groups.

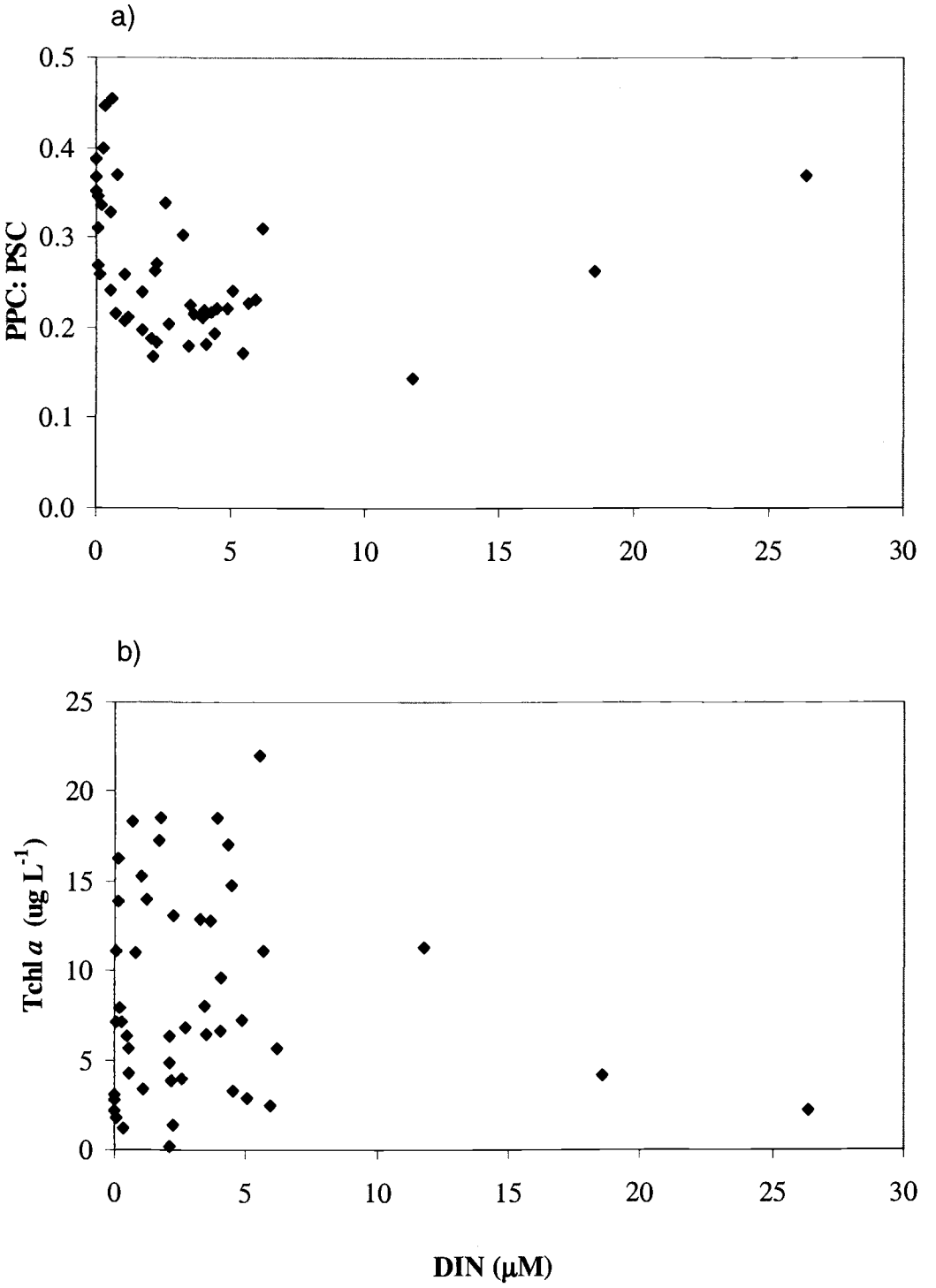

Figure 4.7. Relationship of dissolved inorganic nitrogen (DIN) with a) PPC: PSC and b) Tchl *a* for 5 m samples. Station CP11 data excluded.

Low nutrient concentrations were associated with particular pigment biomarkers, indicative of phytoplankton taxonomic composition. Biomarkers include fuco for diatoms, perid for dinoflagellates, hex for prymnesiophytes and zea for prokaryotes. The highest perid: Tchl *a* ratios and high hex: Tchl *a* ratios occurred over the mid shelf (CP4 and nearby stations) in samples with undetectable Si concentrations (Table 4.1, Figure 4.8a). The PPC: PSC ratios showed similar fluctuations as perid: Tchla (and hex: Tchla to some extent) suggesting that increases in PPC: PSC were associated with increases in the relative abundances of dinoflagellates and prymnesiophytes (Table 4.1, Figure 4.8b). Low Si concentrations (0.2 μM-Si) and low DIN (~2 μM) were also associated with higher zea/lut: Tchl *a* ratios and hex: Tchl *a* ratios at the most offshore station (CP11) (Appendix C). Station CH6 also had low DIN with low fuco: Tchl *a* and high hex: Tchl *a*. The occurrence of non-diatom species groups in these samples, indicated by higher proportions of biomarker pigments such as perid, hex, zea, may have been driven by silicate limitation and/or (possibly) nitrogen limitation.

Light- Since discrete samples were collected throughout the light cycle, we compared the PPS: PSC ratios to the average daytime light exposures for the 24 h prior to sample collection, assuming stratified conditions, (see Method 1 in methods section). We did not find a significant relationship for 5 m samples between PPC: PSC ratios and mean PAR for the prior 24 h ($p > 0.05$, Figure 4.9a).

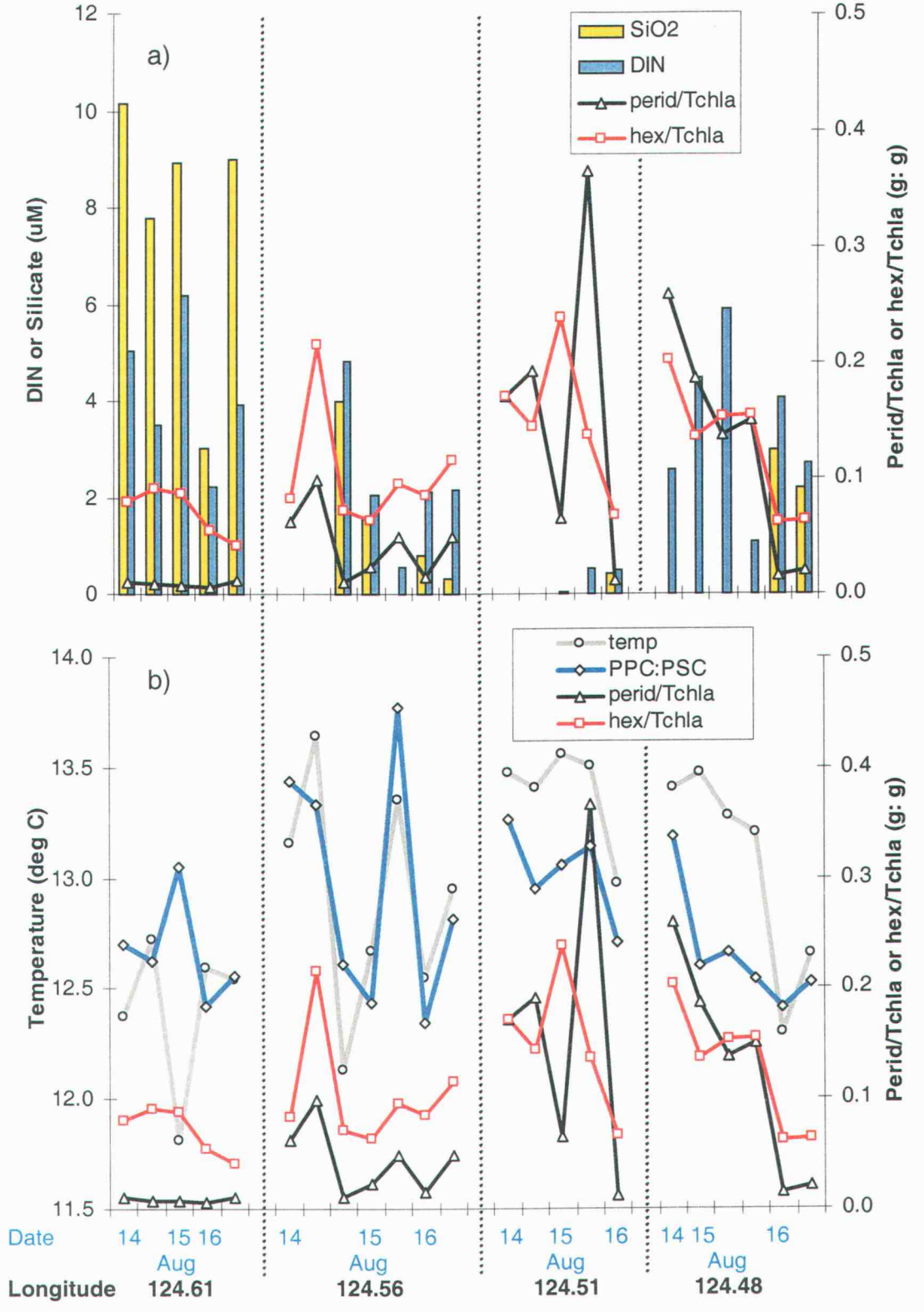

Figure 4.8 5-m samples for CP4 to CP5 time series from 14-16 August grouped into four geographic locations for a) dissolved inorganic nitrogen (DIN), silicate, perid/ Tchla and hex/Tchla and b) perid/Tchla and hex/Tchla, PPC: PSC ratios and temperature.

Figure 4.9. Relationship between PPC: PSC ratios and PAR averaged over prior 24 h for daylight hours assuming 14 h light for a) 5 m samples and c) all depths, and PAR averaged over prior 1 h for samples collected from 0800 to 1800 (local time) for b) 5-m samples and d) all depths. East Sound data averaged over prior 1 h for data collected from1100 and 1600 at depths of 3 to 18 m is shown in panel b.

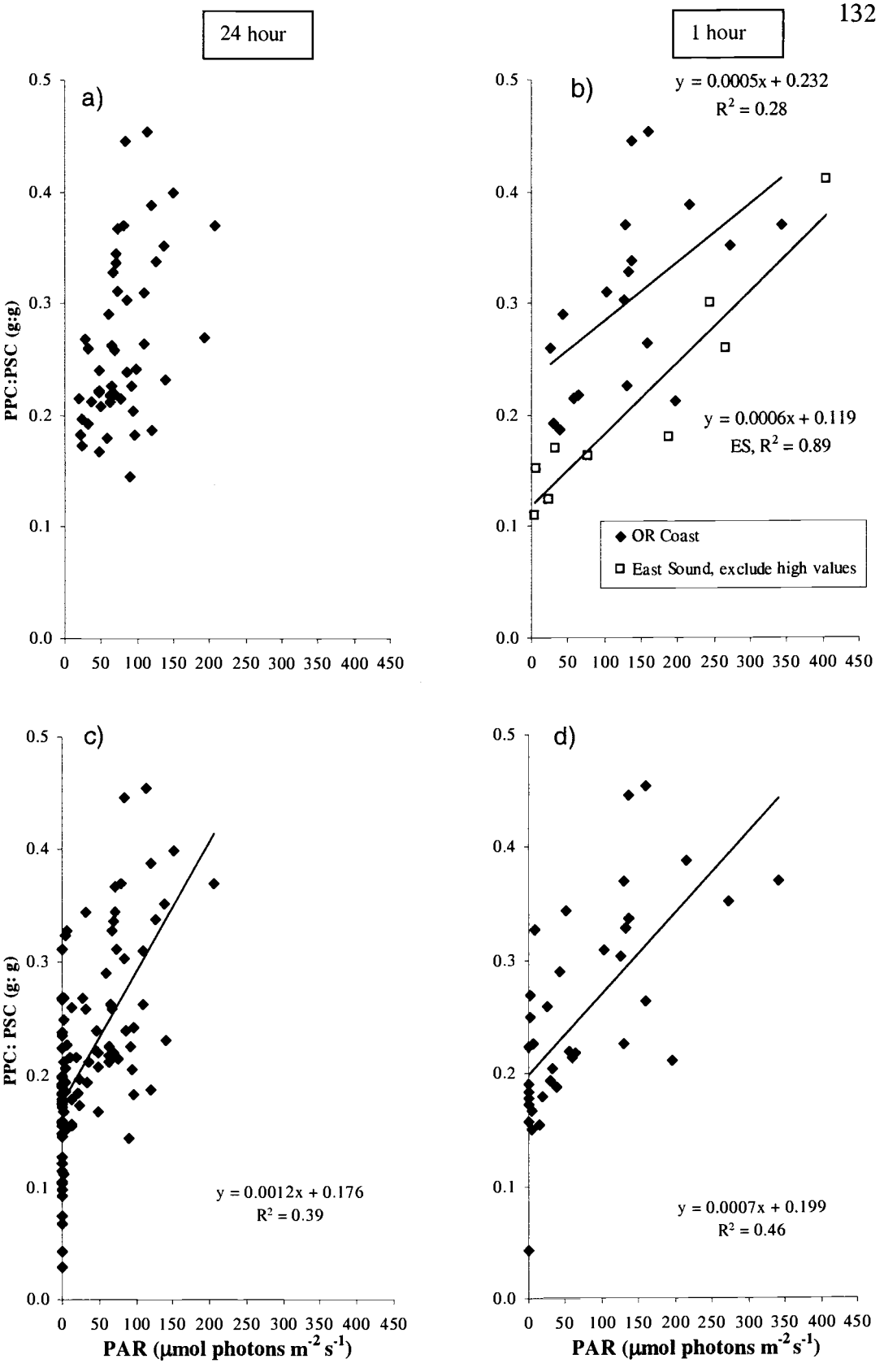
24 hour
1 hour
a)
b)
c)
d)
PPC:PSC (g:g)
PPC: PSC (g: g)
PAR (µmol photons m-2 s-1)
y = 0.0005x + 0.232
R2 = 0.28
y = 0.0006x + 0.119
ES, R2 = 0.89
OR Coast
East Sound, exclude high values
y = 0.0012x + 0.176
R2 = 0.39
y = 0.0007x + 0.199
R2 = 0.46

Figure 4.9.

For those samples collected during daylight (0800 –1800), we found a significant positive relationship between PPC: PSC ratios and PAR averaged over the hour preceding sample collection, assuming stratified conditions ($r^2 = 0.28$, $p < 0.05$, Figure 4.9b). Similar results were seen using PAR values averaged over the depth of mixing (Method 2 in methods section, data not shown). The regression line slope for our 5-m samples was not significantly different than the regression line slope for East Sound samples collected from 1100 h to 1600 h in a similar PAR range ($p < 0.05$, Figure 4.9b). The y-intercept was 2 times higher for these Oregon Coast samples than for East Sound samples (intercepts = 0.23 compared to 0.12, significantly different ($p < 0.05$), Figure 4.9b). The linear regression between the mean PAR for the prior 1 h and PPS: PSC ratios also shows more scatter for Oregon Coast compared to East Sound samples ($r^2 = 0.28$ compared to $r^2 = 0.89$). This higher variability may be due to the greater diversity of the phytoplankton assemblages and water masses seen during the Oregon Coast survey (large area) compared to the East Sound survey (single station).

Temperature- We observed a positive relationship between temperature and PPC: PSC ratios for surface samples, excluding the sample from station CH3, a low temperature outlier that was >2.5 standard deviations from the mean 5 m value ($r^2 = 0.36$, $p<0.001$, Figure 4.10a). Similar, slightly stronger trends were seen between temperature and PPC: total pigment (mol: mol) ratios for these samples ($r^2 = 0.48$, $p<0.001$). We found a weak linear relationship between temperature and Tchl *a* for all samples combined excluding station CH3 ($r^2 = 0.32$, $p<0.05$). Variations in PPC: PSC

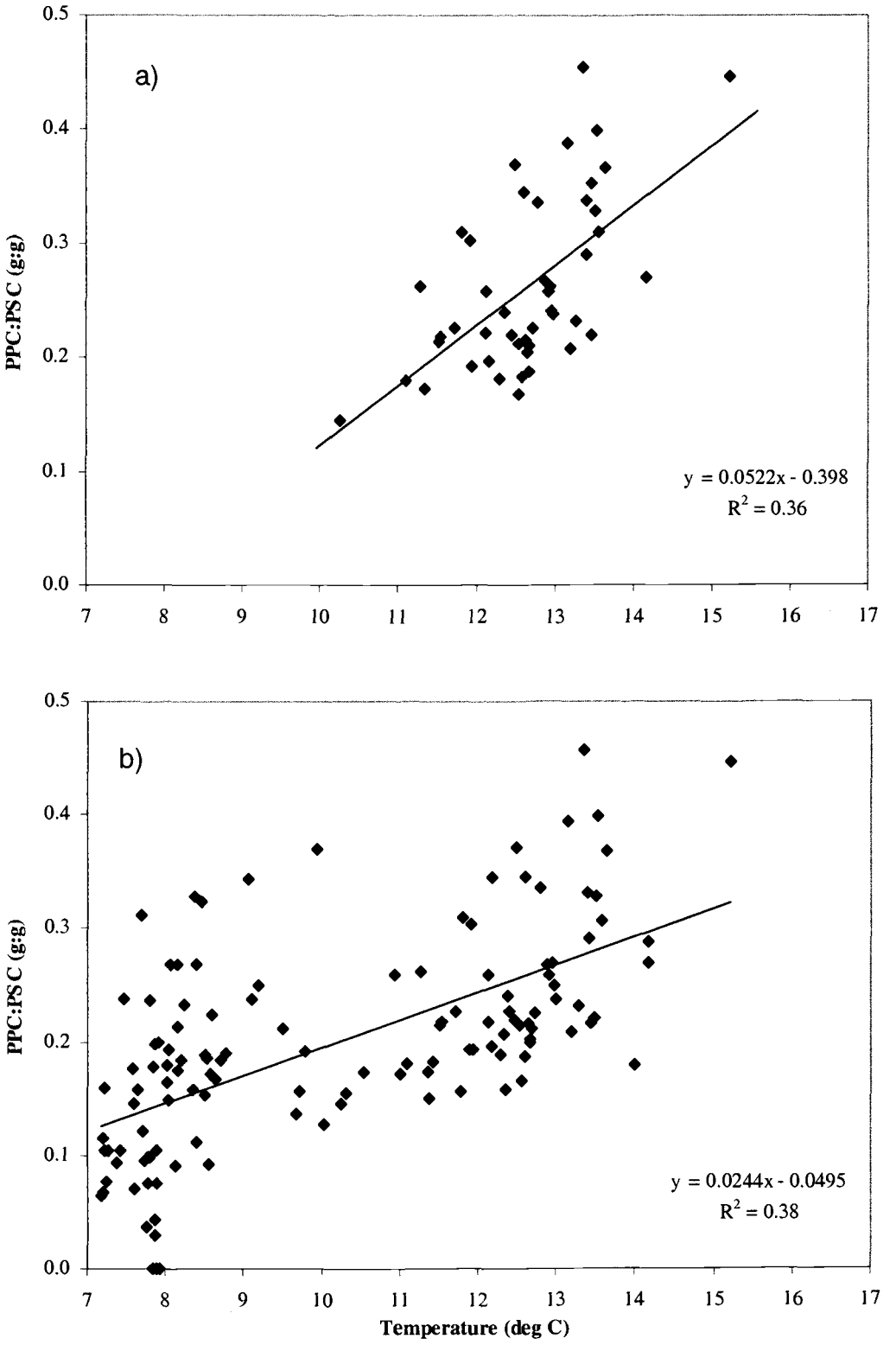

Figure 4.10. Relationship of temperature and PPC: PSC ratios for a) 5-m samples and b) all depths.

ratios were associated with increases in temperature for the CP4 to CP 5 time series (Figure 4.8b). For these time series data, increases in PPC: PSC were also associated with increases in relative abundances of non-diatom species in the higher temperature, higher salinity, low silicate water mass, as discussed earlier.

Interaction of DIN, PAR, temperature, salinity on PPC: PSC ratios- We used multiple linear stepwise regressions to evaluate the influence of DIN, mean PAR (at sample depth) averaged over the prior 24 h, temperature, and salinity on surface PPC: PSC ratios. We found that for all 5 m data, excluding the outlier samples from CP11 and CH3, we could explain 42% of the PPC: PSC variability with temperature and PAR and 36% of the variability with temperature alone (Appendix B). We were able to explain more of the PPC: PSC variability for samples with low nutrient concentrations. For all 5-m samples with DIN values < 2 μM, we could explain 61% of the PPC: PSC variability with an additive model including temperature and PAR and 49% with PAR alone (Table 4.2). These results indicate that variations in surface PPC: PSC ratios are linearly associated with PAR and temperature, with better predictions possible for samples with low DIN concentrations.

Variations in pigment ratios and environmental parameters as a function of depth

Nutrients- For all depths and samples combined, there was a weak inverse linear relationship between PPC: PSC ratios and DIN ($r^2 = 0.24$, $p<0.001$). At pump stations CH6 (11Aug), CP4 (16Aug), HB6, HB8, HB10, the 5-m DIN concentrations

Table 4.2. Multiple linear regression results using stepwise linear regression (SPSS). Separate analyses were conducted for all 5-m samples and for samples with DIN < 2 μM. Y variable is PPC: PSC (g: g). X variables are temperature (T), salinity (S), PAR (par) at sample depth (averaged over prior 24 h assuming 14 h daylight), DIN (N = NO_3+NO_2+NH_4).

All 5-m samples (except CP11 and CH3). n=45

								Extra sum of squares F-test (for each stepwise decrease)			unstandardized coeff		
X variables	r	r2	F	p	SSE	MSE	df	F-stat	signif	variable	B	std error	p-value
T,par,N, S	0.68	0.46	8.51	0.000	0.138	0.003	40			Constant	1.26E+00	1.024	0.227
										Temp	3.69E-02	0.014	0.012
										PAR	5.91E-04	0.000	0.026
										DIN	-2.14E-03	0.003	0.534
										Salin	-4.56E-02	0.031	0.143
T,par,N	0.66	0.43	10.29	0.000	0.146	0.004	41	2.67	p> 0.1	Constant	-2.52E-01	0.179	0.167
										Temp	3.79E-02	0.014	0.011
										PAR	5.55E-04	0.000	0.000
										DIN	-2.54E-03	0.003	0.467
T, par	0.65	0.42	15.34	0.000	0.148	0.004	42	1.67	p> 0.1	Constant	-3.40E-01	0.132	0.014
										Temp	4.46E-02	0.011	0.000
										PAR	5.12E-04	0.000	0.046
T	0.60	0.36	24.62	0.000	0.163	0.004	43	4.26	p<0.05	Constant	-3.99E-01	0.134	0.005
										Temp	5.24E-02	0.011	0.000

5-m samples with DIN< 2 uM. n=20

								Extra sum of squares F-test (for each stepwise decrease)			unstandardized coeff		
X variables	r	r2	F	p	SSE	MSE	df	F-stat	signif	variable	B	std error	p-value
T,par,N, S	0.83	0.69	8.33	0.001	0.038	0.003	15			Constant	1.79E+00	1.288	0.185
										Temp	4.09E-02	0.019	0.052
										PAR	1.20E-03	0.000	0.005
										DIN	-2.55E-02	0.024	0.296
										Salin	-6.39E-02	0.038	0.117
T,par,N	0.80	0.63	9.17	0.001	0.045	0.003	16	2.33	p> 0.1	Constant	-3.09E-01	0.264	0.258
										Temp	4.20E-02	0.020	0.056
										PAR	1.09E-03	0.000	0.011
										DIN	-2.28E-02	0.025	0.371
T, par	0.78	0.61	13.46	0.001	0.048	0.003	17	1.00	p> 0.1	Constant	-3.82E-01	0.251	0.146
										Temp	4.62E-02	0.020	0.033
										PAR	1.18E-03	0.000	0.004
par	0.70	0.49	17.26	0.000	0.063	0.004	18	5.00	p<0.05	Constant	1.98E-01	0.030	0.000
										PAR	1.52E-03	0.000	0.001

were ≤ 1.2 μM and nutrient gradients between 5 m and 10 m were large (concentrations were ~2 to 10 times higher at 10 m than 5 m). These stations also showed higher (10-70% larger) PPC: PSC ratios at 5 m than at 10 m depths.

Light- We compared PPC: PSC ratios to PAR values averaged over the prior 24 h assuming waters stratified conditions (see method 1 in Methods section) and over the prior 1 hour for samples collected from 800 to 1800 (Figure 4.9c,d). We found weak relationships between PPC: PSC ratios and mean PAR over prior the 24 h and prior 1 hour ($r^2 = 0.36$ and 0.46, respectively, $p < 0.001$). The relationship of PPC: PSC ratios to mean PAR over the prior 1 h was similar for 5 m samples and all depths combined (Figure 4.9b,d).

A significant vertical gradient in PPC: PSC ratios was observed between 5 m and 10 m for pump stations CP5, CP4 (15Aug, 2nd profile), MC1, HB6, HB8, HB10 (Appendix B). These gradients correspond to the irradiance gradient near the surface (~5 to 50 μmol photons m^{-2} s^{-1} from 10 m to 5 m, Appendix B). Similar vertical gradients in irradiance were observed at other pump stations (CH1, CP1 and CP4 (15Aug, first profile)), although no significant differences in PPS: PSC ratios were seen.

Temperature- We found positive relationships between temperature and PPC: PSC ratios (Figure 4.10b, $r^2 = 0.36$, $p < 0.001$). As seen for the 5 m data alone (Figure 4.10a), higher PPC: PSC ratios were associated with higher temperatures. However, the slope of the regression line was steeper for data from 5 m depths compared to all

depths combined. We found a weaker relationship between temperature and PPC: PSC ratios for samples from colder deeper waters (r^2= 0.16, p<0.05 for samples from > 10 m). This relationship was not significantly different than that seen for all depths combined (p> 0.05)

Interaction of nutrients, temperature, salinity, PAR and depth- We used multiple regression to evaluate the interaction of the explanatory variables: depth, temperature, salinity, PAR (averaged over prior 24 h) and DIN on PPC: PSC ratios for all depths combined (excluding CP11 at 5 and 10 m). Using an additive model with all five explanatory variables, we could explain 58% of the variability (Table 4.3). We can simplify this model and explain 50% of the variability using two parameters (depth, PAR) and 39% using a single parameter (depth). For this data set, we also calculated partial correlation coefficients between temperature, salinity, PAR, DIN and PPC: PSC ratios with the effects due to depth held constant. These results indicated that after accounting for depth effects, significant linear correlations to PPC: PSC ratios are seen for temperature and PAR but not for salinity and DIN.

Spatial distributions of optical and hydrographic properties

Examples of higher resolution horizontal variations of a_p slopes and pigment ratios

To examine higher resolution spatial variations in the optical and hydrographic parameters we evaluated surface ac-9 and CTD data (3 to 7 m depth bins) collected along two transects (HB transect on 21 August and ST transect on 25 August, *see*

Table 4.3. Multiple linear regression results using stepwise linear regression (SPSS) for all depths combined. Y variable is PPC: PSC (g: g). X variables are temperature (T), salinity (S), PAR (par) at sample depth (averaged over prior 24 h assuming 14 h daylight), DIN (N = NO_3+NO_2+NH_4) and depth (D).

All depths combined, n=127								Extra sum of squares F-test (for each stepwise decrease)			unstandardized coeff		
X variables	r	r2	F	p	SSE	MSE	df	F-stat	signif	variable	B	std error	p-value
D,T,S,par,N	0.76	0.57	32.74	0.000	0.463	0.0038	121			Constant	1.476E+00	0.614	0.018
										Depth	-8.653E-04	0.000	0.002
										Temp	3.064E-02	0.007	0.000
										Salin	-5.065E-02	0.019	0.010
										PAR	6.405E-04	0.000	0.000
										DIN	5.558E-03	0.001	0.000
D,T,par,N	0.74	0.55	37.40	0.000	0.489	0.004	122	6.79	p<0.025	Constant	-1.180E-01	0.091	0.195
										Depth	-1.161E-03	0.000	0.000
										Temp	2.613E-02	0.007	0.001
										PAR	6.071E-04	0.000	0.001
										DIN	3.906E-03	0.001	0.001
D, PAR	0.71	0.50	78.93	0.000	0.544	0.0044	124	6.86	p=0.001	Constant	2.100E-01	0.011	0.000
										Depth	-1.263E-03	0.000	0.000
										PAR	7.915E-04	0.000	0.000
D	0.62	0.39	78.93	0.000	0.667	0.0053	125	28.04	p<0.001	Constant	2.500E-01	0.009	0.000
										Depth	-1.819E-03	0.000	0.000

Figure 4.11). Both these transects crossed fronts and display examples of the physical and optical variability encountered in the Oregon coastal region. The surface data in the HB and ST transects are within the spatial and hydrographic domain of the samples in group MID. Therefore, we applied the linear relationship between PPC: PSC ratios and ac-9 derived slopes obtained for that group.

It must be noted that estimates of PPC: PSC ratios from continuous in situ absorption measurements (either surface or vertical sections) rely on realistic estimates of the detrital contribution to the obtained absorption spectra. Alternatively, a reasonable assumption of the spatial uniformity in a_d allows the use of a_p as a proxy for a_{ph} in the relationship between a_p slopes and PPC: PSC ratios. We found that the PPC: PSC to a_p slope relationship for group MID was not significantly different than the PPC: PSC to a_{ph} slope relationship (chapter 3), indicating a relatively low and spatially uniform contribution of detritus to the a_p spectra. Use of a_p slopes to predict pigment ratios in regions with variable and high concentrations of detritus would require additional calibration data from QFT analysis.

We used a model 1 linear regression (PPC: PSC ratio = -34.4 (a_p slope) - 0.26) to estimate the PPC: PSC ratios from the a_p slopes for the HB and ST transects (Figure 4.11). The individual r^2 was 0.91 for the discrete samples collected at ST transect stations on 25 Aug (Figure 4.12), although the linear regression equation was not significantly different than the general regression for all MID samples (3-5 m depths) combined ($p<0.05$). The a_p slopes and estimated PPC: PSC ratios were comparable to values seen for discrete samples from stations in the ST line and station HB12 (Figures 4.12, 4.13, 4.14, Appendix C).

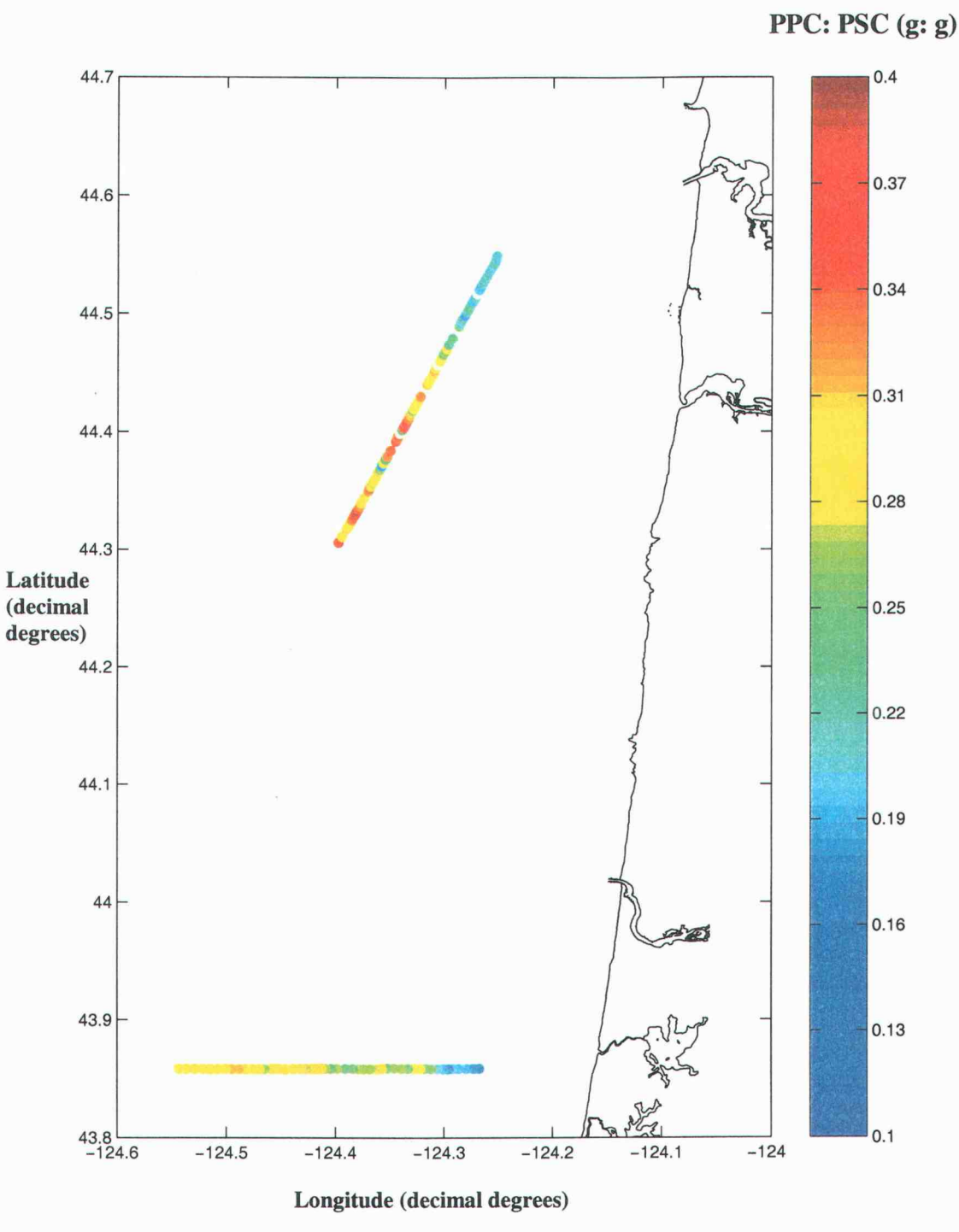

Figure 4.11. Surface PPC: PSC ratios estimated from ac-9 a_p slopes (means for 3-7 m) for the HB transect at 43.86° N on 21 August and the ST transect from 44.31° N, 124.40° W to 44.55° N, 124.25° W on 24-25 August in Oregon coastal waters. Regression used was: PPC: PSC ratio = $-34.39(a_p \text{ slope}) - 0.2632$.

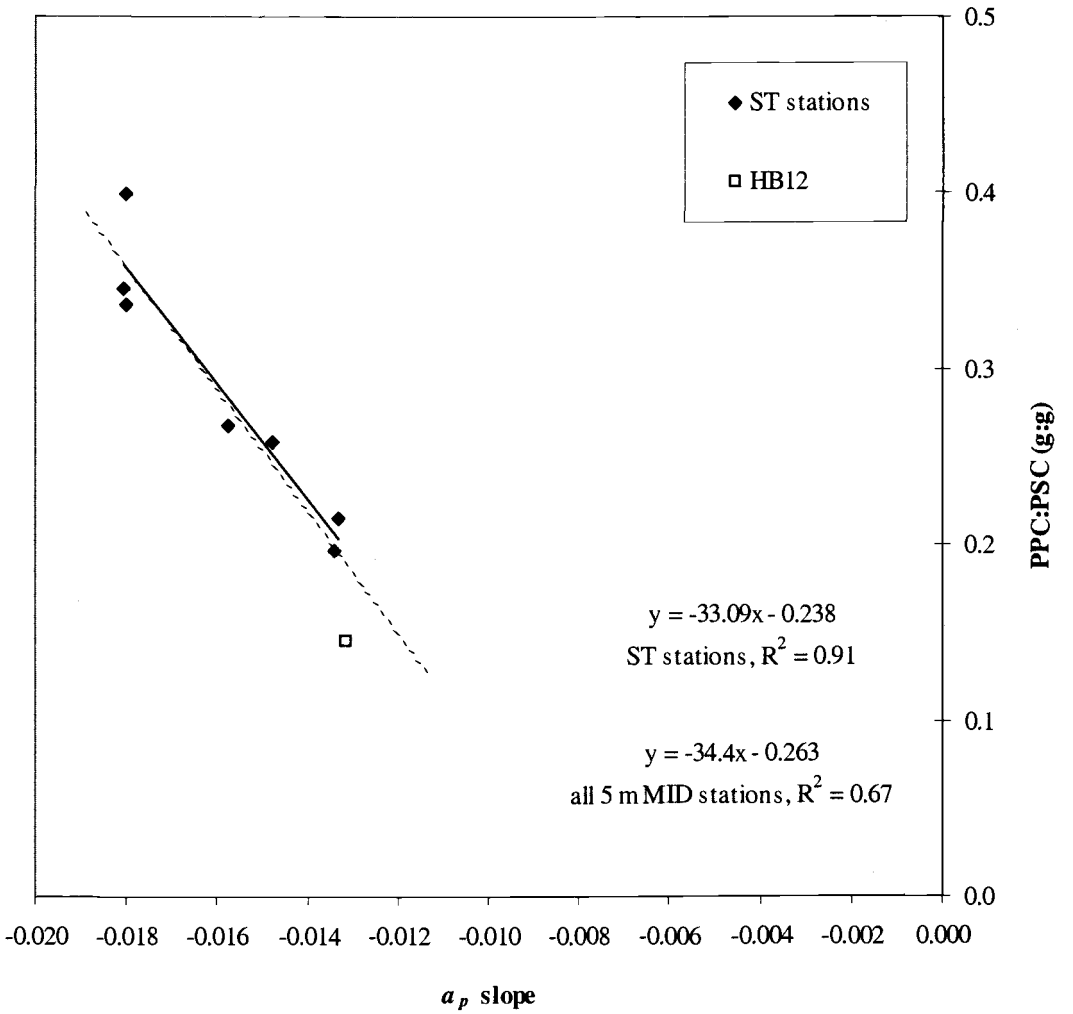

Figure 4.12. Relationship between surface a_p slopes and PPC: PSC ratios for samples from the ST line (ST6 to ST12) on 24-25 August and station HB12 on 21 August. Model 1 regressions for the ST stations (solid line) and for all MID 5 m samples (dashed line).

Figure 4.13. Surface (mean values for 3-7 m depths) optical and hydrographic properties for the HB longitudinal transect on 21 August along 43.86° N from inshore at 124.5° W to further offshore at 124.55° W. Total length of transect was 24 km. Parameters include particulate absorption (a_p) slope parameter (an index of PPC: PSC ratios), c_p440: c_p650 (ratio of particulate beam attenuation at 440 to 650 nm, an index of the particle size distribution), a_p 676: c_p650 (an index of chl a pigment per particle), a_p 676 (an indicator of chl *a* concentration, temperature and salinity.

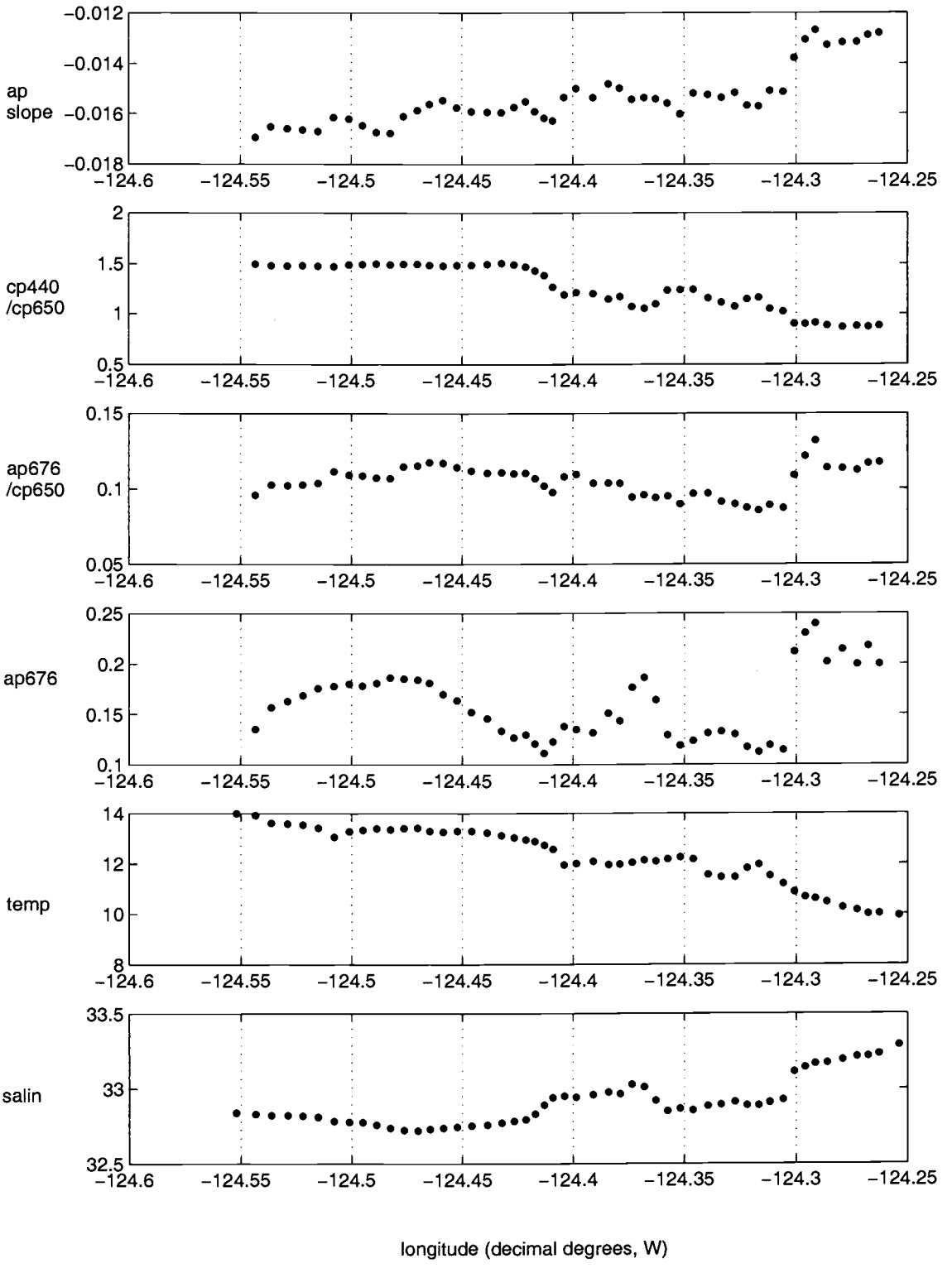
ap slope
-0.012
-0.014
-0.016
-0.018
cp440 /cp650
2
1.5
1
0.5
ap676 /cp650
0.15
0.1
0.05
ap676
0.25
0.2
0.15
0.1
temp
14
12
10
8
salin
33.5
33
32.5
-124.6
-124.55
-124.5
-124.45
-124.4
-124.35
-124.3
-124.25
longitude (decimal degrees, W)

Figure 4.13.

Figure 4.14. Surface (mean values for 3-7 m depths) optical and hydrographic properties for the ST transect on 24-25 August from station ST6 at 44.31° N, 124.40°W to station ST11 at 44.55° N, 124.25° W. Total length of transect was 30 km. Same parameters as described in Figure 4.13.

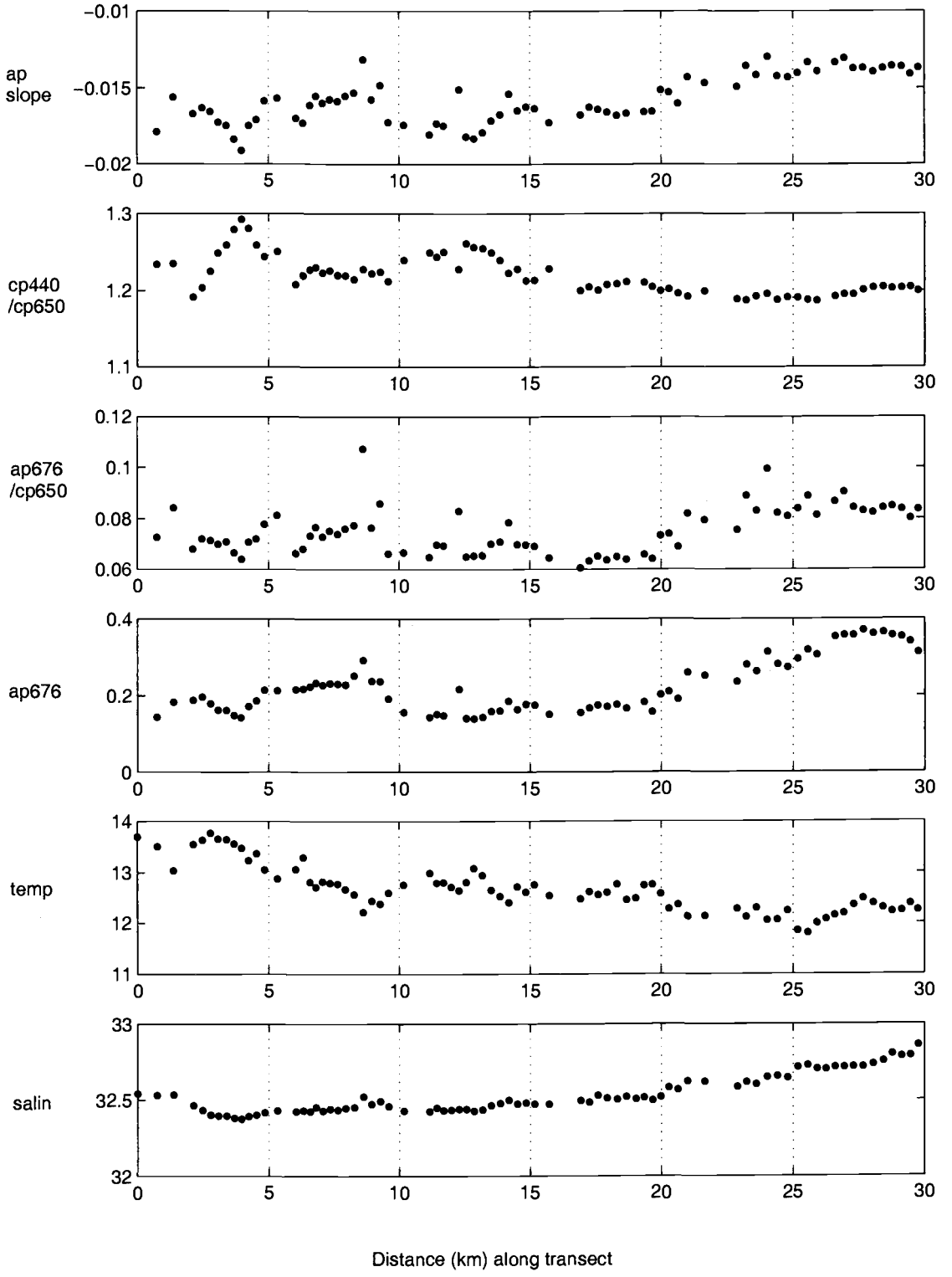
ap
slope
-0.01
-0.015
-0.02
cp440
/cp650
1.3
1.2
1.1
ap676
/cp650
0.12
0.1
0.08
0.06
ap676
0.4
0.2
0
temp
14
13
12
11
salin
33
32.5
32
0
5
10
15
20
25
30
Distance (km) along transect

Figure 4.14.

The HB transect is a longitudinal transect covering ~24 km from 124.6° W to 124.25° W conducted on 21 August. We observed steeper a_p slopes, higher c_p440: c_p650 ratios, lower a_{ph}676: *cp650* ratios, higher temperatures and lower salinities further offshore compared to closer to the coast (Figure 4.13). There was considerable cross shelf variation with large gradients seen at ~124.42° W and, in particular, at 124.3° W. High a_p676 values were seen at various locations along the transect. These data suggest that phytoplankton assemblages located closer to the coast consisted of larger cells with lower PPC: PSC ratios and higher chl *a* per cell, and were in newly upwelled water (T = 10°C and S > 33) with high nutrients (DIN = 11.8 μM near the coast) (Figure 4.12, Figure 4.3a). In contrast, phytoplankton assemblages located further from shore appeared to have smaller cells with higher PPC: PSC ratios and were in warmer, fresher, low nutrient water (at station HB6 located ~15 km NW of this transect, DIN ~ 1.0 μM). High chl *a* concentrations were observed in both these water masses (based on a_p676 values), although the species composition of these assemblages may have been different based on the geographic separation and different water mass characteristics. The discrete 5-m sample from station HB6 on 19 August had T and S characteristics similar to the HB transect at 124.46° W, a further offshore location with high a_p676. The PPC: PSC ratio was 0.26 g: g, the fuco: Tchl *a* ratio was 0.55 g: g, and Tchl *a* was 15.3 μg L^{-1} at station HB6 (Appendix C). Whereas, at station HB12, the innermost location on the HB transect, the PPC: PSC ratio was 0.14 g: g, the fuco: Tchl *a* ratio was 0.43 g: g (with minimal perid: Tchl *a* of 0.04 g: g), and the Tchl *a* was 11.3 μg L^{-1}. These pigment ratios suggest that diatoms dominated the

assemblages at both locations, but the differences in c_p440: c_p650 ratios suggest that these locations possessed different size distributions and likely different species composition. Also, for the area near shore, c_p440: c_p650 were < 1 (negative γ) which suggests that there was a mono disperse assemblage of particles, since particles of a single size can be at a point in the scattering efficiency curve where there is less scattering in the blue compared to the red region of the spectrum. Hence, these data indicate that a monospecific phytoplankton bloom may have occurred near the coast. Variations in the photoacclimation of species common to both locations may also be important.

The ST transect was conducted in a NNE direction from 44.3° N, 124.4° W to 44.55° N, 124.25° W covering ~ 30 km. There were both longitudinal and latitudinal gradients in optical and hydrographic properties. Generally, steeper a_p slopes, higher c_p440: c_p650 ratios, higher a_p676: c_p650 ratios, and lower a_p676 values were seen further south and further offshore (at the start of the transect) compared to samples located further north and onshore. Very high a_p676 values (>0. 4 m^{-1}) were seen inshore at the end of the transect at ~27 to 30 km (Figure 4.14). The spatial patterns for these four parameters generally co-varied with steeper a_p slopes associated with higher c_p440: c_p650, lower a_p676: c_p650 and lower $a_{ph}676$. Temperatures were higher and salinities lower further south and offshore (Figure 4.14, Figure 4.3b). These data suggest that the phytoplankton assemblages were generally smaller further south and offshore (but see variations for 0 to 5 km slice), although the PSD parameter (c_p440: c_p650) had a much narrower range than seen in the HB transect. The a_p slope and $a_{ph}676$ data suggest that PPC: PSC ratios were higher in southern more offshore

waters coinciding with relatively lower chl *a* concentrations. As seen with the HB transect, the higher PPC: PSC ratios are associated with higher temperature, lower salinity, lower nutrient (DIN < 0.25 μM) waters whereas the lower PPC: PSC ratios were associated with lower temperature, higher salinity, somewhat higher nutrient (DIN = 1.7 μM) waters.

Examples of vertical distributions of optical and hydrographic properties

We now compare the vertical variations in chemotaxonomic pigments, Tchl *a*, PPC: PSC ratios and diadinoxanthin + diatoxanthin (Dd+Dt): Tchl *a* ratios, Qa*676 derived from QFT and HPLC data, ac-9 a_{ph} slopes, c_p440: c_p650, and a_{ph}676: c_p650 ratios for selected stations, CH3 and CH6. Data were obtained from analysis of discrete samples within in the upper 50 m of the water column. The Qa*676 values were greater than 1, at CH6, exceeding the theoretical maximum, for all samples, so Qa*676 profile data were not considered for this station.

At station CH3 the Tchl *a* concentrations were higher at the surface, lower at mid-depth (20-25m), and moderate deeper in the water column (40 m) (Figure 4.15, Appendix B). The fuco: Tchl *a* levels (indicative of diatoms) were higher at the surface and at 30-45 m than at mid-depth. Conversely, we saw higher levels of other biomarkers (perid = dinoflagellates, allo = cryptomonads, hex = prymnesiophytes) at mid depth than elsewhere in the water column. We also saw increased Qa*676 values

at mid depth suggesting that packaging was lower for those phytoplankton assemblages, due to at least partially to a shift in species composition. The c_p440:

Figure 4.15. Station CH3 on 9 August: vertical profiles for the top 50 m of the water column of a) HPLC derived pigment: Tchl *a* ratios (g: g) and Tchl *a* concentration (μg L^{-1}) and b) temperature and salinity for pump profile data (symbols only) and cast conducted ~ 1 h after pump profile (dashed line), and parameters derived with in situ optics, HPLC (PPC: PSC ratios and Tchl *a*) or both (Tchl *a*: c_p650) for c) pump profile and d) profile ~1 h after pump profile.

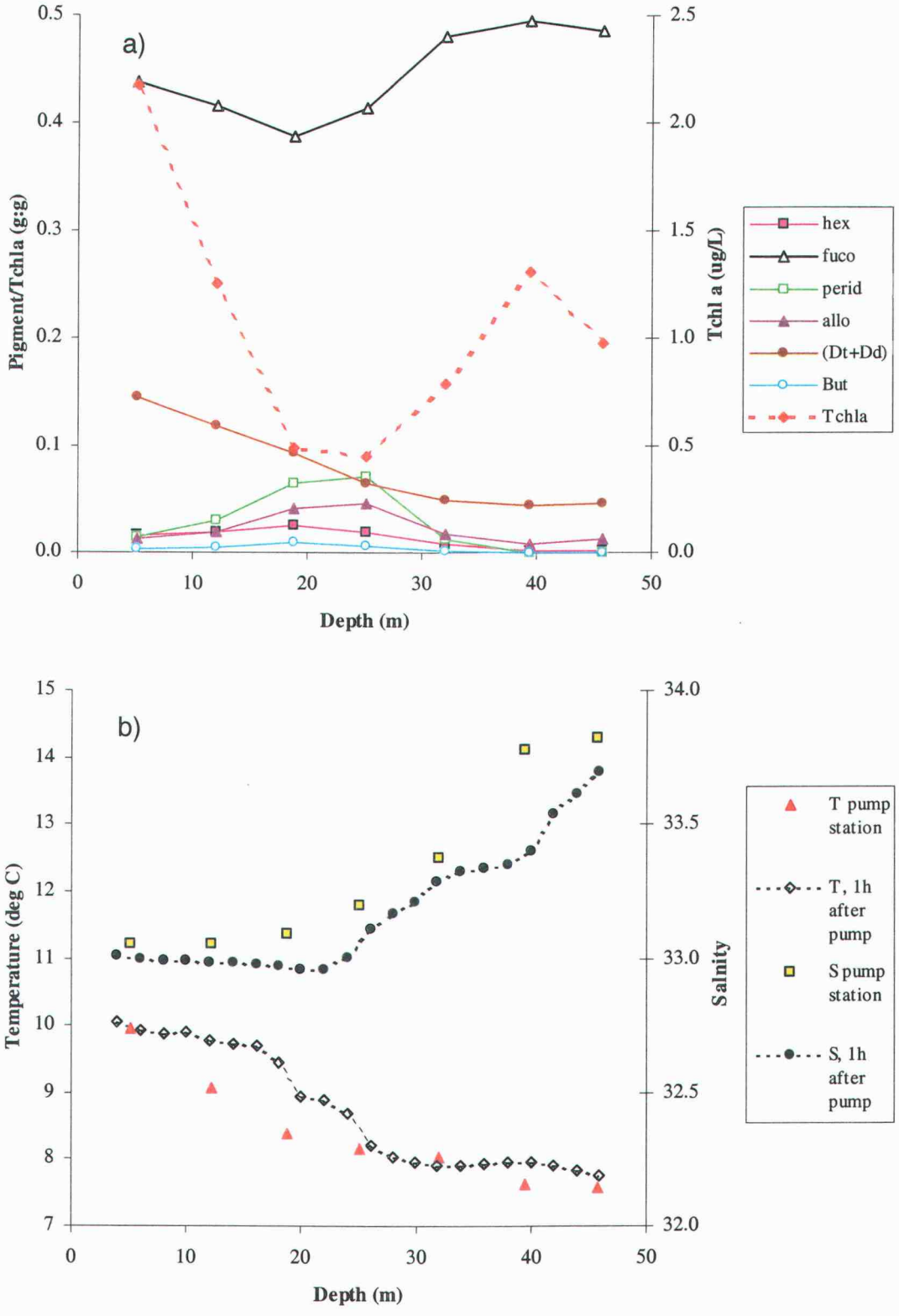
a)
Pigment/Tchla (g:g)
Tchl a (ug/L)
Depth (m)
hex
fuco
perid
allo
(Dt+Dd)
But
Tchla
b)
Temperature (deg C)
Salnity
Depth (m)
T pump station
T, 1h after pump
S pump station
S, 1h after pump

Figure 4.15

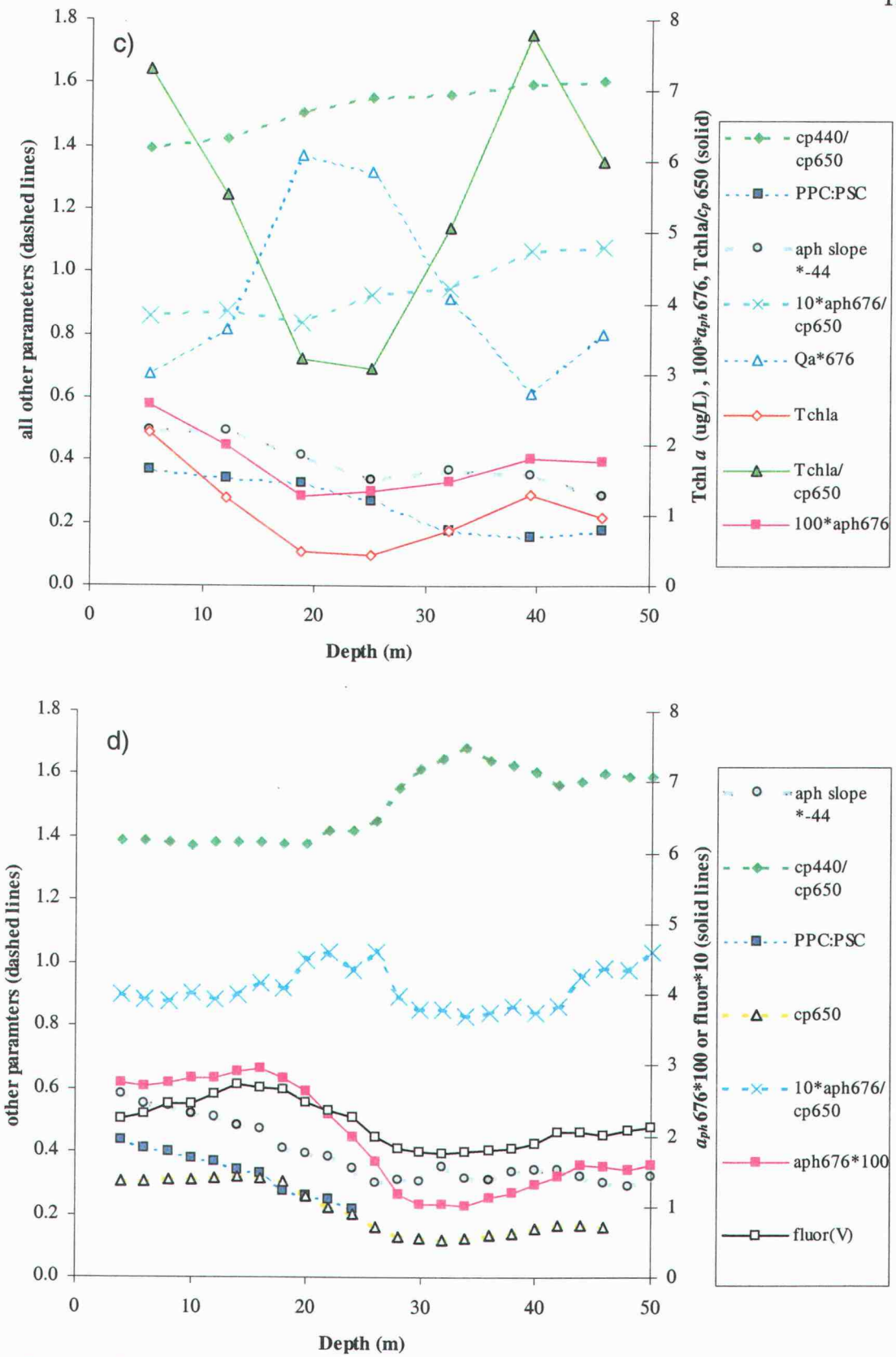

Figure 4.15 continued

c_p650 values were higher deeper in the water column, suggesting that the mean particle size decreased with depth. At this group IN station, the a_d values were high but constant throughout the water column (a_d412: a_p412 = 0.44 to 0.54 from QFT). Thus, the c_p440: c_p650 ratios may reflect PSD variations in both phytoplankton and non-pigmented (detrital) particles. The Tchl *a*: c_p650 ratios appeared to inversely vary with Qa*676 suggesting that the mid-depth packaging increase was partially due to reductions in the Tchl *a* per particle (pigment per cell). The a_{ph}676: c_p650 ratios did not show a similar pattern as Tchl *a*: c_p650 ratios. The PPC: PSC ratios, (Dd+Dt): Tchl *a* ratios and a_{ph} slope magnitude all decreased with depth. There was a significant linear relationship between PPC: PSC ratios and ac-9 a_{ph} slopes for samples collected from 5 to 46 m at this station, (PPC: PSC = -41.38*(a_{ph} slope)-0.110, r^2 = 0.70, $p<$ 0.001, n = 7). The diadinoxanthin + diatoxanthin (Dd+Dt): Tchl *a* ratio was also correlated with a_{ph} slopes ((Dd+Dt): Tchl *a* = -20.22*(a_{ph} slope)-0.101, r^2 = 0.85, p<0.001). Surface nutrients were high throughout the water column, thus the reduction in photoprotective pigments with depth is more likely due to reduced light exposure and or shifts in taxonomic composition.

At station CH6, the Tchl *a* concentrations were higher in the top 20 m than at 30 to 50 m (Figure 4.16). Fuco: Tchl *a* and hex: Tchl *a* ratios were both high and seemed to be inversely correlated. Hex decreased and fuco increased from 10 m to 20 m, and fuco decreased and hex increased from 20 to 50 m. The perid: Tchl *a* and allo: Tchl *a* remained low and constant whereas the but: Tchl *a* increased with depth. Chl *b*: Tchl *a* ratios were relatively high (compared to MID and IN stations), with increased values seen at 50 m where Tchl *a* concentrations were very low. The Tchl

Figure 4.16. Station CH6 on 8 August: vertical profiles for the top 50 m of the water column of a) HPLC derived pigment: Tchl *a* ratios (g: g) and Tchl *a* concentration (μg L^{-1}) and b) temperature and salinity for pump profile data (symbols only) and cast conducted ~ 45 min after pump profile (dashed line), and parameters derived with in situ optics, HPLC (PPC: PSC ratios and Tchl *a*) or both (Tchl *a*: c_p650) for c) pump profile and d) profile ~ 45 min after pump profile.

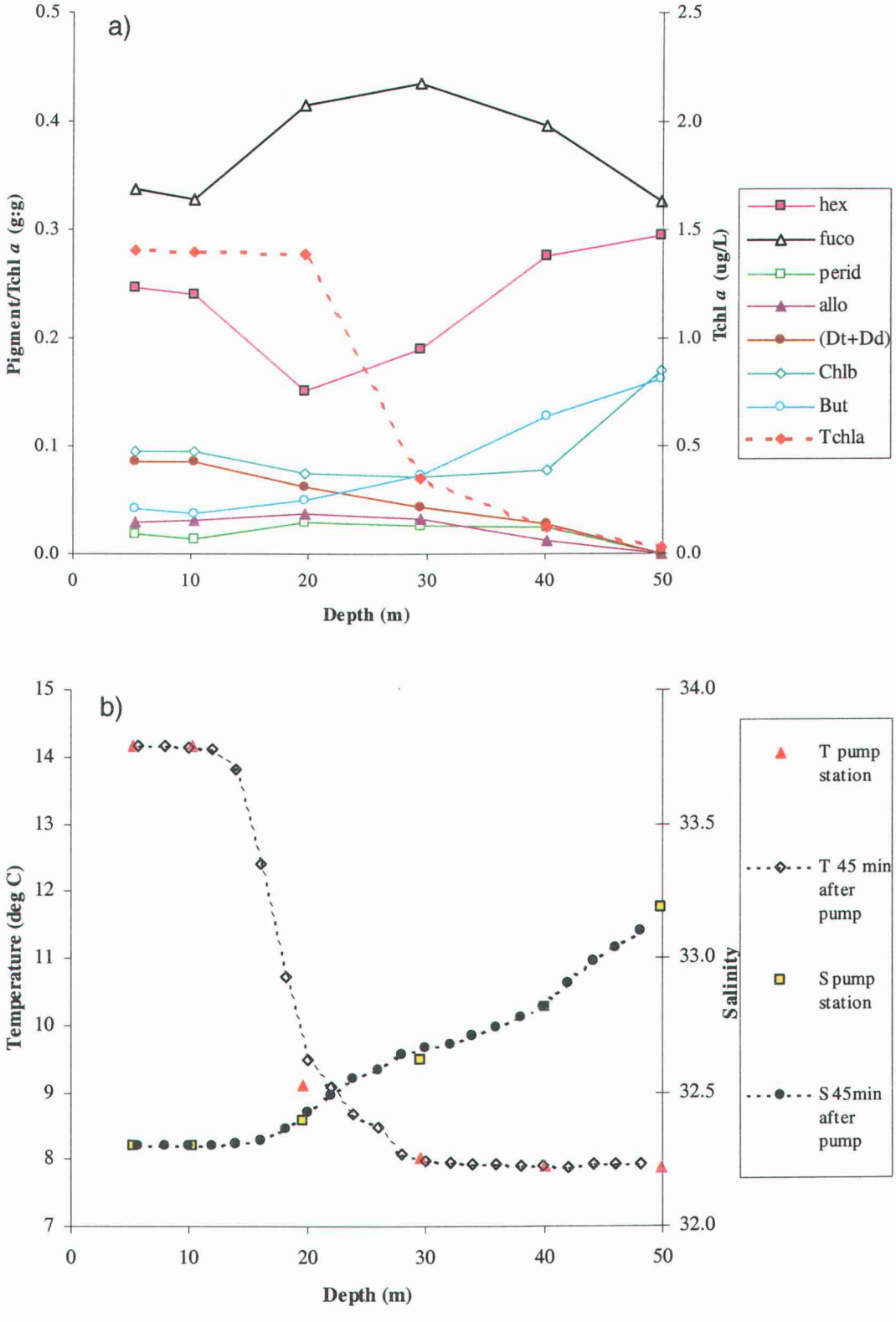
a)
Pigment/Tchl a (g:g)
Tchl a (ug/L)
Depth (m)
hex
fuco
perid
allo
(Dt+Dd)
Chlb
But
Tchla
b)
Temperature (deg C)
Salinity
Depth (m)
T pump station
T 45 min after pump
S pump station
S 45min after pump

Figure 4.16

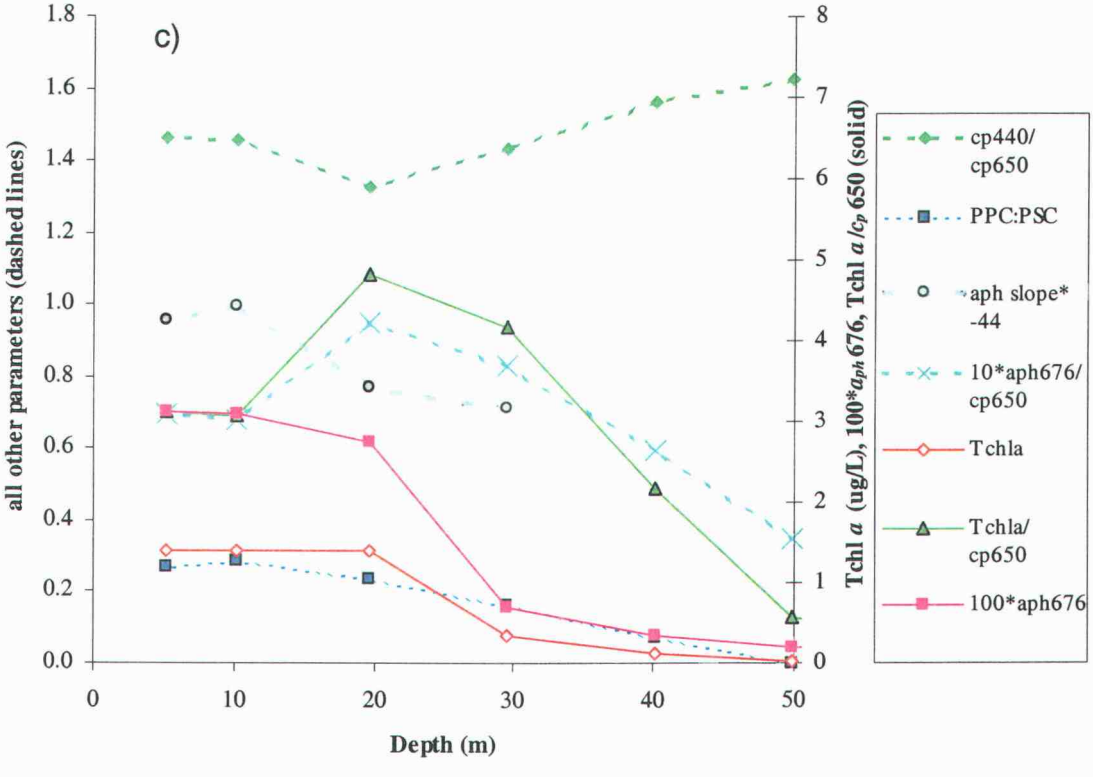

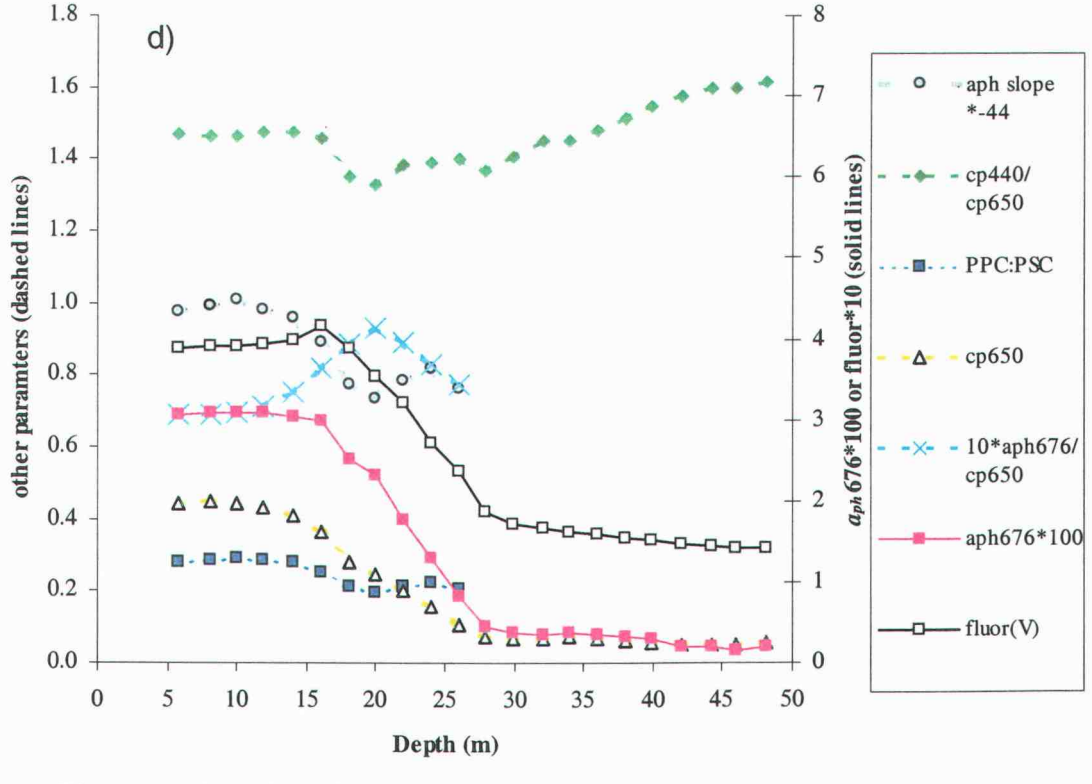

Figure 4.16 continued

a: c_p650 ratios and a_{ph}676: c_p650 ratios showed similar patterns with maxima seen at 20 m. The c_p440: c_p650 ratios were at their minima at 20 m, indicating that the assemblages had PSDs with flatter slopes, suggestive of larger particles, and increased Tchl *a* per cell, suggesting an increase in packaging (perhaps due to an increase in diatom abundance). The a_d412: a_p412 varied from 0.2 to 0.7 for the top 20 m compared to 50 m. Therefore, it is possible that increases in the detrital component may have contributed to the increase in the c_p440: c_p650 ratios seen between 20 and 50 m. The PPC: PSC ratios, (Dd+Dt): Tchl *a* ratios and a_{ph} slope magnitude all decreased from 10 m to 50 m. We found a significant linear relationship between PPC: PSC ratios and ac-9 a_{ph} slopes for samples collected from 5 to 30 m at this station, (PPC: PSC = -15.917*(a_{ph} slope)-0.0.0701, $r^2 = 0.83$, $p < 0.05$, n = 4). The (Dd+Dt): Tchl *a* ratio was also correlated with a_{ph} slopes ((Dd+Dt): Tchl *a* = -6.34*(a_{ph} slope)-0.054, $r^2 = 0.94$, $p<0.05$). This station had fairly low surface nutrient values (DIN = 2.3 μM), thus a combination of low nutrients and higher irradiance may be associated with the higher PPC concentrations near the surface. Taxonomic composition (high hex: Tchl *a*) may also be important.

Vertical variations in PPC: PSC ratios and aph slopes at fine-scale resolution

A vertical profile of optical and hydrographic data was obtained at station CH3 just 45 min after pump profiling of discrete samples was completed. We binned the CTD and ac-9 data into 2-m depth bins for the top 50 m of the water column. We then used the linear relationship between PPC: PSC and a_{ph} slopes for the CH3 pump station to derive estimates of PPC: PSC ratios from a_{ph} slopes. The fine-scale vertical

profile data resemble the discrete sample profile data (Figures 4.15) for the a_{ph} slopes and PPC: PSC ratios. In contrast, the fine scale c_p440: c_p650 ratios are constant in the upper 25 m and then show a shift to higher values (indicative of smaller particles) for deeper waters (Figure 4.15c), whereas the earlier profile shows a more gradual increase in c_p440: c_p650 with depth (Figure 4.15d).

We obtained a vertical profile of optical and hydrographic data at station CH6 (8Aug) approximately 30 min after the pump station. The linear regression found for PPC: PSC ratios to a_{ph} slope from the CH6 pump station was used to predict PPC: PSC ratios from a_{ph} slopes for the upper 30 m. Below 30 m the a_{ph} 676 values were < 0.005 and thus considered to be too low for reliable use. The measured a_{ph} slopes, derived PPC: PSC ratios and measured c_p440: c_p650 ratios all resembled the pump station values, with fine scale variations seen in the 2-m binned data that are missed in the more coarsely sampled discrete profile (Figures 4.16). The $a_{ph}676$: c_p650 ratios varied inversely with the a_{ph} slopes and PPC: PSC ratios in the upper 24 m with the highest ratios seen within the pycnocline. The $a_{ph}676$: c_p650 ratio provides an estimate of the average Tchl *a* absorption per particle (phytoplankton and detritus). Since detrital contribution was low in the upper 20 m (based on pump station QFT data), the $a_{ph}676$: c_p650 ratio provides a rough estimate of the average Tchl *a* per phytoplankton cell for this region of the water column. These data suggest that the average Tchl *a* per cell was higher when PPC: PSC ratios were lower and vise versa, as would be expected during photoadaption of the phytoplankton assemblage. The decrease in $a_{ph}676$: c_p650 from 24 to 28 m may reflect an increase in detrital

contribution (a_d412: a_p412 increased from 0.18 to 0.32 from 20 to 30 m based on QFT data from the pump station).

Discussion

Our results show that optical tools in conjunction with discrete water samples (HPLC and QFT analyses) can offer insight into the phytoplankton photophysiology and taxonomic characteristics of the phytoplankton assemblage in a diverse environment such as the Oregon coastal zone. We have shown that PPC: PSC ratios can be estimated from ac-9 a_{ph} slope measurements using linear relationships and these relationships differ for phytoplankton communities with broadly different water mass characteristics, sampling dates and locations (chapter 3). The relationship between PPC: PSC ratios and a_{ph} slopes was more variable for vertical samples than seen for surface (5 and 10 m) samples (chapter 3) since surface water masses may have quite different origins and light and nutrient histories than those located below the pycnocline and deeper in the water column.

The PPC: PSC ratios can be used to understand variations in photophysiology since phytoplankton can increase PPC concentrations under high light and/or low nutrient conditions (Schluter et al.2000). Taxonomic composition can also affect pigmentation since taxa have different carotenoid compositions that may produce variations in the PPC: PSC ratios. One species may out compete another under various light and nutrient conditions. Increases in PPC: PSC ratios also are associated with low temperatures (5°C in laboratory studies with *Chlorella*, Maxwell 1994,

1995). Cells may produce PPC to alleviate excess light energy since the photosynthetic capacity is reduced at low temperature. This does not appear to be a factor of concern in our study area, however, since temperatures were relatively high (above 7 °C). Also, PPC: PSC ratios were seen to be positively instead of negatively associated with temperature. A relationship between temperature and PPC: PSC ratios may be related to other characteristics such as nutrients, PAR, and phytoplankton taxonomic composition that will vary between water masses. For example, higher PPC: PSC ratios are often seen in higher temperature waters since warmer waters are observed near the top of the water column where irradiance is higher and nutrients are often lower under stratified conditions.

The PPC: PSC ratios likely decreased from surface to depth and from offshore to onshore due to variations in irradiance or nutrient availability. For our data set we analyzed the variability in PPC: PSC ratios due to temperature, salinity, PAR (daytime mean over prior 24 h), DIN and depth. We found that 50% of the variability in PPC: PSC ratios could be explained by PAR and depth for all samples from all depths combined, 42% by temperature and PAR for all 5-m samples combined, and 61% by temperature and PAR for samples with low DIN (< 2 μM) concentrations. These results indicate that prior light exposure has a substantial influence on PPC: PSC variability with the best predictions seen for samples found in low nutrient waters.

PPC can increase under high light and decrease under low light, whereas chl *a* per cell and to some extent, PSC, show the opposite trend (Geider et al.1996). The PPC are thought to be located in the light harvesting antennae and the reaction center of the photosynthetic system and may serve to dissipate excess light energy as heat

(Falkowski and Raven 1997, MacIntyre et al. 2002). Conversely, the energy absorbed by chl *a* and PSC pigments is funneled along the electron transport chain for use in photosynthesis. Thus, higher PPC, lower chl *a* and possibly lower PSC are predicted for high light compared to low light conditions. Accordingly, PPC: PSC ratios may provide an indication of the recent light history of the phytoplankton assemblage.

Our results indicate that changes in PPC: PSC ratios are influenced by light history (over prior 1 h or prior 24 h). We found similar regression line slopes for PPC: PSC ratios and mean PAR over the prior 1 h for Oregon Coast data and East Sound data (Eisner et al. 2003) (Figure 4.9b). This suggests that PPC: PSC ratios for Oregon Coast and East Sound assemblages are responding to prior light exposure in a similar manner. In contrast, the differences in the y-intercepts of the regression lines suggest that the PPC: PSC ratios for assemblages exposed to very low PAR are higher for the Oregon Coast samples compared to the East Sound samples. These differences are likely partially due to taxonomic variations. Both areas were dominated by diatoms, indicated by high fuco: Tchl *a* levels, but there may be regional differences between diatom species in the "baseline" PPC: PSC ratios for assemblages that are exposed to low light (and high nutrients).

DIN concentrations also appear to influence PPC: PSC ratios under low nutrient conditions. When N is limiting phytoplankton may have less functional photochemical reaction centers since the cell may have reduced ability to repair damaged reaction centers, consequently less of the absorbed energy can be used in photosynthesis (Babin et al.1996). Under these conditions PPC may be in higher concentrations allowing more energy to be dissipated as heat and thereby minimize the

damage due to excess light energy. The higher PPC: PSC ratios seen at 5 m compared to deeper depths may be due to N limitation, as well as higher PAR exposure for select stations (Heceta Bank stations HB6, HB8, HB10, for example). Nutrient availability can induce modifications in light absorption, energy transfer and charge separation, although these effects may be difficult to assess in the natural marine environment (Babin et al.1996).

Phytoplankton photophysiology and taxonomic composition both can show variations in response to fluctuations in the nutrient and light environment (Johnsen and Sakshaug 1996). At stations HB6 and HB8, nutrients were in much lower concentration at 5 m compared to 10 m (DIN = 1.0 and 12.0), however the chemotaxonomic composition suggested by HPLC pigments was essentially unchanged (Appendix B). In contrast, at station HB10 some chemotaxonomic variations are suggested between surface depths (5 and 10 m) where nutrients were low and 20 m where nutrients were high (DIN ~1 compared to 18 μM, respectively). For samples from 5 - 10 m compared to 20 m, the HPLC data indicate that the fuco: Tchl *a* ratios were slightly higher (0.60 compared to 0.53 g: g), hex: Tchl *a* ratios was lower (0.026 compared to 0.042 g: g) and chl *b*: Tchl *a* ratios were lower (0.02 compared to 0.054 g: g). Tchl *a* concentrations were also much higher at the surface than at 20 m (18.5 compared to 3.5 $\mu g\ L^{-1}$). Since we cannot differentiate between species within a chemotaxonomic group (diatoms for example) using HPLC analyses, there are likely additional taxonomic variations that were not quantified. Other optical parameters that provide an indication of particle size, such as c_p440: c_p650 ratios, may help clarify taxonomic variations within assemblages.

Variation in PPC: PSC ratios appear to be influenced more by prior light exposure than by nutrients under nutrient-replete conditions, as shown by the multiple linear regression analyses for Oregon Coast data and East Sound data (Eisner et al. 2003). If nutrients are sufficient, we may be able to describe qualitatively the recent light and mixing history based on the relative PPC: PSC ratios. For example, at stations CH1 (8 and 10 August pump profiles) we saw no significant difference in PPC: PSC ratios between 5 m and 10 m depths although there were large differences in sigma-t and estimated prior PAR exposure. We speculate that these samples may have come from a well-mixed water column that was recently stratified. Within these two profiles (CH1 on 7 and 10 Aug), the chemotaxonomic composition between 5 and 10 m depths was similar. At station CP1, we also saw similar PPC: PSC ratios and large differences in sigma-t for 5 m compared to 10 m. However, at this station there were differences in chemotaxonomic composition with higher perid: Tchl *a* ratios seen at 10 m. Thus, for station CP1 the similarities in PPC: PSC ratios between 5 m and 10 m depths are more difficult to interpret (we cannot infer that the 5 m and 10 m samples were recently stratified).

The spatial patterns in optically derived parameters: PPC: PSC ratios, c_p440: c_p650, a_{ph}676, and a_{ph}676: c_p650 along with CTD measurements of water mass characteristics can help us understand the interaction of coastal upwelling and intrusions by other water masses (Columbia River plume water, eddies, etc.) on phytoplankton ecology. In our results, we showed examples from two surface transects (HB and ST) of variations in ac-9 optically derived properties and hydrographic parameters. These analyses indicated that the derived PPC: PSC ratios,

relative size and chl *a* varied from onshore to offshore with larger cells, higher chl *a*, lower PPC: PSC ratios seen in the cold salty newly upwelled water close to shore and smaller cells, lower chl *a*, and higher PPC: PSC ratios seen further offshore (Figures 4.11, 4.13). The high inshore and low offshore chl *a* concentrations seen during normal coastal upwelling seasons on the Oregon Coast have been well documented (Small and Menzies 1981, Hill and Wheeler 2002, Landry et al.1989). In addition, particle size distributions have been shown to vary between the shelf and slope based on chl a size fractionation (Corwith and Wheeler 2002) and across the shelf, based on Coulter Counter measurements collected at 45° N in August 1974 (Small et al.1989). Small et al. (1989) estimated the slopes of the cumulative size distribution, with steeper slopes indicating a relatively greater percentage of small particles, and found a greater percentage of large particles inshore than further offshore, with particle size decreasing with depth for stations inshore of 10 km.

Mesoscale cross-shelf variability was also observed in our data (Figures 4.11, 4.13, 4.14). Data from the CP4 to CP5 time series suggest that there were filaments from northward flowing warm salty "spicy" water (Barth et al.2000) at some mid-shelf locations within a background of fresher colder water (Appendix B, Figure 4.8). The PPC: PSC ratios were higher, large cells may have been in greater relative abundance, silicate and occasionally DIN concentrations were low, and perid: Tchl *a* ratios were high in the spicy water compared to the fresher water. Overall, the low Si and fairly low DIN levels in this spicy water mass may have led to higher PPC: PSC ratios and allowed dinoflagellates (possibly large species) to become a greater proportion of the phytoplankton assemblage.

The influences of episodic coastal upwelling on hydrography and phytoplankton photophysiology and taxonomic characteristics are also apparent in our results. For example, at station CH1 the water was colder and more saline, and nutrient (nitrate, phosphate, silicate) concentrations were much higher throughout the water column on 10 August compared to 7 August (5 m nitrate was 17 μM compared to 3 μM), likely due to upwelling driven by the southward winds on 7 to 9 August (Figure 4.2). Diatoms appeared to be the prominent taxonomic group and fuco: Tchl *a* ratios were similar for both dates. The chl *c*1/*c*2: Tchl *a* ratios and Tchl *a* concentrations were lower throughout the water column on 10 Aug compared to 7 Aug (mean chl *c*1/*c*2: Tchl *a* was 0.10 compared 0.17 g: g, and mean Tchl *a* was 9.1 compared to 4.2 μg L^{-1} (Appendix B). The values are consistent with post bloom (2-9 μg L^{-1}) and upwelling (1-4 μg L^{-1}) chl *a* levels seen in Oregon coastal waters during the upwelling season (Dickson and Wheeler, 1995). We also looked at the relative concentrations of chlorophyll *a* epimer, a colored degradation product of chl *a* (Porra et al. 1997). The epimer: Tchl *a* ratios were higher throughout the water column on 10 Aug compared to 7Aug (0.02 to 0.09 on 10 Aug compared to undetectable levels on 7Aug). The increase in chlorophyll *a* epimer also suggests that cells on 10 Aug may have been more recently upwelled. For 5 m data the Qa*676 values and PPC: PSC ratios were slightly higher on 10 Aug relative to 7 Aug (Qa* = 0.67 compared to 0.44 and PPC: PSC = 0.26 to 0.22), perhaps due to a shift in diatom species (as suggested by the variation in chl *c*1/*c*2: Tchl *a* ratios) and/or a different light history (on time scales of hours to days).

We have shown that in situ ac-9 data in concert with discrete samples can be used to help characterize the photophysiological and taxonomic variations of field phytoplankton assemblages. With careful calibrations using HPLC pigments and QFT a_d data, we have been able to obtain high-resolution information on vertical and horizontal spatial patterns in PPC: PSC ratios, relative size differences, chl *a* per cell and Tchl *a* concentration. However, the limitations of these analyses must also be considered. We have determined that the noise of the ac-9 absorption can be as high as 0.005 m^{-1} (R. Desiderio pers. comm.). This equates to ~ 0.2 $\mu g\ L^{-1}$ for $a_{ph}676$, levels which are commonly observed in coastal systems particularly at depth. Since $a_{ph}676$ is in the denominator of our slope equation, this equation is particularly sensitive to uncertainties in a_{ph} 676 at low concentrations. Thus, we were unable to evaluate the a_{ph} slopes for many of the deep samples in our data set. This uncertainty would also be problematic in oceanic samples with low phytoplankton biomass.

The estimation of a_d for the calculation of a_{ph} values and slopes is also important. To estimate a_{ph} slopes from ac-9 data without concurrent QFT measurements of a_d, we need to model the a_d spectra (Roesler et al.1989) or use a_d collected at nearby stations and times (Eisner et al., 2003). Additionally, we had errors in our Qa*676 estimates, since we found values above 1, incorrect theoretically. These errors in Qa*676 may be due to either incorrect estimation of the QFT spectra (perhaps to the β correction) and/or pigments not quantified by HPLC such as phycobilipigments which are water soluble and not extracted by standard HPLC analyses (Bricaud et al.1995, Nelson et al.1993), or pigment loss from incomplete extraction.

Finally, one important limitation of HPLC analyses is that you cannot easily differentiate between species within a taxonomic group. For example, using HPLC data alone, we were unable to distinguish one diatom species from another. Metrics for classification based on relative size such as c_p440: c_p650 ratios, may aid in taxonomic categorization, although, detrital particle contribution will complicate these results. In addition, chains of colonial diatoms, which commonly occur in Oregon coastal waters (Kokkinakis and Wheeler 1987), will appear as large particles, while the cells themselves may be small. Ideally, microscopic enumeration, flow cytometry and/or Coulter Counter measurements should be used to identify species and size structure (Ciotti et al. 2002).

Our results form the Oregon coastal waters and from more protected waters (Eisner et al. 2003) indicate that in situ absorption and beam attenuation measurements can provide high resolution information on optical properties (PPC: PSC ratios, particle size) of the in-water phytoplankton assemblage. This high-resolution data is valuable for understanding the complex interaction of physical and biological parameters and will offer substantial insight into the factors influencing photophysiology and taxonomic variations in marine environments.

Acknowledgements

This research was supported by a Coastal Advances in Ocean Transport (COAST) grant (#OCE-9907854) from the National Science Foundation. We thank Ricardo Letelier for water sample collection and particulate absorption analyses, Pat Wheeler

for nutrient data, Burke Hales for hydrographic data, Jack Barth for contour maps of chlorophyll *a* and temperature, Chris Wingard and Russ Desiderio for help with data processing, and Margaret Sparrow for advice and support with HPLC analysis. Wind data were obtained from the National Data Buoy Center (http://www.ndbc.noaa.gov).

References

Anning, T., H.L. MacIntyre, S.M. Pratt, P.J. Sammes, S. Gibb and R.J. Geider. 2000. Photoacclimation in the marine diatom *Skeletonema costatum.* Limnol. Oceanogr. **45**: 1807-1817.

Atlas, E.L., Hager, S., Gordon, L., and P. Park. 1971. *A practical manual for use of the Technicon AutoAnalyzer in seawater nutrient analyses.* Revised O.S.U. Tech Report 215, Ref. 71-22, Dept. of Oceanography, Oregon State University, Corvallis.

Babin M., A. Morel, H. Claustre, A. Bricaud, Z. Kolber and P.G. Falkowski. 1996. Nitrogen-and-irradiance-dependent variations of the maximum quantum yield of carbon fixation in eutrophic, mesotrophic and oligotrophic marine systems. Deep Sea Res. I **43**: 1241-1272.

Barth, J.A., Pierce, S.D. and R.L. Smith. 2000. A separating coastal upwelling jet at Cape Blanco, Oregon and its connection to the California Current system. Deep Sea Res. II. 783-810.

Barth, J.A and R.L. Smith. 1998. Separation of a coastal upwelling jet at Cape Blanco, Oregon, USA. S. Afr. J. Mar. Sci. **19**: 5-14.

Bidigare, R.R, M.E. Ondrusek, J.H. Morrow, and D.E. Kiefer. 1990. In vivo absorption properties of algal pigments. SPIE Ocean Optics X. **1302**: 290-302.

Boss E., W.S. Pegau, W.D. Gardner, J.R. Zaneveld, A.H. Barnard, M.S. Twardowski, G.C. Chang and T.D. Dickey. 2001. Spectral particulate attenuation and particle size distribution in the bottom boundary layer of a continental shelf. J. Geophys. Res. **106**: 9509-9516.

Bricaud, A., M. Babin, A. Morel, and H. Claustre. 1995. Variability in the chlorophyll-specific absorption coefficients of natural phytoplankton: Analysis and parameterization. J. Geophys. Res. **100**: 13321-13332.

Chisholm, S.W. 1992. Phytoplankton size. In: Primary Productivity and Biogeochemical Cycles in the Sea. P. G. Falkowski and A. D. Woodhead, eds., Plenum Press, New York.

Ciotti, A.M., M.R. Lewis and J.J. Cullen. 2002. Assessment of the relationships between dominant cell size in natural phytoplankton communities and the spectral shape of the absorption coefficient. Limnol. Oceanogr. **47**: 404-417.

Corwith, H.L. and P.A.Wheeler. 1987. El nino related variations in nutrient and chlorophyll distributions off Oregon. Progr. Oceanogr. **54**: 361-380.

Dickson, M.L. and P.A.Wheeler. 1995. Nitrate uptake rates in a coastal upwelling regime: A comparison of PN-specific, absolute, and Chl a-specific rates. Limnol. Oceanogr. **40**: 533-543.

Eisner, L.B., M.S. Twardowski, T.J. Cowles and M.J. Perry. 2003. Resolving phytoplankton photoprotective: photosynthetic carotenoid ratios on fine scales using in situ spectral absorption measurements. Limnol. Oceanogr. **48**: 632-646.

Falkowski, P.G., and J.A. Raven. 1997. Aquatic Photosynthesis. Blackwell Science.

Geider, R.J., H. L. MacIntyre and T.M. Kana. 1996. A dynamic model of photoadaptation in phytoplankton. Limnol. Oceanogr. **41**: 1-15.

Geider, R.J., J. La Roche, R.M. Greene, and M. Olaizola. 1993. Response of the photosynthetic apparatus of *Phaeodactylum tricornutum* (Bacillariophyceae) to nitrate, phosphate, or iron starvation. J. Phycol. **29**: 755-766.

Hermann, A.J., B.M. Hickey, M.R. Landry and D.F. Winter. 1989. Coastal upwelling dynamics. In M.R. Landry & B.M. Hickey (eds.), Coastal Oceanography of Washington and Oregon (p. 211). Elsevier Oceanography Series, 47. Elsevier.

Hickey, B. M. 1989. Patterns and processes of circulation over the Washington continental shelf and slope. In M.R. Landry & B.M. Hickey (eds.), Coastal Oceanography of Washington and Oregon (p. 607). Elsevier Oceanography Series, 47. Elsevier.

Hill, J.K. and P.A. Wheeler. 2002. Organic carbon and nitrogen in the northern California current system: comparison of offshore, river plume, and coastally upwelled waters. Progr. Oceanogr. **53**: 369-387.

Hood, R.R., M.R. Abbott and A. Huyer. 1991. Phytoplankton and photosynthetic light response in the coastal transition zone off northern California in June 1987. J. Geophys. Res. **96**: 14769-14780.

Johnsen G., and E. Sakshaug. 1996. Light harvesting in bloom-forming marine phytoplankton: species-specificity and photoacclimation. Sci. Mar. **60** (Supl.1): 47-56.

Kishino, M., M. Takahashi, N. Okami, and S. Ichimura. 1985. Estimation of the spectral absorption coefficients of phytoplankton in the sea. Bull. Mar. Sci. **37**: 634-642.

Kitchen, J.C., J.R. Zaneveld and H.Pak. 1982. Effect of particle size distribution and chlorophyll content on beam attenuation spectra. Applied Optics. **21**: 3913-3918.

Kokkinakis, S.A. and P.A. Wheeler. 1987. Nitrogen uptake and phytoplankton growth in coastal upwelling regions. Limnol. Oceanogr. **32**: 1112-1123.

Landry, M.R., J.R. Postel, W.K. Peterson and J. Newman. 1989. Broad-scale distributional patterns of hydrographic variables on the Washington/Oregon Shelf. In M. R. Landry, & B. Hickey (Eds.) Coastal Oceanography of Washington and Oregon (p.1) Elsevier Oceanography Series, 47. New York. Elsevier.

Maxwell, D.P., S. Falk, C. G. Trick and N.P.A. Huner. 1994. Growth at low temperature mimics high light acclimation in Chlorella vulgaris. Plant Physiology. **105**: 535-543.

Maxwell, D.P., D.E. Laudenbach and N.P.A. Huner. 1995. Redox regulation of light-harvesting complex II and cab mRNA abundance in Dunaliella salina. Plant Physiology. **109**: 787-795.

Mitchell, B.G., and D.A. Kiefer. 1988. Chlorophyll a specific absorption and fluorescence excitation spectra for light-limited phytoplankton. Deep Sea Res. **35**: 639-663.

Moline, M.A. 1998. Photoadaptive response during the development of a coastal Antarctic diatom bloom and relationship to water column stability. Limnol. Oceanogr. **43**: 146-153.

Morel, A. and A. Bricaud. 1981. Theoretical results concerning light absorption in a discrete medium, and application to specific absorption of phytoplankton. Deep Sea Res. **28A**:1375-1393.

Nelson, N.B., B.B. Prezelin and R.R. Bidigare. 1993. Phytoplankton light absorption and the package effect in California coastal waters. Mar. Ecol. Prog. Ser. **94**: 217-227

Pegau, W.S., D. Gray, and J.R.V. Zaneveld. 1997. Absorption and attenuation of visible near-infrared light in water: dependence on temperature and salinity. Applied Optics. **36**: 6035-6046.

Porra R.J., E.E. Pfundel and N. Engel. 1997. Metabolism and function of photosynthetic pigment, p.104. *In:* S.W. Jeffrey, R.F. Mantoura, and S.W. Wright [eds.], Phytoplankton pigments in oceanography: guidelines to modern methods. Unesco Publishing.

Roesler, C.S., M.J. Perry, and K.L. Carder. 1989. Modeling in situ phytoplankton absorption from total absorption spectra in productive inland marine waters. Limnol. Oceanogr. **34**: 1510-1523.

Roesler, C.S. 1998. Theoretical and experimental approaches to improve the accuracy of particulate absorption coefficients derived form the quantitative filter technique. Limnol. Oceanogr. **43**: 1649-1660.

Schluter L., F. Mohlenberg, H. Havskum and S. Larsen. 2000. The use of phytoplankton pigments for identifying and quantifying phytoplankton groups in coastal areas: testing the influence of light and nutrients on pigment/chlorophyll a ratios. Mar. Ecol. Prog. Ser. **192**: 49-63.

Small, L.F. and D.W. Menzies. 1981. Patterns of primary productivity and biomass in a coastal upwelling region. Deep Sea Res. **28A**: 123-149.

Small, L.F., H. Pak, D.M. Nelson, and C.S. Weimer. 1989 Seasonal dynamics of suspended particulate matter. In M. R. Landry, & B. Hickey (Eds.) Coastal Oceanography of Washington and Oregon (p.255) Elsevier Oceanography Series, 47. New York. Elsevier.

Strub P. T. and C. James. 2000. Altimeter-derived variability of surface velocities in the California Current System: 2. Seasonal circulation and eddy statistics. Deep Sea Res. **47**: 831-870.

Twardowski, M.S., J.M. Sullivan, P.L. Donaghay, and J.R.V. Zaneveld. 1999. Microscale quantification of the absorption by dissolved and particulate material in coastal waters with an ac-9. J. Atmos. Ocean. Technol. **16**: 691-707.

Wright, S.W., and S.W. Jeffrey. 1997. High-resolution HPLC system for chlorophylls and carotenoids of marine phytoplankton, p.327-341. *In:* S.W. Jeffrey, R.F. Mantoura, and S.W. Wright [eds.], Phytoplankton pigments in oceanography: guidelines to modern methods. Unesco Publishing.

Yentsch, C.S. 1962. Measurement of visible light absorption by particulate matter in the ocean. Limnol. Oceanogr. **7**: 207-217.

Zaneveld, J.R.V., J.C. Kitchen, and C.C. Moore. 1994. Scattering error correction of reflecting tube absorption meters. Proc. SPIE Int. Soc. Opt. Eng. **12**: 44-55.

CHAPTER 5

GENERAL CONCLUSIONS

Changes in phytoplankton photophysiology affect the growth, survival and competition between taxa. Variations in environmental parameters such as light, temperature, and nutrients also affect growth and survival, and so, lead to changes in photophysiology and taxonomic composition. One of the central goals of my research is to observe and compare phytoplankton photophysiology and taxonomy with environmental parameters in an attempt to understand the factors influencing phytoplankton ecology in natural marine assemblages.

Measures of phytoplankton pigment composition can be used to monitor photophysiology and taxonomic variations (Jeffrey and Vesk 1997, Porra et al.1997) and thus provide valuable information on characteristics of the phytoplankton assemblages. Phytoplankton pigments serve to absorb light and then transfer this absorbed energy to the reaction center for photosynthesis or dissipate excess energy as fluorescence or heat (Raven and Falkowski 1997). Different pigments are involved in these pathways, with photoprotective carotenoids (PSC) involved in heat dissipation and photosynthetic pigments involved in photochemistry. The ratios of these pigment types will vary in response to light, nutrient and temperature with higher ratios of PPC: photosynthetic pigments observed for high light, low nutrient and low temperature conditions (Latasa 1995, Maxwell 1994). It is well documented that phytoplankton pigmentation can affect the shape and magnitude of phytoplankton

absorption spectra (Roesler et al.1989, Bidigare et al.1990). Absorption spectra have traditionally been evaluated for discrete water samples collected on filters (Yentsch 1962; Mitchell and Kiefer 1988). Now, in situ optical instruments for measurement of spectral absorption and beam attenuation allows acquisition of bio-optical data on time and space scales comparable to hydrographic data from CTDs. Therefore, my research focused on evaluating 1) the relationship between phytoplankton PPC: photosynthetic carotenoids (PSC) and the shape of the in situ absorption spectra, so that in situ absorption spectral shapes could be used to understand fine-scale changes in these pigment ratios, and 2) the relationship between PPC: PSC ratios, absorption spectral shapes and environmental parameters to provide information on the phytoplankton photophysiology and ecology.

In chapter 2, I developed an index for the PPC: PSC ratios based on the shape of the in situ absorption spectra using data collected in protected coastal waters in East Sound, Washington. This index, denoted the a_{ph} slope, was calculated as (a_{ph}488-a_{ph}532)/((a_{ph}676) · (488-532 nm)). I found a single linear relationship between PPC: PSC ratios and a_{ph} slopes (r^2 = 0.93) for these diatom-dominated waters. The detrital absorption in these waters was low and dissolved absorption (from constituents smaller than 0.2 μm) was constant, so there were also strong relationships between PPC: PSC ratios and particulate absorption (a_p) slopes, and PPC: PSC ratios and particulate + dissolved absorption (a_{pg}) slopes (r^2 = 0.93, for both). I also modeled the potential influence of variations in detrital absorption and packaging on this relationship. Model results for the relationship of a_{ph} slopes and PPC: PSC ratios indicated that the y-intercept increased as packaging decreased, although the slopes of

regression lines remained constant. Comparisons to environmental parameters indicated that the PPC: PSC ratios, (diadinoxanthin + diatoxanthin): chlorophyll *a* (chl *a*), and a_{ph} slopes were strongly associated with the recent (1 h) light history, suggesting that light was the primary factor driving photophysiological variations in this study.

In chapter 3, I applied the techniques developed in chapter 2 to surface waters in the Oregon upwelling region. I found separate linear relationships between PPC: PSC ratios and a_{ph} slopes for samples located 1) inshore, close to areas of active upwelling, 2) mid-shelf, influenced by a wide variety of water masses, and 3) further offshore, influenced by the Columbia River plume (r^2 = 0.61, 0.66 and 0.95, respectively). These results indicate that PPC: PSC ratios can be predicted from the ac-9 a_{ph} slope parameter using the appropriate calibration. For the relationship between a_{ph} slopes and PPC: PSC ratios, the regression line slopes for all three groups were similar, however, the y-intercepts of these relationships were significantly different, suggestive of packaging variations.

Packaging was estimated by Qa*676 (Morel and Bricaud 1981) by dividing the measured $a_{ph}676$ value by the estimated unpackaged value, $a_{ph}676'$ (derived by multiplying the HPLC determined concentration for chl *a* by the specific absorption coefficient, Bidigare et al.1990). For East Sound and all three groups from Oregon waters, the mean Qa*676 values were linearly related to the y-intercept from the a_{ph} slope and PPC: PSC relationships. These results suggest that the y-intercept of the PPC: PSC to a_{ph} slope relationship provides an indication of the mean packaging within these four different areas. The y-intercepts were also linearly related to

gamma, the hyperbolic slope of the c_p spectra (a measure of the relative particle size distribution, Boss et al.2001) and the total chl *a*: c_p650 (a measure of chl *a* per particle), both of which contribute to packaging variations.

In chapter 4, the relationship between PPC: PSC ratios and environmental factors (light, nutrients, temperature) were compared for surface (5-m) samples and all depths combined using bivariate and multivariate stepwise linear regression analyses (SPSS). Temperature, mean PAR for the prior 24 h and depth (for all depths combined) proved to be the parameters that could explain the greatest amount of variability in PPC: PSC ratios using additive models. More variability in PPC: PSC ratios could be explained by evaluating only samples with < 2 μM dissolved inorganic nitrogen (DIN). For these samples, 61% of the variability could be explained by PAR and temperature, and 49% by PAR alone suggesting that there may be an interaction between PAR and nutrients at DIN levels that are potentially limiting to phytoplankton (1 to 2 μM for coastal diatoms, Wheeler pers. comm.).

I also evaluated spatial (horizontal and vertical) variations in optical parameters, pigment ratios and hydrography. For surface horizontal transects in the mid-shelf region, a_p slopes were able to estimate PPC: PSC ratios since detrital absorption (a_d) was low (a_d412: a_p412 ~0.2). PPC: PSC ratios were calculated from these higher resolution a_p slope estimates using relationships determined for HPLC-derived PPC: PSC ratios and ac-9 a_p slopes when discrete samples were available. These observations indicated that PPC: PSC ratios were lower, larger particles made a greater contribution to the relative particle size distribution, and chl *a* per particle was higher in waters located closer compared to further from shore. The inshore waters

were influenced by upwelling as indicated by lower temperatures and higher nutrients, which likely affected both the photophysiology and taxonomic composition of the phytoplankton assemblages. As expected, considerable mesoscale cross-shore variability was observed in pigment ratios, and optical and hydrographic properties throughout the mid-shelf region (Small and Menzies 1981). Vertical distributions showed gradients in PPC: PSC ratios, taxonomic composition, relative particle size distribution, and packaging, likely driven in part by light and nutrient gradients. At stations without discrete samples, a_{ph} values were corrected for a_d using discrete samples collected during the prior hour. PPC: PSC were estimated from a_{ph} slopes using a linear relationship seen between HPLC-derived PPC: PSC ratios and a_{ph} slopes from the earlier cast. These data show that there were fine scale variations in PPC: PSC ratios and relative particle size distribution that related to the hydrographic profiles, suggesting variations in phytoplankton photophysiology and taxonomy varied with water mass characteristics.

The data from all three chapters indicate that in situ spectral absorption measurements can offer useful information on phytoplankton pigments in coastal environments. Insights may be gained by using these optical tools to monitor indices of pigmentation such as PPC: PSC ratios, and particle size distributions at high-resolution, concurrent with measurements of water mass characteristics (such as temperature and salinity), irradiance and data from automated or in-line nutrient sensors. Estimates of PPC: PSC ratios may help assess the role of heat dissipation in photosynthesis in natural assemblages, which may be a high percentage of the total energy absorbed (up to 50%) under certain conditions (Falkowski and Raven 1997).

PPC: photosynthetic pigment ratios also provide an index of light or nutrient history of the cell and may be used to predict prior mixing history (Cullen and Lewis 1988, Culver and Perry 1999). These ratios will also vary with community composition, however. The relative importance of taxonomic and photophysiological variations on this pigment index remains to be determined.

These field observations raise a number of questions that could be addressed through a series of controlled laboratory experiments. Laboratory incubation chemostat experiments using cultures representative of coastal species could be used to study the effects of varying irradiance and nutrient concentrations on the synthesis and degradation of photoprotective and photosynthetic pigments, so that photophysiology and taxonomic affects could be better understood. Sub-samples for HPLC analysis should be collected during the course of the incubation to estimate pigment kinetics. Samples should be continuously monitored with an ac-9, or if this proves damaging to the cells, sub-samples for ac-9 measurements should be collected periodically. Rapid shifts in light (and possibly nutrients) could be evaluated as well as the effects of long-term exposure to established nutrient and light conditions. Xanthophyll cycling, on the scale of 1 to 10 min, would be expected with rapid light shifts. Synthesis or degradation of pigments will be on the order of hours to days. Photoadaption based on chl *a*: carbon ratios may be more rapid following a shift to high light than following a shift to low light (Geider et al.1996), although Cullen and Lewis (1988) reported the opposite finding. The interaction of light and nutrients could be evaluated with a factorial study design. A factorial experimental design has treatment combinations for all the possible combinations of factor levels (Ramsey and

Shafer, 1997). For example, a 2 by 2 design involves two factors each at two levels (e.g. low and high light and low and high dissolved inorganic nitrogen (DIN)) on estimates of a dependent variable (e.g. PPC: PSC ratios). If there is an interaction between light and DIN at low DIN levels, we may expect to see a greater increase in PPC: PSC ratios for low compared to high DIN at high light, than seen for low compared to high DIN at low light. Several species should be compared including, at the minimum, diatoms (*Chaetoceros*, *Skeletonema*, *Thalassiosira*, if possible), dinoflagellates, prymnesiophytes and prokaryotes.

Shipboard experiments with natural assemblages would also be useful in assessing the effects of irradiance on pigment ratios. Samples could be placed in UV transparent containers in deck board incubators or (preferably) returned to the depth of collection. Sub-samples would be collected at the initiation of the experiment and periodically thereafter for HPLC analysis, taxonomic identification, Coulter Counter size estimates, nutrients and ac-9 measurements. Samples could be incubated at a range of light levels (at the minimum, at the sample's original light level and one higher and one lower level) to evaluate the effects of irradiance on pigment synthesis and degradation. The variations in PPC: PSC and other ratios could be compared to shifts in taxonomy to distinguish the photophysiological and taxonomic influences on pigment ratios and optical properties.

Additional information on phytoplankton photophysiology will be gained by comparing Fast Repetition Rate fluorometer (FRRf) measurements with PPC: photosynthetic pigment ratios and a_{ph} slopes from the ac-9. The FRRf measures fluorescence in darkness when all the functional reaction centers are potentially open

and under gradually saturating flashes of light that cause all the reaction centers to eventually close (Falkowski and Raven 1997). The difference in fluorescence yield for closed and open reaction centers is termed variable fluorescence. Cells with a lower percentage of functional reaction centers, such as nutrient stressed cells, will have lower variable fluorescence. Thus, FRRf measurements offer a measure of the health of the cell and its capacity to absorb light energy for photochemistry (Falkowski and raven 1997). Variable fluorescence also may be related to the maximum quantum yield of carbon fixation in nutrient stressed cells. The PPC: PSC ratios may show a stronger relationship to variable fluorescence in nutrient stressed cells compared to nutrient replete cells if, for example, nutrient limitation rather than high light is driving increases in the PPC: PSC ratios. FRRf data were collected by Dr. R. Letelier for the Oregon Coast samples, so this type of analysis is possible.

Taxonomic identification using microscopy and flow cytometry would be extremely valuable for discerning taxonomic variations in our Oregon Coast samples. We assume this area was primarily dominated by diatoms based on the high fucoxanthin: chl *a* ratios obtained from HPLC analysis, but we do not know which diatom species were present, with the exception of four surface samples, three of which contained *Chaetoceros* and one *Leptocylindrus* (M. Wetz pers. comm.). Drs. L. Karp-Boss and K. Ruttenberg collected phytoplankton samples at select stations, so this data may become available in the future. Some differences in diatom species are suggested by the ac-9 c_p440: c_p650 ratios, which indicate that relative particle size distributions varied over the study area. Coulter Counter measurements of discrete samples would allow us to calibrate the relative particle size distributions estimated

from the ac-9 measurements. In future studies, samples for taxonomic and Coulter Counter analyses should be collected concurrently with HPLC pigment samples and in situ optical measurements.

Other complimentary information on phytoplankton cellular fluorescence and scattering properties could be obtained with a Flow Cytometer And Microscope (FlowCAM), newly developed by Bigelow laboratory (http://www.bigelow.org/flowcam). This instrument continuously counts, images and sizes phytoplankton and particles between 10 and 1000 μm diameter that exhibit chlorophyll or phycoerythrin fluorescence. With a FlowCAM in our in-line optical system, we could directly identify the phytoplankton species producing the in situ spectral absorption and beam transmission signatures, and evaluate the effects of taxonomy on PPC: photosynthetic pigment ratios in coastal upwelling areas where particle sizes may be large (Corwith and Wheeler, 2002). Obviously, if a sizable fraction of the assemblage is < 10 μm, the FlowCAM will be less applicable.

During the Coastal Advances in Ocean Transport (COAST) cruises in 2001, nutrients (nitrate, nitrite, ammonium, phosphate and silicate) and dissolved oxygen were collected by Dr. B. Hales from the same flow stream as our in-line optics system. Once analyses of these data are completed, we will be able to extend our observations of PPC: photosynthetic pigment ratios (derived from in situ absorption) and estimated particle size distribution (derived from in situ beam attenuation) to nutrient concentrations, as well as hydrography, on fine scales (~ 1-2 m vertical resolution). This information would enable us to better evaluate the effects of nutrient availability on the relative concentrations of PPC.

We found noticeable levels of chlorophyll *a* epimer, a degradation product of chl *a* (Porra et al, 1997) in many of our samples, with the highest concentrations seen at depth. The chl *a* epimer was also detected throughout the water column in water that appeared to be recently upwelled (station CH1 on 11 August, discussed in chapter 4), thus the presence of this pigment may provide another means to discriminate upwelled water masses. This pigment could also be detected with our ac-9 in situ absorption data (see methods chapter 4), thus we can obtain fine scale information on its presence. Low oxygen concentrations were observed in deep waters during our August 2001 survey (Dr. B. Hales pers. comm.) and it is possible the chl *a* epimer concentrations are associated with these low oxygen conditions. Comparisons of the in-line dissolved oxygen data with ac-9 determinations of epimer may shed some light on this hypothesis.

I have limited my analyses of photoprotection to the visible portion of the absorption spectrum. Phytoplankton can be strongly affected by ultraviolet radiation (UV) exposure (Cullen et al.1992). Information on the pigments that that absorb UV light such as mycrosporine-like amino acids (MAA) could be obtained by modifying the ac-9 or some other in situ absorption instrument to use UV light as a source, and a detector with sensitivity in the UV. The MAA serve as a sunscreen for the cell and increase under high light conditions (Neale et al.1998; Litchman et al.2002). Comparisons between MAA and PPC would be informative for understanding the conditions that promote formation of both these types of pigments and how they relate to one another within and between taxa. A hyperspectral in situ absorption detector (such as one in development by S. Laney and Dr. R. Letelier) could be used to obtain

more detailed absorption spectra, so that individual pigment types and detrital contributions could be more easily detected. This information would also enable taxonomic groups to be identified more readily.

There is considerable and spatial variability in the Oregon Coastal waters (Small and Menzies 1981, Landry et al.1989, Barth et al.2000). Shipboard sampling cannot accommodate the simultaneous measurements of two areas at one time. Thus, for example, evaluating the differences between the northern compared to southern region of our study area (which are very different bathymetrically) during an upwelling event, requires at least two research vessels, moorings or remote sensing via aircraft over flights or satellite imagery. For the work described in chapters two through four, I have used in situ spectral absorption measurements to evaluate ratios of PPC: PSC ratios. However, moored instrumentation and remote sensing generally collect spectral reflectance rather than absorption data. Inversion of the a_{ph} slope calculation and substitution of some of the wavelengths may provide information on PPC: PSC ratios. For East Sound data (Eisner unpublished results), I evaluated this possibility using ac-9 a_{pg} data and Tethered Spectral Radiometer (TSRB) reflectance data. The ac-9 a_{pg} slopes (defined in this case as ($a_{pg}488$- $a_{pg}555$)/ a_{pg} 676) were linearly related (r^2 = 0.90) to TSRB measurements of $R_{rs}443/(R_{rs}488-R_{rs}555)$ collected from 0800 to 1800, where $R_{rs}(\lambda)$ is the upwelled radiance divided by the downwelled irradiance (Figure 5.1a). In turn, the HPLC-derived PPC: PSC ratios were linearly related (r^2 = 0.94) to the a_{pg} slope for surface (< 5m samples) (Figure 5.1b). These preliminary results suggest that surface PPC: PSC ratios can be predicted from TSRB estimates for this particular data set. The constant dissolved absorption (a_g) during

this study allowed a tight correlation between a_{pg} slopes and PPC: PSC ratios. In areas with variable a_g, this analysis may be confounded (see difference between a_{ph} slopes and a_{pg} slopes for the Oregon Coast data, chapter 3, Figure 3.5). Ideally PPC: PSC ratios and reflectance data should be compared directly. We had limited concurrent HPLC and TSRB data (only 5 samples) in East Sound, even so a strong linear association was observed ($r^2 \sim 0.95$). If a solid relationship between pigment ratios and moored TSRB reflectance data can be established, then a pigment ratio may be derived from aircraft and satellite imagery as well. Both TSRB and over flight (Dr. J. Bane, UNC) spectral reflectance data exist for the Oregon Coast survey, and could be compared to HPLC derived pigment ratios and ac-9 spectral absorption measurements in future analyses.

Further research efforts should continue to examine the interaction of physical oceanographic parameters, nutrients (organic and inorganic, micro (such as iron) and macro), and irradiance with phytoplankton photophysiology and taxonomy, as there remain several unanswered questions about time scales of variability of phytoplankton photophysiological processes. The role of top-down effects from grazers will also influence phytoplankton taxonomic composition and should not be overlooked in an integrated research design. Indices of phytoplankton photophysiology, such as those developed here, offer new techniques for understanding fine scale processes, and provide new insights into phytoplankton ecology. The application of in situ optical tools to questions on photophysiology brings us another step closer to understanding the complex biological and physical interactions in our oceans.

Figure 5.1. Relationship of a) Tethered Spectral Radiometer Buoy (TSRB) reflectance parameter: ((1/R_{rs}488)-(1/R_{rs}555)) * R_{rs}443 to ac-9 a_{pg} slope parameter: (a_{pg}488-a_{pg}555)/a_{pg}676, and b) ac-9 a_{pg} slope parameter and PPC: PSC ratios (photoprotective carotenoids: photosynthetic carotenoids for data collected between 0800 and 1800 on 15-24 June 1998 in East Sound, Washington. Pigment samples and ac-9 data collected at depths < 5 m. Model 1 linear regressions are shown.

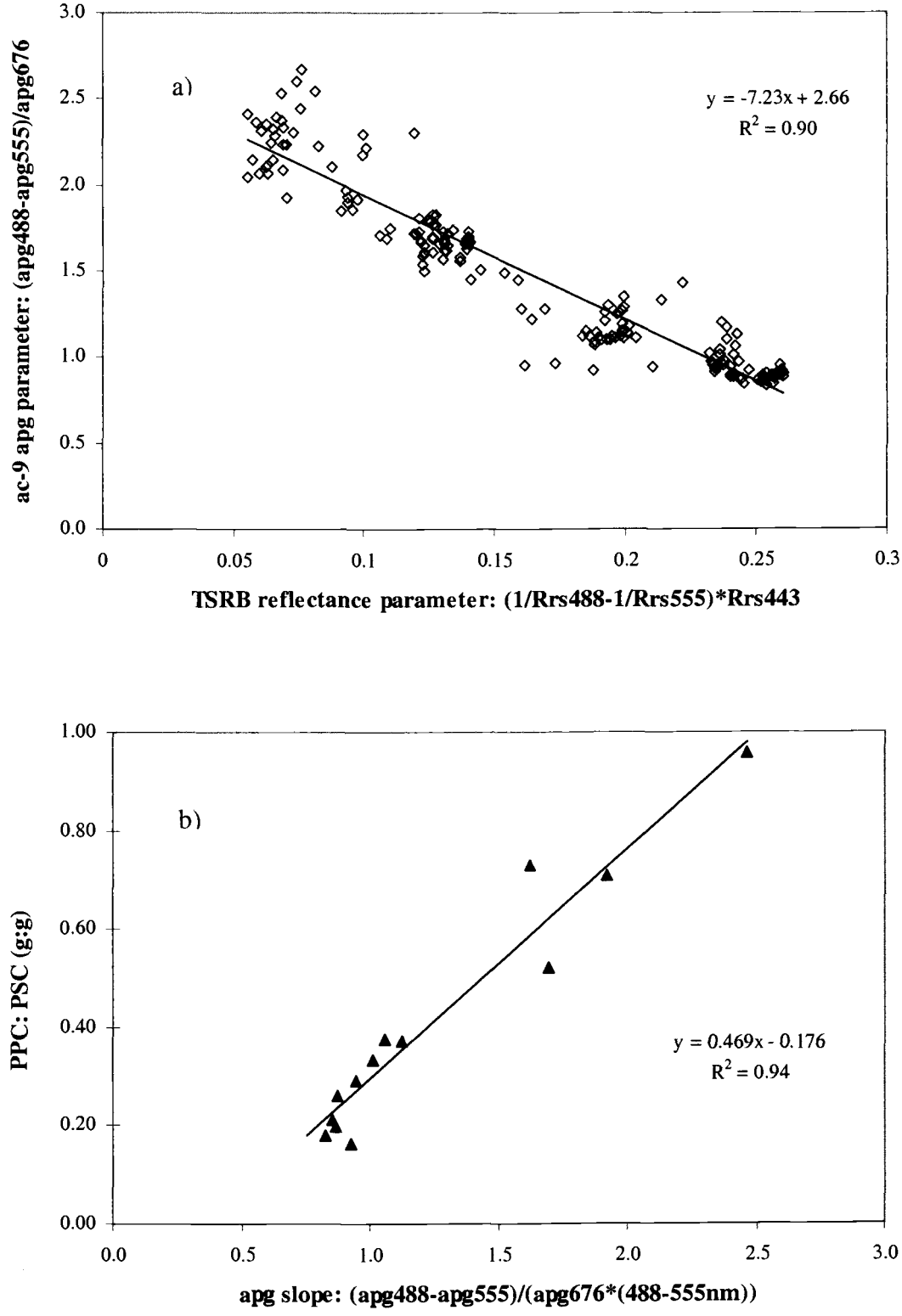
a)
y = -7.23x + 2.66
R2 = 0.90
ac-9 apg parameter: (apg488-apg555)/apg676
TSRB reflectance parameter: (1/Rrs488-1/Rrs555)*Rrs443
b)
y = 0.469x - 0.176
R2 = 0.94
PPC: PSC (g:g)
apg slope: (apg488-apg555)/(apg676*(488-555nm))

Figure 5.1.

BIBLIOGRAPHY

Alldredge, A.L., T.J. Cowles, S. MacIntyre, J.E.B. Rines, P.L. Donaghay, C.F. Greenlaw, D.V. Holliday, M.M. Dekshenieks, J.M. Sullivan, J.R.V. Zaneveld. 2002. Occurrence and mechanisms of formation of a dramatic thin layer of marine snow in a shallow Pacific fjord. Mar. Ecol. Prog. Ser. **233**: 1-12

Anning, T., H.L. MacIntyre, S.M. Pratt, P.J. Sammes, S. Gibb and R.J. Geider. 2000. Photoacclimation in the marine diatom *Skeletonema costatum.* Limnol. Oceanogr. **45**: 1807-1817.

Atlas, E.L., Hager, S., Gordon, L., and P. Park. 1971. *A practical manual for use of the Technicon AutoAnalyzer in seawater nutrient analyses.* Revised O.S.U. Tech Report 215, Ref. 71-22, Dept. of Oceanography, Oregon State University, Corvallis.

Babin M., A. Morel, H. Claustre, A. Bricaud, Z. Kolber and P.G. Falkowski. 1996. Nitrogen-and-irradiance-dependent variations of the maximum quantum yield of carbon fixation in eutrophic, mesotrophic and oligotrophic marine systems. Deep Sea Res. I **43**: 1241-1272.

Barnard A., W.S. Pegau and J.R. Zaneveld. 1998. Global relationships of the inherent optical properties of the oceans. J. Geophys. Res. **103**: 24955-24968.

Barth, J.A., Pierce, S.D. and R.L. Smith. 2000. A separating coastal upwelling jet at Cape Blanco, Oregon and its connection to the California Current system. Deep Sea Res. II. 783-810.

Barth, J.A and R.L. Smith. 1998. Separation of a coastal upwelling jet at Cape Blanco, Oregon, USA. S. Afr. J. Mar. Sci.

Bidigare, R.R, M.E. Ondrusek, J.H. Morrow, and D.E. Kiefer. 1990. In vivo absorption properties of algal pigments. SPIE Ocean Optics X. **1302**: 290-302.

Bjornsen, P.K. and T.G. Nielsen. 1991. Decimeter scale heterogeneity in plankton during a pycnocline bloom of Gyrodinium aureolum. Mar. Ecol. Prog. Ser. **73**: 263-267.

Boss E., W.S. Pegau, W.D. Gardner, J.R. Zaneveld, A.H. Barnard, M.S. Twardowski, G.C. Chang and T.D. Dickey. 2001. Spectral particulate attenuation and particle size distribution in the bottom boundary layer of a continental shelf. J. Geophys. Res. **106**: 9509-9516.

Bricaud, A., M. Babin, A. Morel, and H. Claustre. 1995. Variability in the chlorophyll-specific absorption coefficients of natural phytoplankton: Analysis and parameterization. J. Geophys. Res. **100**: 13321-13332.

Bricaud, A., A. Morel and L. Prieur. 1983. Optical efficiency factors of some phytoplankters. Limnol. Oceanogr. **28**: 816-832.

Chisholm, S.W. 1992. Phytoplankton size. In: Primary Productivity and Biogeochemical Cycles in the Sea. P. G. Falkowski and A. D. Woodhead, eds., Plenum Press, New York.

Ciotti, A.M., M.R. Lewis and J.J. Cullen. 2002. Assessment of the relationships between dominant cell size in natural phytoplankton communities and the spectral shape of the absorption coefficient. Limnol. Oceanogr. **47**: 404-417.

Claustre, H., P. Kerherve, J.C. Marty, and L. Prieur. 1994. Phytoplankton photoadaption related to some frontal physical processes. J. Mar. Systems. **5**: 251-265.

Cleveland, J.S., and M.J. Perry. 1994. A model for partitioning absorption into phytoplanktonic and detrital components. Deep Sea Res. Part I. **41**: 197-221.

Corwith, H.L. and P.A.Wheeler. 1987. El nino related variations in nutrient and chlorophyll distributions off Oregon. Progr. Oceanogr. **54**: 361-380.

Cowles, T.J., R.A. Desiderio, and S. Neuer. 1993. *In situ* characterization of phytoplankton from vertical profiles of fluorescence emission spectra. Mar. Biol. **115**: 217-222

Cowles, T.J., R.A. Desiderio, and M-E. Carr. 1998. Small-scale planktonic structure: persistence and trophic consequences. Oceanography **11**: 4-9

Cullen, J.J., A.M. Ciotti, R.F. Davis, and M.L. Lewis. 1997. Optical detection and assessment of algal blooms. Limnol. Oceanogr. **42**: 1223-1239.

Cullen, J.J. and M.R. Lewis. 1988. The kinetics of algal photoadaptation in the context of vertical mixing. J. Plankton Res. **10**: 1039-1063.

Cullen, J.J., P.J. Neale and M.P. Lesser. 1992. Biological weighting function for the inhibition of phytoplankton photosynthesis by ultraviolet radiation. Science. **258**: 646-650.

Culver, M.E., and M.J. Perry. 1999. The response of photosynthetic absorption coefficients to irradiance in culture and in tidally mixed estuarine waters. Limnol. Oceanogr. **44**: 24-36.

Dekshenieks, M.M., P.L. Donaghay, and J.M. Sullivan, J.E. Rines, T.R. Osborn, and M.S. Twardowski. 2001. Temporal and spatial occurrence of thin phytoplankton layers in relation to physical processes. Mar. Ecol. Prog. Ser. **223**: 61-71.

Dickson, M.L. and P.A.Wheeler. 1995. Nitrate uptake rates in a coastal upwelling regime: A comparison of PN-specific, absolute, and Chl a-specific rates. Limnol. Oceanogr. **40**: 533-543.

Diehl, P. and H. Haardt. 1980. Measurement of the spectral attenuation to support biological research in a "plankton tube" experiment. Oceanol. Acta. **3**: 89-96.

Duysens, L.N.M. 1956. The flattening of the absorption spectrum of suspensions, as compared to that of solutions. Biochim. Biophys. Acta. **19**: 1-12.

Eisner, L.B., M.S. Twardowski, T.J. Cowles and M.J. Perry. 2003. Resolving phytoplankton photoprotective: photosynthetic carotenoid ratios on fine scales using in situ spectral absorption measurements. Limnol. Oceanogr. **48**: 632-646.

Eppley, R.W. 1972. Temperature and phytoplankton growth in the sea. Fish Bulletin. **70**: 1063-1085.

Falkowski, P.G., and J.A. Raven. 1997. Aquatic Photosynthesis. Blackwell Science. Barth, J.A., Pierce, S.D. and R.L. Smith. 2000. A separating coastal upwelling jet at Cape Blanco, Oregon and its connection to the California Current system. Deep Sea Res. II. 783-810.

Geider, R.J., J. La Roche, R.M. Greene, and M. Olaizola. 1993. Response of the photosynthetic apparatus of *Phaeodactylum tricornutum* (Bacillariophyceae) to nitrate, phosphate, or iron starvation. J. Phycol. **29**: 755-766.

Geider R.J., H.I. MacIntyre, L. Graziano and R.M.M. McKay. 1998. Response of the photosynthetic apparatus of Dunaliella tertiolecta (Chlorophyceae) to nitrogen and phosphorus limitation. Eur. J. Phycol. **29**: 755-766.

Geider, R.J., H. L. MacIntyre and T.M. Kana. 1996. A dynamic model of photoadaptation in phytoplankton. Limnol. Oceanogr. **41**: 1-15.

Hermann, A.J., B.M. Hickey, M.R. Landry and D.F. Winter. 1989. Coastal upwelling dynamics. In M.R. Landry & B.M. Hickey (eds.), Coastal Oceanography of Washington and Oregon (p. 211). Elsevier Oceanography Series, 47. Elsevier.

Hickey, B. M. 1989. Patterns and processes of circulation over the Washington continental shelf and slope. In M.R. Landry & B.M. Hickey (eds.), Coastal Oceanography of Washington and Oregon (p. 607). Elsevier Oceanography Series, 47. Elsevier.

Hill, J.K. and P.A. Wheeler. 2002. Organic carbon and nitrogen in the northern California current system: comparison of offshore, river plume, and coastally upwelled waters. Progr. Oceanogr. **53**: 369-387.

Hoepffner, N., and S. Sathyendranath. 1991. Effect of pigment composition on absorption properties of phytoplankton. Mar. Ecol. Prog. Ser. **73**:11-23.

Hood, R.R., M.R. Abbott and A. Huyer. 1991. Phytoplankton and photosynthetic light response in the coastal transition zone off northern California in June 1987. J. Geophys. Res. **96**: 14769-14780.

Huyer, A. A comparison of upwelling events in two locations: Oregon and northwest Africa. J. Mar. Res. **34**: 531-546.

Jeffrey, S.W. 1997. Application of pigment methods to oceanography, p.127-166. *In:* S.W. Jeffrey, R.F. Mantoura, and S.W. Wright [eds.], Phytoplankton pigments in oceanography: guidelines to modern methods. Unesco Publishing.

Jeffrey, S.W., and M. Vesk. 1997. Introduction to marine phytoplankton and their pigment signatures, p.37-84. *In:* S.W. Jeffrey, R.F. Mantoura, and S.W. Wright [eds.], Phytoplankton pigments in oceanography: guidelines to modern methods. Unesco Publishing.

Johnsen G., and E. Sakshaug. 1996. Light harvesting in bloom-forming marine phytoplankton: species-specificity and photoacclimation. Sci. Mar. **60 (Supl.1)**: 47-56.

Johnsen, G., O. Samset, L. Granskog, and E. Sakshaug. 1994. In vivo absorption characteristics in 10 classes of bloom-forming phytoplankton: taxonomic characteristics and responses to photoadaptation by means of discriminate and HPLC analysis. Mar. Ecol. Prog. Ser. **105**: 149-157.

Kirk, J.T. 1994. Light and photosynthesis in aquatic ecosystems. 2nd ed. Cambridge Univ. Press.

Kishino, M., M. Takahashi, N. Okami, and S. Ichimura. 1985. Estimation of the spectral absorption coefficients of phytoplankton in the sea. Bull. Mar. Sci. **37**: 634-642.

Kitchen, J.C., J.R. Zaneveld and H.Pak. 1982. Effect of particle size distribution and chlorophyll content on beam attenuation spectra. Applied Optics. **21**: 3913-3918.

Kokkinakis, S.A. and P.A. Wheeler. 1987. Nitrogen uptake and phytoplankton growth in coastal upwelling regions. Limnol. Oceanogr. **32**: 1112-1123.

Landry, M.R., J.R. Postel, W.K. Peterson and J. Newman. 1989. Broad-scale distributional patterns of hydrographic variables on the Washington/Oregon Shelf. In M. R. Landry, & B. Hickey (Eds.) Coastal Oceanography of Washington and Oregon (p.1) Elsevier Oceanography Series, 47. New York. Elsevier.

Latasa, M. 1995. Pigment composition of *Heterocapsa* sp. and *Thalassiosira weissflogii* growing in batch cultures under different irradiances. Sci. Mar. **59**: 25-37.

Litchman E., P.J. Neale and A.T. Banaszak. 2002. Increased sensitivity to ultraviolet radiation in nitrogen-limited dinoflagellates: Photoprotection and repair. Limnol. Oceanogr. **47**: 86-94.

MacIntyre, H.I., T.M. Kana, T. Anning and R.J. Geider. 2002. Photoacclimation of photosynthesis irradiance response curves and photosynthetic pigments in microalgae and cyanobacteria. J. Phycol. **38**: 17-37.

Mann, K.H. and J.R.N. Lazier. 1991. Dynamics of marine ecosystems: biological-physical interactions in the oceans. Blackwell Scientific.

Maxwell, D.P., S. Falk, C. G. Trick and N.P.A. Huner. 1994. Growth at low temperature mimics high light acclimation in Chlorella vulgaris. Plant Physiology. **105**: 535-543.

Maxwell, D.P., D.E. Laudenbach and N.P.A. Huner. 1995. Redox regulation of light-harvesting complex II and cab mRNA abundance in Dunaliella salina. Plant Physiology. **109**: 787-795.

Mitchell, B.G., and D.A. Kiefer. 1988. Chlorophyll *a* specific absorption and fluorescence excitation spectra for light-limited phytoplankton. Deep Sea Res. **35**: 639-663.

Moline, M.A. 1998. Photoadaptive response during the development of a coastal Antarctic diatom bloom and relationship to water column stability. Limnol. Oceanogr. **43**: 146-153.

Morel, A. and A. Bricaud. 1981. Theoretical results concerning light absorption in a discrete medium, and application to specific absorption of phytoplankton. Deep Sea Res. **28A**:1375-1393.

Neale, P.J. A.T. Banaszak and C.R. Jarriel. 1998. Ultraviolet sunscreens in Gymnodinium sanguineum (Dinophyceae): Mycrosporine-like amino acids protect against inhibition in photosynthesis. J. Phycol. **34**: 928-938.

Nelson, N.B., B.B. Prezelin and R.R. Bidigare. 1993. Phytoplankton light absorption and the package effect in California coastal waters. Mar. Ecol. Prog. Ser. **94**: 217-227.

Porra R.J., E.E. Pfundel and N. Engel. 1997. Metabolism and function of photosynthetic pigment, p.104. *In:* S.W. Jeffrey, R.F. Mantoura, and S.W. Wright [eds.], Phytoplankton pigments in oceanography: guidelines to modern methods. Unesco Publishing.

Parsons, T. R., Y. Maita, and C.M. Lalli. 1984. A manual of chemical and biological methods for seawater analysis. Pergamon Press.

Pegau, W.S., D. Gray, and J.R.V. Zaneveld. 1997. Absorption and attenuation of visible near-infrared light in water: dependence on temperature and salinity. Applied Optics. **36**: 6035-6046.

Press, W.H., B.P. Flannery, S.A. Teukolsky, and W.T. Vetterling. 1986. Numerical Recipes: The Art of Scientific Computing. Cambridge University Press, Cambridge.

Ramsey, F.L. and D.W. Schafer. 1997. The statistical sleuth: A course in methods of data analysis. Duxbery Press. Belmont, CA.

Riley, G.A. 1942. The relationship of vertical turbulence and spring diatom flowering. J. Mar. Res. **5**: 67-87.

Rines, J.E.B., P.L. Donaghay, M.M. Dekshenieks, J.M. Sullivan, and M.S. Twardowski. 2002. Thin layers and camouflage: hidden Pseudo-nitzschia populations in a fjord in the San Juan Islands, Washington, USA. Mar. Ecol. Prog. Ser. **225**: 123-137.

Roesler, C.S. 1992. The determination of in situ phytoplankton spectral absorption coefficients: Direct measurements, modeled estimates, and applications to bio-optical modeling. PhD. Dissertation, Univ. of Washington, Seattle.

Roesler, C.S. 1998. Theoretical and experimental approaches to improve the accuracy of particulate absorption coefficients derived form the quantitative filter technique. Limnol. Oceanogr. **43**: 1649-1660.

Roesler, C.S., M.J. Perry, and K.L. Carder. 1989. Modeling in situ phytoplankton absorption form total absorption spectra in productive inland marine waters. Limnol. Oceanogr. **34**: 1510-1523.

Rowan, K.S. 1989. Photosynthetic pigments of algae. Cambridge University Press, Cambridge.

Schluter L., F. Mohlenberg, H. Havskum and S. Larsen. 2000. The use of phytoplankton pigments for identifying and quantifying phytoplankton groups in coastl areas: testing the influence of light and nutrients on pigment/chlorophyll a ratios. Mar. Ecol. Prog. Ser. **192**: 49-63.

Small, L.F., H. Pak, D.M. Nelson, and C.S. Weimer. 1989 Seasonal dynamics of suspended particulate matter. In M. R. Landry, & B. Hickey (Eds.) Coastal Oceanography of Washington and Oregon (p.255) Elsevier Oceanography Series, 47. New York. Elsevier.

Small, L.F. and D.W. Menzies. 1981. Patterns of primary productivity and biomass in a coastal upwelling region. Deep Sea Res. **28A**: 123-149.

SooHoo, J.B., D.A. Kiefer, D.J. Collins, and I.S. McDermid. 1986. In vivo fluorescence excitation and absorption spectra of marine phytoplankton: I. Taxonomic characteristics and responses to photoadaptation. J. Plankton Res. **8**: 197-214.

Strub P. T. and C. James. 2000. Altimeter-derived variability of surface velocities in the California Current System: 2. Seasonal circulation and eddy statistics. Deep Sea Res. **47**: 831-870.

Sverdrup, H.U. 1953. On conditions for the vernal blooming of phytoplankton. Journal du Consiel pour l'Exploration de la Mer. **18**: 287-295.

Twardowski, M.S. and P.L. Donaghay. 2002. Photobleaching of aquatic and dissolved materials: Absorption removal, spectral alteration and their relationship. J. Geophys. Res. **107**, no. 0, 10.1029/1999JC000281.

Twardowski, M.S., J.M. Sullivan, P.L. Donaghay, and J.R.V. Zaneveld. 1999. Microscale quantification of the absorption by dissolved and particulate material in coastal waters with an ac-9. J. Atmos. Ocean. Technol. **16**: 691-707

UNESCO. 1994. Protocols for the Joint Global Ocean Flux Study (JGOFS) core measurements. IOC Manual and Guides **29**.

Vidussi, F., H. Claustre, B.B. Manca, A. Luchetta and J. Marty. 2001. Phytoplankton pigment distribution in relation to upper thermocline circulation in the eastern Mediterranean Sea during winter. J. Geophys. Res. **106**: 19,939-19,956.

Wright, S.W., and S.W. Jeffrey. 1997. High-resolution HPLC system for chlorophylls and carotenoids of marine phytoplankton, p.327-341. *In:* S.W. Jeffrey, R.F. Mantoura, and S.W. Wright [eds.], Phytoplankton pigments in oceanography: guidelines to modern methods. Unesco Publishing.

Yentsch, C.S. 1962. Measurement of visible light absorption by particulate matter in the ocean. Limnol. Oceanogr. **7**: 207-217.

Zaneveld, J.R.V., J.C. Kitchen, and C.C. Moore. 1994. Scattering error correction of reflecting tube absorption meters. Proc. SPIE Int. Soc. Opt. Eng. **12**: 44-55.

Zinkel, Z.V. 2001. Light absorption and size scaling of light-limited metabolism in marine diatoms. Limnol. Oceanogr. **46**: 86-94.

APPENDICES

Appendix A. Model 2 linear regression equations for pigment ratios vs. absorption "slope" parameter (a_{ph}, a_p, a_{pg} slopes) and ratios from ac-9 and QFT data. Regression line slopes and intercepts with 95% CI, correlation coefficient (r), coefficient of determination (r^2), p-value and t-statistic are shown.

Model 2 regressions (all surface data)

PPC:PSC (g:g) vs ac9 aph slope

Station	Group		n	slope	intercept	r	r2	p	t
CH1, CH3, CP1	**IN**	**mean**	**7**	**-0.025**	**-0.004**	**-0.78**	**0.61**	**<0.05**	**-2.80**
		lower 95%CI		-0.013	-0.009				
		upper 95% CI		-0.048	0.001				
CH6, CP11	**CR**	**mean**	**6**	**-0.021**	**-0.016**	**-0.99**	**0.98**	**<0.05**	**-16.07**
		lower 95%CI		-0.018	-0.042				
		upper 95% CI		-0.025	0.010				
CH6 only		**mean**	**4**	**-0.025**	**-0.015**	**-0.97**	**0.95**	**<0.05**	**-5.92**
		lower 95%CI		-0.013	-0.027				
		upper 95% CI		-0.047	-0.003				
TS45, CP5, CP4, HB, MC BLM, ST	**MID**	**mean**	**48**	**-0.025**	**-0.009**	**-0.81**	**0.66**	**<0.05**	**-9.49**
		lower 95%CI		-0.021	-0.010				
		upper 95% CI		-0.030	-0.007				
all groups combined, except CP11		**mean**	**59**	**-0.042**	**-0.004**	**-0.60**	**0.36**	**<0.05**	**-5.61**
		lower 95%CI		-0.034	-0.007				
		upper 95% CI		-0.051	-0.002				
East Sound		**mean**	**36**	**-0.017**	**-0.005**	**-0.97**	**0.93**	**<0.05**	**-21.72**
		lower 95%CI		-0.016	-0.008				
		upper 95% CI		-0.019	-0.003				

Model 2 regressions (all surface data)

PPC:PSC (g:g) vs ac9 ap slope

Station	Group		n	slope	intercept	r	r2	p	t
CH1, CH3, CP1	**IN**	**mean**	**7**	**-0.016**	**-0.008**	**-0.63**	**0.39**	**not sig**	**-1.80**
		lower 95%CI		-0.007	-0.011				
		upper 95% CI		-0.035	-0.004				
CH6, CP11	**CR**	**mean**	**6**						
		lower 95%CI							
		upper 95% CI							
CH6 only		**mean**	**4**	**-0.020**	**-0.015**	**-0.97**	**0.94**	**<0.05**	**-5.42**
		lower 95%CI		-0.010	-0.025				
		upper 95% CI		-0.041	-0.005				
TS45, CP5, CP4, HB, MC BLM, ST	**MID**	**mean**	**48**	**-0.023**	**-0.009**	**-0.82**	**0.67**	**<0.05**	**-9.59**
		lower 95%CI		-0.019	-0.011				
		upper 95% CI		-0.027	-0.008				
all groups combined, except CP11		**mean**	**59**	**-0.034**	**-0.007**	**-0.63**	**0.40**	**<0.05**	**-6.16**
		lower 95%CI		-0.028	-0.009				
		upper 95% CI		-0.042	-0.004				
East Sound		**mean**	**36**	**-0.017**	**-0.006**	**-0.96**	**0.93**	**<0.05**	**-20.36**
		lower 95%CI		-0.015	-0.009				
		upper 95% CI		-0.018	-0.004				

Model 2 regressions (all surface data)

PPC:PSC (g:g) vs ac9 apg slope

Station	Group		n	slope	intercept	r	r2	p	t
CH1, CH3, CP1	**IN**	**mean**	**7**	**-0.043**	**-0.005**	**-0.98**	**0.96**	**<0.05**	**-10.66**
		lower 95%CI		-0.034	-0.010				
		upper 95% CI		-0.055	0.001				
CH6, CP11	**CR**	**mean**	**6**						
		lower 95%CI							
		upper 95% CI							
CH6 only		**mean**	**4**	**-0.027**	**-0.019**	**-1.00**	**0.99**	**<0.05**	**-15.43**
		lower 95%CI		-0.021	-0.032				
		upper 95% CI		-0.036	-0.006				
TS45, CP5, CP4, HB, MC BLM, ST	**MID**	**mean**	**48**	**-0.037**	**-0.008**	**-0.67**	**0.45**	**<0.05**	**-6.12**
		lower 95%CI		-0.030	-0.011				
		upper 95% CI		-0.046	-0.006				
all groups combined, except CP11		**mean**	**59**	**-0.051**	**-0.005**	**-0.62**	**0.39**	**<0.05**	**-6.00**
		lower 95%CI		-0.041	-0.008				
		upper 95% CI		-0.062	-0.002				
East Sound		**mean**	**36**	**-0.031**	**-0.008**	**-0.96**	**0.93**	**<0.05**	**-20.61***
		lower 95%CI		-0.028	-0.012				
		upper 95% CI		-0.034	-0.003				

*n=35

Model 2 regressions (all surface data)

PP: total pigs (mol:mol) vs ac9 aph slope

Station	Group		n	slope	intercept	r	r2	p	t
CH1, CH3, CP1	**IN**	**mean**	**7**	**-0.074**	**-0.004**	**-0.78**	**0.60**	**<0.05**	**-2.76**
		lower 95%CI		-0.038	-0.009				
		upper 95% CI		-0.150	0.001				
CH6, CP11	**CR**	**mean**	**6**						
		lower 95%CI							
		upper 95% CI							
CH6 only		**mean**	**4**	**-0.071**	**-0.014**	**-0.94**	**0.89**	**not sig**	**-4.06**
		lower 95%CI		-0.030	-0.027				
		upper 95% CI		-0.172	-0.001				
TS45, CP5, CP4, HB, MC BLM, ST	**MID**	**mean**	**48**	**-0.076**	**-0.008**	**-0.84**	**0.71**	**<0.05**	**-10.62**
		lower 95%CI		-0.065	-0.010				
		upper 95% CI		-0.089	-0.007				
all groups combined, except CP11		**mean**	**59**	**-0.124**	**-0.004**	**-0.68**	**0.46**	**<0.05**	**-7.02**
		lower 95%CI		-0.102	-0.006				
		upper 95% CI		-0.151	-0.001				
East Sound		**mean**	**36**						
		lower 95%CI							
		upper 95% CI							

Model 2 regressions (all surface data)

PP: total pigs (mol:mol) vs ac9 ap slope

Station	Group		n	slope	intercept	r	r2	p	t
CH1, CH3, CP1	**IN**	**mean**	**7**	**-0.046**	**-0.008**	**-0.61**	**0.37**	**not sig**	**-1.71**
		lower 95%CI		-0.020	-0.011				
		upper 95% CI		-0.105	-0.004				
CH6, CP11	**CR**	**mean**	**6**						
		lower 95%CI							
		upper 95% CI							
CH6 only		**mean**	**4**	**-0.059**	**-0.015**	**-0.94**	**0.88**	**not sig**	**-3.81**
		lower 95%CI		-0.023	-0.025				
		upper 95% CI		-0.148	-0.004				
TS45, CP5, CP4, HB, MC BLM, ST	**MID**	**mean**	**48**	**-0.070**	**-0.009**	**-0.85**	**0.73**	**<0.05**	**-11.04**
		lower 95%CI		-0.060	-0.010				
		upper 95% CI		-0.082	-0.007				
all groups combined, except CP11		**mean**	**59**	**-0.102**	**-0.006**	**-0.71**	**0.51**	**<0.05**	**-7.64**
		lower 95%CI		-0.084	-0.008				
		upper 95% CI		-0.122	-0.004				
East Sound		**mean**	**36**						
		lower 95%CI							
		upper 95% CI							

Model 2 regressions (all surface data)

PP: total pigs (mol:mol) vs ac9 apg slope

Station	Group		n	slope	intercept	r	r2	p	t
CH1, CH3, CP1	**IN**	**mean**	**7**	**-0.129**	**-0.005**	**0.97**	**0.94**	**<0.05**	**-8.50**
		lower 95%CI		-0.097	-0.011				
		upper 95% CI		-0.172	0.002				
CH6, CP11	**CR**	**mean**	**6**						
		lower 95%CI							
		upper 95% CI							
CH6 only		**mean**	**4**	**-0.080**	**-0.019**	**-0.99**	**0.97**	**<0.05**	**-8.06**
		lower 95%CI		-0.048	-0.032				
		upper 95% CI		-0.132	-0.005				
TS45, CP5, CP4, HB, MC BLM, ST	**MID**	**mean**	**48**	**-0.113**	**-0.007**	**-0.71**	**0.50**	**<0.05**	**-6.81**
		lower 95%CI		-0.092	-0.010				
		upper 95% CI		-0.139	-0.005				
all groups combined, except CP11		**mean**	**59**	**-0.151**	**-0.004**	**-0.69**	**0.47**	**<0.05**	**-7.12**
		lower 95%CI		-0.124	-0.007				
		upper 95% CI		-0.183	-0.001				
East Sound		**mean**	**36**						
		lower 95%CI							
		upper 95% CI							

Model 2 regressions (all surface data)

PPC:PSC (g:g) vs QFT aph slope

Station	Group		n	slope	intercept	r	r2	p	t
CH1, CH3, CP1	**IN**	**mean**	**7**	**-0.022**	**-0.005**	**-0.69**	**0.48**	**not sig**	**-2.15**
		lower 95%CI		-0.010	-0.009				
		upper 95% CI		-0.047	0.000				
CH6, CP11	**CR**	**mean**	**6**	**-0.013**	**-0.016**	**-0.93**	**0.87**	**<0.05**	**-5.20**
		lower 95%CI		-0.008	-0.032				
		upper 95% CI		-0.021	0.000				
CH6 only		**mean**	**4**	**-0.040**	**-0.009**	**-1.00**	**0.99**	**<0.05**	**-14.55**
		lower 95%CI		-0.030	-0.028				
		upper 95% CI		-0.053	0.010				
TS45, CP5, CP4, HB, MC BLM, ST	**MID**	**mean**	**48**	**-0.032**	**-0.006**	**-0.66**	**0.43**	**<0.05**	**-5.81**
		lower 95%CI		-0.026	-0.008				
		upper 95% CI		-0.040	-0.004				
all groups combined, except CP11		**mean**	**59**						
		lower 95%CI							
		upper 95% CI							
East Sound		**mean**	**36**						
		lower 95%CI							
		upper 95% CI							

Model 2 regressions (all surface data)

PPC:PSC (g:g) vs QFT ap slope

Station	Group		n	slope	intercept	r	r2	p	t
CH1, CH3, CP1	**IN**	**mean**	**7**	**-0.021**	**-0.006**	**-0.68**	**0.47**	**not sig**	**-2.10**
		lower 95%CI		-0.010	-0.011				
		upper 95% CI		-0.044	-0.002				
CH6, CP11	**CR**	**mean**	**6**	**-0.010**	**-0.017**	**-0.88**	**0.78**	**<0.05**	**-3.74**
		lower 95%CI		-0.006	-0.030				
		upper 95% CI		-0.019	-0.004				
CH6 only		**mean**	**4**	**-0.039**	**-0.009**	**-0.99**	**0.98**	**<0.05**	**-10.78**
		lower 95%CI		-0.026	-0.028				
		upper 95% CI		-0.057	0.010				
TS45, CP5, CP4, HB, MC BLM, ST	**MID**	**mean**	**48**	**-0.034**	**-0.006**	**-0.61**	**0.37**	**<0.05**	**-5.19**
		lower 95%CI		-0.027	-0.008				
		upper 95% CI		-0.043	-0.003				
all groups combined, except CP11		**mean**	**59**						
		lower 95%CI							
		upper 95% CI							
East Sound		**mean**	**36**						
		lower 95%CI							
		upper 95% CI							

Model 2 regressions (all surface data)

PPC:PSC (g:g) vsac9 aph440/aph676

Station	Group		n	slope	intercept	r	r2	p	t
CH1, CH3, CP1	**IN**	**mean**	**7**	**2.68**	**1.12**	**0.87**	**0.76**	**<0.05**	**3.94**
		lower 95%CI		1.56	0.80				
		upper 95% CI		4.60	1.45				
CH6, CP11	**CR**	**mean**	**6**						
		lower 95%CI							
		upper 95% CI							
CH6 only		**mean**	**4**	**1.41**	**2.24**	**0.99**	**0.98**	**<0.05**	**10.68**
		lower 95%CI		0.95	2.12				
		upper 95% CI		20.76	2.37				
TS45, CP5, CP4, HB, MC BLM, ST	**MID**	**mean**	**48**	**2.28**	**1.43**	**0.69**	**0.47**	**<0.05**	**6.40**
		lower 95%CI		1.84	1.30				
		upper 95% CI		2.82	1.55				
all groups combined, except CP11		**mean**	**59**						
		lower 95%CI							
		upper 95% CI							
East Sound		**mean**	**36**						
		lower 95%CI							
		upper 95% CI							

Model 2 regressions (all surface data)

PPC:PSC (g:g) vsac9 aph488/aph532

Station	Group		n	slope	intercept	r	r2	p	t
CH1, CH3, CP1	**IN**	**mean**	**7**	**-0.49**	**1.67**	**-0.75**	**0.56**	**not si**	**-1.944**
		lower 95%CI		-0.18	1.53				
		upper 95% CI		-1.38	1.82				
CH6, CP11	**CR**	**mean**	**6**						
		lower 95%CI							
		upper 95% CI							
CH6 only		**mean**	**4**	**1.03**	**1.61**	**0.93**	**0.86**	**not si**	**3.47**
		lower 95%CI		0.38	1.35				
		upper 95% CI		2.74	1.88				
TS45, CP5, CP4, HB, MC BLM, ST	**MID**	**mean**	**48**	**1.39**	**1.46**	**0.52**	**0.27**	**<0.05**	**4.08**
		lower 95%CI		1.08	1.37				
		upper 95% CI		1.79	1.55				
all groups combined, except CP11		**mean**	**59**						
		lower 95%CI							
		upper 95% CI							
East Sound		**mean**	**36**						
		lower 95%CI							
		upper 95% CI							

Model 2 regressions (all surface data)

Station	Group		n	Tchl a (ug/L) vs ac9 aph slope	intercept	r	r2	p	t
CH1, CH3, CP1	**IN**	**mean**	**7**	**0.00060**	**-0.014**	**0.50**	**0.25**	**not sig**	**1.29**
		lower 95%CI		0.00020	-0.017				
		upper 95% CI		0.00140	-0.010				
CH6, CP11	**CR**	**mean**	**6**	**0.01790**	**-0.048**	**0.99**	**0.99**	**<0.05**	**19.06**
		lower 95%CI		0.01550	-0.050				
		upper 95% CI		0.02070	-0.045				
CH6 only		**mean**	**4**	**0.01190**	**-0.039**	**0.99**	**0.98**	**<0.05**	**9.87**
		lower 95%CI		0.00780	-0.044				
		upper 95% CI		0.01810	-0.034				
TS45, CP5, CP4, HB, MC BLM, ST	**MID**	**mean**	**48**	**0.00033**	**-0.018**	**0.42**	**0.18**	**<0.05**	**3.14**
		lower 95%CI		0.00026	-0.019				
		upper 95% CI		0.00044	-0.017				
all groups combined, except CP11		**mean**	**59**	**0.00058**	**-0.020**	**0.34**	**0.11**	**<0.05**	**2.71**
		lower 95%CI		0.00045	-0.021				
		upper 95% CI		0.00074	-0.018				
East Sound		**mean**	**36**						
		lower 95%CI							
		upper 95% CI							

Model 2 regressions (all surface data)

Station	Group		n	chl c: Tchl a (g:g) vs ac9 aph slope	intercept	r	r2	p	t
CH1, CH3, CP1	**IN**	**mean**	**7**	**0.032**	**-0.018**	**0.93**	**0.86**	**<0.05**	**5.55**
		lower 95%CI		0.021	-0.021				
		upper 95% CI		0.049	-0.015				
CH6, CP11	**CR**	**mean**	**6**	**0.072**	**-0.054**	**0.95**	**0.89**	**<0.05**	**5.84**
		lower 95%CI		0.046	-0.064				
		upper 95% CI		0.111	-0.044				
CH6 only		**mean**	**4**	**0.033**	**-0.036**	**0.93**	**0.86**	**not sig**	**3.52**
		lower 95%CI		0.012	-0.048				
		upper 95% CI		0.087	-0.025				
TS45, CP5, CP4, HB, MC BLM, ST	**MID**	**mean**	**48**	**-0.044**	**-0.001**	**-0.04**	**0.00**	**not sig**	**-0.26**
		lower 95%CI		-0.033	-0.005				
		upper 95% CI		-0.059	0.003				
all groups combined, except CP11		**mean**	**59**	**-0.052**	**0.002**	**-0.44**	**0.20**	**<0.05**	**-3.75**
		lower 95%CI		-0.041	-0.003				
		upper 95% CI		-0.066	0.006				
East Sound		**mean**	**36**						
		lower 95%CI							
		upper 95% CI							

Model 2 regressions (all surface data)

Station	Group		n	chl b: Tchl a (g:g) vs ac9 aph slope	intercept	r	r2	p	t
CH1, CH3, CP1	**IN**	**mean**	**7**	**-0.208**	**-0.008**	**-0.72**	**0.52**	**not sig**	**-2.32**
		lower 95%CI		-0.100	-0.011				
		upper 95% CI		-0.433	-0.005				
CH6, CP11	**CR**	**mean**	**6**	**-0.221**	**-0.002**	**-0.94**	**0.88**	**<0.05**	**-5.32**
		lower 95%CI		-0.138	-0.030				
		upper 95% CI		-0.353	0.026				
CH6 only		**mean**	**4**	**0.255**	**-0.045**	**0.76**	**0.58**	**not sig**	**1.68**
		lower 95%CI		0.061	-0.077				
		upper 95% CI		1.061	-0.013				
TS45, CP5, CP4, HB, MC BLM, ST	**MID**	**mean**	**48**	**-0.105**	**-0.011**	**-0.30**	**0.09**	**<0.05**	**-2.15**
		lower 95%CI		-0.079	-0.013				
		upper 95% CI		-0.139	-0.010				
all groups combined, except CP11		**mean**	**59**	**-0.127**	**-0.010**	**-0.64**	**0.41**	**<0.05**	**-6.19***
		lower 95%CI		-0.135	-0.012				
		upper 95% CI		-0.156	-0.009				
East Sound		**mean**	**36**						
		lower 95%CI							
		upper 95% CI							

n=57, did not include CP1

Appendix B. Pump station data. Includes station, date (PDT), depth (m), nutrients (μM), PPC: PSC ratios (g: g), PPC: Tchl *a* (g: g), ac-9 a_{ph} slope, ac-9 a_p slope, ac-9 $a_{ph}676$ (m^{-1}), T (°C), S, sigma-t (kg m^{-3}), daytime mean PAR at sample depth over prior 24 h (μmol photons m^{-2} s^{-1}), k_d (m^{-1}), HPLC-derived pigments including Tchl *a* (μg L^{-1}) and ratios of pigments to Tchl *a* (g: g), QFT a_d12: a_p412, Qa*676 from QFT and HPLC data and from ac-9 and HPLC data, gamma (slope of hyperbolic fit to c_p spectra), ac-9 c_p440: c_p650, c_p650 (m^{-1}), Tchl *a*: c_p650, ac-9 $a_{ph}676$: c_p650.

Station	Date	Depth	PO_4	NH4	SiO_2	NO_2	NO_3	DIN	N:P	Si:N
CH1	7-Aug	5	0.68	0.83	2.56	0.07	3.11	4.01	4.66	0.64
CH1	7-Aug	10	0.59	0.88	2.43	0.05	2.67	3.59	4.64	0.68
CH1	7-Aug	15	1.07	2.69	4.80	0.12	5.73	8.55	5.45	0.56
CH1	7-Aug	20	1.26	1.85	4.98	0.11	8.38	10.34	6.76	0.48
CH1	7-Aug	28	1.87	3.28	9.80	0.18	14.19	17.64	7.66	0.56
CH6	8-Aug	5	0.51	0.18	9.89	0.12	1.95	2.24	4.02	4.41
CH6	8-Aug	10	0.54	0.21	10.16	0.13	2.21	2.56	4.32	3.97
CH6	8-Aug	20	1.47	0.03	15.52	0.36	12.46	12.85	8.72	1.21
CH6	8-Aug	30	1.66	0.07	17.40	0.05	15.94	16.05	9.60	1.08
CH6	8-Aug	40	1.74	0.00	18.87	0.05	17.56	17.61	10.15	1.07
CH6	8-Aug	50	2.10	0.01	26.24	0.03	21.36	21.40	10.17	1.23
CH6	8-Aug	60	2.32	0.02	30.40	0.02	27.17	27.22	11.74	1.12
CH3	9-Aug	5	2.45	2.12	51.04	0.16	24.12	26.40	9.91	1.93
CH3	9-Aug	12	2.72	1.95		0.20	28.07	30.22	10.40	
CH3	9-Aug	19	2.82	1.32	33.91	0.24	30.60	32.15	10.95	1.05
CH3	9-Aug	25	2.96	0.85	36.33	0.22	32.27	33.34	10.99	1.09
CH3	9-Aug	32	2.91	1.65	36.22	0.20	31.93	33.79	11.03	1.07
CH3	9-Aug	39	2.89	0.73	43.03	0.21	33.33	34.27	11.59	1.26
CH3	9-Aug	46	2.87	0.55	43.18	0.23	33.33	34.11	11.70	1.27
CH1	10-Aug	5	1.85	1.35	19.11	0.19	17.03	18.57	9.33	1.03
CH1	10-Aug	10	1.99	1.39	20.20	0.18	18.77	20.35	9.55	0.99
CH1	10-Aug	15	2.68	1.95	29.94	0.28	26.50	28.73	10.01	1.04
CH1	10-Aug	20	2.91	2.29	37.42	0.29	29.38	31.96	10.19	1.17
CH1	10-Aug	28.6	3.14	2.87	47.29	0.36	32.20	35.43	10.35	1.33
CH6	11-Aug	5	0.33	0.34	5.54	0.00	nd	0.35	0.01	16.02
CH6	11-Aug	10	0.94	0.65	6.50	0.11	1.35	2.11	1.54	3.08
CH6	11-Aug	20	1.71	0.52	17.83	0.41	16.38	17.31	9.82	1.03
CH6	11-Aug	25	1.81	0.09	18.79	0.24	18.21	18.54	10.21	1.01
CH6	11-Aug	30	1.89	0.00	20.67	0.12	20.03	20.15	10.66	1.03
CH6	11-Aug	40	2.00	2.14	24.43	0.05	21.75	23.95	10.91	1.02
CH6	11-Aug	60	1.99	1.62	21.91	0.05	21.48	23.15	10.80	0.95
CH6	11-Aug	80	2.36	0.10	30.59	0.04	29.15	29.29	12.37	1.04
CH6	11-Aug	100	2.45	0.18	35.14	0.07	31.68	31.93	12.95	1.10
CH6	11-Aug	150	2.64	0.74	42.75	0.16	29.88	30.78	11.39	1.39
CH6	11-Aug	170	3.09	0.80	51.56	0.28	35.81	36.89	11.67	1.40
CP1	12-Aug	5	1.08	1.11	2.29	0.11	2.19	3.41	2.13	0.67
CP1	12-Aug	10	1.49	1.35	4.78	0.14	10.10	11.59	6.90	0.41
CP1	12-Aug	20	3.90	6.55	24.10	0.21	20.22	26.97	5.24	0.89
CP1	12-Aug	26	2.92	5.06	25.39	0.19	24.63	29.88	8.50	0.85
CP1	12-Aug	32	3.18	6.13	31.33	0.21	27.86	34.21	8.82	0.92
CP11	13-Aug	5	0.21	2.05	0.23	0.05	nd	2.10	0.22	0.11
CP11	13-Aug	10	0.29	0.02	1.02	0.03	nd	0.04	0.09	24.90
CP11	13-Aug	17	0.61	2.51	1.79	0.06	0.41	2.98	0.78	0.60
CP11	13-Aug	25	0.87	1.33	3.62	0.27	2.41	4.00	3.07	0.90
CP11	13-Aug	40	1.20	0.11	8.49	0.22	9.08	9.42	7.79	0.90
CP11	13-Aug	50	1.58	0.13	15.22	0.11	15.39	15.63	9.79	0.97

Station	Date	Depth	PO_4	NH4	SiO_2	NO_2	NO_3	DIN	N:P	Si:N
CP5	14-Aug	5	0.79	0.44	10.16	0.15	4.46	5.05	5.81	2.01
CP5	14-Aug	10	0.68	1.69	15.41	0.14	3.26	5.09	4.96	3.03
CP5	14-Aug	20	2.55	1.49	30.17	0.14	27.28	28.91	10.74	1.04
CP5	14-Aug	30	2.60	0.63	38.83	0.14	29.28	30.05	11.32	1.29
CP5	14-Aug	40	2.52	0.54	32.81	0.16	27.64	28.34	11.03	1.16
CP5	14-Aug	50	2.93	0.89	35.28	0.15	27.08	28.12	9.29	1.25
CP5	14-Aug	60	3.10	1.25	50.94	0.16	31.98	33.39	10.35	1.53
CP5	14-Aug	70	2.86	1.19	46.40	0.20	32.96	34.35	11.60	1.35
CP5	14-Aug	80	3.12	nd	52.64	0.13	35.04	35.17	11.27	1.50
CP5	14-Aug	90	2.96	0.11	48.91	0.16	28.77	29.04	9.78	1.68
CP5	14-Aug	95	3.30	0.04	62.85	0.32	33.67	34.03	10.29	1.85
CP5	14-Aug	101	3.50	0.57	66.82	0.33	29.94	30.84	8.66	2.17
CP4	15-Aug	5	0.25	0.64	nd	0.03	3.81	4.48	15.65	
CP4	15-Aug	10	0.27	0.62	nd	0.02	3.94	4.58	14.58	
CP4	15-Aug	20	1.53	2.43	7.54	0.10	13.18	15.72	8.70	0.48
CP4	15-Aug	25	2.95	5.61	24.88	0.11	28.37	34.09	9.65	0.73
CP4	15-Aug	30	3.05	5.78	30.41	0.11	30.40	36.29	10.01	0.84
CP4	15-Aug	40	4.08?	2.72	37.04	0.12	32.36	35.20	7.96	1.05
CP4	15-Aug	50	3.13	0.03	49.73	0.24	36.79	37.05	11.82	1.34
CP4	15-Aug	5	0.24	1.04	nd	0.02	nd	0.02	0.08	
CP4	15-Aug	10	0.72	1.02	nd	0.06	4.69	5.77	6.63	
CP4	15-Aug	20	2.88	5.90	14.88	0.08	24.62	30.61	8.57	0.49
CP4	15-Aug	25	3.19	5.60	25.16	0.07	28.71	34.39	9.02	0.73
CP4	15-Aug	30	3.00	2.92	34.34	0.15	31.58	34.65	10.59	0.99
CP4	15-Aug	40	2.99	2.53	37.37	0.15	31.20	33.89	10.50	1.10
CP4	15-Aug	90	3.80	0.78	73.57	0.45	35.49	36.72	9.46	2.00
MC1	17-Aug	5	0.78	0.45	9.96	0.09	3.87	4.41	5.07	2.26
MC1	17-Aug	10	1.67	1.45	18.67	0.22	15.34	17.01	9.30	1.10
MC1	17-Aug	20	2.26	0.82	28.03	0.21	24.79	25.83	11.06	1.09
MC1	17-Aug	30	2.35	0.06	31.48	0.02	27.26	27.34	11.59	1.15
MC1	17-Aug	50	2.79	1.06	42.82	0.25	32.12	33.43	11.59	1.28
HB6	19-Aug	5	0.49	0.48	6.27	0.03	0.52	1.04	1.13	6.05
HB6	19-Aug	10	1.23	2.06	15.99	0.16	9.78	12.00	8.08	1.33
HB6	19-Aug	20	2.62	0.93	33.25	0.23	28.40	29.56	10.92	1.12
HB6	19-Aug	30	2.60	1.08	32.73	0.23	27.93	29.24	10.83	1.12
HB6	19-Aug	50	2.59	0.87	34.80	0.06	29.91	30.84	11.58	1.13
HB8	20-Aug	5	0.61	0.19	10.01	0.04	0.98	1.21	1.68	8.28
HB8	20-Aug	10	0.85	0.07	12.22	0.10	4.46	4.63	5.39	2.64
HB8	20-Aug	20	2.04	0.04	23.31	0.11	21.19	21.34	10.43	1.09
HB8	20-Aug	30	2.07	nd	24.02	0.05	24.33	24.38	11.78	0.99
HB8	20-Aug	50	2.23	0.00	27.46	0.05	25.80	25.85	11.57	1.06
HB10	20-Aug	5	0.52	0.40	9.62	0.01	0.29	0.70	0.57	13.78
HB10	20-Aug	10	0.74	0.30	10.51	0.05	0.84	1.19	1.20	8.81
HB10	20-Aug	20	1.83	0.37	49.07	0.16	17.40	17.93	9.57	2.74
HB10	20-Aug	30	2.37	0.05	30.04	0.08	26.27	26.40	11.11	1.14
HB10	20-Aug	50	2.53	0.27	32.17	0.12	28.75	29.14	11.41	1.10
HB10	20-Aug	70	2.98	1.83	38.77	0.17	16.53	18.53	5.61	2.09
HB10	20-Aug	90	2.91	0.87	40.90	0.18	34.31	35.36	11.84	1.16
HB10	20-Aug	110	2.96	0.00	43.95	0.01	36.23	36.24	12.22	1.21
HB10	20-Aug	130	2.97	0.01	47.26	0.11	36.08	36.20	12.19	1.31
HB12	21-Aug	5	1.57	0.15	16.31	0.03	11.62	11.80	7.41	1.38

NOTES: blank = no data
nd = not detectable

Station	Date	Depth	Comments on nutrients
CH1	7-Aug	5	
CH1	7-Aug	10	
CH1	7-Aug	15	
CH1	7-Aug	20	
CH1	7-Aug	28	
CH6	8-Aug	5	
CH6	8-Aug	10	
CH6	8-Aug	20	
CH6	8-Aug	30	
CH6	8-Aug	40	
CH6	8-Aug	50	low reps drop for all nuts
CH6	8-Aug	60	
CH3	9-Aug	5	
CH3	9-Aug	12	variable NH4 reps
CH3	9-Aug	19	variable NH4 reps
CH3	9-Aug	25	
CH3	9-Aug	32	low PO4 rep drop, var NH4 reps
CH3	9-Aug	39	
CH3	9-Aug	46	
CH1	10-Aug	5	variable NH4 reps
CH1	10-Aug	10	
CH1	10-Aug	15	
CH1	10-Aug	20	low PO4 rep dropped
CH1	10-Aug	28.6	
CH6	11-Aug	5	
CH6	11-Aug	10	
CH6	11-Aug	20	
CH6	11-Aug	25	
CH6	11-Aug	30	low PO4 rep dropped
CH6	11-Aug	40	
CH6	11-Aug	60	
CH6	11-Aug	80	
CH6	11-Aug	100	
CH6	11-Aug	150	variable NH4 reps
CH6	11-Aug	170	
CP1	12-Aug	5	
CP1	12-Aug	10	
CP1	12-Aug	20	
CP1	12-Aug	26	
CP1	12-Aug	32	
CP11	13-Aug	5	variable NH4 reps
CP11	13-Aug	10	
CP11	13-Aug	17	variable NH4 reps
CP11	13-Aug	25	
CP11	13-Aug	40	
CP11	13-Aug	50	

Station	Date	Depth	Comments on nutrients
CP5	14-Aug	5	variable NH4 reps
CP5	14-Aug	10	variable NH4 reps
CP5	14-Aug	20	
CP5	14-Aug	30	variable NH4 reps
CP5	14-Aug	40	
CP5	14-Aug	50	low PO4 rep drop, nuts variable
CP5	14-Aug	60	variable NH4 reps
CP5	14-Aug	70	variable NH4 reps
CP5	14-Aug	80	
CP5	14-Aug	90	
CP5	14-Aug	95	
CP5	14-Aug	101	variable reps
CP4	15-Aug	5	variable NH4 reps
CP4	15-Aug	10	
CP4	15-Aug	20	
CP4	15-Aug	25	low PO4 rep dropped
CP4	15-Aug	30	
CP4	15-Aug	40	
CP4	15-Aug	50	
CP4	15-Aug	5	
CP4	15-Aug	10	variable reps
CP4	15-Aug	20	
CP4	15-Aug	25	high PO4 rep dropped
CP4	15-Aug	30	
CP4	15-Aug	40	
CP4	15-Aug	90	
MC1	17-Aug	5	variable NH4, Si(OH)4 reps
MC1	17-Aug	10	variable NH4 reps
MC1	17-Aug	20	
MC1	17-Aug	30	
MC1	17-Aug	50	low PO4 rep dropped
HB6	19-Aug	5	variable NH4 reps
HB6	19-Aug	10	variable NH4 reps
HB6	19-Aug	20	variable NH4 reps
HB6	19-Aug	30	variable NH4 reps
HB6	19-Aug	50	variable NH4 reps
HB8	20-Aug	5	
HB8	20-Aug	10	
HB8	20-Aug	20	variable NH4 reps
HB8	20-Aug	30	
HB8	20-Aug	50	high NH4 dropped
HB10	20-Aug	5	variable NH4 reps
HB10	20-Aug	10	
HB10	20-Aug	20	variable NH4 reps
HB10	20-Aug	30	
HB10	20-Aug	50	
HB10	20-Aug	70	
HB10	20-Aug	90	variable NH4 reps
HB10	20-Aug	110	
HB10	20-Aug	130	
HB12	21-Aug	5	

Station	Date	Depth	PPC/PSC	PPC/Tchla	aph slope	ap slope	ac9 aph676
CH1	7-Aug	5	0.220	0.10	-0.0102	-0.0118	0.146
CH1	7-Aug	10	0.226	0.10	-0.0100	-0.0120	0.142
CH1	7-Aug	15	0.183	0.08	-0.0094	-0.0121	0.123
CH1	7-Aug	20	0.172	0.08	-0.0096	-0.0124	0.112
CH1	7-Aug	28	0.191	0.10	-0.0118	-0.0159	0.122
CH6	8-Aug	5	0.270	0.17	-0.0236	-0.0231	0.031
CH6	8-Aug	10	0.289	0.18	-0.0245	-0.0232	0.031
CH6	8-Aug	20	0.238	0.15	-0.0193	-0.0180	0.027
CH6	8-Aug	30	0.165	0.12	-0.0241	-0.0228	0.007
CH6	8-Aug	40	0.076	0.06	-0.0355	-0.0326	0.003
CH6	8-Aug	50	0.000	0.00	-0.0258	-0.0328	0.002
CH6	8-Aug	60	0.000	0.00	-0.0583	-0.0385	0.002
CH3	9-Aug	5	0.370	0.17	-0.0128	-0.0138	0.026
CH3	9-Aug	12	0.344	0.16	-0.0133	-0.0141	0.020
CH3	9-Aug	19	0.328	0.16	-0.0122	-0.0150	0.013
CH3	9-Aug	25	0.269	0.14	-0.0102	-0.0147	0.013
CH3	9-Aug	32	0.179	0.09	-0.0108	-0.0144	0.015
CH3	9-Aug	39	0.158	0.08	-0.0100	-0.0133	0.018
CH3	9-Aug	46	0.177	0.09	-0.0083	-0.0138	0.018
CH1	10-Aug	5	0.263	0.12	-0.0116	-0.0131	0.076
CH1	10-Aug	10	0.260	0.12	-0.0125	-0.0132	0.064
CH1	10-Aug	15	0.212	0.10	-0.0097	-0.0126	0.058
CH1	10-Aug	20	0.184	0.09	-0.0089	-0.0126	0.064
CH1	10-Aug	28.6	0.198	0.11	-0.0084	-0.0135	0.073
CH6	11-Aug	5	0.446	0.31	-0.0271	-0.0256	0.034
CH6	11-Aug	10	0.179	0.15	-0.0196	-0.0192	0.048
CH6	11-Aug	20	0.250	0.14	-0.0143	-0.0149	0.025
CH6	11-Aug	25	0.224	0.13	-0.0148	-0.0135	0.020
CH6	11-Aug	30	0.158	0.11	-0.0137	-0.0136	0.016
CH6	11-Aug	40	0.042	0.03	-0.0186	-0.0156	0.006
CH6	11-Aug	60	0.000	0.00	-0.0062	-0.0134	0.003
CH6	11-Aug	80	0.000	0.00	-0.0024	-0.0132	0.002
CH6	11-Aug	100	0.029	0.03	-0.0138	-0.0138	0.006
CH6	11-Aug	150	0.076	0.08	-0.0095	-0.0130	0.002
CH6	11-Aug	170	0.067	0.06	-0.0089	-0.0121	0.016
CP1	12-Aug	5	0.181	0.08	no ag data		0.129
CP1	12-Aug	10	0.174	0.08	no ag data		0.178
CP1	12-Aug	20	0.191	0.09	no ag data		0.114
CP1	12-Aug	26	0.171	0.09	no ag data		0.122
CP1	12-Aug	32	0.233	0.11	no ag data		0.144
CP11	13-Aug	5	1.427	0.42	-0.0601	-0.0498	0.006
CP11	13-Aug	10	1.248	0.45	-0.0606	-0.0491	0.006
CP11	13-Aug	17	0.345	0.21	-0.0288	-0.0284	0.013
CP11	13-Aug	25	0.136	0.11	-0.0221	-0.0236	0.013
CP11	13-Aug	40	0.092	0.07	-0.0285	-0.0273	0.006
CP11	13-Aug	50	0.090	0.07	-0.0322	-0.0393	0.003

Station	Date	Depth	PPC/PSC	PPC/Tchla	aph slope	ap slope	ac9 aph676
CP5	14-Aug	5	0.240	0.12	-0.0153	-0.0154	0.099
CP5	14-Aug	10	0.206	0.11	-0.0132	-0.0136	0.128
CP5	14-Aug	20	0.112	0.06	-0.0110	-0.0142	0.015
CP5	14-Aug	30	0.104	0.07	-0.0124	-0.0147	0.013
CP5	14-Aug	40	0.075	0.06	-0.0097	-0.0138	0.012
CP5	14-Aug	50	0.122	0.08	-0.0125	-0.0144	0.011
CP5	14-Aug	60	0.093	0.08	-0.0128	-0.0146	0.012
CP5	14-Aug	70	0.105	0.11	-0.0133	-0.0142	0.010
CP5	14-Aug	80	0.104	0.13	-0.0102	-0.0137	0.016
CP5	14-Aug	90	0.105	0.11	-0.0092	-0.0138	0.022
CP5	14-Aug	95	0.159	0.14	-0.0076	-0.0135	0.031
CP5	14-Aug	101	0.115	0.14	-0.0080	-0.0135	0.032
CP4	15-Aug	5	0.221	0.16			0.061
CP4	15-Aug	10	0.216	0.16			0.063
CP4	15-Aug	20	0.128	0.09	-0.0146	-0.0150	0.037
CP4	15-Aug	25	0.184	0.12	-0.0144	-0.0160	0.014
CP4	15-Aug	30	0.193	0.12	-0.0126	-0.0158	0.011
CP4	15-Aug	40	0.236	0.14	-0.0122	-0.0154	0.009
CP4	15-Aug	50	0.238	0.19	-0.0128	-0.0160	0.009
CP4	15-Aug	5	0.208	0.14	-0.0139	-0.0139	0.079
CP4	15-Aug	10	0.157	0.11	-0.0120	-0.0121	0.039
CP4	15-Aug	20	0.153	0.12	-0.0012	-0.0024	0.010
CP4	15-Aug	25	0.175	0.13	-0.0004	-0.0007	0.009
CP4	15-Aug	30	0.199	0.14		NaN	0.010
CP4	15-Aug	40	0.146	0.10		NaN	0.008
CP4	15-Aug	90	0.064	0.15	-0.0076	-0.0109	0.026
MC1	17-Aug	5	0.193	0.12	-0.0151	-0.0147	0.255
MC1	17-Aug	10	0.155	0.09	-0.0140	-0.0131	0.109
MC1	17-Aug	20	0.167	0.10	-0.0163	-0.0183	0.015
MC1	17-Aug	30	0.178	0.14	-0.0146	-0.0172	0.007
MC1	17-Aug	50	0.312	0.20	-0.0127	-0.0187	0.011
HB6	19-Aug	5	0.259	0.16	-0.0162	-0.0164	0.283
HB6	19-Aug	10	0.150	0.09	-0.0144	-0.0138	0.203
HB6	19-Aug	20	0.185	0.11	-0.0146	-0.0149	0.012
HB6	19-Aug	30	0.189	0.10	-0.0153	-0.0163	0.011
HB6	19-Aug	50	0.098	0.09	-0.0066	-0.0123	0.005
HB8	20-Aug	5	0.212	0.13	-0.0160	-0.0155	0.263
HB8	20-Aug	10	0.194	0.12	-0.0157	-0.0152	0.192
HB8	20-Aug	20	0.324	0.16	-0.0135	-0.0115	0.018
HB8	20-Aug	30	0.268	0.15	-0.0125	-0.0112	0.010
HB8	20-Aug	50	0.214	0.15	-0.0069	-0.0092	0.007
HB10	20-Aug	5	0.216	0.14	-0.0147	-0.0151	0.387
HB10	20-Aug	10	0.158	0.10	-0.0136	-0.0137	0.373
HB10	20-Aug	20	0.156	0.09	-0.0139	-0.0137	0.080
HB10	20-Aug	30	0.269	0.16	-0.0124	-0.0132	0.020
HB10	20-Aug	50	0.148	0.11	-0.0110	-0.0123	0.012
HB10	20-Aug	70	0.095	0.08	-0.0043	-0.0110	0.011
HB10	20-Aug	90	0.037	0.03	-0.0051	-0.0110	0.012
HB10	20-Aug	110	0.098	0.13	-0.0121	-0.0099	0.006
HB10	20-Aug	130	0.070	0.08	-0.0029	-0.0098	0.013
HB12	21-Aug	5	0.145	0.07	-0.0123	-0.0134	0.211

Station	Date	Depth	temp	salin	sig-t	average for prior 24 h PAR	kd
CH1	7-Aug	5	12.457	32.789	24.812	69.63	0.49
CH1	7-Aug	10	12.398	32.851	24.872	6.45	0.49
CH1	7-Aug	15	11.435	33.199	25.321	0.72	0.47
CH1	7-Aug	20	10.995	33.352	25.518	0.09	0.45
CH1	7-Aug	28	9.796	33.569	25.894	0.00	0.52
CH6	8-Aug	5	14.164	32.304	24.096	193.90	0.31
CH6	8-Aug	10	14.160	32.304	24.097	40.88	0.31
CH6	8-Aug	20	9.110	32.394	25.087	3.12	0.28
CH6	8-Aug	30	8.026	32.620	25.427	0.59	0.25
CH6	8-Aug	40	7.894	32.814	25.598	0.07	0.24
CH6	8-Aug	50	7.893	33.190	25.894	0.01	0.24
CH6	8-Aug	60	7.886	33.452	26.100	0.00	0.24
CH3	9-Aug	5	9.947	33.056	25.468	206.94	0.29
CH3	9-Aug	12	9.040	33.054	25.613	30.50	0.28
CH3	9-Aug	19	8.370	33.089	25.744	5.48	0.27
CH3	9-Aug	25	8.149	33.201	25.865	1.14	0.27
CH3	9-Aug	32	8.030	33.369	26.014	0.17	0.27
CH3	9-Aug	39	7.632	33.780	26.395	0.03	0.27
CH3	9-Aug	46	7.574	33.826	26.439	0.00	0.26
CH1	10-Aug	5	11.281	33.000	25.194	64.50	0.36
CH1	10-Aug	10	10.968	33.135	25.355	12.58	0.34
CH1	10-Aug	15	9.499	33.480	25.875	2.04	0.35
CH1	10-Aug	20	8.693	33.620	26.111	0.23	0.37
CH1	10-Aug	28.6	7.852	33.758	26.345	0.00	0.41
CH6	11-Aug	5	15.216	32.264	23.843	84.43	0.31
CH6	11-Aug	10	13.991	32.341	24.161	13.24	0.34
CH6	11-Aug	20	9.194	32.469	25.132	1.42	0.28
CH6	11-Aug	25	8.596	32.560	25.295	0.50	0.27
CH6	11-Aug	30	8.353	32.623	25.382	0.16	0.26
CH6	11-Aug	40	7.869	32.897	25.667	0.02	0.25
CH6	11-Aug	60	7.838	33.361	26.036	0.00	0.24
CH6	11-Aug	80	7.929	33.620	26.226	0.00	0.24
CH6	11-Aug	100	7.857	33.747	26.336	0.00	0.24
CH6	11-Aug	150	7.248	33.911	26.552	0.00	0.27
CH6	11-Aug	170	7.198	33.915	26.562	0.00	0.32
CP1	12-Aug	5	11.102	33.447	25.574	58.62	0.42
CP1	12-Aug	10	10.529	33.500	25.716	4.13	0.48
CP1	12-Aug	20	8.777	33.629	26.105	0.09	0.43
CP1	12-Aug	26	8.550	33.642	26.150	0.01	0.42
CP1	12-Aug	32	8.232	33.665	26.217	0.00	0.49
CP11	13-Aug	5	15.577	32.304	23.795	58.62	0.26
CP11	13-Aug	10	15.475	32.306	23.818	4.13	0.26
CP11	13-Aug	17	12.160	32.356	24.532	3.16	0.27
CP11	13-Aug	25	9.683	32.428	25.022	0.52	0.26
CP11	13-Aug	40	8.541	32.507	25.262	0.02	0.24
CP11	13-Aug	50	8.121	32.728	25.498	0.00	0.24

Station	Date	Depth	temp	salin	sig-t	average for prior 24 h PAR	kd
CP5	14-Aug	5	12.379	32.566	24.654	46.21	0.40
CP5	14-Aug	10	12.337	32.791	24.836	4.42	0.43
CP5	14-Aug	20	8.389	33.167	25.803	1.64	0.27
CP5	14-Aug	30	7.896	33.284	25.967	0.13	0.26
CP5	14-Aug	40	7.781	33.442	26.107	0.01	0.25
CP5	14-Aug	50	7.698	33.663	26.293	0.00	0.26
CP5	14-Aug	60	7.379	33.865	26.497	0.00	0.26
CP5	14-Aug	70	7.408	33.894	26.516	0.00	
CP5	14-Aug	80	7.272	33.935	26.567	0.00	
CP5	14-Aug	90	7.219	33.934	26.574	0.00	
CP5	14-Aug	95	7.217	33.936	26.576	0.00	
CP5	14-Aug	101	7.202	33.934	26.576	0.00	
CP4	15-Aug	5	13.476	33.124	24.870	47.41	0.35
CP4	15-Aug	10	13.429	33.121	24.878	11.31	0.36
CP4	15-Aug	20	10.028	33.262	25.614	0.76	0.31
CP4	15-Aug	25	8.188	33.448	26.053	0.49	0.27
CP4	15-Aug	30	8.051	33.580	26.177	0.15	0.26
CP4	15-Aug	40	7.803	33.663	26.278	0.01	0.26
CP4	15-Aug	50	7.459	33.770	26.411	0.00	0.25
CP4	15-Aug	5	13.199	33.095	24.904	48.49	0.39
CP4	15-Aug	10	11.787	33.128	25.201	12.43	0.33
CP4	15-Aug	20	8.509	33.428	25.989	1.43	0.27
CP4	15-Aug	25	8.149	33.518	26.113	0.48	0.26
CP4	15-Aug	30	7.912	33.590	26.205	0.15	0.26
CP4	15-Aug	40	7.605	33.705	26.340	0.01	0.25
CP4	15-Aug	90	7.177	33.903	26.555	0.00	0.31
MC1	17-Aug	5	12.000	32.645	24.785	33.18	0.59
MC1	17-Aug	10	10.328	32.710	25.135	12.66	0.39
MC1	17-Aug	20	8.621	33.002	25.638	3.11	0.27
MC1	17-Aug	30	7.846	33.251	25.948	0.39	0.25
MC1	17-Aug	50	7.680	33.652	26.287	0.00	0.25
HB6	19-Aug	5	12.910	32.706	24.660	31.79	0.66
HB6	19-Aug	10	11.356	32.642	24.902	4.29	0.53
HB6	19-Aug	20	8.530	33.028	25.672	3.89	0.27
HB6	19-Aug	30	8.508	33.066	25.705	0.27	0.27
HB6	19-Aug	50	7.801	33.444	26.106	0.00	0.25
HB8	20-Aug	5	12.684	32.600	24.622	36.60	0.62
HB8	20-Aug	10	11.889	32.556	24.739	4.25	0.52
HB8	20-Aug	20	8.451	32.636	25.377	3.99	0.27
HB8	20-Aug	30	8.060	32.861	25.611	0.45	0.25
HB8	20-Aug	50	8.149	33.385	26.009	0.00	0.24
HB10	20-Aug	5	12.637	32.565	24.604	18.37	0.77
HB10	20-Aug	10	12.346	32.685	24.752	0.60	0.73
HB10	20-Aug	20	9.711	32.654	25.194	0.72	0.35
HB10	20-Aug	30	8.387	32.829	25.538	0.29	0.27
HB10	20-Aug	50	8.038	33.215	25.892	0.00	0.25
HB10	20-Aug	70	7.738	33.647	26.275	0.00	0.25
HB10	20-Aug	90	7.759	33.750	26.353	0.00	0.25
HB10	20-Aug	110	7.773	33.911	26.477	0.00	0.25
HB10	20-Aug	130	7.597	33.943	26.528	0.00	0.26
HB12	21-Aug	5	10.252	33.196	25.526	89.39	0.50

Station	Date	Depth	Tchla	fuco/Tchla	perid/Tchla	hex/Tchla	zea+lut /Tchla	allo/Tchla	chlb/Tchla
CH1	7-Aug	5	9.60	0.41	0.01	0.02	0.00	0.01	0.01
CH1	7-Aug	10	9.09	0.41	0.01	0.02	0.00	0.01	0.01
CH1	7-Aug	15	8.86	0.43	0.01	0.01	0.00	0.01	0.01
CH1	7-Aug	20	8.71	0.45	0.00	0.01	0.00	0.00	0.00
CH1	7-Aug	28	9.41	0.50	0.00	0.00	0.00	0.00	0.00
CH6	8-Aug	5	1.41	0.34	0.02	0.25	0.03	0.03	0.10
CH6	8-Aug	10	1.40	0.33	0.01	0.24	0.02	0.03	0.10
CH6	8-Aug	20	1.39	0.42	0.03	0.15	0.02	0.04	0.08
CH6	8-Aug	30	0.35	0.44	0.03	0.19	0.01	0.03	0.07
CH6	8-Aug	40	0.13	0.40	0.03	0.28	0.01	0.01	0.08
CH6	8-Aug	50	0.03	0.33	0.00	0.30	0.00	0.00	0.17
CH6	8-Aug	60	0.02	0.39	0.00	0.15	0.00	0.00	0.27
CH3	9-Aug	5	2.18	0.44	0.01	0.02	0.00	0.01	0.00
CH3	9-Aug	12	1.26	0.42	0.03	0.02	0.00	0.02	0.00
CH3	9-Aug	19	0.49	0.39	0.07	0.03	0.00	0.04	0.00
CH3	9-Aug	25	0.45	0.41	0.07	0.02	0.00	0.05	0.00
CH3	9-Aug	32	0.79	0.48	0.01	0.01	0.00	0.02	0.00
CH3	9-Aug	39	1.31	0.50	0.00	0.00	0.00	0.01	0.00
CH3	9-Aug	46	0.98	0.49	0.00	0.00	0.00	0.01	0.00
CH1	10-Aug	5	4.21	0.42	0.01	0.03	0.00	0.01	0.02
CH1	10-Aug	10	4.33	0.42	0.01	0.03	0.00	0.01	0.02
CH1	10-Aug	15	4.66	0.45	0.00	0.01	0.00	0.00	0.00
CH1	10-Aug	20	4.59	0.45	0.00	0.00	0.00	0.00	0.00
CH1	10-Aug	28.6	3.12	0.55	0.00	0.00	0.00	0.00	0.00
CH6	11-Aug	5	1.18	0.21	0.01	0.41	0.04	0.05	0.07
CH6	11-Aug	10	1.73	0.52	0.02	0.24	0.03	0.02	0.10
CH6	11-Aug	20	0.99	0.37	0.03	0.12	0.01	0.07	0.10
CH6	11-Aug	25	0.74	0.40	0.03	0.13	0.01	0.06	0.07
CH6	11-Aug	30	0.57	0.41	0.03	0.19	0.00	0.05	0.04
CH6	11-Aug	40	0.15	0.48	0.04	0.15	0.00	0.00	0.03
CH6	11-Aug	60	0.02	0.48	0.00	0.18	0.00	0.00	0.18
CH6	11-Aug	80	0.01	0.70	0.00	0.24	0.00	0.00	0.00
CH6	11-Aug	100	0.01	0.66	0.00	0.30	0.00	0.00	0.00
CH6	11-Aug	150	0.05	0.94	0.00	0.09	0.00	0.00	0.00
CH6	11-Aug	170	0.07	0.93	0.00	0.02	0.00	0.00	0.00
CP1	12-Aug	5	8.07	0.36	0.06	0.01	0.00	0.00	0.00
CP1	12-Aug	10	5.78	0.34	0.14	0.00	0.00	0.00	0.00
CP1	12-Aug	20	5.85	0.49	0.00	0.00	0.00	0.01	0.00
CP1	12-Aug	26	8.75	0.50	0.00	0.00	0.00	0.00	0.00
CP1	12-Aug	32	12.01	0.48	0.00	0.00	0.00	0.00	0.00
CP11	13-Aug	5	0.21	0.10	0.00	0.19	0.27	0.04	0.17
CP11	13-Aug	10	0.25	0.12	0.01	0.21	0.28	0.04	0.20
CP11	13-Aug	17	0.53	0.24	0.02	0.32	0.11	0.01	0.18
CP11	13-Aug	25	0.60	0.35	0.02	0.35	0.02	0.01	0.13
CP11	13-Aug	40	0.25	0.28	0.00	0.42	0.00	0.01	0.14
CP11	13-Aug	50	0.10	0.29	0.04	0.33	0.00	0.02	0.18

Station	Date	Depth	Tchla	fuco/Tchla	perid/Tchla	hex/Tchla	zea+lut /Tchla	allo/Tchla	chlb/Tchla
CP5	14-Aug	5	2.90	0.39	0.01	0.08	0.01	0.02	0.08
CP5	14-Aug	10	3.82	0.42	0.02	0.06	0.00	0.02	0.05
CP5	14-Aug	20	0.93	0.52	0.01	0.01	0.00	0.00	0.00
CP5	14-Aug	30	0.55	0.68	0.03	0.00	0.00	0.00	0.01
CP5	14-Aug	40	0.25	0.81	0.04	0.01	0.00	0.00	0.00
CP5	14-Aug	50	0.45	0.63	0.02	0.00	0.00	0.00	0.00
CP5	14-Aug	60	0.33	0.88	0.02	0.00	0.00	0.00	0.00
CP5	14-Aug	70	0.17	1.04	0.00	0.00	0.00	0.00	0.00
CP5	14-Aug	80	0.10	1.22	0.05	0.00	0.00	0.00	0.06
CP5	14-Aug	90	0.12	1.03	0.00	0.00	0.00	0.00	0.00
CP5	14-Aug	95	0.48	0.86	0.05	0.00	0.00	0.00	0.00
CP5	14-Aug	101	0.53	1.19	0.00	0.00	0.01	0.00	0.00
CP4	15-Aug	5	3.29	0.37	0.19	0.14	0.00	0.01	0.03
CP4	15-Aug	10	3.24	0.40	0.17	0.14	0.00	0.01	0.03
CP4	15-Aug	20	2.19	0.55	0.13	0.05	0.00	0.01	0.01
CP4	15-Aug	25	0.61	0.43	0.19	0.02	0.00	0.01	0.00
CP4	15-Aug	30	0.49	0.41	0.22	0.01	0.00	0.01	0.00
CP4	15-Aug	40	0.42	0.39	0.21	0.01	0.00	0.01	0.00
CP4	15-Aug	50	0.20	0.72	0.07	0.01	0.01	0.00	0.00
CP4	15-Aug	5	3.37	0.33	0.15	0.15	0.00	0.01	0.05
CP4	15-Aug	10	2.07	0.46	0.15	0.07	0.00	0.01	0.02
CP4	15-Aug	20	0.38	0.41	0.30	0.10	0.00	0.03	0.00
CP4	15-Aug	25	0.31	0.28	0.43	0.02	0.00	0.01	0.00
CP4	15-Aug	30	0.42	0.18	0.53	0.01	0.00	0.00	0.00
CP4	15-Aug	40	0.29	0.42	0.22	0.01	0.00	0.00	0.00
CP4	15-Aug	90	1.93	0.45	1.87	0.00	0.00	0.00	0.00
MC1	17-Aug	5	14.78	0.55	0.01	0.04	0.00	0.01	0.04
MC1	17-Aug	10	6.62	0.52	0.01	0.04	0.00	0.02	0.04
MC1	17-Aug	20	0.59	0.51	0.03	0.03	0.00	0.01	0.04
MC1	17-Aug	30	0.09	0.54	0.18	0.04	0.01	0.00	0.04
MC1	17-Aug	50	0.15	0.66	0.00	0.00	0.01	0.00	0.00
HB6	19-Aug	5	15.31	0.55	0.01	0.03	0.00	0.01	0.03
HB6	19-Aug	10	9.58	0.55	0.01	0.04	0.00	0.01	0.04
HB6	19-Aug	20	0.56	0.47	0.07	0.03	0.00	0.03	0.02
HB6	19-Aug	30	0.51	0.44	0.07	0.02	0.00	0.03	0.03
HB6	19-Aug	50	0.10	0.55	0.28	0.03	0.00	0.00	0.00
HB8	20-Aug	5	13.96	0.56	0.01	0.05	0.00	0.01	0.03
HB8	20-Aug	10	10.12	0.55	0.01	0.05	0.00	0.01	0.03
HB8	20-Aug	20	0.61	0.31	0.03	0.12	0.02	0.06	0.12
HB8	20-Aug	30	0.28	0.37	0.04	0.11	0.01	0.05	0.09
HB8	20-Aug	50	0.04	0.48	0.04	0.12	0.05	0.03	0.14
HB10	20-Aug	5	18.33	0.59	0.00	0.03	0.00	0.01	0.02
HB10	20-Aug	10	18.76	0.61	0.01	0.03	0.00	0.01	0.02
HB10	20-Aug	20	3.53	0.53	0.01	0.04	0.00	0.02	0.05
HB10	20-Aug	30	0.52	0.40	0.07	0.08	0.01	0.04	0.09
HB10	20-Aug	50	0.17	0.45	0.19	0.04	0.00	0.02	0.00
HB10	20-Aug	70	0.06	0.68	0.14	0.03	0.00	0.00	0.00
HB10	20-Aug	90	0.05	0.83	0.08	0.04	0.00	0.00	0.00
HB10	20-Aug	110	0.01	1.26	0.00	0.08	0.00	0.00	0.00
HB10	20-Aug	130	0.02	1.11	0.00	0.00	0.00	0.00	0.00
HB12	21-Aug	5	11.28	0.43	0.04	0.02	0.00	0.00	0.01

Station	Date	Depth	but/Tchla	(diad+diat) /Tchla	chla epimer /Tchla	chl c1+c2 /Tchla	chlc3 /Tchla	Total Carot +Chl b+Chlc /Tchla	QFT ad412/ ap412
CH1	7-Aug	5	0.00	0.06	0.00	0.17	0.01	0.74	0.39
CH1	7-Aug	10	0.00	0.06	0.00	0.17	0.01	0.74	0.40
CH1	7-Aug	15	0.00	0.05	0.00	0.17	0.02	0.71	0.48
CH1	7-Aug	20	0.00	0.05	0.00	0.17	0.01	0.72	0.50
CH1	7-Aug	28	0.00	0.05	0.00	0.14	0.02	0.76	0.53
CH6	8-Aug	5	0.04	0.09	0.00	0.16	0.14	1.22	0.17
CH6	8-Aug	10	0.04	0.09	0.00	0.16	0.11	1.16	0.19
CH6	8-Aug	20	0.05	0.06	0.00	0.16	0.12	1.16	0.18
CH6	8-Aug	30	0.07	0.04	0.00	0.13	0.16	1.21	0.32
CH6	8-Aug	40	0.13	0.03	0.00	0.13	0.15	1.25	0.43
CH6	8-Aug	50	0.16	0.00	0.00	0.08	0.14	1.17	0.68
CH6	8-Aug	60	0.10	0.00	0.00	0.14	0.00	1.06	0.56
CH3	9-Aug	5	0.00	0.14	0.00	0.14	0.02	0.81	0.47
CH3	9-Aug	12	0.01	0.12	0.00	0.15	0.01	0.79	0.44
CH3	9-Aug	19	0.01	0.09	0.00	0.16	0.03	0.83	0.52
CH3	9-Aug	25	0.01	0.07	0.00	0.17	0.01	0.83	0.52
CH3	9-Aug	32	0.00	0.05	0.00	0.15	0.01	0.76	0.54
CH3	9-Aug	39	0.00	0.04	0.00	0.16	0.01	0.74	0.44
CH3	9-Aug	46	0.00	0.05	0.00	0.16	0.00	0.73	0.53
CH1	10-Aug	5	0.01	0.08	0.01	0.10	0.04	0.74	0.33
CH1	10-Aug	10	0.00	0.08	0.02	0.12	0.02	0.73	0.33
CH1	10-Aug	15	0.01	0.06	0.04	0.10	0.00	0.66	0.48
CH1	10-Aug	20	0.01	0.05	0.05	0.10	0.02	0.67	0.58
CH1	10-Aug	28.6	0.02	0.06	0.09	0.10	0.01	0.78	0.63
CH6	11-Aug	5	0.06	0.18	0.00	0.17	0.09	1.33	0.15
CH6	11-Aug	10	0.04	0.08	0.01	0.24	0.16	1.45	0.22
CH6	11-Aug	20	0.04	0.03	0.02	0.15	0.09	1.05	0.24
CH6	11-Aug	25	0.04	0.04	0.04	0.15	0.13	1.08	0.24
CH6	11-Aug	30	0.04	0.03	0.08	0.15	0.15	1.13	0.29
CH6	11-Aug	40	0.11	0.03	0.41	0.10	0.14	1.09	0.58
CH6	11-Aug	60	0.00	0.00	0.48	0.08	0.00	0.92	0.77
CH6	11-Aug	80	0.00	0.00	0.53	0.00	0.00	0.94	0.95
CH6	11-Aug	100	0.00	0.03	0.56	0.00	0.00	1.00	0.27
CH6	11-Aug	150	0.02	0.08	0.28	0.14	0.00	1.28	0.81
CH6	11-Aug	170	0.00	0.05	0.31	0.10	0.00	1.11	0.77
CP1	12-Aug	5	0.00	0.06	0.05	0.18	0.04	0.72	0.35
CP1	12-Aug	10	0.00	0.06	0.08	0.18	0.03	0.77	0.28
CP1	12-Aug	20	0.00	0.06	0.00	0.17	0.01	0.77	0.62
CP1	12-Aug	26	0.00	0.06	0.05	0.17	0.01	0.77	0.36
CP1	12-Aug	32	0.00	0.07	0.01	0.15	0.00	0.74	0.62
CP11	13-Aug	5	0.00	0.04	0.00	0.07	0.00	0.96	0.19
CP11	13-Aug	10	0.03	0.06	0.00	0.11	0.04	1.16	0.18
CP11	13-Aug	17	0.04	0.06	0.00	0.15	0.12	1.28	0.21
CP11	13-Aug	25	0.06	0.06	0.00	0.17	0.18	1.37	0.20
CP11	13-Aug	40	0.10	0.05	0.00	0.16	0.16	1.33	0.26
CP11	13-Aug	50	0.16	0.04	0.00	0.15	0.14	1.37	0.32

Station	Date	Depth	but/Tchla	(diad+diat) /Tchla	chla epimer /Tchla	chl c1+c2 /Tchla	chlc3 /Tchla	Total Carot +Chl b+Chlc /Tchla	QFT ad412/ ap412
CP5	14-Aug	5	0.02	0.06	0.01	0.13	0.05	0.88	0.22
CP5	14-Aug	10	0.01	0.06	0.00	0.14	0.05	0.85	0.22
CP5	14-Aug	20	0.00	0.03	0.11	0.14	0.01	0.74	0.43
CP5	14-Aug	30	0.00	0.04	0.13	0.16	0.01	0.96	0.47
CP5	14-Aug	40	0.00	0.03	0.27	0.14	0.01	1.07	0.44
CP5	14-Aug	50	0.00	0.04	0.15	0.15	0.00	0.88	0.55
CP5	14-Aug	60	0.00	0.04	0.18	0.17	0.00	1.16	0.28
CP5	14-Aug	70	0.00	0.04	0.25	0.16	0.00	1.31	0.34
CP5	14-Aug	80	0.00	0.05	0.27	0.14	0.00	1.60	0.53
CP5	14-Aug	90	0.00	0.04	0.11	0.16	0.00	1.30	0.73
CP5	14-Aug	95	0.00	0.09	0.07	0.16	0.00	1.22	0.68
CP5	14-Aug	101	0.00	0.07	0.02	0.24	0.01	1.58	0.77
CP4	15-Aug	5	0.01	0.12	0.00	0.20	0.08	1.17	0.24
CP4	15-Aug	10	0.01	0.11	0.00	0.20	0.08	1.19	0.21
CP4	15-Aug	20	0.01	0.06	0.00	0.22	0.12	1.17	0.27
CP4	15-Aug	25	0.00	0.09	0.00	0.20	0.06	1.00	0.35
CP4	15-Aug	30	0.00	0.09	0.00	0.21	0.04	1.02	0.38
CP4	15-Aug	40	0.00	0.11	0.00	0.19	0.02	0.96	0.42
CP4	15-Aug	50	0.00	0.16	0.00	0.25	0.03	1.26	0.45
CP4	15-Aug	5	0.01	0.09	0.00	0.19	0.07	1.10	0.24
CP4	15-Aug	10	0.02	0.07	0.00	0.19	0.10	1.11	0.30
CP4	15-Aug	20	0.00	0.09	0.00	0.25	0.13	1.31	0.39
CP4	15-Aug	25	0.00	0.10	0.00	0.23	0.04	1.13	0.37
CP4	15-Aug	30	0.00	0.12	0.00	0.21	0.00	1.07	0.39
CP4	15-Aug	40	0.00	0.07	0.00	0.18	0.01	0.94	0.42
CP4	15-Aug	90	0.00	0.11	0.00	0.18	0.00	2.65	0.50
MC1	17-Aug	5	0.01	0.08	0.00	0.19	0.04	1.00	0.15
MC1	17-Aug	10	0.01	0.04	0.00	0.15	0.06	0.93	0.13
MC1	17-Aug	20	0.01	0.06	0.00	0.16	0.08	0.96	0.47
MC1	17-Aug	30	0.00	0.10	0.00	0.20	0.06	1.19	0.58
MC1	17-Aug	50	0.00	0.15	0.00	0.17	0.02	1.05	0.49
HB6	19-Aug	5	0.01	0.13	0.01	0.18	0.06	1.03	0.17
HB6	19-Aug	10	0.01	0.05	0.01	0.16	0.07	0.96	0.16
HB6	19-Aug	20	0.04	0.05	0.05	0.17	0.07	0.97	0.41
HB6	19-Aug	30	0.02	0.05	0.06	0.12	0.03	0.83	0.54
HB6	19-Aug	50	0.06	0.06	0.11	0.14	0.00	1.15	0.64
HB8	20-Aug	5	0.01	0.10	0.00	0.20	0.05	1.03	0.14
HB8	20-Aug	10	0.02	0.08	0.00	0.19	0.06	1.02	0.16
HB8	20-Aug	20	0.02	0.05	0.00	0.16	0.12	1.04	0.28
HB8	20-Aug	30	0.03	0.05	0.00	0.14	0.11	1.03	0.41
HB8	20-Aug	50	0.07	0.06	0.00	0.17	0.08	1.25	0.54
HB10	20-Aug	5	0.01	0.11	0.01	0.17	0.03	1.00	0.19
HB10	20-Aug	10	0.01	0.07	0.01	0.21	0.05	1.03	0.11
HB10	20-Aug	20	0.01	0.05	0.01	0.15	0.10	1.00	0.19
HB10	20-Aug	30	0.03	0.07	0.13	0.12	0.07	1.03	0.33
HB10	20-Aug	50	0.05	0.07	0.26	0.14	0.02	1.01	0.43
HB10	20-Aug	70	0.00	0.05	0.33	0.10	0.00	1.10	0.54
HB10	20-Aug	90	0.00	0.03	0.37	0.13	0.00	1.16	0.36
HB10	20-Aug	110	0.00	0.08	0.52	0.04	0.00	1.58	0.51
HB10	20-Aug	130	0.00	0.02	0.18	0.09	0.00	1.28	0.67
HB12	21-Aug	5	0.00	0.05	0.00	0.20	0.08	0.85	0.20

Station	Date	Depth	QFT Qa*676	ac-9 Qa*676	fit to cp spectra gamma	cp440 /cp650	Tchla cp650	Tchla /cp650	aph676 /cp650
CH1	7-Aug	5	0.65	0.76	0.69	1.31	1.29	7.43	0.11
CH1	7-Aug	10	0.77	0.78	0.71	1.32	1.30	6.97	0.11
CH1	7-Aug	15	0.66	0.69	0.84	1.38	1.19	7.47	0.10
CH1	7-Aug	20	0.76	0.64	0.88	1.40	1.12	7.76	0.10
CH1	7-Aug	28	0.55	0.65	0.92	1.43	1.59	5.90	0.08
CH6	8-Aug	5	1.64	1.11	0.87	1.46	0.45	3.13	0.07
CH6	8-Aug	10	1.61	1.11	0.87	1.46	0.46	3.07	0.07
CH6	8-Aug	20	1.47	0.98	0.66	1.33	0.29	4.82	0.09
CH6	8-Aug	30	1.57	1.00	0.92	1.43	0.09	4.17	0.08
CH6	8-Aug	40	1.83	1.37	1.19	1.56	0.06	2.18	0.06
CH6	8-Aug	50	1.10	3.07	1.32	1.63	0.06	0.57	0.04
CH6	8-Aug	60	2.70	5.37	1.34	1.63	0.05	0.35	0.04
CH3	9-Aug	5	0.68	0.59	0.88	1.39	0.30	7.31	0.09
CH3	9-Aug	12	0.82	0.79	0.97	1.42	0.23	5.55	0.09
CH3	9-Aug	19	1.37	1.31	1.16	1.51	0.15	3.22	0.08
CH3	9-Aug	25	1.32	1.52	1.25	1.55	0.15	3.07	0.09
CH3	9-Aug	32	0.92	0.94	1.26	1.57	0.16	5.08	0.10
CH3	9-Aug	39	0.62	0.69	1.27	1.60	0.17	7.79	0.11
CH3	9-Aug	46	0.80	0.90	1.29	1.61	0.16	6.00	0.11
CH1	10-Aug	5	0.99	0.91	0.56	1.25	0.84	5.03	0.09
CH1	10-Aug	10	0.87	0.74	0.67	1.30	0.72	6.01	0.09
CH1	10-Aug	15	0.70	0.62	0.96	1.45	0.68	6.87	0.09
CH1	10-Aug	20	0.77	0.70	1.02	1.48	0.80	5.78	0.08
CH1	10-Aug	28.6	1.12	1.18	0.94	1.44	1.05	2.97	0.07
CH6	11-Aug	5	1.63	1.46	0.91	1.50	0.58	2.03	0.06
CH6	11-Aug	10	1.61	1.37	0.94	1.54	0.53	3.25	0.09
CH6	11-Aug	20	1.67	1.27	0.72	1.36	0.25	3.94	0.10
CH6	11-Aug	25	1.59	1.32	0.62	1.29	0.19	3.84	0.10
CH6	11-Aug	30	1.52	1.38	0.67	1.30	0.15	3.70	0.10
CH6	11-Aug	40	1.46	2.06	1.12	1.52	0.07	1.97	0.08
CH6	11-Aug	60	1.74	5.72	1.29	1.60	0.06	0.35	0.04
CH6	11-Aug	80	2.65	10.09	1.35	1.63	0.06	0.19	0.04
CH6	11-Aug	100		20.83	1.41	1.66	0.06	0.24	0.10
CH6	11-Aug	150		2.42	1.04	1.49	0.18	0.28	0.01
CH6	11-Aug	170	3.69	11.75	0.81	1.37	0.51	0.13	0.03
CP1	12-Aug	5	0.74	0.80			0.95	8.51	
CP1	12-Aug	10	0.66	1.55			1.05	5.50	
CP1	12-Aug	20	0.89	0.98			0.94	6.21	
CP1	12-Aug	26	0.63	0.70			0.92	9.52	
CP1	12-Aug	32	0.46	0.60			1.45	8.30	
CP11	13-Aug	5	2.52	1.41	1.55	1.88	0.11	1.98	0.06
CP11	13-Aug	10	2.40	1.15	1.55	1.88	0.11	2.34	0.05
CP11	13-Aug	17	1.88	1.16	1.31	1.72	0.14	3.82	0.09
CP11	13-Aug	25	1.78	1.07	0.77	1.37	0.13	4.49	0.10
CP11	13-Aug	40	1.59	1.09	0.83	1.34	0.06	3.93	0.09
CP11	13-Aug	50	2.30	1.67	1.12	1.48	0.05	1.98	0.07

Station	Date	Depth	QFT Qa*676	ac-9 Qa*676	fit to cp spectra gamma	cp440 /cp650	Tchla cp650	Tchla /cp650	aph676 /cp650
CP5	14-Aug	5	1.86	1.70	0.63	1.32	1.06	2.74	0.09
CP5	14-Aug	10	1.84	1.68	0.49	1.24	1.29	2.97	0.10
CP5	14-Aug	20	1.03	0.79	1.12	1.49	0.15	6.36	0.10
CP5	14-Aug	30	1.35	1.18	1.20	1.55	0.14	3.94	0.09
CP5	14-Aug	40	2.42	2.37	1.27	1.59	0.11	2.25	0.11
CP5	14-Aug	50	1.07	1.27	1.26	1.59	0.13	3.55	0.09
CP5	14-Aug	60	1.56	1.82	1.31	1.61	0.12	2.68	0.10
CP5	14-Aug	70	2.74	3.07	1.34	1.63	0.11	1.49	0.09
CP5	14-Aug	80	3.74	7.93	1.16	1.56	0.23	0.44	0.07
CP5	14-Aug	90	5.50	9.55	1.07	1.51	0.41	0.28	0.05
CP5	14-Aug	95	1.75	3.21	1.02	1.49	0.48	1.00	0.06
CP5	14-Aug	101	1.86	3.08	0.99	1.47	0.56	0.95	0.06
CP4	15-Aug	5	1.22	0.92	0.23	1.11	0.97	3.39	0.06
CP4	15-Aug	10	0.63	0.97	0.25	1.12	0.97	3.36	0.07
CP4	15-Aug	20	1.16	0.84	0.51	1.20	0.39	5.54	0.09
CP4	15-Aug	25	1.18	1.15	0.95	1.38	0.16	3.87	0.09
CP4	15-Aug	30	1.26	1.12	1.21	1.50	0.12	4.21	0.09
CP4	15-Aug	40	1.16	1.12	1.24	1.52	0.10	4.23	0.09
CP4	15-Aug	50	2.05	2.38	1.28	1.55	0.09	2.21	0.11
CP4	15-Aug	5	1.26	1.17	0.35	1.16	1.08	3.11	0.07
CP4	15-Aug	10	1.13	0.95	0.53	1.23	0.51	4.06	0.08
CP4	15-Aug	20	1.89	1.30	0.99	1.38	0.15	2.53	0.07
CP4	15-Aug	25	1.09	1.54	1.10	1.43	0.11	2.81	0.09
CP4	15-Aug	30	0.95	1.22	1.10	1.44	0.10	4.26	0.10
CP4	15-Aug	40	1.03	1.47	1.23	1.50	0.08	3.37	0.10
CP4	15-Aug	90	0.81	0.68	1.13	1.53	0.32	6.13	0.08
MC1	17-Aug	5	0.89	0.87	0.51	1.28	2.51	5.88	0.10
MC1	17-Aug	10	1.18	0.82	0.66	1.35	0.81	8.16	0.13
MC1	17-Aug	20	1.20	1.25	1.29	1.58	0.16	3.78	0.09
MC1	17-Aug	30	2.06	4.04	1.50	1.64	0.08	1.08	0.09
MC1	17-Aug	50	1.93	3.51	1.58	1.69	0.10	1.51	0.11
HB6	19-Aug	5	0.93	0.93	0.64	1.35	2.96	5.17	0.10
HB6	19-Aug	10	0.87	1.06	0.65	1.37	1.70	5.62	0.12
HB6	19-Aug	20	1.66	1.08	1.01	1.47	0.14	3.93	0.08
HB6	19-Aug	30	1.57	1.07	1.05	1.48	0.14	3.58	0.08
HB6	19-Aug	50	2.04	2.59	1.15	1.54	0.08	1.20	0.06
HB8	20-Aug	5	1.01	0.94	0.67	1.37	2.74	5.09	0.10
HB8	20-Aug	10	1.08	0.95	0.69	1.39	1.93	5.26	0.10
HB8	20-Aug	20	1.80	1.49	0.88	1.44	0.14	4.35	0.13
HB8	20-Aug	30	1.98	1.86	1.07	1.50	0.08	3.50	0.13
HB8	20-Aug	50	3.64	8.97	1.27	1.59	0.06	0.62	0.11
HB10	20-Aug	5	0.98	1.06	0.58	1.33	4.27	4.29	0.09
HB10	20-Aug	10	0.87	1.00	0.66	1.38	3.12	6.02	0.12
HB10	20-Aug	20	1.06	1.13	0.79	1.44	0.59	6.01	0.14
HB10	20-Aug	30	1.95	1.91	1.11	1.53	0.14	3.59	0.14
HB10	20-Aug	50	1.74	3.72	1.46	1.67	0.10	1.74	0.13
HB10	20-Aug	70	1.97	10.17	1.65	1.75	0.08	0.67	0.14
HB10	20-Aug	90	2.22	11.49	1.62	1.71	0.08	0.64	0.15
HB10	20-Aug	110	5.53	20.41	1.47	1.65	0.09	0.17	0.07
HB10	20-Aug	130	6.98	28.34	1.18	1.54	0.15	0.15	0.08
HB12	21-Aug	5	0.90	0.94	-0.38	0.87	1.91	5.90	0.11

Appendix C. 5-m data. Includes collection date and time (PDT), group, latitude and longitude (decimal degrees), nutrients (μM), PPC: PSC ratios (g: g), PPC: Tchl *a* (g: g), ac-9 a_{ph} slope, ac-9 a_p slope, ac-9 $a_{ph}676$ (m^{-1}), T (°C), S, sigma-t (kg m^{-3}), daytime mean PAR at sample depth over prior 24 h (μmol photons m^{-2} s^{-1}), k_d (m^{-1}), HPLC-derived pigments including Tchl *a* (μg L^{-1}) and ratios of pigments to Tchl *a* (g: g), QFT a_d12: a_p412, Qa*676 from QFT and HPLC data and from ac-9 and HPLC data, gamma (slope of hyperbolic fit to c_p spectra), ac-9 c_p440: c_p650, c_p650 (m^{-1}), Tchl *a*: c_p650, ac-9 $a_{ph}676$: c_p650.

Station	date (local)	time (local)	depth	group	lat (N)	long (W)
CH1	7-Aug	17:46	5	IN	45.01	124.04
CH6	8-Aug	4:25	5	CR	45.01	124.36
CH3	9-Aug	14:21	5	IN	45.01	124.12
CH1	10-Aug	20:18	5	IN	45.01	124.04
CH6	11-Aug	10:47	5	CR	45.01	124.33
CP1	12-Aug	3:01	5	IN	44.22	124.15
CP11	13-Aug	15:28	5	CR	44.23	125.00
CP5	14-Aug	3:15	5	MID	44.23	124.61
CP45 ts	14-Aug	12:16	4	MID	44.23	124.56
CP45 ts	14-Aug	14:07	3	MID	44.23	124.51
CP45 ts	14-Aug	16:07	3	MID	44.23	124.49
CP45 ts	14-Aug	16:47	5	MID	44.22	124.51
CP45 ts	14-Aug	18:09	5	MID	44.22	124.55
CP45 ts	14-Aug	20:06	4	MID	44.23	124.61
CP45 ts	14-Aug	21:56	5	MID	44.23	124.56
CP45 ts	15-Aug	0:09	5	MID	44.23	124.51
CP4	15-Aug	3:55	6	MID	44.23	124.47
CP45 ts	15-Aug	6:24	3	MID	44.23	124.50
CP45 ts	15-Aug	8:01	3	MID	44.23	124.55
CP45 ts	15-Aug	9:50	3	MID	44.22	124.60
CP45 ts	15-Aug	12:09	3	MID	44.22	124.57
CP45 ts	15-Aug	14:09	4	MID	44.22	124.51
CP4	15-Aug	20:28	5	MID	44.23	124.47
CP45 ts	16-Aug	0:00	3	MID	44.22	124.53
CP45 ts	16-Aug	2:12	5	MID	44.22	124.61
CP45 ts	16-Aug	4:07	5	MID	44.23	124.55
CP45 ts	16-Aug	6:07	3	MID	44.23	124.49
CP45 ts	16-Aug	7:46	3	MID	44.23	124.49
CP45 ts	16-Aug	10:00	3	MID	44.23	124.56
CP45 ts	16-Aug	12:07	3	MID	44.22	124.61
BLM	16-Aug	18:43	3	MID	44.19	124.72
MC 1	17-Aug	16:43	5	MID	44.19	124.65
HB6	19-Aug	8:08	5	MID	44.03	124.68
HB8	20-Aug	1:11	5	MID	43.95	124.78
HB10	20-Aug	21:45	5	MID	43.86	124.74
HB12	21-Aug	2:57	5	MID	43.86	124.28
ST1	24-Aug	6:22	5	MID	44.55	124.25
ST2	24-Aug	8:31	4	MID	44.55	124.31
ST3	24-Aug	10:33	4	MID	44.55	124.37
ST4	24-Aug	12:33	4	MID	44.55	124.44
ST5	24-Aug	14:06	4	MID	44.55	124.49
ST6	24-Aug	18:22	4	MID	44.31	124.40
ST7	24-Aug	20:24	6	MID	44.34	124.37
ST8	24-Aug	22:29	5	MID	44.38	124.35
ST9	25-Aug	0:33	5	MID	44.43	124.32
ST10	25-Aug	2:36	4	MID	44.48	124.29
ST11	25-Aug	5:54	5	MID	44.55	124.25
ST12	25-Aug	7:58	4	MID	44.57	124.31

Station	date (local)	depth	group	PO4	NH4	SiO2	NO2	NO3	DIN	N:P	Si:N
CH1	7-Aug	5	IN	0.68	0.83	2.56	0.07	3.11	4.01	5.88	0.64
CH6	8-Aug	5	CR	0.51	0.18	9.89	0.12	1.95	2.24	4.37	4.41
CH3	9-Aug	5	IN	2.45	2.12	51.04	0.16	24.12	26.40	10.77	1.93
CH1	10-Aug	5	IN	1.85	1.35	19.11	0.19	17.03	18.57	10.06	1.03
CH6	11-Aug	5	CR	0.33	0.34	5.54	0.00	0.00	0.35	1.05	16.02
CP1	12-Aug	5	IN	1.08	1.11	2.29	0.11	2.19	3.41	3.16	0.67
CP11	13-Aug	5	CR	0.21	2.05	0.23	0.05	0.00	2.10	10.15	0.11
CP5	14-Aug	5	MID	0.79	0.44	10.16	0.15	4.46	5.05	6.36	2.01
CP45 ts	14-Aug	4	MID	0.28	0.00	0.00	0.00	0.00	0.00		
CP45 ts	14-Aug	3	MID	0.33	0.00	0.00	0.00	0.00	0.00		
CP45 ts	14-Aug	3	MID	0.43	1.46	0.00	0.10	1.02	2.58	6.02	0.00
CP45 ts	14-Aug	5	MID								
CP45 ts	14-Aug	5	MID	0.33	0.00	0.00	0.00	0.00	0.00		
CP45 ts	14-Aug	4	MID	0.78	0.00	7.79	0.10	3.42	3.52	4.53	2.22
CP45 ts	14-Aug	5	MID	0.84	0.00	3.99	0.12	4.72	4.84	5.76	0.82
CP45 ts	15-Aug	5	MID	0.28	0.05	0.00	0.00	0.00	0.05	0.18	0.00
CP4	15-Aug	6	MID	0.25	0.64	0.00	0.03	3.81	4.48	18.26	0.00
CP45 ts	15-Aug	3	MID	0.33	1.47	0.00	0.05	4.40	5.92	17.91	0.00
CP45 ts	15-Aug	3	MID	0.57	0.20	1.60	0.07	1.79	2.06	3.61	0.78
CP45 ts	15-Aug	3	MID	0.91	0.28	8.94	0.16	5.74	6.18	6.79	1.45
CP45 ts	15-Aug	3	MID	0.35	0.15	0.00	0.02	0.39	0.57	1.62	0.00
CP45 ts	15-Aug	4	MID	0.39	0.52	0.00	0.01	0.00	0.53	1.35	0.00
CP4	15-Aug	5	MID	0.24	1.04	0.00	0.02	0.00	1.06	4.40	0.00
CP45 ts	16-Aug	3	MID	0.29	0.47	0.42	0.03	0.00	0.50	1.69	0.84
CP45 ts	16-Aug	5	MID	0.68	0.20	3.03	0.09	1.93	2.22	3.24	1.36
CP45 ts	16-Aug	5	MID	0.59	0.19	0.79	0.06	1.86	2.11	3.61	0.37
CP45 ts	16-Aug	3	MID	0.53	0.26	2.99	0.11	3.69	4.06	7.66	0.74
CP45 ts	16-Aug	3	MID	0.53	0.14	2.18	0.04	2.53	2.71	5.16	0.80
CP45 ts	16-Aug	3	MID	0.40	0.19	0.30	0.03	1.92	2.15	5.33	0.14
CP45 ts	16-Aug	3	MID	0.72	0.51	9.00	0.09	3.33	3.93	5.47	2.29
BLM	16-Aug	3	MID	0.54	0.83	18.33	0.08	0.79	1.69	3.12	10.84
MC 1	17-Aug	5	MID	0.78	0.45	9.96	0.09	3.87	4.41	5.65	2.26
HB6	19-Aug	5	MID	0.49	0.48	6.27	0.03	0.52	1.04	2.12	6.05
HB8	20-Aug	5	MID	0.61	0.19	10.01	0.04	0.98	1.21	1.99	8.28
HB10	20-Aug	5	MID	0.52	0.40	9.62	0.01	0.29	0.70	1.35	13.78
HB12	21-Aug	5	MID	1.57	0.15	16.31	0.03	11.62	11.80	7.51	1.38
ST1	24-Aug	5	MID	1.11	0.19	6.57	0.09	5.20	5.48	4.95	1.20
ST2	24-Aug	4	MID	1.08	0.13	9.58	0.11	4.05	4.29	3.97	2.23
ST3	24-Aug	4	MID	0.84	0.13	10.45	0.10	2.98	3.21	3.82	3.26
ST4	24-Aug	4	MID	1.13	0.20	11.46	0.10	5.35	5.66	5.03	2.03
ST5	24-Aug	4	MID	0.80	0.08	9.54	0.07	0.63	0.78	0.97	12.28
ST6	24-Aug	4	MID	0.67	0.02	8.85	0.22	0.00	0.24	0.36	36.73
ST7	24-Aug	6	MID	0.58	0.09	8.95	0.01	0.00	0.10	0.16	93.87
ST8	24-Aug	5	MID	0.62	0.10	8.63	0.02	0.08	0.20	0.32	42.91
ST9	25-Aug	5	MID	0.60	0.01	8.57	0.01	0.07	0.08	0.14	103.06
ST10	25-Aug	4	MID	0.75	0.11	7.29	0.03	0.02	0.16	0.21	45.29
ST11	25-Aug	5	MID	0.86	0.93	5.77	0.05	0.76	1.74	2.03	3.32
ST12	25-Aug	4	MID	0.96	0.68	3.85	0.08	2.88	3.63	3.78	1.06

Station	date (local)	depth	group	PPC/PSC	PPC:Tchla	aph slope	ap slope	ac9 aph676
CH1	7-Aug	5	IN	0.22	0.10	-0.010	-0.011	0.146
CH6	8-Aug	5	CR	0.27	0.17	-0.022	-0.021	0.031
CH3	9-Aug	5	IN	0.37	0.17	-0.011	-0.012	0.026
CH1	10-Aug	5	IN	0.26	0.12	-0.011	-0.012	0.076
CH6	11-Aug	5	CR	0.45	0.31	-0.025	-0.024	0.034
CP1	12-Aug	5	IN	0.18	0.08	-0.008	-0.011	
CP11	13-Aug	5	CR	1.43	0.42		-0.034	0.006
CP5	14-Aug	5	MID	0.24	0.12	-0.015	-0.015	0.099
CP45 ts	14-Aug	4	MID	0.39	0.21	-0.019	-0.019	0.041
CP45 ts	14-Aug	3	MID	0.35	0.23	-0.017	-0.017	0.057
CP45 ts	14-Aug	3	MID	0.34	0.23	-0.017	-0.017	0.082
CP45 ts	14-Aug	5	MID	0.29	0.20	-0.016	-0.016	0.090
CP45 ts	14-Aug	5	MID	0.37	0.24	-0.018	-0.018	0.053
CP45 ts	14-Aug	4	MID	0.23	0.12	-0.015	-0.015	0.143
CP45 ts	14-Aug	5	MID	0.22	0.12	-0.015	-0.014	0.129
CP45 ts	15-Aug	5	MID	0.31	0.21	-0.017	-0.017	0.048
CP4	15-Aug	6	MID	0.22	0.16	-0.016	-0.016	0.061
CP45 ts	15-Aug	3	MID	0.23	0.15	-0.017	-0.017	0.052
CP45 ts	15-Aug	3	MID	0.19	0.10	-0.014	-0.014	0.094
CP45 ts	15-Aug	3	MID	0.31	0.16	-0.016	-0.016	0.108
CP45 ts	15-Aug	3	MID	0.45	0.23	-0.018	-0.018	0.071
CP45 ts	15-Aug	4	MID	0.33	0.22	-0.015	-0.016	0.093
CP4	15-Aug	5	MID	0.21	0.14	-0.014	-0.015	0.079
CP45 ts	16-Aug	3	MID	0.24	0.13	-0.015	-0.015	0.104
CP45 ts	16-Aug	5	MID	0.18	0.10	-0.012	-0.012	0.234
CP45 ts	16-Aug	5	MID	0.17	0.10	-0.014	-0.014	0.088
CP45 ts	16-Aug	3	MID	0.18	0.10	-0.014	-0.014	0.116
CP45 ts	16-Aug	3	MID	0.20	0.11	-0.014	-0.014	0.118
CP45 ts	16-Aug	3	MID	0.26	0.15	-0.016	-0.016	0.077
CP45 ts	16-Aug	3	MID	0.21	0.13	-0.014	-0.014	0.302
BLM	16-Aug	3	MID	0.24	0.14	-0.015	-0.015	0.307
MC 1	17-Aug	5	MID	0.19	0.12	-0.015	-0.014	0.255
HB6	19-Aug	5	MID	0.26	0.16	-0.016	-0.016	0.283
HB8	20-Aug	5	MID	0.21	0.13	-0.016	-0.015	0.263
HB10	20-Aug	5	MID	0.22	0.14	-0.015	-0.015	0.387
HB12	21-Aug	5	MID	0.14	0.07	-0.012	-0.013	0.211
ST1	24-Aug	5	MID	0.17	0.09	-0.011	-0.011	0.324
ST2	24-Aug	4	MID	0.22	0.12	-0.013	-0.013	0.282
ST3	24-Aug	4	MID	0.30	0.16	-0.014	-0.014	0.231
ST4	24-Aug	4	MID	0.23	0.13	-0.014	-0.014	0.198
ST5	24-Aug	4	MID	0.37	0.20	-0.017	-0.016	0.211
ST6	24-Aug	4	MID	0.40	0.22	-0.019	-0.018	0.132
ST7	24-Aug	6	MID	0.27	0.16	-0.015	-0.016	0.204
ST8	24-Aug	5	MID	0.34	0.20	-0.018	-0.018	0.138
ST9	25-Aug	5	MID	0.35	0.21	-0.018	-0.018	0.129
ST10	25-Aug	4	MID	0.26	0.15	-0.015	-0.015	0.241
ST11	25-Aug	5	MID	0.20	0.11	-0.013	-0.013	0.300
ST12	25-Aug	4	MID	0.21	0.12	-0.013	-0.013	0.208

Station	date (local)	depth	group	temp	salin	sig-t	average for prior 24h PAR	kd from ac9 at
CH1	7-Aug	5	IN	12.457	32.789	24.812	69.63	0.49
CH6	8-Aug	5	CR	14.164	32.304	24.096	193.90	0.31
CH3	9-Aug	5	IN	9.947	33.056	25.468	206.94	0.29
CH1	10-Aug	5	IN	11.277	33.001	25.195	64.50	0.36
CH6	11-Aug	5	CR	15.216	32.264	23.843	84.43	0.31
CP1	12-Aug	5	IN	11.102	33.447	25.574	58.62	0.42
CP11	13-Aug	5	CR	15.578	32.304	23.795	88.64	0.26
CP5	14-Aug	5	MID	12.373	32.567	24.656	46.21	0.40
CP45 ts	14-Aug	4	MID	13.154	33.068	24.892	120.28	0.33
CP45 ts	14-Aug	3	MID	13.472	33.118	24.867	137.97	0.35
CP45 ts	14-Aug	3	MID	13.404	33.095	24.863	126.70	0.38
CP45 ts	14-Aug	5	MID	13.409	33.121	24.881	59.16	0.38
CP45 ts	14-Aug	5	MID	13.644	33.113	24.828	72.08	0.34
CP45 ts	14-Aug	4	MID	12.722	32.573	24.594	63.70	0.46
CP45 ts	14-Aug	5	MID	12.128	32.679	24.789	46.22	0.43
CP45 ts	15-Aug	5	MID	13.562	33.115	24.846	73.53	0.34
CP4	15-Aug	6	MID	13.478	33.124	24.870	47.41	0.35
CP45 ts	15-Aug	3	MID	13.276	33.103	24.896	140.19	0.35
CP45 ts	15-Aug	3	MID	12.671	32.998	24.934	120.62	0.39
CP45 ts	15-Aug	3	MID	11.808	32.608	24.794	109.68	0.41
CP45 ts	15-Aug	3	MID	13.356	33.062	24.847	113.56	0.37
CP45 ts	15-Aug	4	MID	13.508	33.092	24.839	67.33	0.40
CP4	15-Aug	5	MID	13.199	33.095	24.904	48.49	0.39
CP45 ts	16-Aug	3	MID	12.971	33.168	25.005	97.70	0.41
CP45 ts	16-Aug	5	MID	12.593	32.826	24.814	20.39	0.56
CP45 ts	16-Aug	5	MID	12.545	33.149	25.074	47.98	0.39
CP45 ts	16-Aug	3	MID	12.299	32.942	24.961	96.25	0.41
CP45 ts	16-Aug	3	MID	12.658	33.028	24.958	94.61	0.42
CP45 ts	16-Aug	3	MID	12.953	33.158	25.002	109.81	0.38
CP45 ts	16-Aug	3	MID	12.538	32.695	24.723	62.43	0.64
BLM	16-Aug	3	MID	12.994	32.679	24.624	85.63	0.65
MC 1	17-Aug	5	MID	11.942	32.645	24.794	33.18	0.59
HB6	19-Aug	5	MID	12.910	32.706	24.660	31.79	0.66
HB8	20-Aug	5	MID	12.684	32.600	24.622	36.60	0.62
HB10	20-Aug	5	MID	12.637	32.565	24.604	18.37	0.77
HB12	21-Aug	5	MID	10.253	33.195	25.526	89.39	0.50
ST1	24-Aug	5	MID	11.349	32.801	25.027	22.99	0.66
ST2	24-Aug	4	MID	11.544	32.599	24.834	63.11	0.64
ST3	24-Aug	4	MID	11.915	32.447	24.648	85.06	0.58
ST4	24-Aug	4	MID	11.717	32.494	24.722	92.45	0.55
ST5	24-Aug	4	MID	12.489	32.357	24.472	80.50	0.59
ST6	24-Aug	4	MID	13.531	32.532	24.402	150.66	0.47
ST7	24-Aug	6	MID	12.880	32.429	24.451	28.22	0.56
ST8	24-Aug	5	MID	12.796	32.424	24.464	70.34	0.49
ST9	25-Aug	5	MID	12.605	32.461	24.529	71.07	0.49
ST10	25-Aug	4	MID	12.129	32.614	24.738	67.60	0.62
ST11	25-Aug	5	MID	12.177	32.906	24.958	23.09	0.71
ST12	25-Aug	4	MID	11.522	32.809	25.001	76.12	0.58

					pigment/Tchla (g:g):					
Station	date (local)	depth	group	Tchla	fuco	perid	hex	zea+lut	allo	chlb
CH1	7-Aug	5	IN	9.60	0.41	0.01	0.02	0.00	0.01	0.01
CH6	8-Aug	5	CR	1.41	0.34	0.02	0.25	0.03	0.03	0.10
CH3	9-Aug	5	IN	2.18	0.44	0.01	0.02	0.00	0.01	0.00
CH1	10-Aug	5	IN	4.21	0.42	0.01	0.03	0.00	0.01	0.02
CH6	11-Aug	5	CR	1.18	0.21	0.01	0.41	0.04	0.05	0.07
CP1	12-Aug	5	IN	8.07	0.36	0.06	0.01	0.00	0.00	0.00
CP11	13-Aug	5	CR	0.21	0.10	0.00	0.19	0.27	0.04	0.17
CP5	14-Aug	5	MID	2.90	0.39	0.01	0.08	0.01	0.02	0.08
CP45 ts	14-Aug	4	MID	3.12	0.37	0.06	0.08	0.01	0.02	0.03
CP45 ts	14-Aug	3	MID	2.75	0.29	0.17	0.17	0.00	0.01	0.04
CP45 ts	14-Aug	3	MID	3.95	0.19	0.26	0.20	0.01	0.02	0.06
CP45 ts	14-Aug	5	MID	4.94	0.35	0.19	0.14	0.00	0.01	0.03
CP45 ts	14-Aug	5	MID	2.19	0.32	0.10	0.22	0.00	0.01	0.05
CP45 ts	14-Aug	4	MID	6.42	0.43	0.01	0.09	0.01	0.01	0.09
CP45 ts	14-Aug	5	MID	7.25	0.43	0.01	0.07	0.01	0.02	0.07
CP45 ts	15-Aug	5	MID	1.82	0.34	0.07	0.24	0.01	0.01	0.07
CP4	15-Aug	6	MID	3.29	0.37	0.19	0.14	0.00	0.01	0.03
CP45 ts	15-Aug	3	MID	2.47	0.32	0.14	0.15	0.00	0.01	0.04
CP45 ts	15-Aug	3	MID	6.35	0.44	0.02	0.06	0.00	0.02	0.04
CP45 ts	15-Aug	3	MID	5.67	0.41	0.01	0.09	0.01	0.02	0.07
CP45 ts	15-Aug	3	MID	4.29	0.35	0.05	0.10	0.01	0.03	0.07
CP45 ts	15-Aug	4	MID	5.64	0.14	0.37	0.14	0.00	0.02	0.03
CP4	15-Aug	5	MID	3.37	0.33	0.15	0.15	0.00	0.01	0.05
CP45 ts	16-Aug	3	MID	6.36	0.47	0.01	0.07	0.00	0.01	0.03
CP45 ts	16-Aug	5	MID	13.06	0.48	0.01	0.06	0.00	0.01	0.03
CP45 ts	16-Aug	5	MID	4.87	0.46	0.02	0.09	0.00	0.01	0.03
CP45 ts	16-Aug	3	MID	6.67	0.46	0.02	0.06	0.00	0.02	0.04
CP45 ts	16-Aug	3	MID	6.86	0.46	0.02	0.06	0.00	0.02	0.04
CP45 ts	16-Aug	3	MID	3.84	0.39	0.05	0.12	0.00	0.01	0.04
CP45 ts	16-Aug	3	MID	18.52	0.54	0.01	0.04	0.00	0.01	0.03
BLM	16-Aug	3	MID	17.27	0.54	0.01	0.04	0.00	0.01	0.03
MC 1	17-Aug	5	MID	14.78	0.55	0.01	0.04	0.00	0.01	0.04
HB6	19-Aug	5	MID	15.31	0.55	0.01	0.03	0.00	0.01	0.03
HB8	20-Aug	5	MID	13.96	0.56	0.01	0.05	0.00	0.01	0.03
HB10	20-Aug	5	MID	18.33	0.59	0.00	0.03	0.00	0.01	0.02
HB12	21-Aug	5	MID	11.28	0.43	0.04	0.02	0.00	0.00	0.01
ST1	24-Aug	5	MID	21.99	0.51	0.01	0.02	0.00	0.01	0.01
ST2	24-Aug	4	MID	17.02	0.50	0.02	0.02	0.00	0.02	0.02
ST3	24-Aug	4	MID	12.87	0.48	0.02	0.03	0.00	0.02	0.03
ST4	24-Aug	4	MID	11.15	0.53	0.01	0.03	0.00	0.02	0.03
ST5	24-Aug	4	MID	11.05	0.48	0.02	0.04	0.01	0.03	0.03
ST6	24-Aug	4	MID	7.17	0.50	0.00	0.04	0.01	0.02	0.03
ST7	24-Aug	6	MID	11.11	0.54	0.00	0.04	0.01	0.01	0.03
ST8	24-Aug	5	MID	7.91	0.54	0.01	0.05	0.01	0.01	0.03
ST9	25-Aug	5	MID	7.17	0.53	0.01	0.05	0.01	0.01	0.03
ST10	25-Aug	4	MID	13.85	0.51	0.01	0.03	0.00	0.02	0.02
ST11	25-Aug	5	MID	18.57	0.52	0.02	0.02	0.00	0.02	0.02
ST12	25-Aug	4	MID	12.84	0.50	0.02	0.02	0.00	0.02	0.02

				pigment/Tchla (g:g):					total carot	ad412/
Station	date (local)	depth	group	but	diad+diat	chla epimer	chlc1/c2	chlc3	+chlb+chlc	ap412
CH1	7-Aug	5	IN	0.00	0.06	0.00	0.17	0.01	0.74	0.39
CH6	8-Aug	5	CR	0.04	0.09	0.00	0.16	0.14	1.22	0.17
CH3	9-Aug	5	IN	0.00	0.14	0.00	0.14	0.02	0.81	0.47
CH1	10-Aug	5	IN	0.01	0.08	0.01	0.10	0.04	0.74	0.33
CH6	11-Aug	5	CR	0.06	0.18	0.00	0.17	0.09	1.33	0.15
CP1	12-Aug	5	IN	0.00	0.06	0.05	0.18	0.04	0.72	0.35
CP11	13-Aug	5	CR	0.00	0.04	0.00	0.07	0.00	0.96	0.19
CP5	14-Aug	5	MID	0.02	0.06	0.01	0.13	0.05	0.88	0.22
CP45 ts	14-Aug	4	MID	0.01	0.14	0.00	0.17	0.05	0.99	0.28
CP45 ts	14-Aug	3	MID	0.01	0.18	0.00	0.20	0.07	1.19	0.23
CP45 ts	14-Aug	3	MID	0.02	0.16	0.00	0.21	0.06	1.22	0.20
CP45 ts	14-Aug	5	MID	0.01	0.16	0.00	0.20	0.07	1.20	0.09
CP45 ts	14-Aug	5	MID	0.02	0.18	0.00	0.18	0.07	1.19	0.10
CP45 ts	14-Aug	4	MID	0.02	0.06	0.00	0.16	0.03	0.94	0.25
CP45 ts	14-Aug	5	MID	0.01	0.06	0.00	0.17	0.04	0.91	0.14
CP45 ts	15-Aug	5	MID	0.02	0.14	0.00	0.17	0.06	1.16	0.13
CP4	15-Aug	6	MID	0.01	0.12	0.00	0.20	0.08	1.17	0.24
CP45 ts	15-Aug	3	MID	0.01	0.10	0.00	0.18	0.06	1.05	0.29
CP45 ts	15-Aug	3	MID	0.01	0.05	0.00	0.16	0.03	0.86	0.14
CP45 ts	15-Aug	3	MID	0.02	0.09	0.00	0.14	0.04	0.94	0.14
CP45 ts	15-Aug	3	MID	0.02	0.15	0.00	0.16	0.03	1.00	0.20
CP45 ts	15-Aug	4	MID	0.02	0.16	0.00	0.22	0.03	1.17	0.12
CP4	15-Aug	5	MID	0.01	0.09	0.00	0.19	0.07	1.10	0.24
CP45 ts	16-Aug	3	MID	0.01	0.10	0.00	0.15	0.04	0.91	0.24
CP45 ts	16-Aug	5	MID	0.01	0.06	0.00	0.16	0.03	0.88	0.24
CP45 ts	16-Aug	5	MID	0.01	0.05	0.00	0.15	0.06	0.91	0.20
CP45 ts	16-Aug	3	MID	0.01	0.05	0.00	0.17	0.05	0.90	0.20
CP45 ts	16-Aug	3	MID	0.01	0.06	0.00	0.17	0.04	0.91	0.19
CP45 ts	16-Aug	3	MID	0.02	0.11	0.00	0.16	0.06	0.97	0.24
CP45 ts	16-Aug	3	MID	0.01	0.10	0.00	0.18	0.05	0.99	0.13
BLM	16-Aug	3	MID	0.01	0.10	0.00	0.19	0.03	1.01	0.12
MC 1	17-Aug	5	MID	0.01	0.08	0.00	0.19	0.04	1.00	0.15
HB6	19-Aug	5	MID	0.01	0.13	0.01	0.18	0.06	1.03	0.17
HB8	20-Aug	5	MID	0.01	0.10	0.00	0.20	0.05	1.03	0.14
HB10	20-Aug	5	MID	0.01	0.11	0.01	0.17	0.03	1.00	0.19
HB12	21-Aug	5	MID	0.00	0.05	0.00	0.20	0.08	0.85	0.20
ST1	24-Aug	5	MID	0.01	0.05	0.00	0.16	0.04	0.85	0.23
ST2	24-Aug	4	MID	0.01	0.07	0.00	0.16	0.04	0.88	0.17
ST3	24-Aug	4	MID	0.01	0.11	0.00	0.16	0.04	0.93	0.15
ST4	24-Aug	4	MID	0.01	0.08	0.00	0.17	0.06	0.95	0.21
ST5	24-Aug	4	MID	0.01	0.14	0.00	0.17	0.05	1.00	0.19
ST6	24-Aug	4	MID	0.01	0.15	0.00	0.17	0.03	1.01	0.21
ST7	24-Aug	6	MID	0.01	0.11	0.00	0.18	0.04	1.00	0.22
ST8	24-Aug	5	MID	0.01	0.15	0.00	0.18	0.04	1.06	0.24
ST9	25-Aug	5	MID	0.01	0.15	0.00	0.18	0.04	1.05	0.24
ST10	25-Aug	4	MID	0.01	0.10	0.00	0.18	0.04	0.95	0.17
ST11	25-Aug	5	MID	0.01	0.06	0.00	0.17	0.04	0.91	0.22
ST12	25-Aug	4	MID	0.01	0.07	0.00	0.15	0.04	0.88	0.27

Station	date (local)	depth	group	QFT Qa*676	ac-9 Qa*676	fit to cp spectra gamma	cp440/ cp650	cp650	Tchla/ cp650	aph676/ cp650
CH1	7-Aug	5	IN	0.65	0.76	0.69	1.31	1.29	7.43	0.11
CH6	8-Aug	5	CR	1.64	1.11	0.87	1.46	0.45	3.13	0.07
CH3	9-Aug	5	IN	0.68	0.59	0.88	1.39	0.30	7.31	0.09
CH1	10-Aug	5	IN	0.99	0.91	0.56	1.25	0.84	5.03	0.09
CH6	11-Aug	5	CR	1.63	1.46	0.91	1.50	0.58	2.03	0.06
CP1	12-Aug	5	IN	0.74	0.80			0.95	8.51	
CP11	13-Aug	5	CR	2.52	1.41	1.55	1.88	0.11	1.98	0.06
CP5	14-Aug	5	MID	1.86	1.70	0.63	1.32	1.06	2.74	0.09
CP45 ts	14-Aug	4	MID	1.11	0.66	0.50	1.22	0.66	4.75	0.06
CP45 ts	14-Aug	3	MID	1.20	1.04	0.27	1.12	0.92	3.00	0.06
CP45 ts	14-Aug	3	MID	1.16	1.03	0.34	1.16	1.16	3.40	0.07
CP45 ts	14-Aug	5	MID	0.60	0.91	0.07	1.03	1.21	4.08	0.07
CP45 ts	14-Aug	5	MID	1.36	1.21	0.24	1.11	0.98	2.22	0.05
CP45 ts	14-Aug	4	MID	0.95	1.11	0.48	1.24	1.67	3.83	0.09
CP45 ts	14-Aug	5	MID	1.02	0.89	0.44	1.21	1.44	5.03	0.09
CP45 ts	15-Aug	5	MID	1.51	1.31	0.41	1.19	0.86	2.12	0.06
CP4	15-Aug	6	MID	1.22	0.92	0.23	1.11	0.97	3.39	0.06
CP45 ts	15-Aug	3	MID	1.18	1.06	0.59	1.27	0.82	3.01	0.06
CP45 ts	15-Aug	3	MID	1.00	0.74	0.51	1.24	1.01	6.32	0.09
CP45 ts	15-Aug	3	MID	1.12	0.95	0.70	1.37	1.06	5.33	0.10
CP45 ts	15-Aug	3	MID	1.00	0.83	0.37	1.17	1.04	4.14	0.07
CP45 ts	15-Aug	4	MID	1.27	0.83	0.37	1.17	1.11	5.10	0.08
CP4	15-Aug	5	MID	1.26	1.17	0.35	1.16	1.08	3.11	0.07
CP45 ts	16-Aug	3	MID	0.93	0.82	0.27	1.14	1.46	4.35	0.07
CP45 ts	16-Aug	5	MID	0.39	0.90	0.24	1.11	2.22	5.90	0.11
CP45 ts	16-Aug	5	MID	1.34	0.90	0.48	1.24	1.02	4.79	0.09
CP45 ts	16-Aug	3	MID		0.87	0.53	1.26	1.15	5.80	0.10
CP45 ts	16-Aug	3	MID	0.99	0.86	0.52	1.26	1.17	5.85	0.10
CP45 ts	16-Aug	3	MID	1.08	1.01	0.51	1.25	0.99	3.86	0.08
CP45 ts	16-Aug	3	MID	0.77	0.82	0.44	1.24	2.58	7.19	0.12
BLM	16-Aug	3	MID	0.94	0.89	0.36	1.19	3.52	4.90	0.09
MC 1	17-Aug	5	MID	0.89	0.87	0.51	1.28	2.51	5.88	0.10
HB6	19-Aug	5	MID	0.93	0.93	0.64	1.35	2.96	5.17	0.10
HB8	20-Aug	5	MID	1.01	0.94	0.67	1.37	2.74	5.09	0.10
HB10	20-Aug	5	MID	0.98	1.06	0.58	1.33	4.27	4.29	0.09
HB12	21-Aug	5	MID	0.90	0.94	-0.38	0.87	1.91	5.90	0.11
ST1	24-Aug	5	MID	0.56	0.74	0.40	1.21	2.51	8.78	0.13
ST2	24-Aug	4	MID	0.66	0.83	0.39	1.20	2.68	6.35	0.11
ST3	24-Aug	4	MID	0.94	0.90	0.42	1.21	2.36	5.46	0.10
ST4	24-Aug	4	MID	0.84	0.89	0.43	1.22	2.05	5.45	0.10
ST5	24-Aug	4	MID	0.88	0.96	0.36	1.18	2.87	3.84	0.07
ST6	24-Aug	4	MID	0.95	0.92	0.45	1.24	1.96	3.66	0.07
ST7	24-Aug	6	MID	0.87	0.92	0.48	1.25	2.61	4.26	0.08
ST8	24-Aug	5	MID	0.94	0.87	0.46	1.24	2.31	3.42	0.06
ST9	25-Aug	5	MID	1.02	0.90	0.46	1.24	2.24	3.19	0.06
ST10	25-Aug	4	MID	0.95	0.87	0.40	1.20	3.12	4.44	0.08
ST11	25-Aug	5	MID	0.78	0.81			3.77	4.92	0.08
ST12	25-Aug	4	MID	0.80	0.81	0.51	1.26	1.70	7.54	0.12